The role of mitochondrial proteins CHCHD10 and CHCHD2 in neurodegenerative disease

by

Isabella Romana Straub

Department of Human Genetics
McGill University, Montréal, Canada
February 2020

A thesis submitted to McGill University in partial fulfillment of the requirements of the degree of Doctor of Philosophy

If you can't explain it simply, you don't understand it well enough.

Albert Einstein

Abstract

Dysfunctional mitochondria have been suggested to contribute to a number of neurodegenerative diseases including some of the most prevalent such as amyotrophic lateral sclerosis (ALS) and Parkinson's disease (PD). Our studies focused on two proteins, CHCHD10 and CHCHD2, which have been linked to ALS and PD, respectively. CHCHD10 and CHCHD2 are paralogues, belonging to the CX_9C family of proteins that primarily localize to the mitochondrial intermembrane space. Our first two studies focused on the investigation of the function of CHCHD10, using a fibroblast cell line from an ALS patient, harbouring the p.R15L variant. Patient fibroblasts presented with a variety of mitochondrial defects: (1) lower levels of complex I, (2) mitochondrial hyperfusion and (3) a growth defect in galactose. This phenotype could be rescued by expression of the wild-type CHCHD10 protein suggesting that it is haploinsufficient. Analysis of the patient cells in medium in which glucose is replaced by galactose, forcing cells to rely on oxidative phosphorylation as an energy supply, revealed deficits in energy production and imbalances in the $NADH/NAD^+$ ratio as well as dysregulation of the nucleotide producing one-carbon cycle. Moreover, the change in nutrient supply activated the integrated stress response in the ER as well as the unfolded protein response in mitochondria and resulted in an increase in FGF21 and GDF15, two biomarkers previously associated with mitochondrial disease caused by mutations in mitochondrial DNA. We discovered protein-protein interactions between CHCHD10, CHCHD2 and C1QBP/p32, and identified a high molecular weight complex containing CHCHD10 and CHCHD2 that was not present in patient cells.

The third study analysed the effects of two different pathogenic variants of CHCHD2, p.T61I and p.R145Q, as well as the CRISPR-Cas9 mediated knockout of CHCHD2 in fibroblasts. The loss of CHCHD2 resulted in altered mitochondrial morphology, decreased levels of oxidative phosphorylation complexes, disassembly of complex V and an accumulation of CHCHD10 in the high molecular weight complex. Expression of wild-type CHCHD2, but not the pathogenic variants, rescued the OXPHOS phenotype as well as the complex formation with CHCHD10. The more hydrophobic CHCHD2 p.T61I variant caused an accumulation of CHCHD2 and CHCHD10 at a high molecular weight, perhaps suggesting that it is prone to form aggregates. Moreover, we identified short forms of CHCHD2, but not CHCHD10. Levels of

CHCHD10 as well as all long and short forms of CHCHD2 increased when cells were exposed to different stress conditions. Transcript and protein levels of RNA binding proteins showed the largest changes in cells expressing wildtype or pathogenic variants compared to knockout cell lines. Interestingly, we discovered additional interaction partners of CHCHD2 in DNA/RNA binding proteins outside of mitochondria (ALYREF, YBX1, CHTOP, LBR), an interaction that was lost or significantly reduced when CHCHD2 p.T61I and p.R145Q variants were expressed, suggesting that CHCHD2 may play an important function outside mitochondria.

Overall, our findings contribute to a better understanding of the molecular mechanisms underlying CHCHD10 and CHCHD2 related disorders in ALS and PD patients, while providing detailed insights into the mitochondrial dysfunction of pathogenic variants of these proteins.

Résumé

Il a été montré qu'une dysfonction mitochondriale pouvait contribuer à la physiopathologie de certaines maladies neurodégénératives, comme la sclérose latérale amyotrophique (SLA) et la maladie de Parkinson (MD). Nos études se sont concentrées sur deux protéines, CHCHD10 et CHCHD2, qui ont été liées à la SLA et la MD, respectivement. CHCHD10 et CHCHD2 sont des gènes paralogues, codant pour des protéines appartenant à la famille CX9C, qui se localisent généralement dans l'espace inter membranaire mitochondrial. Nos deux premières études se sont concentrées sur la fonction de CHCHD10, en utilisant une lignée cellulaire de fibroblastes issue d'un patient SLA p.R15L. Ces fibroblastes présentent plusieurs défauts mitochondriaux : (1) un niveau bas de complexe I, (2) une hyperfusion mitochondriale et (3) un défaut de croissance en présence de galactose. Ce phénotype est sauvé par l'expression de la protéine CHCHD10 de type sauvage, suggérant une haplo insuffisance. L'analyse des fibroblastes de patient en présence de galactose, forçant ainsi les cellules à s'appuyer sur la phosphorylation oxydative comme source d'énergie, a révélé un déficit de production d'énergie, un déséquilibre du rapport $NADH/NAD^+$, ainsi qu'une dérégulation des nucléotides participant à la production des métabolites à un carbone. Ce changement de nutriment active la réponse au stress du réticulum endoplasmique, ainsi que la réponse au stress de la mitochondrie. Ceci entraîne une augmentation de FGF21 et GDF15, deux biomarqueurs précédemment associés aux maladies mitochondriales causées par des mutations de l'ADN mitochondrial. Nous avons de plus découvert une interaction protéique entre CHCHD10, CHCHD2 et C1QBP/p32, et identifié un complexe de poids moléculaire élevé contenant CHCHD10 et CHCHD2, qui est absent dans les cellules de patient.

La troisième étude concerne les effets de deux variants pathogènes de CHCHD2, p.T61I et p.R145Q, ainsi que l'invalidation de CHCHD2 par CRISPR-Cas9 dans les fibroblastes. L'absence de CHCHD2 entraîne une modification de la morphologie mitochondriale, une diminution des niveaux des complexes de la phosphorylation oxydative, le désassemblage du complexe V et une accumulation de CHCHD10 dans le complexe de haut poids moléculaire. La réexpression de CHCHD2 de type sauvage, mais pas des variants pathogènes, sauve le phénotype de la chaine respiratoire ainsi que la formation du complexe avec CHCHD10. Le variant CHCHD2 p.T61I, plus hydrophobe, entraine une accumulation de CHCHD2 et CHCHD10 dans un complexe de poids moléculaire très élevé, suggérant une tendance à former des agrégats. Nous avons de plus identifié des formes plus courtes de CHCHD2. Les niveaux de

toutes les isoformes de CHCHD2 ainsi que de CHCHD10 augmentent lorsque les cellules sont exposées à différents stress. En comparant le transcriptome et le protéome des cellules sauvages à celui des cellules mutantes ou invalidées, nous avons observé que les niveaux d'ARN et de protéine des protéines de liaison à l'ARN sont les plus dérégulés. Nous avons de plus découvert d'autres partenaires de CHCHD2 en dehors de la mitochondrie, impliqués dans la liaison à l'ADN ou l'ARN (ALYREF, YBX1, CHTOP, LBR). Ces interactions sont perdues, ou significativement réduites lorsque CHCHD2 p.T61I et p.R145Q sont exprimées, suggérant que CHCHD2 puisse jouer un rôle important en dehors de la mitochondrie.

Dans l'ensemble, nos résultats contribuent à une meilleure compréhension des mécanismes physiopathologiques liés à CHCHD10 et CHCHD2 chez les patients SLA et PD, tout en fournissant des informations détaillées sur les dysfonctions mitochondriales dues aux variants pathogènes.

Table of Contents

List of Abbreviations

°C	degree Celsius
2D-PAGE	second dimension SDS-PAGE
5-MTHF	5-methyltetrahydrofolate
aa	amino acid
Ab	antibody
ACAT2	acetyl-CoA acetyltransferase 2
ACLY	ATP citrate synthase
ACSS3	acyl-CoA synthetase short chain 3
AD	Alzheimer's disease
ADMM	autosomal dominant mitochondrial myopathy
ADP	adenosine diphosphate
AFF4	AF4/FMR2 Family Member 4
AKT	AKT serine/threonine kinase
ALDH1L2	aldehyde dehydrogenase 1 family member L2
ALDH3A2	aldehyde dehydrogenase 3 family member A2
ALDOA	aldolase, fructose-bisphosphate A
ALR	augmenter of the liver regeneration
ALS	Amyotrophic Lateral Sclerosis
ALYREF	Aly/REF Export Factor
AMP	adenosine monophosphate
AMPK	acetyl-CoA carboxylase kinase
AMS	4-acetamido-4'-((iodoacetyl)amino)stilbene-2,2'-disulfonic acid
ANPEP	alanyl aminopeptidase
ASAH1	N-acylsphingosine amidohydrolase 1
ASNS	asparagine synthetase (glutamine-hydrolyzing)
ATF3	activating transcription factor 3
ATF4	activating transcription factor 4
ATF5	activating transcription factor 5
ATF6	activating transcription factor 6
ATP	adenosine triphosphate
ATP6	mitochondrially encoded ATP synthase membrane subunit 6
ATP6V1G1	ATPase H+ transporting V1 subunit G1
BAX	BCL2 associated X, apoptosis regulator
Bcl-xL	B-cell lymphoma-extra large
BDH1	3-hydroxybutyrate dehydrogenase 1
BIP	binding immunoglobulin protein
BirA	biotin-protein ligase A
BN	blue native
BSA	bovine serum albumin
C1QBP	complement C1q binding protein
Cas9	CRISPR-associated protein 9
CAT	catalase
CCCP	carbonyl cyanide m-chlorophenyl hydrazone
cDNA	complementary DNA

CHAC1	ChaC glutathione specific gamma-glutamylcyclotransferase 1
CHCH	coiled-helix coiled-helix
CHCHD10	coiled-helix coiled-helix domain containing protein 10
CHCHD2	coiled-helix coiled-helix domain containing protein 2
CHCHD3	coiled-helix coiled-helix domain containing protein 3
CHCHD4	coiled-helix coiled-helix domain containing protein 4
CHCHD5	coiled-helix coiled-helix domain containing protein 5
CHCHD6	coiled-helix coiled-helix domain containing protein 6
CHCHD7	coiled-helix coiled-helix domain containing protein 7
CHCHD8	coiled-helix coiled-helix domain containing protein 8
CHTOP	chromatin target of PRMT1
CLPP	caseinolytic mitochondrial matrix peptidase proteolytic subunit
CLTB	clathrin light chain B
CMC1	C-X9-C motif containing 1
CMC2	C-X9-C motif containing 2
CMC3	C-X9-C motif containing 3
CMC4	C-X9-C motif containing 4
CMPK2	cytidine/uridine monophosphate kinase 2
CMT2	Charcot-Marie Tooth type 2
CO2	carbon dioxide
CoA	coenzyme A
COA4	cytochrome C oxidase assembly factor 4
COA5	cytochrome C oxidase assembly factor 5
COA6	cytochrome C oxidase assembly factor 6
COX1	cytochrome C oxidase subunit 1
COX12	cytochrome C oxidase assembly factor COX12
COX17	cytochrome C oxidase assembly factor COX17
COX19	cytochrome C oxidase assembly factor COX19
COX2	cytochrome C oxidase subunit 2
COX4	cytochrome C oxidase subunit 4I2
COX4I2	cytochrome C oxidase subunit 4I2
COX6B1	cytochrome C oxidase subunit 6B1
COX6B2	cytochrome C oxidase subunit 6B2
CRISPR	clustered regularly interspaced short palindromic repeats
CTNND1	catenin delta 1
CTSB	cathepsin B
CTSD	cathepsin D
CTSK	cathepsin K
CTSL	cathepsin L
CTSZ	cathepsin Z
CYCS	cytochrome C, somatic
dCMP	deoxycytidine monophosphate
DDM	n-dodecyl β-D-maltoside
DDX6	DEAD-box helicase 6
DHFR	dihydrofolate reductase
DIABLO	direct IAP-binding protein with low PI

DJ-1	protein deglycase
DLD	dihydrolipoamide dehydrogenase
DMEM	Dulbecco's Modified Eagle Medium
DMP	dimethyl pimelimidate
DNA	deoxyribonucleic acid
DNASE2	deoxyribonuclease 2, lysosomal
DRP1	dynamin-1-like protein
DSG	disuccinimidyl glutarate
DSP	dithiobis (succinimidyl propionate)
DTT	dithiothreitol
dUMP	deoxyuridine monophosphate
dUTP	deoxyuridine triphosphate
ECAR	extracellular acidification rate
EGLN2	Egl-9 family hypoxia inducible factor 2
EGLN3	Egl-9 family hypoxia inducible factor 3
EHD2	EH domain containing 2
EIF2A	eukaryotic translation initiation factor 2A
EIF2AK1	eukaryotic translation initiation factor 2 alpha kinase 1
EIF2AK2	eukaryotic translation initiation factor 2 alpha kinase 2
EIF2AK3	eukaryotic translation initiation factor 2 alpha kinase 3
EIF2AK4	eukaryotic translation initiation factor 2 alpha kinase 4
EMI1	early mitotic inhibitor
ENO1	enolase 1
ENO2	enolase 2
ENO3	enolase 3
ER	endoplasmic reticulum
ERK	extracellular signal-regulated kinase
ERN1	endoplasmic reticulum to nucleus signaling 1
F6P	fructose-6-phosphate
FARSA	phenylalanyl-TRNA synthetase subunit alpha
FASN	fatty acid synthetase
FBS	fetal bovine serum
FC	fold change
FCCP	carbonyl cyanide-4-(trifluoromethoxy)phenylhydrazone
FDR	false discovery rate
FGF21	fibroblast growth factor 21
FH	fumarate hydratase
FLNC	filamin C
FOXO3	forkhead box O3
FPD	familial Parkinson's disease
FPGS	folylpolyglutamate synthase
FTD	frontotemporal dementia
FUBP3	far upstream element binding protein 3
FUS	fused in sarcoma
g	gravity (rcf)
G6P	glucose-6-phosphate

GABA	gamma aminobutyric acid
GADD34	growth arrest and DNA-damage-inducible 34
Gal	galactose
GAPDHS	glyceraldehyde-3-phosphate dehydrogenase, spermatogenic
GDF15	growth/differentiation factor 15
GDP	guanosine diphosphate
GEO	Gene Expression Omnibus
Glc	glucose
GMP	guanosine monophosphate
GNS	glucosamine (N-acetyl)-6-sulfatase
GO	gene ontology
GO_BP	gene ontology biological process
GOMF	gene ontology molecular function
GOT1	glutamic-oxaloacetic transaminase 1
GRSF1	G-rich RNA sequence binding factor 1
GSH	glutathione reduced
GSSG	glutathione oxidized
GSTO1	glutathione S-transferase omega 1
GSTP1	glutathione S-transferase pi 1
GTP	guanosine diphosphate
h	hour
H. sapiens	homo sapiens
HA	human influenza hemagglutinin
har-1	hemi-asterlin resistant 1
HCl	hydrochloric acid
HEK	human embryonic kidney
HeLa	Henrietta Lacks (cells)
HEPES	4-(2-hydroxyethyl)-1-piperazineethanesulfonic acid
HEXB	hexosaminidase subunit beta
HMG-CoA	3-hydroxy-3-methyl-glutaryl-coenzyme A reductase
HPS	HEPES buffered saline
HPV	human papillomavirus
HSP10	heat shock 10kD protein 1
HSP60	heat shock 60kD protein 1
HSP70	heat shock 70kD protein 1
HSPA5	heat shock protein family A (Hsp70) member 5
HSPA9	heat shock protein family A (Hsp70) member 9
HSPD1	heat shock protein family D (Hsp60) member 1
HSPE1	heat shock protein family E (Hsp10) member 1
htert	human telomerase
HTRA2	high temperature requirement protein A2
IDH3A	isocitrate dehydrogenase (NAD(+)) 3 catalytic subunit alpha
IMMP1L	mitochondrial inner membrane protease subunit 1
IMMP2L	mitochondrial inner membrane protease subunit 2
IMMT	inner membrane mitochondrial protein
IMP	inosine monophosphate

IMS	intermembrane space
IP	immunoprecipitation
IRCM	Institut de recherches cliniques de Montréal
ISR	integrated stress response
kDa	kilodalton
KIAA0391	mitochondrial ribonuclease P protein 3
KIF5B	kinesin family member 5B
KO	knockout
KUB3	ku70-binding protein 3
kV	kilovolt
L	litre
LAMP1	lysosomal associated membrane protein 1
LBD	Lewy Body disease
LBR	lamin B receptor
LC-MS/MS	liquid chromatography with tandem mass spectrometry
LC3-A/B	light chain 3 alpha/beta
LDHA	lactate dehydrogenase A
LDHAL6B	lactate dehydrogenase A like 6B
LGMN	legumain
LONP1	lon peptidase 1
LRKK2	leucine rich repeat kinase 2
M	molar
M. musculus	mus musculus
MAP1LC3 A/B	microtubule-associated proteins 1A/1B light chain 3 A/B
MAPK	mitogen-activated protein kinase
MDH1	malate dehydrogenase 1
MDH2	malate dehydrogenase 2
MDM35	mitochondrial distribution and morphology protein 35
metab.	metabolism
MFN1	mitofusin 1
MFN2	mitofusin 2
MGST1	microsomal glutathione S-transferase 1
Mia40	mitochondrial IMS import and assembly protein 40
Mic14	mitochondrial IMS cysteine motif-containing protein 14
Mic17/ Mix17	mitochondrial IMS cysteine motif-containing protein 17
Mic19	mitochondrial IMS cysteine motif-containing protein 19
Mic25	mitochondrial IMS cysteine motif-containing protein 25
Mic27	mitochondrial IMS cysteine motif-containing protein 27
Mic60	mitochondrial IMS cysteine motif-containing protein 60
MICOS	mitochondrial contact site and cristae organizing system
MICS1	mitochondrial morphology and cristae structure 1
min	minutes
mL	millilitre
MM	mitochondrial myopathy
MMP1	matrix metallopeptidase 1
MMP3	matrix metallopeptidase 3

MPP	Mitochondrial processing peptidase
mRNA	messenger ribonucleic acid
MRP10	mitochondrial ribosomal protein 10
MS	mass spectrometry
MSA	multiple systems atrophy
mtDNA	mitochondrial deoxyribonucleic acid
MTFMT	mitochondrial methionyl-tRNA formyltransferase
MTHFD1	methylenetetrahydrofolate dehydrogenase (NADP+ dependent) 1 like
MTHFD1L	methylenetetrahydrofolate dehydrogenase (NADP+ dependent) 1 like
MTHFD2	methylenetetrahydrofolate dehydrogenase (NADP+ dependent) 2
MTHFD2L	methylenetetrahydrofolate dehydrogenase (NADP+ dependent) 2 like
MTHFR	methylenetetrahydrofolate reductase
MTHFS	methenyltetrahydrofolate synthetase
mTOR	mechanistic target of rapamycin
mTORC1	mammalian target of rapamycin complex 1
MTR	5-methyltetrahydrofolate-homocysteine methyltransferase
MTRR	5-methyltetrahydrofolate-homocysteine methyltransferase reductase
MTS	mitochondrial targeting sequence
mut.	mutation
MVP	major vault protein
MYL12A	myosin light chain 12A
n.s.	non-significant
NaCl	sodium chloride
NAD	nicotinamide adenine dinucleotide
NADH	nicotinamide adenine dinucleotide hydrogen
NADP	nicotinamide adenine dinucleotide phosphate
NDUFA10	NADH:ubiquinone oxidoreductase subunit A10
NDUFA5	NADH:ubiquinone oxidoreductase subunit A5
NDUFA7	NADH:ubiquinone oxidoreductase subunit A7
NDUFA9	NADH:ubiquinone oxidoreductase subunit A9
NDUFB10	NADH:ubiquinone oxidoreductase subunit B10
NDUFB8	NADH:ubiquinone oxidoreductase subunit B8
NDUFS2	NADH:ubiquinone oxidoreductase core subunit S2
NDUFS4	NADH:ubiquinone oxidoreductase subunit S4
NDUFS5	NADH:ubiquinone oxidoreductase subunit S5
NDUFS7	NADH:ubiquinone oxidoreductase core subunit S7
NDUFS8	NADH:ubiquinone oxidoreductase core subunit S8
NDUFV1	NADH:ubiquinone oxidoreductase core subunit V1
NEB	New England Biolabs
nm	nanometre
nmol	nanomolar
NPC2	NPC intracellular cholesterol transporter 2

NRF1	nuclear respiratory factor 1
Nter	N-terminal
OCR	oxygen consumption rate
OGDH	oxoglutarate dehydrogenase
Oligom.	oligomycin
OMA1	overlapping activity with m-AAA protease
OPA1	optic atrophy protein 1
ORE	oxygen responsive element
OXPHOS	oxidative phosphorylation
P	phosphate
p-	phosphorylated
p-value	probability value
p62	SQSTM1
PAGE	polyacrylamide gel electrophoresis
PARL	presenilins-associated rhomboid-like protein
PARP	poly(ADP-ribose) polymerase
Pat	patient
PBS	phosphate buffered saline
PC	principal component
PCA	principle component analysis
PCK2	phosphoenolpyruvate carboxykinase 2
PCR	polymerase chain reaction
PD	Parkinson's disease
PDHA1	pyruvate dehydrogenase E1 alpha 1 subunit
PDHB	pyruvate dehydrogenase E1 beta subunit
PDK4	pyruvate dehydrogenase kinase 4
PERK	PRKR-like endoplasmic reticulum kinase
PET191	mitochondrial protein PET191
PGAM1	phosphoglycerate mutase 1
PGAM4	phosphoglycerate mutase 4
PGK1	phosphoglycerate kinase 1
PHGDH	phosphoglycerate dehydrogenase
PICALM	phosphatidylinositol binding clathrin assembly protein
PINK1	PTEN induced kinase 1
PKLR	pyruvate kinase L/R
PPARGC1A	peroxisome proliferator-activated receptor gamma coactivator 1 alpha
PPP1CA	protein phosphatase 1 catalytic subunit alpha
PPP1R15A	protein phosphatase 1 regulatory subunit 15A
PPP1R15B	protein phosphatase 1 regulatory subunit 15B
PPT1	palmitoyl-protein thioesterase 1
PRMT1	protein arginine methyltransferase 1
PRPP	phosphoribosyl pyrophosphate
PSAP	prosaposin
PSAT1	phosphoserine aminotransferase 1
psi	pound per square inch

PSPH	phosphoserine phosphatase
qRT-PCR	quantitative real-time PCR
R5P	ribulose-5-phosphate
RIDD	Ire1-dependent decay of mRNA
RNA	ribonucleic acid
RT	room temperature
RT-PCR	real-time polymerase chain reaction
S6	ribosomal protein S6
SAH	S-adenosyl-L-homocysteine
SAM	S-adenosyl methionine
SCAF1	SR-related CTD associated factor 1
sCMOS	scientific complementary metal–oxide–semiconductor
SCO1	SCO cytochrome C oxidase assembly protein 1
SCO2	SCO cytochrome C oxidase assembly protein 2
SD	semantic dementia
SDHA	succinate dehydrogenase complex flavoprotein subunit A
SDS	sodium dodecyl sulphate
SEM	standard error of the mean
sgRNA	single guide RNA
SHMT1	serine hydroxymethyltransferase 1
SHMT2	serine hydroxymethyltransferase 2
siRNA	small interfering RNA
SIRT3	sirtuin 3
SIRT7	sirtuin 7
SLC	solute carrier
SMA	spinal muscular atrophy Jokela type
SMAD4	mothers against decapentaplegic homolog 4
SOD1	superoxide dismutase 1
SOD2	superoxide dismutase 2
SPD	sporadic Parkinson's disease
SQSTM1	sequestosome 1
SUCLA1	succinate-CoA ligase alpha subunit
SUCLA2	succinate-CoA ligase ADP-forming beta subunit
t-test	statistical hypothesis test
TBST	tris-buffered saline and Tween 20
TCA	citric acid cycle
TCEP	tris(2-carboxyethyl)phosphine)
TDP-43	TAR DNA-binding protein 43
TEAB	triethylammonium bicarbonate
TGFβ	transforming growth factor beta
THF	tetrahydrofolat
TIM	translocase of inner mitochondrial membrane
TMT	tandem mass tag
TOMM20	translocase of outer mitochondrial membrane 20
TOMM40	translocase of outer mitochondrial membrane 40
TOMM70	translocase of outer mitochondrial membrane 70

TPI1	triosephosphate isomerase 1
TREX	THO transcription elongation complex
TRIAP1	transient receptor potential ankyrin 1
Tris	tris(hydroxymethyl)aminomethane
tRNA	transfer ribonucleic acid
TXNDC12	thioredoxin domain containing 12
TYMS	thymidylate synthetase
UCP4	uncoupling protein 4
UCP5	uncoupling protein 5
UPR	unfolded protein response
VDAC	voltage dependent anion channel 1
vs.	versus
w/w	weight by weight
WT	wild-type
XBP1	X-box binding protein 1
YBX1	Y-box binding protein 1
YME1L	YME1 like 1 ATPase
ZNHIT3	Zinc finger HIT-type containing 3
µg	microgram
µL	microliter
µM	micromolar

List of Figures

List of Supplementary Figures

List of Tables

Acknowledgments

I would like to thank Dr. Eric Shoubridge for supporting me throughout my PhD wherever he could. I greatly appreciated his style of guidance, being human, taking time and letting people evolve in their own ways. Thank you for giving me scientific freedom and financial support throughout all this time. I learned a lot from you and your lab about how to do science well. Results are results and there is no judgment to be made.

I would like to acknowledge the members of my thesis advisory committee Dr. Heidi McBride and Dr. Colin Crist for their time, effort and guidance.

I would also like to thank the members of the Shoubridge lab, Dr. Hana Antonicka, Dr. Alexandre Janer, Kathleen Daigneault, Jana Schüttpelz, Dr. Archita Rajasekharan, Dr. Mari Aaltonen, Dr. Diane Nakamura, and past members and interns Ziyang Chen, Dr. Woranontee Weraarpachai, Dr. Olga Zurita-Rendon, Dr. Shamisa Honarmand, Dr. Vincent Paupe, Timothe Langlois-Therien and Dr. Vijayaraghava Rao.

A special thank you goes to Hana Antonicka, for guiding me through my PhD, for always answering my questions, and for giving me your support whenever I needed it. Thank you for proofreading all texts, presentations and posters during all this time. You are someone I learned so much from, and from whom I learned how to organize my science.

To Alexandre Janer, thank you for being my best friend here, my papa-requin. I learned so much from you in science and non-science related matters. Thank you for always answering my questions, for being human, and for being you.

A special thank you also goes to Woranontee Weraarpachai who helped with a lot of experiments every time she came back to Montreal. You are an inspiration with your endless energy and positive attitude.

I would also like to thank Kathleen Daigneault in particular. She helped out with any matters, took a lot of work load from me, and is such a kind person.

To Jana Schüttpelz, my partner in crime the last two years, thanks for having returned. Montréal would not be the same without you.

I want to thank all the members of the laboratories of Dr. McBride, Dr. Brais, Dr. Hastings and Dr. Armstrong. The atmosphere on the 6th floor of the MNI is special, and I have enjoyed many scientific but also non-scientific conversations with you. Special thanks goes to a

former member of the McBride lab, Maxime Jacoupy, who made sure my blood glucose levels never dropped too low, and for always cheering me up.

To my family, a big thank you goes to my husband Andrés, without whom I would have not embarked on this endeavour. Thank you for always being there with me.

I would also like to thank my parents, for giving me the wings I needed to leave home for six years, and for giving me the confidence and support to follow my dreams.

To my brothers, Alexander and Volker, who I missed a whole lot during these six years, thank you for being always there for me. It gave me a lot of strength to know that I can count on you.

To my grandmother, Hildegard, who understood this step was important for me, thank you for letting me go even though it was hard for you.

Importantly, I don't want to forget to thank this city, Montréal, and this country for its people. You taught me how to be friendlier, more patient, more helpful and more attentive with my surroundings. I will take it back to Europe and wherever I go.

Lastly, I am thankful for the financial support from the following institutions and organizations for my project: DAAD (Deutscher Akademischer Auslands Dienst), Healthy Brain for Healthy Lives (HBHL, McGill), Internal Medicine studentship (McGill), Parkinson Canada, and the department of Human Genetics at McGill.

Contribution to Original Knowledge

1. Identification of the interaction between CHCHD10, CHCHD2 and C1QBP (p32) and the complex formation between CHCHD10 and CHCHD2.

2. Characterization of the CHCHD10 p.R15L mutation in a patient with sporadic ALS and identification that this mutation as being haploinsufficient. The CHCHD10 p.R15L variant causes a complex I deficiency and comprised mitochondrial function. The high molecular weight CHCHD10/2 complex is greatly diminished in this patient.

3. Finding that the phenotypic consequences of the CHCHD10 variant p.R15L are similar to other mitochondrial diseases caused by mtDNA alterations. The CHCHD10 p.R15L variant causes an activation of the integrated stress response in the ER and mitochondria and a release of metabolic cytokines GDF15 and FGF21 in galactose medium.

4. Discovery that the loss of CHCHD2 leads to OXPHOS defects, alterations of mitochondrial morphology and that more hydrophobic CHCHD2 variant p.T61I affects the assembly of the high molecular weight CHCHD10/2 complex.

5. Identification of a new interactome consisting of CHCHD2, CHCHD10 and C1QBP with RNA/DNA binding proteins, ALYREF, YBX1, CHTOP and LBR outside of mitochondria.

6. The disulfide bonds of CHCHD10 and CHCHD2 are structural and are not redox sensitive.

7. Identification of a short form of CHCHD2 and not CHCHD10.

Format of the Thesis

This thesis was prepared in a manuscript-based format, in agreement with the guidelines from the department of Human Genetics at McGill University. This thesis is composed of 7 chapters. **Chapter 1** comprises the general introduction and contains a comprehensive review of the literature related to the topic covered in this thesis. **Chapter 2** contains a study describing mitochondrial alterations in a patient with ALS and a mutation in *CHCHD10*. This study was published in the journal of *Human Molecular Genetics*. The study in **chapter 3** reports the metabolic alterations observed when exposing CHCHD10 patient cells to nutrient stress and is a manuscript near completion and about to be submitted. **Chapter 4** provides insights into the mitochondrial and cellular pathogenesis of two CHCHD2 variants and is a manuscript in preparation, to be submitted once additional experiments are performed by Diane Nakamura. **Chapter 5** consists of a general discussion of the thesis and puts acquired data in context with the literature. **Chapter 6** summarizes this thesis with conclusions and gives ideas for future research directions. Finally, **chapter 7** comprises the master reference list.

Contribution of Authors

With the guidance of my committee consisting of Dr. McBride, Dr. Crist and Dr. Shoubridge, I planned and conducted experiments for the following manuscripts. The particular contribution of co-authors is described in detail below:

Chapter 2:

Straub IR, Janer A, Weraarpachai W, Zinman L, Robertson J, Rogaeva E, Shoubridge EA. (**2018**) Loss of CHCHD10-CHCHD2 complexes required for respiration underlies the pathogenicity of a CHCHD10 mutation in ALS. Hum. Mol. Genet. 1;27(1):178-189.

For chapter 2 of this thesis Dr. Janer managed the immunoprecipitation experiments and guided the start of this project. Dr. Weraarpachai conducted preliminary experiments for the 2D-PAGE and the identification of the CHCHD10/CHCHD2 complex. And Dr. Zinman, Dr. Robertson and Dr. Rogaeva provided the patient cell line. Finally, Dr. Hana Antonicka proofread the manuscript. The IRCM platform conducted the mass spectrometry for the immunoprecipitation experiment.

Chapter 3:

Straub IR, Weraarpachai W, Shoubridge EA. (**2020**) The CHCHD10 variant p.R15L causes an energy deficit and activates the integrated stress response during nutrient stress. *Manuscript in preparation.*

For chapter 3 of this thesis Dr. Logan Walsh helped discussing and analysing the RNA sequencing data and Dr. Weraarpachai conducted several immunoblot experiments for the quantification of the integrated stress response. Finally, Dr. Hana Antonicka proofread the manuscript. The IRCM platform conducted the mass spectrometry for the TMT-labelling experiment. GENEWIZ conducted the RNA sequencing experiment after receiving RNA from us. Human Metabolome Technologies conducted the targeted metabolomic study after receiving the extracted material from us.

Chapter 4:

Straub IR, Chen Z, Nakamura D, Janer A, Weraarpachai W, Shoubridge EA. (**2020**) CHCHD2 interacts with RNA binding proteins outside of mitochondria and pathogenic variant p.T61I causes disturbed interaction with CHCHD10. *Manuscript in preparation.*

For chapter 4 of this thesis, Ziyang Chen, a summer intern through the MITACS program at McGill, contributed and executed immunoblots, immunofluorescence analysis, and cell culture. Furthermore, Dr. Janer managed all immunoprecipitation experiments, and Dr. Weraarpachai assisted with the immunoblot experiments. Finally, Dr. Nakamura assisted with the repetition of several immunoblots to obtain quantitative data and will continue the project. Finally, Dr. Hana Antonicka proofread the manuscript. The IRCM platform conducted the mass spectrometry for the TMT-labelling and the immunoprecipitation experiment. GENEWIZ conducted the RNA sequencing experiment after receiving RNA from us.

Chapter 1: General Introduction

1. Introduction

Neurodegenerative diseases are a heterogeneous group of debilitating diseases causing a progressive degeneration of different types of neurons, resulting primarily in problems with movement or mental capabilities. The pathogenesis of the most common neurodegenerative diseases, like Alzheimer's, Parkinson's disease (PD), Amyotrophic lateral sclerosis (ALS) and frontotemporal dementia (FTD), have been linked to mitochondrial dysfunction (Park et al., 2018, Smith et al., 2019). Recently, two homologous mitochondrial proteins of unknown function (coiled-helix coiled-helix domain containing protein 10/2, CHCHD10/ CHCHD2) have been associated with ALS, FTD and PD. While CHCHD10 is associated with ALS and FTD (Bannwarth et al., 2014, Chaussenot et al., 2014, Chio et al., 2015, Dols-Icardo et al., 2015, Johnson et al., 2014, Kurzwelly et al., 2015, Muller et al., 2014, Ronchi et al., 2015, Ryan et al., 2019, Shen et al., 2017, Zhang et al., 2015, Zhou et al., 2017a), CHCHD2 has been found to cause primarily PD when mutated (Foo et al., 2015, Funayama et al., 2015, Ikeda et al., 2017, Imai et al., 2019b, Jansen et al., 2015, Koschmidder et al., 2016, Lee et al., 2018, Li et al., 2016, Nicoletti et al., 2018, Ogaki et al., 2015, Shi et al., 2016, Wu et al., 2016).

1.1 CHCHD10 is a mitochondrial protein linked predominantly to ALS-FTD

Amyotrophic lateral sclerosis is a neurodegenerative disease affecting motor neurons in the brain and the spinal cord. Only 10% of ALS cases are familial and the majority is inherited in an autosomal dominant fashion, the other 90 % are sporadic and without a known cause (Mathis et al., 2019). To date, mutations in over 20 genes have been discovered to cause ALS, from which solely superoxide dismutase 1 (SOD1) shows partial mitochondrial localization. In 2014, through whole exome sequencing in a French and Spanish family with ALS, frontotemporal dementia-like cognitive decline, and mitochondrial myopathy, the CHCHD10 p.S59L variant identified (Bannwarth et al., 2014, Chaussenot et al., 2014). CHCHD10 was the first ALS-linked protein predicted to be exclusively a mitochondrial protein. Frontotemporal dementia is often linked to ALS; however, it is considered a clinically distinct adult-onset neurodegenerative disease.

Table 1.1 Gene variants of CHCHD10 identified in human neurological disorders. Variant investigated in this thesis is highlighted in red.

Gene variants	Amino acid changes	Human disease	Age of onset	Ethnicity	# of cases	References
c.34C>T	p.Pro12Ser	ALS	58	Spanish	1	(Dols-Icardo et al., 2015)
c.43C>A with c.172G>C	p.Arg15Ser with p.Gly58Arg	ADMM	first decade	Hispanic	15	(Ajroud-Driss et al., 2015, Heiman-Patterson et al., 1997)
c.44C>A	**p.Arg15Leu**	Familial ALS	35-73	German, USA	13	(Johnson et al., 2014, Muller et al., 2014)
		Sporadic ALS	**54**	**Caucasian**	**1**	(Zhang et al., 2015)
c.64C>T	p.His22Tyr	Sporadic FTD	54	Chinese	1	(Jiao et al., 2016)
c.67C>A	p.Pro23Thr	Familial FTD	50	Italian	1	(Zhang et al., 2015)
c.67C>T	p.Pro23Ser	Sporadic FTD	66	Chinese	1	(Jiao et al., 2016)
c.68C>T	p.Pro23Leu	Sporadic FTD	52	Chinese	1	(Jiao et al., 2016)
c.71G>A	p.Pro24Leu	FTD	?	Chinese	1	(Che et al., 2017)
c.89C>T	p.Ser30Leu	Sporadic PD	42	Chinese	1	(Zhou et al., 2017b)
c.95C>A	p.Ala32Asp	Sporadic FTD	76	Chinese	1	(Jiao et al., 2016)
c.100C>T	p.Pro34Ser	ALS/FTD	59-67	French	2	(Chaussenot et al., 2014)
		Sporadic ALS	44-75	Italian	4	(Chio et al., 2015, Ronchi et al., 2015)
		PD	?	Caucasian	1	(Zhang et al., 2015)
		Alzheimer's disease	?	Caucasian	2	(Zhang et al., 2015)
		FTD, ALS		Belgian	17	(Perrone et al., 2017)
c.104C>A	p.Ala35Asp	Sporadic FTD	51	Italian	1	(Zhang et al., 2015)
		Sporadic late onset AD	86	Chinese	1	(Xiao et al., 2017)
c.170T>A	p.Val57Glu	Sporadic FTD	60	Chinese	1	(Jiao et al., 2016)
c.176C>T	p.Ser59Leu	ALS/FTD, Cerebellar sign, Parkinsonism	49-67	French	9	(Bannwarth et al., 2014, Chaussenot et al., 2014)
		FTD and FTD-ALS	57	Spanish	1	(Chaussenot et al., 2014)
c.197G>T	p.Gly66Val	Familial ALS	35-73	Finnish	1	(Muller et al., 2014)
		SMAJ	14-72	Caucasian	55	(Penttila et al., 2015)
		CMT2	30-55	European	12	(Auranen et al., 2015)
?	p.Gly66Ser	ALS	?	?	1	(Lehmer et al., 2018)
c.239C>T	p.Pro80Leu	Sporadic ALS	25-59	Italian	3	(Ronchi et al., 2015)
		Familial ALS	43	Caucasian	1	(Zhang et al., 2015)
c.244C>T	p.Glu82X	FTD	58	Spanish	1	(Dols-Icardo et al., 2015)
c.275A>G	p.Tyr92Cys	Sporadic ALS	54±12	Chinese	1	(Zhou et al., 2017a)
c.306G>C	p.Gln102His	Sporadic ALS	54±12	Chinese	1	(Zhou et al., 2017a)
c.322C>T	p.Gln108Pro/Gln 108X	FTD, PD	48	Belgian	1	(Perrone et al., 2017)
?	p.Cys122Arg	ALS	?	?	1	(Lehmer et al., 2018)
?	p.Glu127Lys	ALS	?	?	1	(Lehmer et al., 2018)

PD = Parkinson's disease; AD = Alzheimer's disease; FTD = frontotemporal dementia; ALS = amyotrophic lateral sclerosis; SMAJ = spinal motor neuropathy Jokela type; CMT2 = Charcot Marie Tooth neuropathy type 2; ADMM = autosomal dominant mitochondrial myopathy

Subsequently, other cohorts were screened for CHCHD10 mutations and were found (Table 1.1) to be a cause for sporadic and familial ALS often associated with FTD (Chio et al., 2015, Dols-Icardo et al., 2015, Johnson et al., 2014, Kurzwelly et al., 2015, Muller et al., 2014, Ronchi et al., 2015, Ryan et al., 2019, Shen et al., 2017, Zhang et al., 2015, Zhou et al., 2017a), spinal muscular atrophy Jokela type (SMAJ) and Charcot-Marie Tooth type 2 (CMT2) (Auranen et al., 2015, Pasanen et al., 2016, Penttila et al., 2015), mitochondrial myopathy (MM) (Ajroud-Driss et al., 2015, Rubino et al., 2018), Alzheimer's disease (AD) (Xiao et al., 2017) and PD (Rubino et al., 2017, Zhou et al., 2017b). All CHCHD10 variants are inherited in an autosomal dominant fashion. For our study we received patient fibroblasts from a patient with sporadic ALS, with typical ALS-like symptoms and severe loss of lower motor neurons (Julia L. Keith, 2020, Zhang et al., 2015), carrying p.R15L variant (highlighted in red in Table 1.1). The variant has been also described in two families with familial ALS and one independent patient with sporadic ALS that was not been associated with FTD or other symptoms (Johnson et al., 2014, Muller et al., 2014, Zhang et al., 2015).

1.2 CHCHD2 is a mitochondrial protein linked to PD

At approximately the same time, autosomal dominant mutations in CHCHD2 (a paralogue of CHCHD10), were reported as a rare cause of familial PD (Foo et al., 2015, Funayama et al., 2015, Ikeda et al., 2017, Jansen et al., 2015, Koschmidder et al., 2016, Lee et al., 2018, Li et al., 2016, Nicoletti et al., 2018, Ogaki et al., 2015, Shi et al., 2016, Wu et al., 2016) (Table 1.2). PD-associated CHCHD2 variants seem to be ethnic-specific, as variants found in Asian patients are not found in Caucasians and vice versa (Jansen et al., 2015, Puschmann et al., 2015, Zhang et al., 2016). In contrast to ALS, Parkinson's Disease affects dopaminergic neurons in the substantia nigra pars compacta. Two mutations in particular are considered to be most pathogenic as they were found in large families. Funayama et al. discovered a *CHCHD2* missense mutation (c.182C>T, p.Thr61Ile) in a family with dominantly inherited late-onset PD (8 cases). Further screening revealed another patient with the same mutation and two potential splice site mutation in two additional families (c.424G>A, p.Arg145Gln; in intron: c.300+5G>A) (Funayama et al., 2015). The CHCHD2 p.T61I variant was discovered in an additional family with autosomal dominant PD (Shi et al., 2016).

Table 1.2 Gene variants of CHCHD2 identified in human neurological disorders. Most pathogenic variants are highlighted in bold.

Gene variants	Amino acid changes	Human disease	Age of onset	Ethnicity	# of cases	References
c.5C>T	p.Pro2Leu	SPD	?	Japanese	?	(Funayama et al., 2015)
		PD	61	Chinese	5	(Foo et al., 2015)
		SPD	?	Chinese	?	(Shi et al., 2016)
		AD, SD	65.6	Chinese	3	(Che et al., 2018)
c.10G>A	p.Gly4Arg	LBD	69	Caucasian	1	(Ogaki et al., 2015)
c.15C>G	p.Ser5Arg	AD	75	Chinese	1	(Che et al., 2018)
c.23G>H	p.Arg8His	SPD	38	Japanese	1	(Ikeda et al., 2017)
c.40C>T	p.Pro14Ser	PD	71	Caucasian	1	(Ogaki et al., 2015)
c.48C>T	p.Ala16Ala	PD	60	Caucasian	1	(Ogaki et al., 2015)
c.53G>A	p.Arg18Gln	SPD	65	Chinese	1	(Yang et al., 2016)
c.94G>A	p.Ala32Thr	AD	70	Chinese	1	(Che et al., 2018)
		PD	20-51	Caucasian	1	(Jansen et al., 2015)
c.101C>T	p.Pro34Leu	PD	20-51	Caucasian	1	(Jansen et al., 2015)
		LBD	90	Caucasian	1	(Ogaki et al., 2015)
		PD	70	Caucasian	1	(Ogaki et al., 2015)
c.110C>T	p.Ala37Val	LBD	?	Caucasian	1	(Ogaki et al., 2015)
c.146C>T	p.Ala49Val	PD	76	Caucasian	1	(Ogaki et al., 2015)
c.182C>T	**p.Thr61Ile**	PD	55.5	Japanese	**8**	(Funayama et al., 2015)
		PD	48	Chinese	**7**	(Shi et al., 2016)
c.196G>A	p.Val66Met	MSA	60	Italian	1	(Nicoletti et al., 2018)
c.211G>C	p.Ala71Pro and TOPIMT mut.	Early onset PD	26	Caucasian	1	(Lee et al., 2018)
c.238A>G	p.Ile80Val	FPD	?	Caucasian	1	(Jansen et al., 2015)
c.255T>A	p.Ser85Arg	FTD	65	Chinese	1	(Che et al., 2018)
c.278C>T	p.Ala93Val	LBD	85	Caucasian	1	(Ogaki et al., 2015)
c.376C>T	p.Gln126X	PD	>40	German	1	(Koschmidder et al., 2016)
c.434G>A	**p.Arg145Gln**	FPD	?	Japanese	**3**	(Funayama et al., 2015)
		PD	41	Chinese	**1**	(Yang et al., 2016)
c.-9T>G	Intron	FPD	?	Japanese	1	(Funayama et al., 2015)
c.300+5G>A	Intron	FPD	?	Japanese	2	(Funayama et al., 2015)

PD = Parkinson's disease; FPD = familial PD; SPD = sporadic PD; AD = Alzheimer's disease; FTD = frontotemporal dementia; SD = semantic dementia: LBD = Lewy Body disease; MSA = multiple systems atrophy;

1.3 Localization and structure of CHCHD10 and CHCHD2

CHCHD10 and CHCHD2 contain a predicted mitochondrial targeting sequence (MTS), a hydrophobic stretch between amino acids 50-80 and the CHCH-domain which forms a helix-turn-helix fold, stabilized through two disulfide bonds formed by four cysteines (Fig. 1.1).

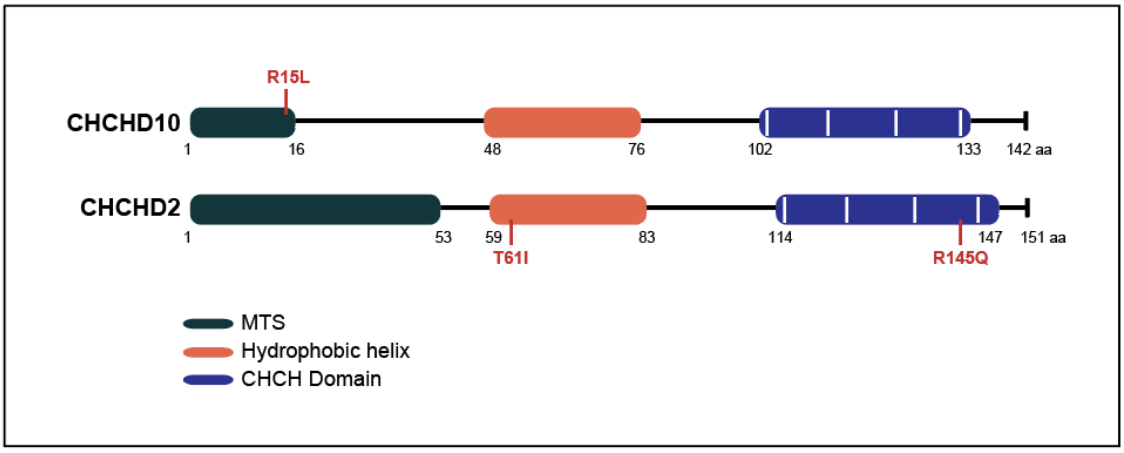

Figure 1.1 Schematic representation of the CHCHD10 and CHCHD2 protein structure.

Predicted structural and functional domains are indicated in different colours. In this study addressed reported mutations associated with ALS and PD are indicated in red. Four cysteines in the coiled-helix coiled-helix domain (CHCH) are indicated with white bars.

Human CHCHD10 and CHCHD2 share a 51% sequence identity at the amino acid level and in particular the hydrophobic helix as well as the CHCH domain share high similarities (Fig. 1.2). Mic17 the orthologue of CHCHD10 and CHCHD2 in yeast was first reported to localize to the nucleus and the cytosol (Huh et al., 2003); however, it was later clearly assigned to the mitochondrial intermembrane space (Gabriel et al., 2007).

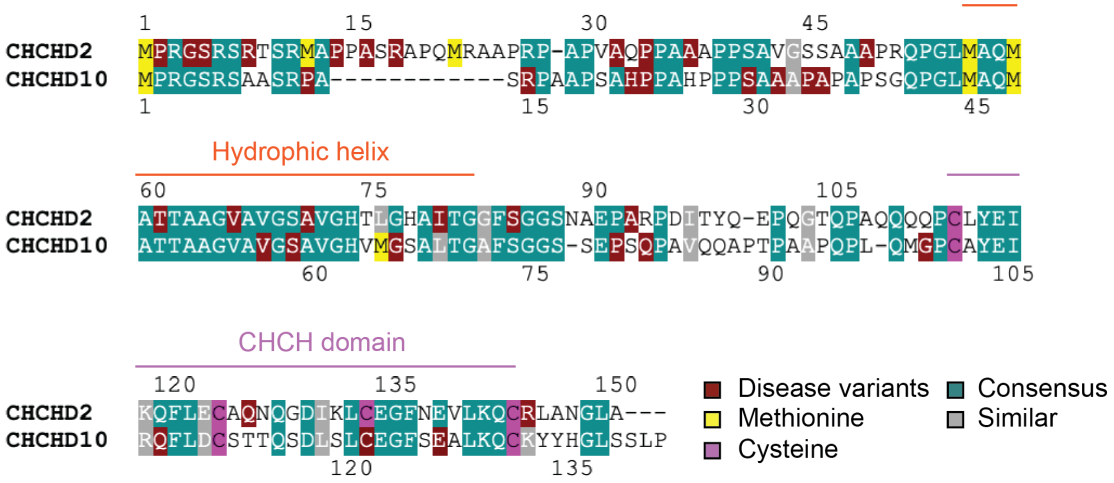

Figure 1.2 Alignment of human CHCHD10 and CHCHD2.

Hydrophobic helix, CHCH-domain, potential disease variants, alternative transcription start sites (methionine), disulfide-bond forming cysteines are highlighted in different colors.

The CHCH-domain and not the MTS was demonstrated to be responsible for targeting CHCHD10 and CHCHD2 to mitochondria and in particular the intermembrane space (Burstein et al., 2018, Lehmer et al., 2018). CHCHD10 and CHCHD2 are classical substrates of the mitochondrial disulfide-relay system Mia40-ALR (mitochondrial intermembrane space import and assembly protein 40-augmenter of liver regeneration) (Longen et al., 2009). Upon import, the four cysteine residues (which form a so called twin CX_9C motif) are oxidized by Mia40, trapping these proteins in the intermembrane space. Due to their amino acid change, three pathogenic variants, CHCHD10 p.Q108P, CHCHD10 p.C122R and CHCHD2 p.Q126X, localized outside of mitochondria (Lehmer et al., 2018, Zhou et al., 2019). Other CX_9C motif-containing proteins of the mitochondrial intermembrane space are involved in various processes and are listed in Table 1.3. The majority are crucial for the biogenesis of enzyme complexes of the respiratory chain, for example COX17, COX19 and CHCHD7 for complex IV assembly (Longen et al., 2009). Due to the lack of any additional structural domain, it is likely that the CHCH-domain determines the overall structure of these proteins. The crystal structure of COX17 showed two helices harbouring two cysteines each and binding one copper atom (Abajian et al., 2004). Furthermore, the structures of CHCHD5, CHCHD7 and CHCHD4 have been identified and by knowing the structure of other CX_9C motif containing proteins, structures of CHCHD10 and CHCHD2 were extrapolated and are predicted to be similar (Banci et al., 2009, Banci et al., 2012, Imai et al., 2019b).

In total three studies found evidence for the existence of CHCHD10 and CHCHD2 outside of mitochondria (Aras et al., 2015, Liu et al., 2015, Woo et al., 2017). In one study endogenous and exogenous FLAG-tagged CHCHD10 protein was found to co-immunoprecipitate with endogenous and exogenous TDP43 protein, a predominantly nuclear protein (Woo et al., 2017). In another study CHCHD2 was found to interact with Bcl-xL, a mitochondrial outer membrane protein involved in cell death (Liu et al., 2015). And lastly, CHCHD2 and CHCHD10 have been described to localize to the nucleus in hypoxic conditions, where they can act as transcription factors of genes harbouring the oxygen responsive element (ORE) (Purandare et al., 2018).

Table 1.3 Eukaryotic CX_9C motif containing proteins. Modified table from (Cavallaro, 2010).

Human Gene	Yeast Gene	Function
COX6B1	COX12	COX subunit
COX6B2	YMR244C-A	COX subunit
COA6	/	COX subunit
COX17	COX17	Copper assembly chaperone for COX
COX19	COX19	COX assembly
CHCHD7	COX23	COX assembly
CMC1	CMC1	COX assembly
COA5	PET191	COX assembly
CMC2	CMC2	COX assembly
COA4 (CHCHD8)	CMC3	COX assembly
CHCHD4 (MIA40)	MIA40	IMS protein import
TRIAP1	MDM35	Mitochondrial apoptosis Lipid handling
C22orf39	EMI1	Mitochondrial structure/function
CHCHD3 (MIC19)	MIC19	MICOS
CHCHD6	MIC25	MICOS
CHCHD2	MIC17	Mitochondrial respiration
CHCHD10	MIC17	Mitochondrial respiration
CHCHD5	MIC14	Unknown
CMC4	CMC4	Unknown
NDUFAF8	/	Complex I assembly
NDUFB7	/	Complex I assembly
NDUFA8	/	Complex I assembly
CHCHD1	MRP10	Translation in cytosol and mitochondria; Component of the mitoribosome

1.4 Tissue expression and evolutionary conservation of CHCHD10 and CHCHD2

mRNA expression of *CHCHD10* and *CHCHD2* is enriched in skeletal muscle, one of the organs ultimately affected in ALS and PD. The CHCHD10 protein is enriched in heart and skeletal muscle whereas the CHCHD2 protein shows no tissue specificity and is expressed in many different tissues (Thul et al., 2017) (www.proteinatlas.org). One recent study which found CHCHD10 expression to be particularly high at the post synapse of neuromuscular junctions (NMJ) in skeletal muscle, showed that the protein is required for agrin-induced clustering of acetylcholine receptors, a process important for the proper development of the NMJ (Xiao et al., 2019).

Immunohistochemical analysis revealed the enrichment of CHCHD2 and CHCHD10 in dopaminergic neurons of the substantia nigra, pyramidal neurons of the cortex and the hippocampus, and motor neurons in the anterior horn of the spinal cord (Burstein et al., 2018, Huang et al., 2018).

CHCHD10 and CHCHD2 are evolutionary conserved proteins and are the result of a gene duplication event in metazoans. *Saccharomyces cerevisiae* has only one homologous gene, Mic17, whereas nine genes and pseudogenes are present in mouse (Cavallaro, 2010). Gene duplications occurred independently in different organisms; however, it predated speciation between *M. musculus* and *H. sapiens* (Cavallaro, 2010). *D. melanogaster* harbors three genes, *DmeI/CG5010*, *DmeI/CG31007* and *DmeI/CG31008*, whereas *DmeI/G5010* is the one with the highest similarity to human *CHCHD10* or *CHCHD2*.

1.5 Functional studies on CHCHD10 and CHCHD2

The first functional studies were conducted on the orthologue of *CHCHD10* and *CHCHD2*, *Mic17* in yeast (Cavallaro, 2010, Gabriel et al., 2007, Longen et al., 2009). The loss of Mic17 resulted in a respiratory deficiency with lower oxygen consumption and did not affect mitochondrial structure (Longen et al., 2009). After that one of the first studies on CHCHD10 function associated the protein with the mitochondrial contact site and cristae organizing system (MICOS) in mouse brain (Genin et al., 2015). The MICOS complex consists of several components including, mitofilin/Mic60/IMMT, CHCHD3/Mic19 and CHCHD6/Mic25 (Kozjak-Pavlovic, 2017) and the genetic ablation of one of these results in cristae defects. The MICOS complex is required for the formation of cristae and is evolutionary highly conserved (Huynen et al., 2016, Munoz-Gomez et al., 2015). Furthermore, cristae formation is indispensable for the proper functioning of the mitochondrial respiratory chain and ATP production in mitochondria. One of the first studies addressing CHCHD10 function found the protein to directly co-immunoprecipitate with IMMT and CHCHD3 as well as a co-localize with CHCHD6 (Genin et al., 2015). Additionally, one other study showed the co-localization of MICOS and CHCHD10 and CHCHD2 by super resolution (Zhou et al., 2019). The first group also identified that cristae are not affected the same way for different CHCHD10 variants. The CHCHD10 p.S59L variant showed abnormal mitochondrial cristae whereas the CHCHD10 p.G66V did not cause any cristae abnormalities (Bannwarth et al., 2014, Genin et al., 2018). Various models reported

abnormal mitochondrial cristae structure for CHCHD10 variants and the knockout of CHCHD10/CHCHD2 in flies (Ajroud-Driss et al., 2015, Genin et al., 2015, Meng et al., 2017). With these findings, CHCHD10 and CHCHD2 were proposed to be structural components of the MICOS complex. Other studies however could not confirm the interaction and propose a role of CHCHD10 and CHCHD2 independent of MICOS (Burstein et al., 2018, Huang et al., 2018).

Another aspect of mitochondrial health is mitochondrial morphology, which is coordinated by specialized proteins orchestrating mitochondrial fission and fusion processes (Tilokani et al., 2018). It was found that different CHCHD10 and CHCHD2 variants affect mitochondrial morphology and might even be directly linked to the function of proteins involved in the fission and fusion machinery (Liu et al., 2020, Liu et al., 2019). The overexpression of different CHCHD10 variants including p.R15L, p.G58R, p.S59L, p.G66V and p.E127K, lead to mitochondrial fragmentation (Ajroud-Driss et al., 2015, Huang et al., 2018, Lehmer et al., 2018, Liu et al., 2019, Woo et al., 2017). Also, various patient cells harbouring different variants like for example CHCHD10 p.S59L, CHCHD2 p.A71P showed fragmented mitochondria (Bannwarth et al., 2014, Lee et al., 2018). The CHCHD10 p.G66V variant did not change mitochondrial morphology in patient cells (Genin et al., 2018).

As mentioned above CHCHD10 has been shown to interact with TDP43 and partially localize to the nucleus (Woo et al., 2017). In the same study CHCHD10 variants were suggested to be responsible for the mis-localization of TDP43 outside the nucleus and in mitochondria, although the latter could not be replicated in another study (Brockmann et al., 2018).

CHCHD2 has been identified as a regulator of oxidative phosphorylation (Baughman et al., 2009). Several studies characterized the knockdown of CHCHD2 in different cellular models and discovered reduced mitochondrial oxygen consumption (Baughman et al., 2009, Zhou et al., 2019). CHCHD2 protein levels have been reported to increase in response to different cellular stress signals, like hypoxia, dissipation of the mitochondrial membrane potential, DNA replication stress and CHCHD2 was suggested to have dual localization within the cell (Aras et al., 2015, Aras et al., 2013, Huang et al., 2018, Quiros et al., 2017, Tkach et al., 2012). During hypoxic stress most of CHCHD2 was located in the nucleus where it bound to the promoter of COX4I2 subunit therefore regulating its expression (Aras et al., 2015, Aras et al., 2013). Furthermore, mitochondrial CHCHD2 was found to decrease upon apoptotic stimuli and translocate to the nucleus (Liu et al., 2015). The same study identified an interaction of

CHCHD2 with Bcl-xL, which inhibits BAX oligomerization, thus negatively regulating mitochondria-mediated apoptosis (Liu et al., 2015). The increase of CHCHD2 levels was also observed by stress induced by truncated mitochondrial matrix protein ornithine transcarbamylase causing the mitochondrial unfolded protein response and the overexpression of the mitochondrial DNA polymerase γ subunits causing genomic stress in *Drosophila,* as well as the dissipation of the mitochondrial membrane potential with FCCP (Huang et al., 2018, Meng et al., 2017). Lastly, using a chemical crosslinker, a study detected an interaction of CHCHD2 with cytochrome *c* and MICS1, a mitochondrial protein described as cytochrome *c* binding as well as cristae structure organizing (Oka et al., 2008).

1.6 Animal models of CHCHD10 and CHCHD2 knockout and variants

One of the first animal models used was *Caenorhabditis elegans,* where the orthologue of *CHCHD10* and *CHCHD2, har-1* (41 % sequence identity to human CHCHD10) was studied (Woo et al., 2017). The loss of *har-1* and the introduction of the two conserved CHCHD10 variants p.R15L and p.S59L exhibited mitochondrial dysfunction as well as locomotor dysfunction (Woo et al., 2017).

To date there are four drosophila models in which CHCHD10 and CHCHD2 variants have been investigated. Three studies analyzed the gene orthologue with the highest similarity to human CHCHD10 and CHCHD2 in *Drosophila*, *DmeI\CG5010* (Baek et al., 2019, Liu et al., 2020, Meng et al., 2017), whereas one model overexpressed the human CHCHD2 wild-type and the variants p.P2L, p.T61I and p.R145Q (Tio et al., 2017). Overexpression of the variants produced PD-related phenotypes such as locomotor and mitochondrial dysfunction: however, the two variants p.T61I and p.R145Q showed more severe impairments than the others (Tio et al., 2017). Interestingly, the overexpression of wild-type CHCHD2 also caused a pathogenic phenotype (Tio et al., 2017). The CHCHD2 p.T61I variant as well as the knockout has also been associated with α-synuclein aggregation, a common phenotype of PD (Ikeda et al., 2019). The knockout of CHCHD2 initiated dopaminergic neuron loss, and mitochondrial abnormalities which could be rescued by the enhancement of the mitochondrial proton-motif force and mitochondrial membrane potential with a light-driven proton transporter (Imai et al., 2019a, Meng et al., 2017). And lastly, The CHCHD10 p.S59L variant caused a gain-of-function toxicity and mitochondria defects in *Drosophil*a (Baek et al., 2019).

A morpholino based knock-down of CHCHD10 in zebrafish (66% identity to human protein) caused a motor neuron pathology with reduced axon length and disturbed organization of skeletal muscle (Burstein et al., 2018). In the same study analysis of CHCHD10 p.R15L and p.G66V in patient cells showed reduced CHCHD10 protein levels and suggested a haploinsufficient mode of action for these variants.

Mouse knockout models of CHCHD10 and CHCHD2 did not show mitochondrial abnormalities and the mice appear phenotypically normal (Burstein et al., 2018, Meng et al., 2017), which could be caused by a compensatory effect. This suggestion is also supported by a recent report of a CHCHD10/CHCHD2 double knockout in mice, where mice presented with a cardiomyopathy, disrupted cristae and the activation of the integrated stress response (Liu et al., 2019). More recently three studies reported mitochondrial myopathy, cardiomyopathy and an activation of the integrated stress response for the knock-in mouse models of CHCHD10 p.S55L (human: CHCHD10 p.S59L) (Anderson et al., 2019b, Genin et al., 2019, Liu et al., 2019). To date, CHCHD10 p.S59L appears to be the only toxic gain of function variant for CHCHD10. CHCHD10 p.S59L causes CHCHD10 and CHCHD2 to aggregate in mitochondria, as well as extra nuclear TDP43 aggregates (Anderson et al., 2019b, Genin et al., 2019).

In summary, the findings show involvement of CHCHD10 and CHCHD2 in different mitochondrial and non-mitochondrial processes. Whether, these proteins are playing a role in cristae formation and are a component of MICOS, mitochondrial respiration, apoptosis, TDP43 pathology or nuclear transcription however needs to be confirmed and studied in more detail. From this perspective, we created the following rationale for this thesis.

1.7 Hypothesis and objectives of this thesis

This thesis tried to elucidate the function of CHCHD10 and CHCHD2 in mitochondria and explain the pathogenesis of the variants, CHCHD10 p.R15L, CHCHD2 p.T61I, and CHCHD2 p.R145Q using human fibroblasts as a model system.

Hypothesis #1: The CHCHD10 p.R15L variant in a patient with sporadic ALS is causing mitochondrial dysfunction and underlying the disease pathology.

Objectives:

- Characterization of mitochondrial function in patient fibroblasts
- Comparison of patient fibroblasts with cells were CHCHD10 wild-type protein was reintroduced with a retroviral vector
- Creation of a CRISPR-Cas9 CHCHD10 knock-out model in fibroblasts and the analysis of the functional consequences
- Analysis of CHCHD10 interaction partners

Hypothesis #2: The CHCHD10 p.R15L variant influences metabolic processes in normal physiological conditions as well and in particular under nutrient stress.

Objectives:

- Collection of transcriptomic (RNA sequencing), metabolomic (LC/MS) and proteomic (TMT/MS) datasets from patient and rescued cells
- Analysis of affected metabolomic pathways and integration of the datasets
- Functional analysis of findings with biochemical methods

Hypothesis #3: The CHCHD2 p.T61I and p.R145Q variants and the CHCHD2 knockout influence various mitochondrial functions and this is the cause of PD in patients with these variants.

Objectives:

- Generation of CRISPR-Cas9 CHCHD2 knock-out cells and analysis of functional consequences
- Generation of CHCHD2 variant cell lines and analysis of functional consequences
- Analysis of interaction partners of CHCHD2 variants

Preface to chapter 2

The first study, described in chapter 2 addresses changes of mitochondrial function of fibroblasts from an ALS patient harbouring the heterozygous CHCHD10 p.R15L variant. Different mitochondrial aspects, such as mitochondrial morphology, cristae structure, respiratory chain function and steady state levels as well as interaction partners of CHCHD10 were studied to characterize mitochondrial defects resulting from this variant.

Chapter 2

CHAPTER 2

Loss of CHCHD10-CHCHD2 complexes required for respiration underlies the pathogenicity of a *CHCHD10* mutation in ALS

Isabella R. Straub[1,2], Alexander Janer[1,2], Woranontee Weraarpachai[1,3], Lorne Zinman[4], Janice Robertson[5], Ekaterina Rogaeva[5], Eric A. Shoubridge[1,2,*]

Affiliations:

[1]Department of Human Genetics, McGill University, Montreal, Quebec, Canada

[2]Montreal Neurological Institute, McGill University, Montreal, Quebec, Canada

[3]Department of Biochemistry, Faculty of Medicine, Chiang Mai University, Chiang Mai, Thailand

[4]Sunnybrook Health Sciences Centre, Toronto, Ontario, Canada

[5]Tanz Centre for Research in Neurodegenerative Diseases, University of Toronto, Toronto, Ontario, Canada.

*To whom correspondence should be addressed at: Eric A. Shoubridge, Montreal Neurological Institute, 3801 University Street, Montreal, Quebec, Canada H3A 2B4; Email: eric@ericpc.mni.mcgill.ca, Tel: 514-398-1997; FAX: 514-398-1509

Published in

Hum Mol Genet. **2018**;27(1):178–189. doi:10.1093/hmg/ddx393.

Abstract

CHCHD10 and its paralogue CHCHD2 belong to a family of twin CX_9C motif proteins, most of which localize to the intermembrane space of mitochondria. Dominant mutations in *CHCHD10* cause amyotrophic lateral sclerosis/frontotemporal dementia (ALS/FTD), and mutations in *CHCHD2* have been associated with Parkinson's disease, but the function of these proteins remains unknown. Here we show that the p.R15L CHCHD10 variant in ALS patient fibroblasts destabilizes the protein, leading to a defect in the assembly of complex I, impaired cellular respiration, mitochondrial hyperfusion, an increase in the steady-state level of CHCHD2, and a severe proliferation defect on galactose, a substrate that forces cells to synthesize virtually all of their ATP aerobically. CHCHD10 and CHCHD2 appeared together in distinct foci by immunofluorescence analysis and could be quantitatively immunoprecipitated with antibodies against either protein. BN-PAGE analyses showed that both proteins migrated in a high molecular weight complex (220 kDa) in control cells, which was however absent in patient cells. CHCHD10 and CHCHD2 levels increased markedly in control cells in galactose medium, a response that was dampened in patient cells, and a new complex (40 kDa) appeared in both control and patient cells cultured in galactose. Re-entry of patient cells into the cell cycle, which occurred after prolonged culture in galactose, was associated with a marked increase in complex I, and restoration of the oxygen consumption defect. Our results indicate that CHCHD10-CHCHD2 complexes are necessary for efficient mitochondrial respiration, and support a role for mitochondrial dysfunction in some patients with ALS.

Introduction

Amyotrophic lateral sclerosis (ALS) is the most common motor neuron disease and it is frequently associated with frontotemporal dementia (FTD). Mitochondrial dysfunction has often been suggested to underlie ALS pathology, but mutations in *bona fide* mitochondrial genes have rarely been reported in ALS cohorts. Recent reports of mutations in *CHCHD10* (coiled-helix coiled-helix domain containing protein 10) in autosomal dominant familial ALS have changed this outlook. *CHCHD10* mutations were first uncovered by whole exome sequencing in a family with motor neuron disease, ALS- and FTD-like symptoms, cerebellar ataxia and myopathy (Bannwarth et al., 2014). Subsequent investigations uncovered autosomal dominant mutations in *CHCHD10* in a clinically heterogeneous group of patients, ranging from sporadic and familial ALS (Chio et al., 2015, Dols-Icardo et al., 2015, Johnson et al., 2014, Muller et al., 2014, Ronchi et al., 2015, Zhang et al., 2015), sporadic and familial FTD (Dols-Icardo et al., 2015, Jiao et al., 2016), autosomal dominant mitochondrial myopathy (ADMM) (Ajroud-Driss et al., 2015), spinal muscular atrophy (SMAJ) (Penttila et al., 2012), Charcot-Marie-Tooth neuropathy (CMT2) (Auranen et al., 2015), Alzheimer's disease (AD) (Zhang et al., 2015), and even Parkinson's disease (PD) (Bannwarth et al., 2014, Ikeda et al., 2017, Zhang et al., 2015). Almost all of the reported mutations are missense substitutions in exon 2, with the exception of a stop-gain mutation (p.Q82X) suggesting a loss-of-function mechanism (Dols-Icardo *et al,* 2015.).

CHCHD10 is a member of the twin CX_9C motif family of proteins, most of which localize to the mitochondrial intermembrane space (IMS). The CHCH domain forms a helix-turn-helix fold, stabilized by two disulphide bonds, which are formed upon import of these proteins into the IMS by the redox-regulated MIA40 pathway (Becker et al., 2012). CHCHD2, a paralogue of CHCHD10, arose by gene duplication from a common ancestor predating human speciation (Cavallaro, 2010), and both proteins are conserved in all metazoans (Longen et al., 2009). The yeast *S. cerevisae*, contains a single orthologue, Mix17 (31% identity with CHCHD10, and 35% identity with CHCHD2) (Pfanner et al., 2014). Recently, a missense mutation in *CHCHD2* (c.182C>T, p.T6I) was shown to segregate with dominantly inherited late-onset PD in a large Japanese family and further screening revealed other PD patients with genetic variants in *CHCHD2* (Zhou et al., 2016). PD-associated CHCHD2 variants appear to be ethnic-specific, as variants found in Asian patients are not found in Caucasians and vice versa (Jansen et al., 2015, Puschmann et al., 2015, Zhang et al., 2016).

While mutations in *CHCHD10* and *CHCHD2* appear to be associated with a fairly wide spectrum of neurodegenerative disorders, the mechanisms of pathogenesis remain unclear. It has been reported that CHCHD10 is enriched at cristae junctions as part of the MICOS (mitochondrial contact site and cristae organizing system) complex (Genin et al., 2015), which is crucial for mitochondrial membrane architecture and cristae organization (Rampelt et al., 2016). Multiple different functions have been suggested for CHCHD2: a regulator of oxidative phosphorylation (Baughman et al., 2009), a transcription factor that regulates the expression of the COX4I2 subunit during stress (Aras et al., 2015, Aras et al., 2013), an inhibitor of Bax oligomerization through its interaction with Bcl-xL (Liu et al., 2015), and finally a protein that sequesters SMAD4 to mitochondria, suppressing the activity of the TGFβ signalling pathway (Zhu et al., 2016).

In this study, we have investigated the function of CHCHD10, and the mechanism of pathogenesis using fibroblasts derived from an ALS patient carrying the pathogenic p.R15L CHCHD10 variant.

Results

Reduced steady-state level of CHCHD10 in patient fibroblasts

All reported mutations in *CHCHD10* are heterozygous, suggesting autosomal dominant inheritance; however, whether this results from dominant negative effects, gain of function, or haploinsufficiency is generally unknown. To begin to address this question we performed an immunoblot analysis on fibroblasts from an ALS patient, heterozygous for the c.44G>T (p.R15L) *CHCHD10* variant. CHCHD10 was reduced to 57% of control levels in patient fibroblasts, whereas the level of its paralogue, CHCHD2, was increased 2.5-fold (Fig. 2.1A). Although both CHCHD10 and CHCHD2 have *in silico* predicted mitochondrial targeting sequences, these do not appear to be processed, as the mature forms of both proteins migrate on reducing gels at their predicted molecular masses (14kDa, 16KDa respectively). Although the p.R15L mutation is contained in the putative targeting sequence, overexpression of the p.R15L variant in control cells showed that it localized to mitochondria without producing an obvious alteration in mitochondrial morphology (Fig. 2.1B). The steady-state level of the *CHCHD10* mRNA in patient fibroblasts was not significantly different from control (data not shown), and DNA sequencing of an RT-PCR product indicated similar contributions from the wild-type and mutant alleles, as would be expected for a heterozygous missense mutation (Fig. S2.1). We conclude that the p.R15L variant targets correctly to mitochondria, but is unstable, leading to a loss of CHCHD10 function

Hyperfusion of mitochondria but normal mitochondrial ultrastructure in patient fibroblasts

Immunofluorescence analysis revealed a striking mitochondrial hyperfusion phenotype in patient cells and in control fibroblasts in which CHCHD10 was depleted by siRNA (Fig. 2.2A, B); however, the steady-state levels of the major molecular components of the mitochondrial fusion machinery (OPA1 and MFN1, MFN2) were not significantly altered in patient or CHCHD10-depleted fibroblasts (Fig. 2.2C). Consistent with the hyperfusion phenotype, overall steady-state levels of Drp1, which is responsible for mitochondrial fission, were reduced, and a larger proportion appeared in the cytosolic fraction compared to control (Fig. 2.2D). Interestingly, depletion of CHCHD2 produced a shift toward short OPA1 isoforms (Fig. 2.2C), which was associated with increased mitochondrial fission (data not shown). Retrovirally-

mediated expression of a wild-type *CHCHD10* cDNA (WT CHCHD10) rescued the mitochondrial hyperfusion in patient fibroblasts (from 65% to 9%). Transmission electron microscopy showed mitochondria with normal cristae organization in patient fibroblasts (Fig. 2.2E).

Oxygen consumption and OXPHOS defect in patient fibroblasts

To determine if the p.R15L variant affected mitochondrial respiratory function, we measured oxygen consumption rates (OCR) using an extracellular flux analyser (Seahorse) in control and patient cells, as well as patient cells overexpressing wild-type CHCHD10. The OCR was measured in four steps: (i) basal OCR (ii) after addition of oligomycin (1 μM) which inhibits ATP synthase, (iii) after uncoupling with cyanide-p-trifluoromethoxyphenylhydrazone (FCCP) (2 μM) and (iv) after addition of a mix of rotenone and antimycin A (0.5 μM), inhibitors of complex I and III, respectively. Basal mitochondrial respiration of patient cell lines was reduced by 46±12% ($p < 0.05$) compared to controls (Fig. 2.3A) and the maximal respiratory capacity in response to uncoupling agent FCCP, was reduced by 55±12% ($p < 0.05$). The extracellular acidification rate (ECAR) was increased about two-fold in patient fibroblasts. This result was phenocopied with a CRISPR-Cas9-mediated CHCHD10 knockout cell line; however, not by the siRNA-mediated depletion of CHCHD10 (Fig. 2.3B, S2.2). Overexpression of CHCHD2 in control fibroblasts did not reduce OCR, arguing against role for increased CHCHD2 expression in disease pathogenesis (Fig. S2.3). Consistent with the rescue of the mitochondrial hyperfusion phenotype, overexpression of wild-type CHCHD10 in patient fibroblasts rescued the respiration defect (Fig. 2.3A, B).

To determine the steady-state levels of the oxidative phosphorylation (OXPHOS) complexes we performed a blue native PAGE (BN-PAGE) analysis. Patient fibroblasts showed about a two-fold reduction in the level of fully assembled complex I (Fig. 2.3C, S2.4), while the levels of the other OXPHOS complexes were not significantly altered. Consistent with this, the steady-state level of a complex I subunit (NDUFA9) was reduced by immunoblot analysis (Fig. 2.1A).

CHCHD10 is required for growth in glucose-free medium

To interrogate mitochondrial respiratory function, we grew cells in medium containing a non-fermentable carbon source (in which glucose is replaced by galactose), forcing them to rely almost entirely on OXPHOS for ATP production. In general, cells with OXPHOS deficiencies grow more slowly than control cells in galactose medium or, if the deficiency is severe, undergo apoptosis. About 20% of the patient fibroblasts died within the first 24 hr in galactose, and while the remaining cells stayed attached to the plate (Fig. 2.4A), they only started dividing after an adaptation period of about two weeks (data not shown). Based on the severity of the complex I assembly defect, this behaviour was unexpected, suggesting that other factors are at play.

To further analyse the effects of galactose medium, we performed an immunofluorescence analysis of CHCHD10 in patient and control cells. CHCHD10 levels steadily increased in control, but not in the patient cells, over the time course of the experiment (Fig. S2.5). Consistent with these results, immunoblot analysis showed that CHCHD10 levels increased after 5 days in galactose medium, and continued to increase up to 15 days in control cells, whereas patient cells showed only a slight increase in CHCHD10 levels by day 5, which, however, was not maintained by day 15 (Fig. 2.4B). CHCHD2 levels were increased in both patient and control fibroblasts on day 5 and 15. The changes in the levels of CHCHD10 in control cells were specific and did not reflect the small increase in mitochondrial content; however, there was a ~1.5-fold increase in SDHA in patient cells after 15 days in galactose and strikingly a nearly four-fold increase in NDUFA9, a proxy for complex I assembly (Fig. 2.4B, S2.6A, B).

We next measured the changes in oxygen consumption rates in control and patient cells after 5 and 15 days in galactose medium. As expected, in control cells there was an increase in basal oxygen consumption over that observed in glucose medium, and a partial normalization of oxygen consumption rates in the patient cells after 5 days, which reached control levels after 15 days (Fig. 2.4C, S2.7).

CHCHD10 immunoprecipitates CHCHD2 and C1QBP

To characterize the CHCHD10 interactome we immunoprecipitated the endogenous protein and analysed it by liquid chromatography-tandem mass spectrometry (LC-MS/MS). This analysis identified CHCHD2 and C1QBP (p32), a multifunctional protein involved in

mitochondrial translation (Yagi et al., 2012), as major interactors of CHCHD10. Reciprocal immunoprecipitation of endogenous CHCHD2 also precipitated CHCHD10 and C1QBP (not shown in immunoblot) suggesting a robust interaction between these mitochondrial proteins (Fig. 2.5A).

To further analyse the interdependence between CHCHD10 and CHCHD2 we performed siRNA-mediated depletion of each protein and analysed the levels of its potential partner by immunoblot analysis. Surprisingly, when CHCHD2 was depleted the levels of CHCHD10 decreased, whereas short-term depletion of CHCHD10 did not affect CHCHD2 levels (Fig. 2.5B). Immunofluorescence analysis of CHCHD2 and CHCHD10 using antibodies against the endogenous proteins showed a punctate pattern and a high degree of co-localization, consistent with the immunoprecipitation results (Fig. 2.5C).

CHCHD10 forms high molecular weight complexes with CHCHD2 and is not part of the MICOS complex

To investigate whether CHCHD10 forms stable complexes with CHCHD2 or C1QBP we performed two-dimensional PAGE (2D-PAGE) analysis (Fig. 2.6). In normal glucose-containing medium (Fig. 2.6A, top panel), CHCHD10 and CHCHD2 were present both in low molecular weight complexes (as either monomers (14 kDa and 16 kDa, respectively), or dimers (not possible to distinguish between these possibilities on this gel), and in higher molecular weight complexes (CHCHD10: 170 kDa and 220 kDa, CHCHD2: 220 kDa), whereas C1QBP ran only as a monomer (32 kDa)). As expected, the level of CHCHD10 was reduced in patient mitochondria (Fig. 2.6B, top panel), but strikingly, it was virtually absent in the higher molecular weight complexes. Furthermore, the level of CHCHD2 appeared to compensate for the loss of CHCHD10 in the 170 kDa complex. Neither CHCHD10, nor CHCHD2 co-migrated with IMMT/Mic60 or CHCHD3/Mic19, key components of the MICOS (Mitochondrial contact site and Cristae Organizing System) complex, which itself was unaffected in patient fibroblasts.

To investigate whether these high molecular weight complexes would be influenced by growth in galactose medium we subjected cells grown for 9 days in galactose to 2D-PAGE analysis. CHCHD10 and CHCHD2 levels increased in control cells (Fig. 2.6A, bottom panel), confirming the immunoblot analysis (Fig. 2.4B), and we observed the appearance of additional complexes at 40 and 100 kDa, the appearance of CHCHD2 in the complex at 170 kDa, but no

apparent change in the complex at 220 kDa. Patient fibroblasts (Fig. 2.6B, bottom panel) showed increased CHCHD2 levels in galactose, and a substantial shift into the complex at 40 kDa, but a further decrease in the higher molecular weight complexes containing either CHCHD2 or CHCHD10. These complexes are likely soluble in the IMS as CHCHD10 behaves like a soluble protein after alkaline carbonate extraction (Fig. S2.8).

Discussion

This study shows that two twin CX_9C mitochondrial IMS proteins, CHCHD10 and CHCHD2, both of which have been implicated in neurodegenerative diseases, exist in complexes that support efficient mitochondrial respiration. Fibroblasts from an ALS patient with a mutation in *CHCHD10* displayed a striking mitochondrial hyperfusion phenotype, a deficiency in both basal and maximal respiration, increased anaerobic glycolysis, and a severe growth defect on a non-fermentable carbon source, all strongly suggesting insufficient aerobic energy supply as the underlying disease mechanism.

Three lines of evidence, including immunoprecipitation, immunofluorescence, and 2D-PAGE, place CHCHD10 and CHCHD2 in protein complexes of 40, 100, 170, and 220 kDa depending on culture conditions. In glucose-containing medium about half of the CHCHD10 in control cells was present in the 170 and 220 kDa complexes, which were essentially undetectable in patient fibroblasts. The appearance of the 40 kDa complex, which was only prominent in control and patient cells in galactose medium, correlated with the recovery of the oxygen consumption defect in the patient cells, and the re-entry into a proliferative phase. There appears to be some degree of functional interdependence between the two proteins as reduced levels of CHCHD10 in patient fibroblasts were associated with a marked increase in the levels of CHCHD2, perhaps as a compensatory mechanism, and the siRNA-mediated depletion of CHCHD2 resulted in decreased levels of CHCHD10, suggesting a role for CHCHD2 in CHCHD10 stability. Further, similar increases were observed in the steady-state levels of both proteins in control cells growing in galactose. The immunoprecipitation data suggest that the CHCHD10-CHCHD2 complexes are largely hetero-oligomers. C1QBP (p32), a predominantly mitochondrial matrix protein that behaves as a monomer on second dimension gels, was the only other protein found to co-immunoprecipitate consistently in these experiments. We did not find any evidence for an association of CHCHD2 with cytochrome *c* oxidase, as had been previously reported (Aras et al., 2015). How might the interaction with matrix protein p32 occur? Although it is clear from our data that the majority of CHCHD10 runs on denaturing gels at its predicted (unprocessed) molecular mass, a recent investigation of the N-termini of mitochondrial proteins suggested that murine CHCHD10 is processed at amino acid 80 (full length is 142aa) (Calvo et al., 2017). It is thus possible that some fraction of CHCHD10 engages the TIM machinery and is processed in the matrix; however, this would need to be verified experimentally.

Importantly, our study clearly shows that the CHCHD10-CHCHD2 complex does not associate with MICOS, a multi-subunit complex that determines the architecture of mitochondrial cristae in the inner mitochondrial membrane. Neither CHCHD10 nor CHCHD2 co-immunoprecipitated or co-migrated on second dimension Blue-Native gels with components of the MICOS complex, an observation that contrasts sharply with a recent report (Genin et al., 2015). We previously performed affinity purification/mass spectrometry studies with antibodies directed against the endogenous forms of two *bona fide* MICOS subunits (Mic60, Mic19) and did not recover either CHCHD10 or CHCHD2 in the immunoprecipitates (Janer et al., 2016). Consistent with our results, the MICOS complex was not destabilized in fibroblasts from our patient, and we found no evidence for a mitochondrial ultrastructural abnormality. Significantly, Mix17 the yeast orthologue of CHCHD10 and CHCHD2, does not constitute part of the yeast MICOS complex (Harner et al., 2011).

The oxygen consumption deficiency in patient cells, the growth defect of these cells in galactose medium, and the marked increase (3-4 fold) in CHCHD10 levels in control cells grown in galactose, suggest a key role for CHCHD10 in respiration, particularly under the stress conditions that are induced by forcing mitochondrial oxidative phosphorylation and increasing oxidative stress. In yeast, Mix17 is also required for normal oxygen consumption, and its steady-state level is reported to increase in response to replication stress (Tkach et al., 2012). The level of CHCHD10 in patient cells was largely unresponsive to growth in galactose, despite the fact that these cells still carry one normal allele. However, there was a slow, progressive increase in oxygen consumption in the patient cells that correlated with an increase in mitochondrial volume, an even greater increase in a marker of complex I assembly, and an increase in the level of CHCHD2 - all likely adaptive responses to the low levels of CHCHD10. Whether other metabolic adaptations are also necessary for the recovery of respiration in patient cells remains to be determined.

Loss of CHCHD10 resulted in a hyperfused mitochondrial network, independent of significant changes in the levels of the proteins involved in mitochondrial fusion (MFN1, MFN2, OPA1). Mitochondrial fusion is a common response to nutrient starvation, increased oxidative stress etc. (Aasen et al., 2008). It seems likely that stress induced by the loss of CHCHD10 results in reduced mitochondrial fission, due to the repartitioning of Drp1 in the cell from the mitochondrial surface to the cytosol which we observed in the patient cells.

Overall, our data support a disease mechanism of haploinsufficiency, at least for the CHCHD10 p.R15L variant associated with ALS: (1) the steady-state level of CHCHD10 was reduced in patient fibroblasts, (2) the respiration defect in patient cells (phenocopied in CHCHD10 knockout cells) could be rescued by expression of a wild-type CHCHD10 cDNA, and (3) the defect in mitochondrial morphology was also rescued by expression of a wild-type CHCHD10 cDNA (4) overexpression of the p.R15L variant in control cells did not produce an obvious phenotype. Our results differ from previous findings on the p.S59L variant in which mitochondria appeared fragmented, and mitochondrial cristae disorganized in patient fibroblasts, as well as HeLa cells overexpressing mutant cDNA (Genin et al., 2015), suggesting that some mutations in CHCHD10 could behave as dominant negatives or have a toxic gain of function.

We speculate that the focal expression of CHCHD10-CHCHD2 complexes creates a mitochondrial platform or microenvironment that is necessary for efficient organization and function of the mitochondrial OXPHOS system, which is especially required in times of transient increases in demand for aerobically-produced ATP, a characteristic of neurons and muscle cells. Further studies will be required to determine the precise molecular function of these proteins.

Materials and Methods

Human studies

The research studies on cell lines were approved by the institutional review board of the Montreal Neurological Institute, McGill University.

Cell lines and Media

A primary fibroblast culture was established from a previously published heterozygous carrier of c.44G>T (p.R15L) (patient DNA #8807) diagnosed with sporadic ALS at age 54 (involving his upper limb) who remains alive 14 years later (Zhang et al., 2015). The p.R15L substitution, has been reported in ALS patients in several independent studies (Johnson et al., 2014; Muller et al., 2014; Zhang *et al.*, 2015), including its segregation with disease in large ALS family (Johnson et al., 2014). Control (Montreal Children's Hospital cell repository; Montreal; Canada; MCH58, 64, 65) and patient fibroblasts were immortalized by transduction with retroviral vectors expressing the HPV-16 E7 gene and the catalytic component of human telomerase (htert) as described previously (Lochmuller et al., 1999). Fibroblasts and 143B cells were grown in 4.5 g/L glucose DMEM supplemented with 10% fetal bovine serum (FBS), at 37°C in an atmosphere of 5% CO_2. Cells stably overexpressing *CHCHD10* in patient cells were engineered using retroviral vectors as previously described (Weraarpachai et al., 2009). For carbon source-dependent experiments, cells were grown in DMEM with 10% dialysed FBS supplemented with either 4.5g/L glucose or 4.5g/L galactose.

siRNA transfection

siRNA duplex constructs were used for transient depletion of CHCHD10 (ambion: CHCHD10-1: s53405; CHCHD10-2: s196436; CHCHD10-3: s226550) or CHCHD2 (ambion: CHCHD2-1: s27540; CHCHD2-2: s27541) in control fibroblasts. siRNA duplexes were transiently transfected into cells using Lipofectamine RNAiMAX (Invitrogen), according to the manufacturer's specifications. The transfection was repeated on day 3 and the cells were harvested on day 6 for analysis.

Generation of stable cell lines over-expressing CHCHD10

CHCHD10 was amplified through PCR with Taq-polymerase with 7-deaza GTP/Nucleotide mix (NEB) using cDNA from control fibroblasts as a template, and cloned into pBABE-Puro using Gateway Cloning Technology (Invitrogen). Retroviral constructs were transfected into the Phoenix packaging cell line using the HBS/$Ca_3(PO_4)_2$ method. Control and patient fibroblasts were infected 48 hours later by exposure to virus-containing medium in the presence of 4 μg/ml of polybrene as described previously (Pear et al., 1997).

Generation of CRISPR-Cas9 CHCHD10 knockout cell line

The sgRNA oligomers for CHCHD10 targeting exon 2 were annealed and inserted into plasmid pSpCas9(BB)-2A-Puro (PX459) V2.0 from Addgene (62988) via combined ligation (T7 ligase NEB) and restriction enzyme (BpiI, NEB) reaction.
Sequence for sgRNA targeting exon 2 of CHCHD10:
5'-caccGAAGCCGCAGCGCGGCCTCC-3'
3'- CTTCGGCGTCGCGCCGGAGGcaaa-5'
The plasmid (1.5 μg) was transfected into a fibroblasts cell line with jetPRIME reagent. 24 hours after transfection puromycin was added for 2 days at a concentration of 5μg/μL. Cells were than expanded and single clones were selected and analysed by immunoblot and sequencing for positive CHCHD10 knockout cell lines.

Mitochondrial isolation

Fibroblasts or 143B cells were rinsed twice with phosphate buffered saline (PBS), resuspended in ice-cold 250 mM sucrose/10 mM Tris–HCl (pH 7.4), and homogenized with ten passes of a pre-chilled, zero-clearance homogenizer (Kimble/Kontes). A post-nuclear supernatant was obtained by centrifugation of the samples twice for 10 min at 600 *g*. Mitochondria were pelleted by centrifugation for 10 min at 10,000 *g* and washed once in the same buffer. Protein concentration was determined using the Bradford assay.

Mitochondrial fractionation

Control and patient fibroblasts were rinsed twice in PBS, resuspended in ice-cold 250 mM sucrose/10 mM Tris–HCl (pH 7.4). 10% of the suspension was lysed in 1.5% DDM in

PBS and centrifuged for 15 min at 20,000 *g*, and the supernatant was considered as the total fraction. The rest (90%) of the cells were homogenized in ice-cold 250 mM sucrose/10 mM Tris–HCl (pH 7.4) with ten passes of a pre-chilled, zero-clearance homogenizer (Kimble/Kontes). A post-nuclear supernatant was obtained by centrifugation of the samples three times for 10 min at 600 *g*. Mitochondria were pelleted by centrifugation for 10 min at 10,000 *g*, washed twice in the same buffer, and lysed in 1.5% DDM in PBS. The lysate was considered as crude mitochondrial fraction. The remaining supernatant, was cleared by three further rounds of centrifugation at 10,000 *g* for 10 min. This supernatant was then centrifuged at 100,000 *g* for 1 h. The pellet was washed two times with PBS, lysed in 1.5% DDM in PBS, and considered as light membranes. The supernatant was adjusted to 1.5% DDM and considered as the cytosol fraction. Protein concentration was determined by Bradford assay.

Alkaline carbonate extraction

Mitochondria isolated from control and patient fibroblasts were extracted with 100 mM alkaline carbonate at pH 11.5 as previously described (Weraarpachai et al., 2009), centrifuged at 20,000 g and the pellet and supernatant fractions analysed by SDS–PAGE.

Denaturing, Native and 2D-PAGE

For SDS–PAGE, cells were extracted with 1.5% n-dodecyl-D-maltoside (DDM) in PBS, after which 20 μg of protein was run on denaturing polyacrylamide gels. BN-PAGE was used to separate individual OXPHOS complexes. Isolated mitochondria were solubilized with 1% DDM, and 20 μg of solubilized samples were run in the first dimension on 6-15% or 8–15% polyacrylamide gradient gels as previously described (Leary, 2012). Two-dimensional (2D-BN-PAGE/SDS-PAGE was carried out as detailed previously (Antonicka et al., 2003). The separated proteins were transferred to a nitrocellulose membrane and immunoblot analysis was performed with the indicated antibodies.

Oxygen consumption measurements using the SeaHorse apparatus

Cells were seeded the day before measurement in a 24-well culture plate at 4×10^4 cells/well. Culture media was removed the following day and replaced with XF Assay Media from SeaHorse Bioscience (Billerica, MA) containing 4.5 g/L glucose or galactose and

incubated at 37°C. Oxygen consumption rate (OCR) and the extracellular acidification rate (ECAR) were measured using the SeaHorse XF24 Extracellular Analyzer over a 100-minute time period. The assay consisted of three basal rate measurements followed by sequential injections of oligomycin (1 μM), FCCP (2 μM), and rotenone (0.5 μM) + antimycin (0.5 μM). Three rate measurements were performed after each injection. Error bars represent mean ± SD of four to five independent experiments and the *p*-values were calculated using a *t*-test.

Immunofluorescence analyses

Immunofluorescence analyses were performed by fixation of the cells grown on coverslips with 4% formaldehyde in PBS at room temperature for 20 min, permeabilization in 0.1% Triton X-100 in PBS, blocking with 5% bovine serum albumin (BSA) in PBS, followed by incubation with primary antibodies in 5% BSA in PBS, for 1 hour at RT. The appropriate anti-species secondary antibodies coupled to Alexa fluorochromes (Invitrogen) (1:1,000) were further used for 30 min at RT. Coverslips were mounted onto slides using fluorescence mounting medium (Dako).

Stained cells were imaged using a 60× or a 100× objective lenses (NA1.4) on an Olympus IX81 inverted microscope with appropriate lasers using an Andor/Yokogawa spinning disk system (CSU-X), with a sCMOS camera. Mitochondrial network morphology was classified in a blinded manner as fused, normal reticulum (intermediate), or fragmented. For each condition, 86 cells were analysed. Experiments were done three times independently. Error bars represent mean ± SD and *p*-values were calculated using a *t*-test.

Analysis of mitochondrial ultrastructure by transmission electron microscopy

Cells grown on Nunc™ Lab-Tek™ Chamber Slide System (Thermofisher) were washed in 0.1 M Na cacodylate washing buffer (Electron Microscopy Sciences) and fixed with 2.5% glutaraldehyde (Electron Microscopy Sciences) in 0.1 M Na cacodylate buffer overnight at 4°C. Cells were then washed three times in 0.1 M Na cacodylate washing buffer for a total of 1 hour, incubated in 1% osmium tetroxide (Mecalab) for 1 hour at 4°C, and washed with ddH_2O three times for 10 min. Then, dehydration in a graded series of ethanol/deionized water solutions from 30 to 90% for 8 min each, and 100% twice for 10 min each, was performed. The cells were then

infiltrated with a 1:1 and 3:1 Epon 812 (Mecalab): ethanol mixture, each for 30 min, followed by 100% Epon 812 for 1 hour. Cells were embedded in the culture wells with new 100% Epon 812 and polymerized overnight in an oven at 60°C. Polymerized blocks were trimmed and 100 nm ultrathin sections were cut with an Ultracut E ultramicrotome (Reichert Jung) and transferred onto 200-mesh Cu grids (Electron Microscopy Sciences). Sections were post-stained for 8 min with 4% aqueous uranyl acetate (Electron Microscopy Sciences) and 5 min with Reynold's lead citrate (Fisher Scientific). Samples were imaged with a FEI Tecnai-12 transmission electron microscope (FEI Company) operating at an accelerating voltage of 120 kV equipped with an XR-80C AMT, 8 megapixel CCD camera.

Immunoprecipitation

Mitochondria (200 µg) isolated from 143B cells were pelleted, rinsed once with PBS, and extracted in 200 µL of lysis buffer (10 mM Tris–HCl pH 7.5, 150 mM NaCl, 1% n-dodecyl-D-maltoside (DDM) (Sigma), and complete protease inhibitors (Roche) on ice for 30 min. The extract was centrifuged at 20,000 *g* at 4°C for 20 min, and the supernatant was pre-cleared overnight with non-coated Dynabeads Protein A (Invitrogen) to reduce non-specific protein binding to the beads. Binding of indicated antibodies to Dynabeads Protein A (Invitrogen) was performed overnight. Antibodies were then cross-linked to the beads using 20 mM dimethyl pimelimidate (DMP) (Sigma). The immunoprecipitation reaction was performed overnight at 4°C. Samples were eluted using 0.1 M glycine pH 2.5/0.5% DDM, trichloroacetic acid precipitated, and analysed by mass spectrometry on an Orbitrap (Thermo Scientific) at the Institute de Recherches Cliniques (IRCM) de Montreal. The false discovery rate is < 5% with a Mascot score of 50.

Antibodies

Antibodies directed against the following proteins were used in this study: CHCHD10 (Sigma, HPA003440; Proteintech, 25671-1-AP), CHCHD2 (Sigma, HPA027407; Proteintech, 66302-1-Ig) SDHA (Abcam, ab14715), ATP5A1 (Abcam, ab14748), NDUFA9 (Abcam, ab14713), COX1 (Abcam, ab14705) and COX2 (Abcam, ab110258), COX4 (Abcam, ab110261), IMMT/MIC60 (Proteintech, 10179-1-AP), CHCHD3/MIC19 (Proteintech, 25625-1-AP), TOMM20 (Santa Cruz, sc-11415), Core2 (Abcam, ab14745), Actin (Abcam, ab3280),

cytochrome c (BioSciences, 556432), GRSF1 (Sigma, HPA036984), C1QBP (GC1qR, Abcam, ab24733), anti-HA (Abcam, ab130275), Porin (Calbiochem, 529534), Tubulin (Invitrogen, 32-2500), OPA1 (BD BioSciences, 612606), MFN1 (Cell Signaling, 14739S), MFN2 (Cell Signaling, 11925S).

Cell growth assay

For immortalized fibroblasts, 82,000 cells were seeded in six-well culture dishes at day 0. For the galactose experiments, cells were switched to galactose-containing medium on day 1. After 1, 2, 3, 5 and 7 days of culture, cells were trypsinized, homogenized, and counted using a Bio-Rad TC10 automated cell counter. Experiments were done in independent triplicates. Error bars represent mean ± SD and *p*-values were calculated using a *t*-test.

Statistical analysis

All data are reported as mean ± SD or ±SEM as indicated in the figure legend. Statistical significance was determined using Student's two-tailed, unpaired and paired *t*-tests. *P*-values < 0.05 were considered statistically significant and labelled as follows: $*P < 0.05$, and $**P < 0.01$.

Acknowledgements

We thank Hana Antonicka, Julien Prudent, and Heidi McBride for fruitful discussions and critique of the manuscript, and Philip McGoldrick (ALS Double Play Christopher Chiu Fellow) and Raphael Schneider (Clinical Research Fellowship from ALS Canada) for establishing the patient fibroblast culture. This work was supported by grants from the Canadian Institutes of Health Research, Parkinson Canada, and the Muscular Dystrophy Association (480233) to EAS, and by the James Hunter ALS Initiative (JR, LZ). IS was supported by a scholarship from the DAAD (German Exchange Service).

Conflict of interest statement: The authors report no conflict of interest.

References

Aasen T, Raya A, Barrero MJ, Garreta E, Consiglio A, Gonzalez F, Vassena R, Bilic J, Pekarik V, Tiscornia G, Edel M, Boue S, Belmonte JC (2008) Efficient and rapid generation of induced pluripotent stem cells from human keratinocytes. *Nat Biotechnol* 26: 1276-84

Ajroud-Driss S, Fecto F, Ajroud K, Lalani I, Calvo SE, Mootha VK, Deng HX, Siddique N, Tahmoush AJ, Heiman-Patterson TD, Siddique T (2015) Mutation in the novel nuclear-encoded mitochondrial protein CHCHD10 in a family with autosomal dominant mitochondrial myopathy. *Neurogenetics* 16: 1-9

Antonicka H, Ogilvie I, Taivassalo T, Anitori RP, Haller RG, Vissing J, Kennaway NG, Shoubridge EA (2003) Identification and characterization of a common set of complex I assembly intermediates in mitochondria from patients with complex I deficiency. *J Biol Chem* 278: 43081-8

Aras S, Bai M, Lee I, Springett R, Huttemann M, Grossman LI (2015) MNRR1 (formerly CHCHD2) is a bi-organellar regulator of mitochondrial metabolism. *Mitochondrion* 20: 43-51

Aras S, Pak O, Sommer N, Finley R, Jr., Huttemann M, Weissmann N, Grossman LI (2013) Oxygen-dependent expression of cytochrome c oxidase subunit 4-2 gene expression is mediated by transcription factors RBPJ, CXXC5 and CHCHD2. *Nucleic Acids Res* 41: 2255-66

Auranen M, Ylikallio E, Shcherbii M, Paetau A, Kiuru-Enari S, Toppila JP, Tyynismaa H (2015) CHCHD10 variant p.(Gly66Val) causes axonal Charcot-Marie-Tooth disease. *Neurol Genet* 1: e1

Bannwarth S, Ait-El-Mkadem S, Chaussenot A, Genin EC, Lacas-Gervais S, Fragaki K, Berg-Alonso L, Kageyama Y, Serre V, Moore DG, Verschueren A, Rouzier C, Le Ber I, Auge G, Cochaud C, Lespinasse F, N'Guyen K, de Septenville A, Brice A, Yu-Wai-Man P et al. (2014) A mitochondrial origin for frontotemporal dementia and amyotrophic lateral sclerosis through CHCHD10 involvement. *Brain* 137: 2329-45

Baughman JM, Nilsson R, Gohil VM, Arlow DH, Gauhar Z, Mootha VK (2009) A computational screen for regulators of oxidative phosphorylation implicates SLIRP in mitochondrial RNA homeostasis. *PLoS Genet* 5: e1000590

Becker T, Bottinger L, Pfanner N (2012) Mitochondrial protein import: from transport pathways to an integrated network. *Trends Biochem Sci* 37: 85-91

Calvo SE, Julien O, Clauser KR, Shen H, Kamer KJ, Wells JA, Mootha VK (2017) Comparative Analysis of Mitochondrial N-Termini from Mouse, Human, and Yeast. *Mol Cell Proteomics* 16: 512-523

Cavallaro G (2010) Genome-wide analysis of eukaryotic twin CX9C proteins. *Mol Biosyst* 6: 2459-70

Chio A, Mora G, Sabatelli M, Caponnetto C, Traynor BJ, Johnson JO, Nalls MA, Calvo A, Moglia C, Borghero G, Monsurro MR, La Bella V, Volanti P, Simone I, Salvi F, Logullo FO, Nilo R, Battistini S, Mandrioli J, Tanel R et al. (2015) CHCH10 mutations in an Italian cohort of familial and sporadic amyotrophic lateral sclerosis patients. *Neurobiol Aging* 36: 1767 e3-1767 e6

Dols-Icardo O, Nebot I, Gorostidi A, Ortega-Cubero S, Hernandez I, Rojas-Garcia R, Garcia-Redondo A, Povedano M, Llado A, Alvarez V, Sanchez-Juan P, Pardo J, Jerico I, Vazquez-Costa J, Sevilla T, Cardona F, Indakoechea B, Moreno F, Fernandez-Torron R, Munoz-Llahuna L et al. (2015) Analysis of the CHCHD10 gene in patients with frontotemporal dementia and amyotrophic lateral sclerosis from Spain. *Brain* 138: e400

Genin EC, Plutino M, Bannwarth S, Villa E, Cisneros-Barroso E, Roy M, Ortega-Vila B, Fragaki K, Lespinasse F, Pinero-Martos E, Auge G, Moore D, Burte F, Lacas-Gervais S, Kageyama Y, Itoh K, Yu-Wai-Man P, Sesaki H, Ricci JE, Vives-Bauza C et al. (2015) CHCHD10 mutations promote loss of mitochondrial cristae junctions with impaired mitochondrial genome maintenance and inhibition of apoptosis. *EMBO Mol Med* 8: 58-72

Harner M, Korner C, Walther D, Mokranjac D, Kaesmacher J, Welsch U, Griffith J, Mann M, Reggiori F, Neupert W (2011) The mitochondrial contact site complex, a determinant of mitochondrial architecture. *EMBO J* 30: 4356-70

Ikeda A, Matsushima T, Daida K, Nakajima S, Conedera S, Li Y, Yoshino H, Oyama G, Funayama M, Nishioka K, Hattori N (2017) A novel mutation of CHCHD2 p.R8H in a sporadic case of Parkinson's disease. *Parkinsonism Relat Disord* 34: 66-68

Janer A, Prudent J, Paupe V, Fahiminiya S, Majewski J, Sgarioto N, Des Rosiers C, Forest A, Lin ZY, Gingras AC, Mitchell G, McBride HM, Shoubridge EA (2016) SLC25A46 is required for mitochondrial lipid homeostasis and cristae maintenance and is responsible for Leigh syndrome. *EMBO Mol Med*

Jansen IE, Bras JM, Lesage S, Schulte C, Gibbs JR, Nalls MA, Brice A, Wood NW, Morris H, Hardy JA, Singleton AB, Gasser T, Heutink P, Sharma M, Ipdgc (2015) CHCHD2 and Parkinson's disease. *Lancet Neurol* 14: 678-9

Jiao B, Xiao T, Hou L, Gu X, Zhou Y, Zhou L, Tang B, Xu J, Shen L (2016) High prevalence of CHCHD10 mutation in patients with frontotemporal dementia from China. *Brain : a journal of neurology* 139: e21

Johnson JO, Glynn SM, Gibbs JR, Nalls MA, Sabatelli M, Restagno G, Drory VE, Chio A, Rogaeva E, Traynor BJ (2014) Mutations in the CHCHD10 gene are a common cause of familial amyotrophic lateral sclerosis. *Brain* 137: e311

Leary SC (2012) Blue native polyacrylamide gel electrophoresis: a powerful diagnostic tool for the detection of assembly defects in the enzyme complexes of oxidative phosphorylation. *Methods Mol Biol* 837: 195-206

Liu Y, Clegg HV, Leslie PL, Di J, Tollini LA, He Y, Kim TH, Jin A, Graves LM, Zheng J, Zhang Y (2015) CHCHD2 inhibits apoptosis by interacting with Bcl-x L to regulate Bax activation. *Cell Death Differ* 22: 1035-46

Lochmuller H, Johns T, Shoubridge EA (1999) Expression of the E6 and E7 genes of human papillomavirus (HPV16) extends the life span of human myoblasts. *Exp Cell Res* 248: 186-93.

Longen S, Bien M, Bihlmaier K, Kloeppel C, Kauff F, Hammermeister M, Westermann B, Herrmann JM, Riemer J (2009) Systematic analysis of the twin cx(9)c protein family. *J Mol Biol* 393: 356-68

Muller K, Andersen PM, Hubers A, Marroquin N, Volk AE, Danzer KM, Meitinger T, Ludolph AC, Strom TM, Weishaupt JH (2014) Two novel mutations in conserved codons indicate that CHCHD10 is a gene associated with motor neuron disease. *Brain* 137: e309

Pear WS, Scott ML, Nolan GP (1997) Generation of high-titer, helper-free retroviruses by transient transfection. *Methods Mol Med* 7: 41-57

Penttila S, Jokela M, Hackman P, Maija Saukkonen A, Toivanen J, Udd B (2012) Autosomal dominant late-onset spinal motor neuronopathy is linked to a new locus on chromosome 22q11.2-q13.2. *European journal of human genetics : EJHG* 20: 1193-6

Pfanner N, van der Laan M, Amati P, Capaldi RA, Caudy AA, Chacinska A, Darshi M, Deckers M, Hoppins S, Icho T, Jakobs S, Ji J, Kozjak-Pavlovic V, Meisinger C, Odgren PR, Park SK, Rehling P, Reichert AS, Sheikh MS, Taylor SS et al. (2014) Uniform nomenclature for the mitochondrial contact site and cristae organizing system. *J Cell Biol* 204: 1083-6

Puschmann A, Dickson DW, Englund E, Wszolek ZK, Ross OA (2015) CHCHD2 and Parkinson's disease. *The Lancet Neurology* 14: 679

Rampelt H, Zerbes RM, van der Laan M, Pfanner N (2016) Role of the mitochondrial contact site and cristae organizing system in membrane architecture and dynamics. *Biochim Biophys Acta*

Ronchi D, Riboldi G, Del Bo R, Ticozzi N, Scarlato M, Galimberti D, Corti S, Silani V, Bresolin N, Comi GP (2015) CHCHD10 mutations in Italian patients with sporadic amyotrophic lateral sclerosis. *Brain* 138: e372

Tkach JM, Yimit A, Lee AY, Riffle M, Costanzo M, Jaschob D, Hendry JA, Ou J, Moffat J, Boone C, Davis TN, Nislow C, Brown GW (2012) Dissecting DNA damage response pathways by analysing protein localization and abundance changes during DNA replication stress. *Nat Cell Biol* 14: 966-76

Weraarpachai W, Antonicka H, Sasarman F, Seeger J, Schrank B, Kolesar JE, Lochmuller H, Chevrette M, Kaufman BA, Horvath R, Shoubridge EA (2009) Mutation in TACO1, encoding a translational activator of COX I, results in cytochrome c oxidase deficiency and late-onset Leigh syndrome. *Nat Genet* 41: 833-7

Yagi M, Uchiumi T, Takazaki S, Okuno B, Nomura M, Yoshida S, Kanki T, Kang D (2012) p32/gC1qR is indispensable for fetal development and mitochondrial translation: importance of its RNA-binding ability. *Nucleic Acids Res* 40: 9717-37

Zhang M, Xi Z, Fang S, Ghani M, Sato C, Moreno D, Liang Y, Lang AE, Rogaeva E (2016) Mutation analysis of CHCHD2 in Canadian patients with familial Parkinson's disease. *Neurobiology of aging* 38: 217 e7-8

Zhang M, Xi Z, Zinman L, Bruni AC, Maletta RG, Curcio SA, Rainero I, Rubino E, Pinessi L, Nacmias B, Sorbi S, Galimberti D, Lang AE, Fox S, Surace EI, Ghani M, Guo J, Sato C, Moreno D, Liang Y et al. (2015) Mutation analysis of CHCHD10 in different neurodegenerative diseases. *Brain* 138: e380

Zhou ZD, Saw WT, Tan EK (2016) Mitochondrial CHCHD-Containing Proteins: Physiologic Functions and Link with Neurodegenerative Diseases. *Mol Neurobiol*

Zhu L, Gomez-Duran A, Saretzki G, Jin S, Tilgner K, Melguizo-Sanchis D, Anyfantis G, Al-Aama J, Vallier L, Chinnery P, Lako M, Armstrong L (2016) The mitochondrial protein CHCHD2 primes the differentiation potential of human induced pluripotent stem cells to neuroectodermal lineages. *J Cell Biol* 215: 187-202

Figures

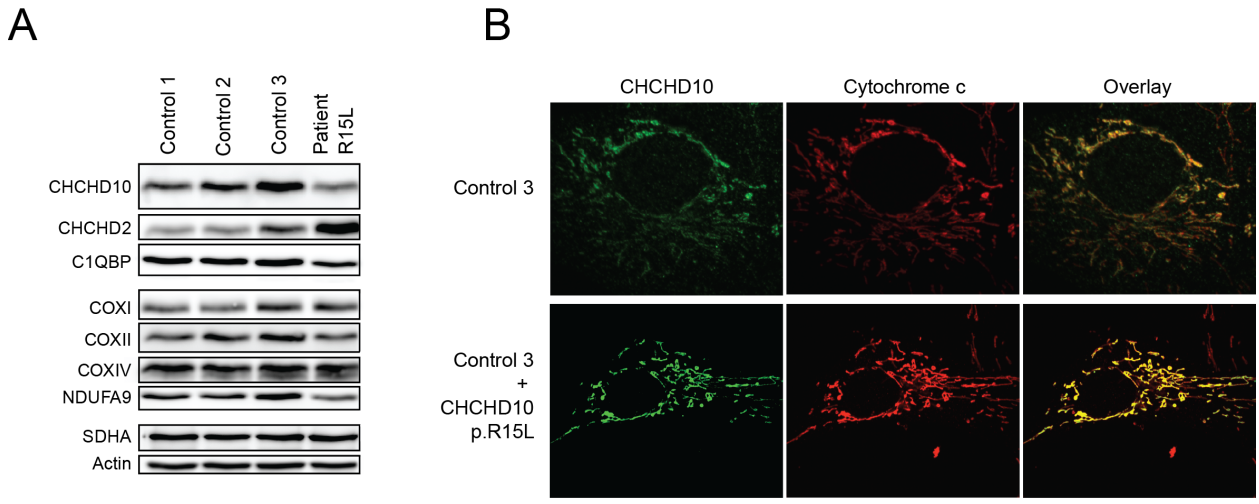

Figure 2.1 Reduced steady-state level of CHCHD10 and localization of CHCHD10 p.R15L to mitochondria.

(A) Whole cell extract from patient and control fibroblasts separated by SDS-PAGE and probed with antibodies against the indicated proteins. Actin was used as a loading control. (B) CHCHD10 p.R15L expression in control fibroblasts. Immunofluorescence analysis of control fibroblasts overexpressing mutant CHCHD10 p.R15L protein. Endogenous CHCHD10 staining is shown in green, the mitochondrial marker cytochrome *c* is shown red.

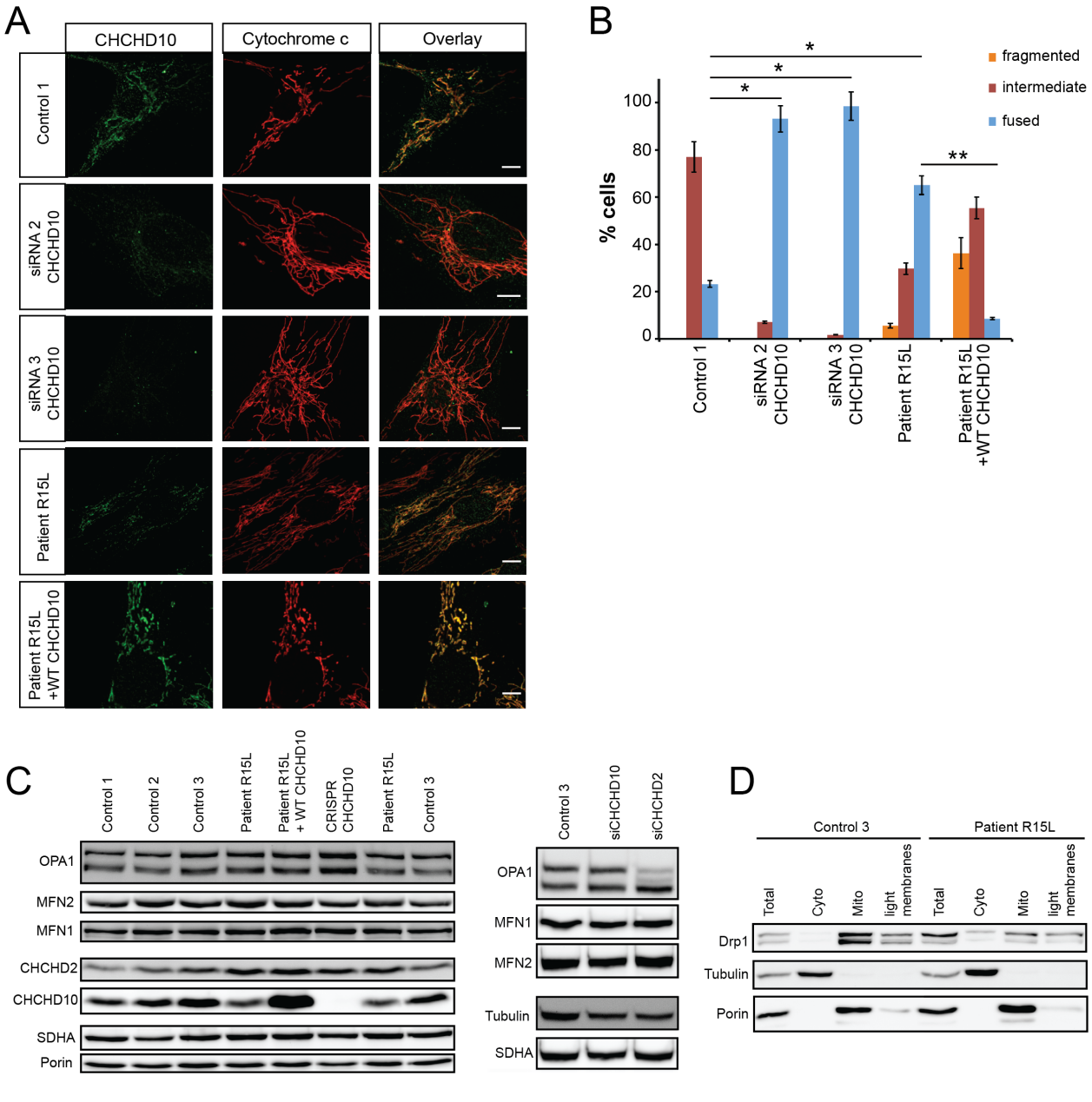
A
CHCHD10
Cytochrome c
Overlay
Control 1
siRNA 2 CHCHD10
siRNA 3 CHCHD10
Patient R15L
Patient R15L +WT CHCHD10
B
fragmented
intermediate
fused
% cells
Control 1
siRNA 2 CHCHD10
siRNA 3 CHCHD10
Patient R15L
Patient R15L +WT CHCHD10
C
Control 1
Control 2
Control 3
Patient R15L
Patient R15L + WT CHCHD10
CRISPR CHCHD10
Patient R15L
Control 3
OPA1
MFN2
MFN1
CHCHD2
CHCHD10
SDHA
Porin
Control 3
siCHCHD10
siCHCHD2
OPA1
MFN1
MFN2
Tubulin
SDHA
D
Control 3
Patient R15L
Total
Cyto
Mito
light membranes
Drp1
Tubulin
Porin
E
Control 3
Patient R15L

Figure 2.2 Mitochondrial hyperfusion in patient fibroblasts without altered fusion machinery.

(A, B) Immunofluorescence analysis of control and patient fibroblasts, control cells treated with siRNA against CHCHD10 and patient fibroblast stably overexpressing wild-type CHCHD10.

(A) Endogenous CHCHD10 staining is shown in green, the mitochondrial marker cytochrome *c* in red. Scale bars: 10 μm.

(B) Quantification analysis of mitochondrial network morphology. In each experimental condition described, 86 cells were analysed and the mitochondrial network organization was classified as fused, normal reticulum (intermediate), or fragmented, in three independent experiments. Data represent mean ± SEM and p-values were calculated using a two-tailed, unpaired *t*-test.

(C) Immunoblot analysis of key players in mitochondrial fusion in patient or siRNA-depleted fibroblasts. Immunoblot analysis of MFN1, MFN2 and OPA1 levels in control and patient fibroblasts as well as fibroblasts where CHCHD10 (siRNA CHCHD10-2) or CHCHD2 (siRNA CHCHD2-2) was depleted by siRNA. SDHA, Porin, and Tubulin were used as loading controls.

(D) Analysis of DRP1 localization in control and patient fibroblasts by immunoblot analysis after cellular fractionation. Porin was used as a mitochondrial marker and tubulin as a cytosolic marker. (E) Analysis of the mitochondrial ultrastructure by transmission electron microscopy in control and patient fibroblasts. Scale bars: 500 nm.

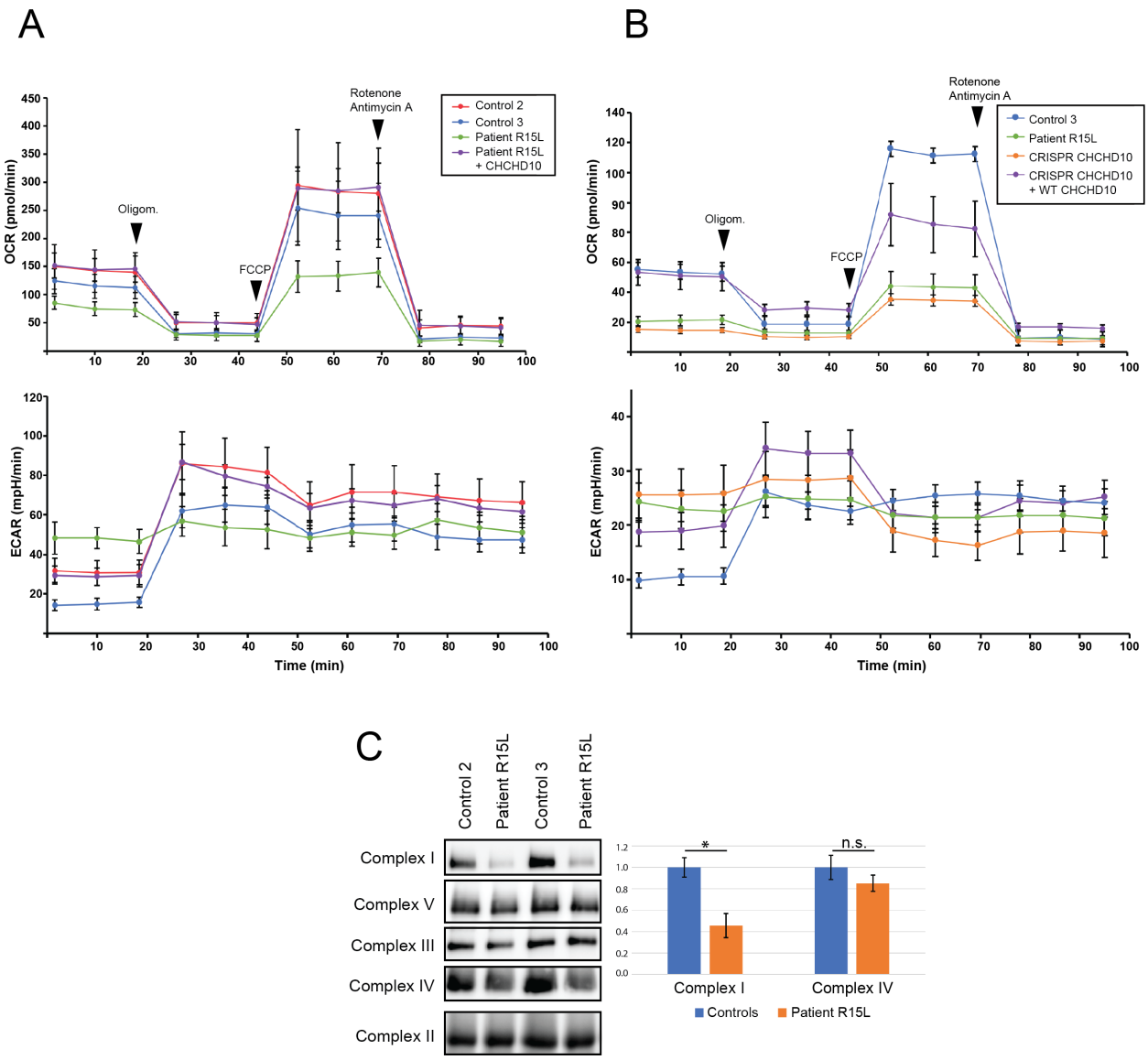

Figure 2.3 Mitochondrial oxygen consumption is impaired in patient fibroblasts as well as CRISPR-Cas9 CHCHD10 knockout cells.

(A, B) Seahorse Bioscience XF24 extracellular flux analyser was used to measure the oxygen consumption rate (OCR) and the extracellular acidification rate (ECAR) in control and

(A) patient fibroblasts, and patient fibroblasts overexpressing wild-type CHCHD10. $n = 3$, data represent mean ± SD.

(B) CRISPR-Cas9 knockout CHCHD10 cells, and CRISPR-Cas9 knockout CHCHD10 cells overexpressing wild-type CHCHD10. $n = 5$, data represent mean ± SD.

(C) BN-PAGE analysis of patient and control fibroblasts shows a Complex I defect as revealed by subunit-specific antibodies against individual OXPHOS complexes. Quantification from 5 independent experiments, data represent mean ± SEM.

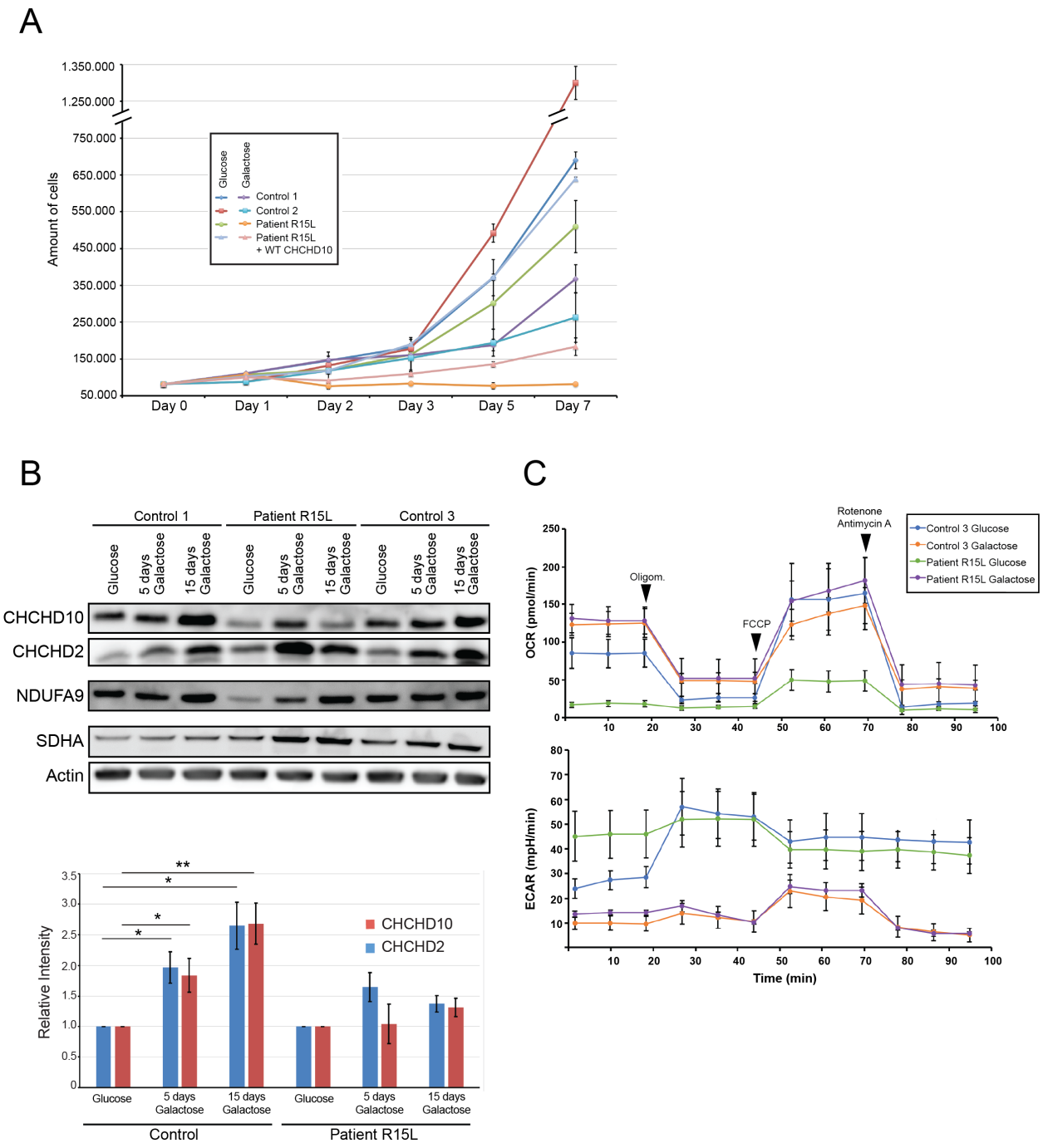

Figure 2.4 CHCHD10 is required for growth in glucose-free medium.

(A) Growth curve for indicated cells grown in glucose- versus galactose-containing medium.

(B) Immunoblot analysis and quantification of CHCHD10 and CHCHD2 levels in control and patient fibroblasts after subjecting the cells to galactose-containing medium for 5 and 15 days, respectively. Actin was used as a loading and normalization control. Graph represents the

relative protein levels of CHCHD10 and CHCHD2 in control and patient cells grown in galactose medium compared to those grown in glucose medium (set to 1). Data represent mean ± SD (control, n=6; patient, n=3). *P*-values were calculated using a two-tailed, paired *t*-test *$P < 0.05$.

(C) Seahorse Bioscience XF24 extracellular flux analyser was used to measure the oxygen consumption rate (OCR) and the extracellular acidification rate (ECAR) in control and patient fibroblasts grown in either glucose or galactose-containing medium. $n = 3$, data represent mean ± SEM.

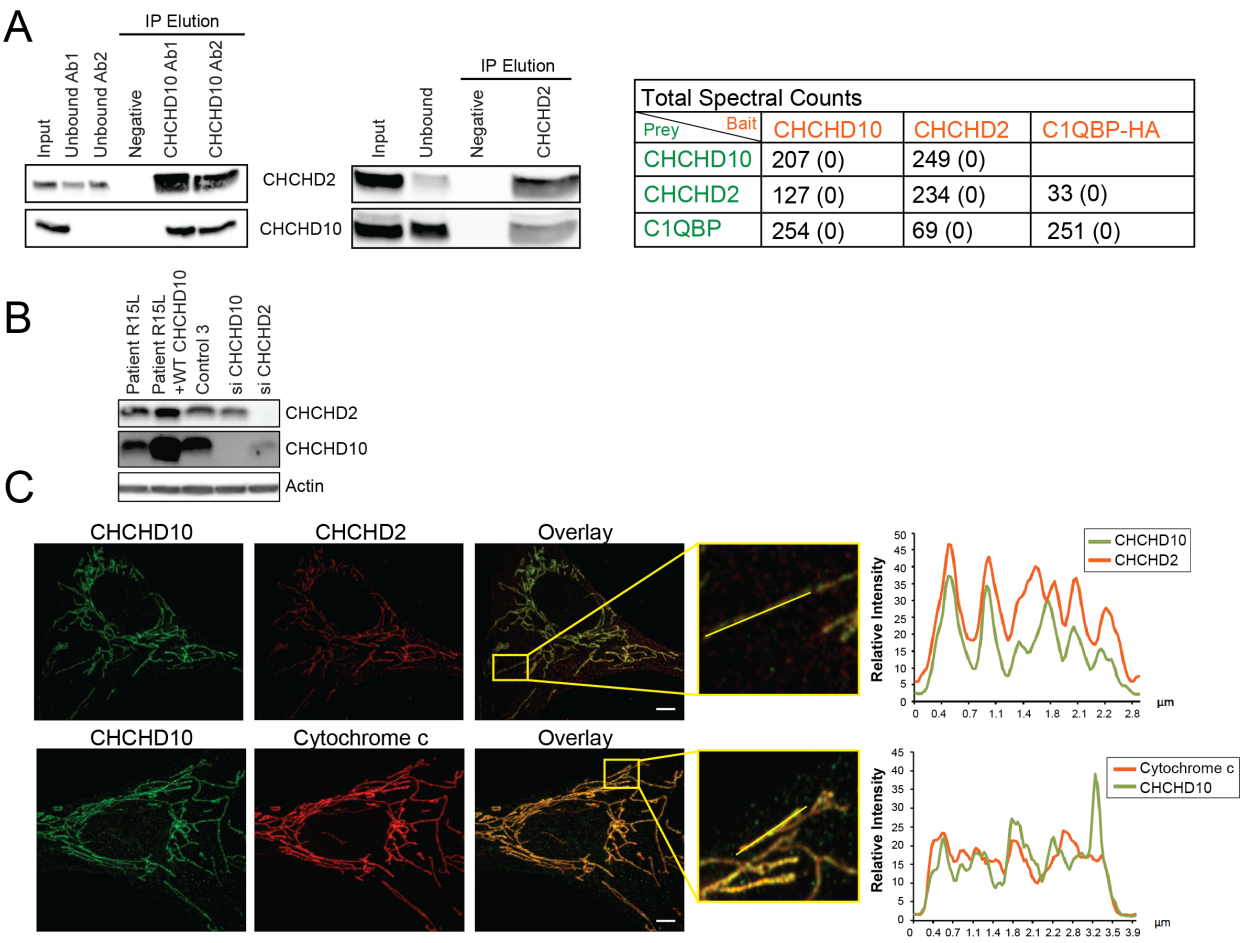

Total Spectral Counts			
Prey \ Bait	CHCHD10	CHCHD2	C1QBP-HA
CHCHD10	207 (0)	249 (0)	
CHCHD2	127 (0)	234 (0)	33 (0)
C1QBP	254 (0)	69 (0)	251 (0)

Figure 2.5 CHCHD10 co-immunoprecipitates with CHCHD2 and appears in distinct foci within mitochondria.

(A) Co-immunoprecipitation experiment of CHCHD10 and CHCHD2 in 143B cells. Immunoprecipitation was performed with two different anti-CHCHD10 antibodies and an anti-CHCHD2 antibody, respectively. Stably overexpressing HA-tagged C1QBP was immunoprecipitated with anti-HA antibody. For negative controls no antibody was bound to the beads. Total Spectral Counts are listed for antibody-specific, versus negative controls (numbers in parentheses).

(B) Immunoblot analysis of the CHCHD10 and CHCHD2 levels in patient and control fibroblasts, patient fibroblasts overexpressing wild-type CHCHD10 and control fibroblasts treated with siRNA against CHCHD10 (CHCHD10-2) and CHCHD2 (CHCHD2-2). Actin was used as a loading control.

(C) Immunofluorescence analysis and line scan of the colocalization of CHCHD10 and CHCHD2. CHCHD10 is shown in green, CHCHD2 and the mitochondrial marker cytochrome *c* in red. Scale bar: 10 μm.

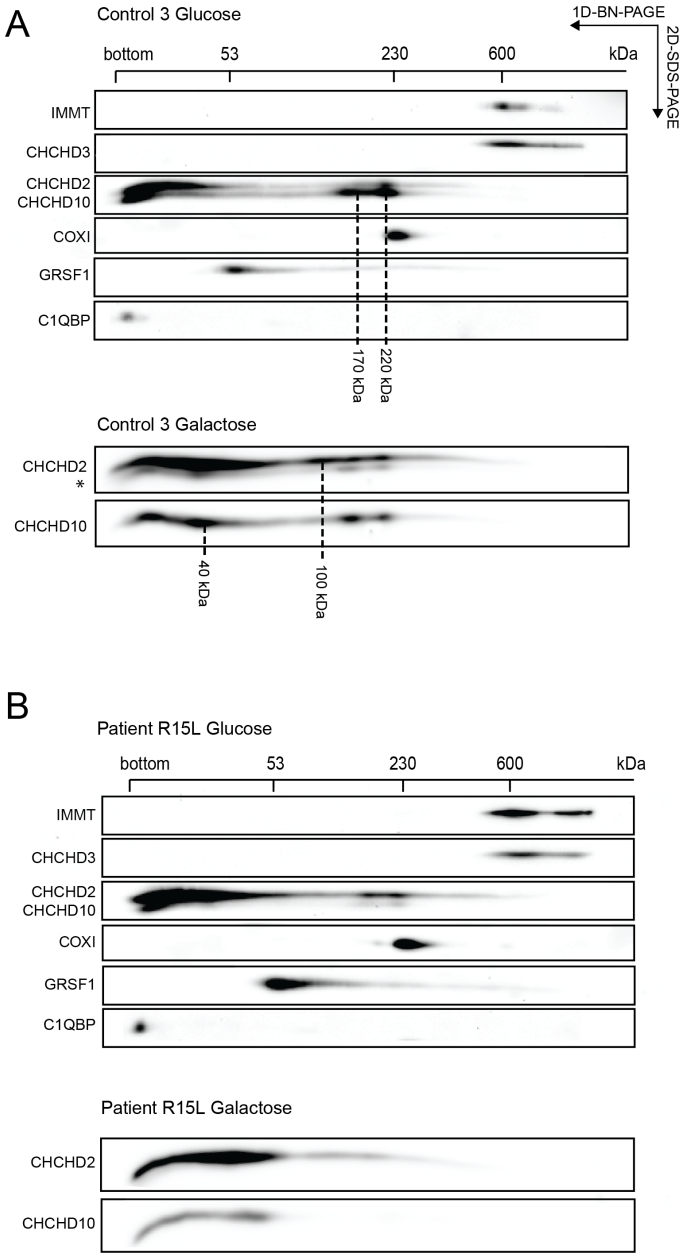

Figure 2.6 CHCHD10 forms a complex with CHCHD2 not MICOS.

(A, B) Two dimensional BN-PAGE/SDS-PAGE electrophoresis analysis of mitochondria from control (A) and patient (B) fibroblasts immunoblotted for indicated proteins. The positions and molecular weight of identified CHCHD10/CHCHD2 containing complexes are indicated in (A).

The monomeric molecular weights of CHCHD2 and CHCHD10 are 15.5 kDa and 14.1 kDa, respectively. The bottom of the gel in the first dimension is indicated as 'bottom'. (A and B bottom) Two-dimensional BN-PAGE/SDS-PAGE electrophoresis analysis of mitochondria from control (A) and patient (B) fibroblasts cultivated for 9 days in galactose-containing medium. * Lower band is a residual signal from a prior CHCHD10 detection. The positions of GRSF1, COX I, and the MICOS complex are indicated on top (in kDa).

Supplemental Figures

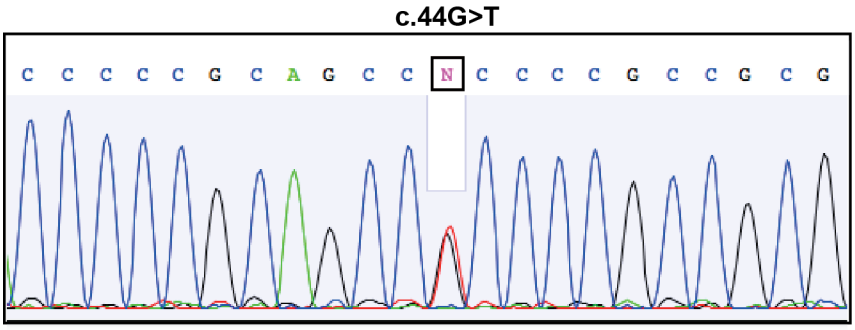

Figure S2.1 cDNA analysis of patient fibroblasts.

The DNA sequence chromatogram shows heterozygosity of the c.44G>T mutation in patient fibroblasts.

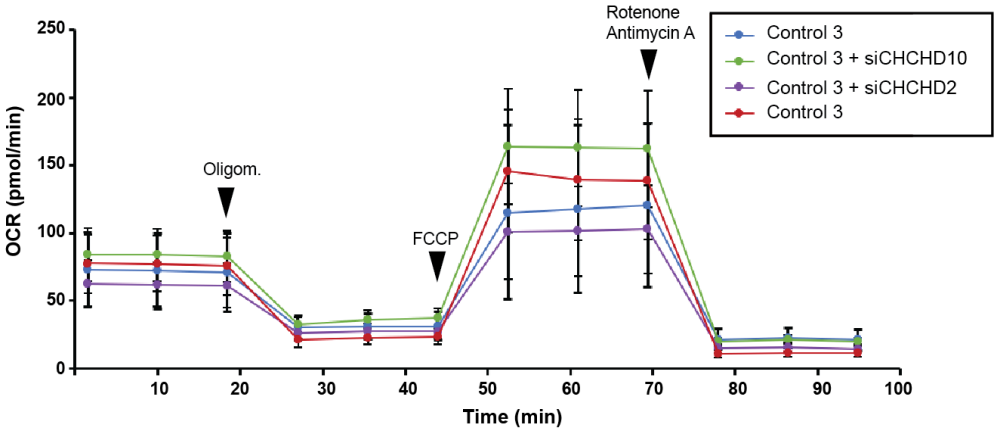

Figure S2.2 Analysis of OCR in control fibroblasts after depletion of CHCHD10 or CHCHD2.

Seahorse Bioscience XF24 extracellular flux analyser was used to measure the oxygen consumption rate (OCR) in control fibroblasts and fibroblasts where CHCHD10 or CHCHD2 was depleted with siRNA. $n = 5$, data represent mean ± SD.

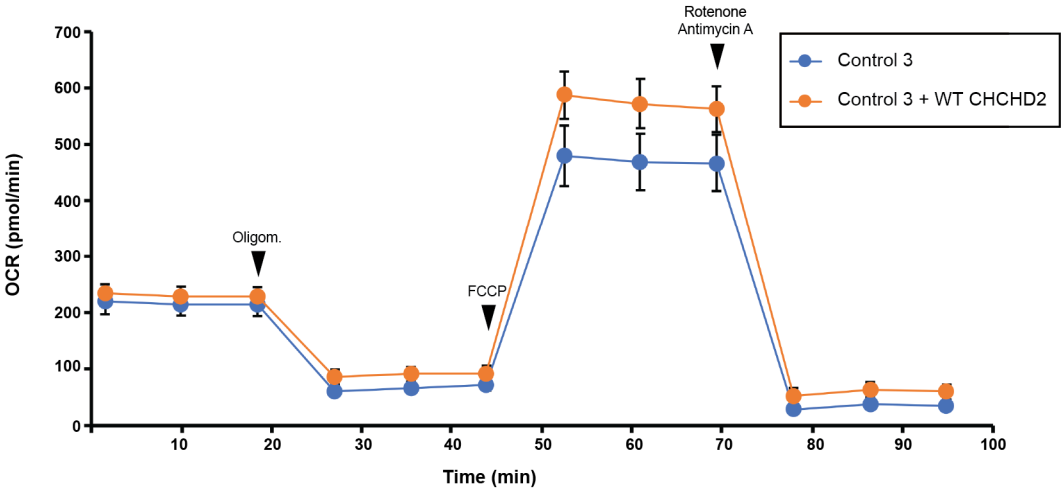

Figure S2.3 Analysis of OCR in control fibroblasts overexpressing CHCHD2.

Seahorse Bioscience XF24 extracellular flux analyser was used to measure the oxygen consumption rate (OCR) in control fibroblasts and fibroblasts in which CHCHD2 was overexpressed. *n* = 5, data represent mean ± SD.

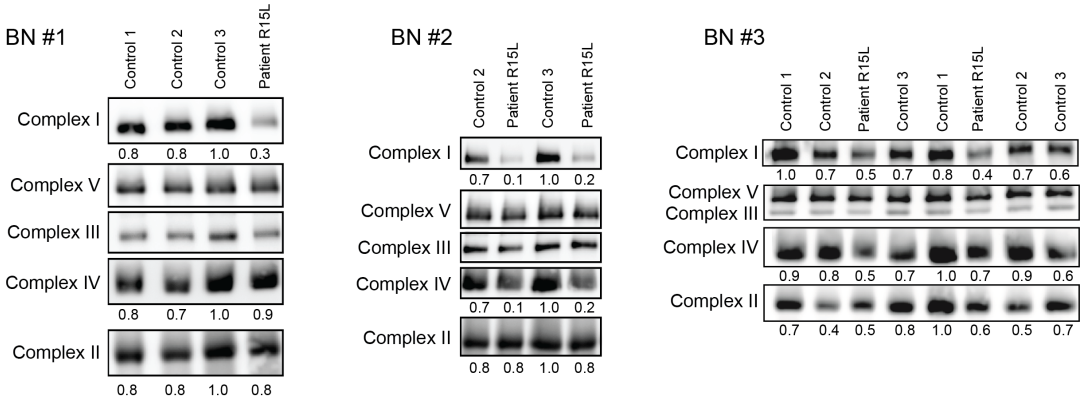

Figure S2.4 BN-PAGE analysis of patient and control fibroblasts.

All BN-PAGE analyses showed a Complex I defect as revealed by subunit-specific antibodies against individual OXPHOS complexes. Numbers represent quantification of bands analysed by Image J, and used for the analysis shown in Fig 1E.

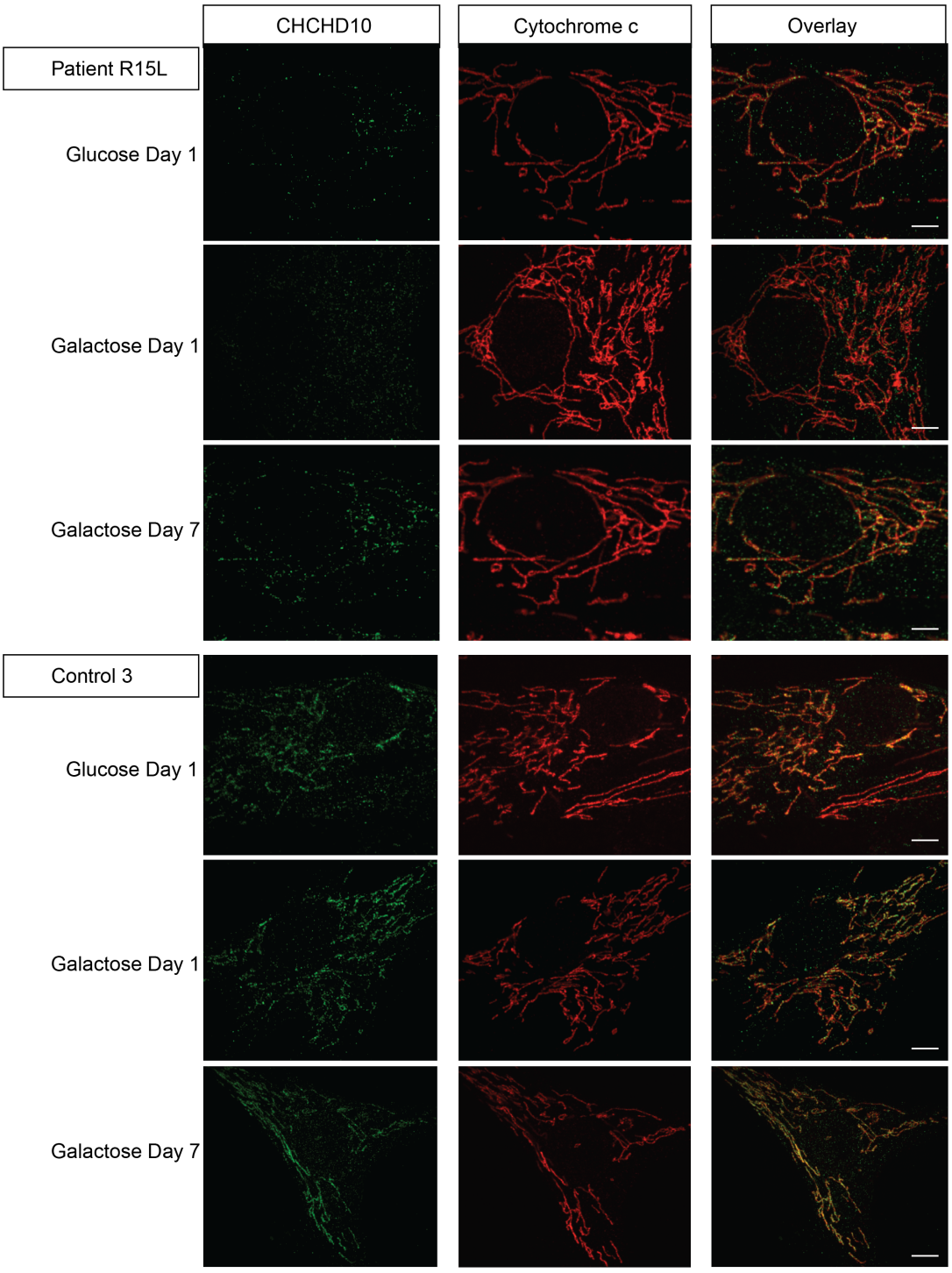

Figure S2.5 Immunofluorescence analysis of control and patient fibroblasts in glucose versus galactose-containing medium.

Endogenous CHCHD10 staining is shown in green, the mitochondrial marker cytochrome *c* is shown in red. Scale bars: 10 μm.

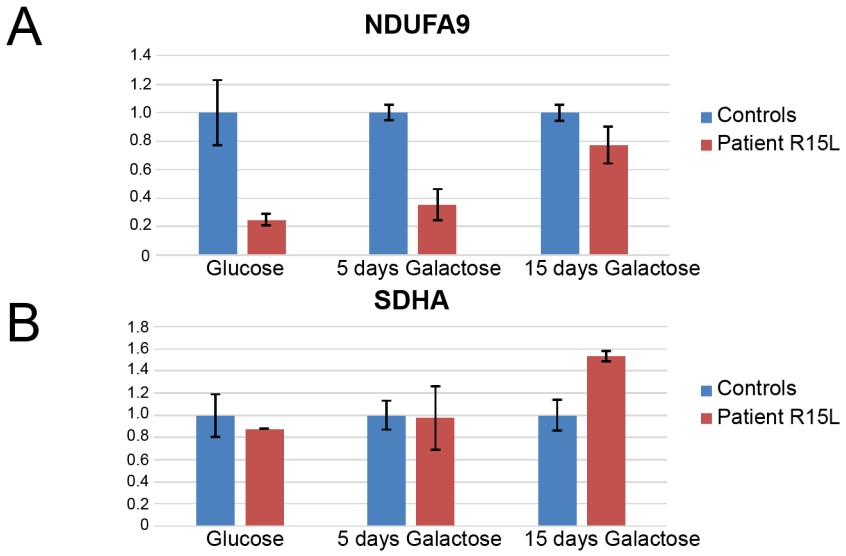

Figure S2.6 Quantification of OXPHOS subunits after subjecting control and patient fibroblasts to galactose for 5 and 15 days.

Calculations represent quantification of two independent blots.

(A) Data represent mean values of NDUFA9 levels normalized to Actin ± SEM.

(B) Data represent mean values of SDHA levels normalized to Actin ± SEM.

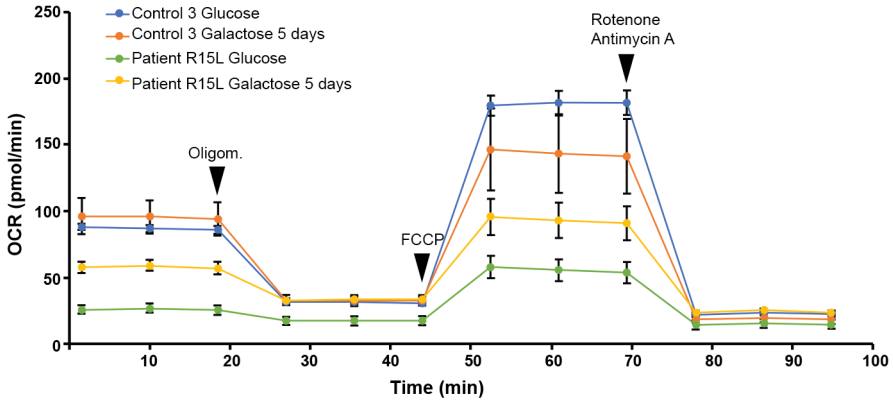

Figure S2.7 Analysis of OCR in control and patient fibroblasts after 5 days in galactose.

Seahorse Bioscience XF24 extracellular flux analyser was used to measure the oxygen consumption rate (OCR) in control fibroblasts and patient fibroblasts suspected to galactose medium for 5 days. n = 5, data represent mean ± SD.

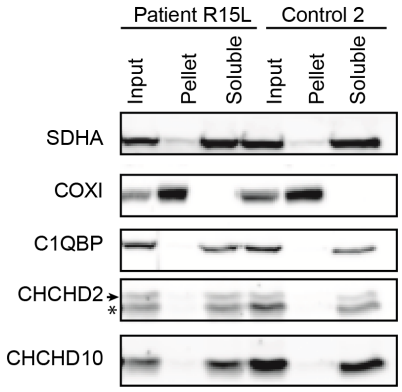

Figure S2.8 CHCHD10 and CHCHD2 are soluble proteins.

Alkaline carbonate extraction of mitochondria from control and patient fibroblasts. Immunoblot analysis shows that CHCHD10, CHCHD2 and C1QBP are soluble proteins. SDHA (membrane-associated protein) and COXI (integral inner membrane protein) were used as controls. Arrow points to CHCHD2 band in the blot. Asterisk marks leftover signal from CHCHD10 antibody.

Preface to chapter 3

The first study on the CHCHD10 p.R15L patient fibroblasts revealed the involvement of CHCHD10 in mitochondrial respiration and a specific complex I deficiency for this variant. The defect could be rescued through the introduction of the wild-type CHCHD10 protein, therefore suggesting a haploinsufficient mode of action. We established an interaction of CHCHD10 with CHCHD2 and C1QBP and the existence of a complex between CHCHD2 and CHCHD10, which was absent in patient cells. In our first study, we identified a severe growth defect of the CHCHD10 p.R15L patient cells in galactose medium, which could be also rescued by the overexpression of the wild-type CHCHD10. In order to understand the mechanisms by which the cells adapted to this energetic stress situation, we used glucose-free medium in which we substituted galactose as a stressor in our second study to profile metabolic differences both in the patient and the rescued cells. For the second study we used an 'omics' approach and collected transcriptomic, metabolomic and proteomic datasets of patient and rescue cells in glucose and galactose conditions.

Chapter 3

CHAPTER 3

The CHCHD10 variant p.R15L causes an energy deficit and activates the integrated stress response through IRE1

Isabella R. Straub[1,2], Woranontee Weraarpachai[3], Eric A. Shoubridge[1,2,*]

Affiliations:

[1]Department of Human Genetics, McGill University, Montreal, Quebec, Canada

[2]Montreal Neurological Institute, McGill University, Montreal, Quebec, Canada

[3]Department of Biochemistry, Faculty of Medicine, Chiang Mai University, Chiang Mai, Thailand

*To whom correspondence should be addressed at: Eric A. Shoubridge, Montreal Neurological Institute, 3801 University Street, Montreal, Quebec, Canada H3A 2B4;

Email: eric@ericpc.mni.mcgill.ca, Tel: 514-398-1997; FAX: 514-398-1509

Manuscript in preparation.

Abstract

Mutations in *CHCHD10*, coding for coiled-helix coiled-helix domain containing 10, a mitochondrial protein of unknown function, are a rare cause of autosomal dominant amyotrophic lateral sclerosis (ALS). The molecular basis for pathogenicity is not well understood, but mutation-specific toxic gain of function or haploinsuffuciency models have been proposed. We investigated the metabolic alterations in patient fibroblasts carrying the haploinsufficient p.R15L variant that we previously showed was unable to proliferate in medium containing galactose, a non-fermentable carbon source. To decipher the metabolic dysfunction associated with this variant we compared transcriptomic, metabolomic and proteomic data in patient cells with those rescued by the expression of the wild-type cDNA. We cultured the cells in medium containing either glucose or galactose to profile differences during nutrient stress. Our study confirmed the complex I deficiency and showed an increase in the NADH/NAD^+ ratio in both glucose and galactose. This was associated with a down-regulation of the TCA cycle and an increase in the entry substrates pyruvate and aspartate. Cells in galactose medium showed a more marked cellular energy deficit, and the increased AMP/ATP ratio resulted in phosphorylation of AMPK, leading to an upregulation of catabolic and apoptotic pathways. Growth in galactose also led to the up-regulation of mitochondrial one-carbon metabolism, activation of the integrated stress response in the endoplasmic reticulum mediated through IRE1, activation of the mitochondrial UPR, and increased production of two metabolic cytokines, GDF15 and FGF21. These results demonstrate that the CHCHD10 p.R15L variant, which causes loss of CHCHD10 function elicits a striking energy deficit phenotype that activates cellular stress and survival pathways, which may underlie the selective vulnerability of motor neurons.

Introduction

Autosomal dominant mutations in *CHCHD10* were recently identified as rare genetic causes of ALS (Bannwarth et al., 2014, Chaussenot et al., 2014, Chio et al., 2015, Dols-Icardo et al., 2015, Johnson et al., 2014, Kurzwelly et al., 2015, Lehmer et al., 2018, Muller et al., 2014, Ronchi et al., 2015, Ryan et al., 2019, Shen et al., 2017, Zhang et al., 2015, Zhou et al., 2017a). Most predicted pathogenic variants are present in the N-terminal half of the protein and not in the defining CHCH-domain at the C-terminus. The mutation c.44C>A (predicting p. R15L) has been reported in sporadic and familial ALS, and motor neuron disease in four studies, and is absent in controls (Johnson et al., 2014, Khan et al., 2017, Muller et al., 2014, Zhang et al., 2015). CHCHD10 is a soluble 14 kDa mitochondrial protein that forms a complex with its paralogue CHCHD2. It has a short half-life and is upregulated in stress conditions (Huang et al., 2018, Straub et al., 2018); however, its precise function remains unknown.

Mitochondrial dysfunction has long been suggested to contribute to ALS disease pathology, but prior to the identification of mutations in CHCHD10, these deficiencies were thought to be pleiotropic effects. Although all reported pathogenic mutations in CHCHD10 are autosomal dominant, the molecular basis of pathogenicity of CHCHD10 is variable. For instance, the p.S59L variant, reported in patients with ALS-FTD, is associated with a fragmented mitochondrial network, protein aggregates in mitochondria, and the activation of the integrated stress response (ISR), ascribed to toxic gain of function (Anderson et al., 2019a, Bannwarth et al., 2014, Genin et al., 2018, Genin et al., 2019). On the other hand, the p.R15L and p.G66V variants, in which reduced levels of CHCHD10 protein are associated with mitochondrial respiratory chain dysfunction, appear to be haploinsufficient (Brockmann et al., 2018, Penttila et al., 2015, Straub et al., 2018).

Emerging lines of evidence suggest a link between endoplasmic reticulum (ER) stress caused by unfolded protein and neurodegenerative diseases like ALS (Hetz & Mollereau, 2014). The stress response of the ER is designed to maintain and recover proteostasis through three distinct signalling pathways: (1) PRKR-like endoplasmic reticulum kinase (PERK), (2) activating transcription factor 6 (ATF6) and (3) inositol-requiring kinase 1 (IRE1) (Hughes & Mallucci, 2019). In particular the IRE1 signalling cascade has been suggested as potential target for treatment as downstream targets such as XBP1 and CHOP have been shown to play a role in several ALS disease models, and knockdown of XBP1 provides significant protection against

neuronal death and delays onset of disease (Hetz et al., 2009, Ito et al., 2009, Jaronen et al., 2014, Medinas et al., 2017).

To investigate the cellular and metabolic remodelling caused by the CHCHD10 variant p.R15L, and to identify whether the integrated stress response plays a role in this ALS model, we collected metabolomic, transcriptomic and proteomic datasets on patient fibroblasts.. We cultured patient and rescued cells (expressing wild-type CHCHD10) in medium containing either glucose or galactose as a nutrient source. Glucose-free galactose medium imposes a nutrient stress, as it forces cells to rely solely on oxidative phosphorylation (OXPHOS) for energy production. Patient cells initially displayed some cell death on transfer to galactose medium, and thereafter a severe growth defect. Our data demonstrate a global remodelling of mitochondrial and cellular metabolic pathways and the activation of the integrated stress response through the IRE1/XBP1 pathway in patient cells under nutrient stress conditions. Maybe a sentence here about the fact that this is not simply mtDNA.

Results

In this study we investigated the mechanisms of pathogenesis in patient fibroblasts with the CHCHD10 p.R15L variant (hereafter referred to as 'patient') compared to the same cells expressing wild-type CHCHD10 cDNA (hereafter called 'rescue'). We previously showed that about 20% of patient cells died over 24 hours after transfer to galactose medium, while the remaining cells remained attached to the plate, but did not re-enter the cell cycle. This phenotype was rescued by expression of wild-type CHCHD10 cDNA. Changes in the transcriptome, proteome, and metabolome of patient versus rescue cells grown in glucose or galactose medium for 48 hours were determined by RNA sequencing, tandem mass tag (TMT) mass spectrometry, and targeted metabolomics analyses to profile the initial response to the galactose challenge. For the analysis we compared patient with rescue in glucose medium ('Glucose') and patient with rescue in galactose medium ('Galactose') (Fig. 3.1A), hence analysing the effect of genotype in different culture media.

RNAseq analysis confirms the respiratory chain deficiency and reveals changes in one-carbon metabolism

To investigate potential transcriptional alterations in patient cells and the response to the stress of exposure to galactose medium we first determined the steady-state mRNA levels by RNA sequencing. The differentially expressed transcripts in 'Glucose' and the 'Galactose' media showed a substantially different distribution; more transcripts had a larger fold change in 'Galactose' compared to 'Glucose' (Fig. 3.1B, S3.1A, S3.1B). We first focused on transcripts of those proteins found in MitoCarta2.0 (Calvo et al., 2016). In 'Glucose', GO terms for biological process enrichment analysis of differentially expressed transcripts identified upregulation of pathways involving ATP synthesis/the respiratory chain and the TCA cycle (Fig. 3.1C). Interestingly, transcripts of the acyl-CoA biosynthetic process, for example ATP citrate synthase (ACLY), fatty acid synthetase (FASN), and the citrate transporter (SLC25A1) were upregulated in glucose even though the biosynthesis of fatty acids seems to be counterproductive in a state of compromised energy supply. At the same time, beta oxidation of fatty acids, a catabolic pathway, was upregulated. Downregulated transcripts encompassed several mitochondrial transporters including SLC25A27 (UCP4), SLC25A14 (UCP5), SLC25A33 and SLC25A36 (pyrimidines),

and SLC25A13 (aspartate/malate). Transcripts coding for enzymes involved in ketone body metabolism, 3-hydroxybutyrate dehydrogenase 1 (BDH1) and acyl-CoA synthetase short chain 3 (ACSS3), were downregulated in the patient in glucose. Lastly, the mitochondrial UMP-CMP kinase (CMPK2), responsible for the phosphorylation of dUMP and dCMP, and thus the local supply of deoxynucleotides as essential precursors for mtDNA replication and transcription was downregulated.

In galactose, upregulated transcripts included those involved in mitochondrial translation, protein targeting, apoptosis, and the assembly of the respiratory chain complexes. However, the transcripts with a log2 fold change >1 mainly involved apoptotic pathways (Fig. 3.1C, 'Galactose'). Furthermore, we observed an upregulation of transcripts of the mitochondrial folate cycle, which is in part responsible for nucleic acid production (Fig. 3.1C and 3.2B). A more detailed analysis of gene transcripts involved in one-carbon metabolism further clarified the effect on this pathway (Fig. 3.2A). Transcripts for mitochondrial proteins involved in folate synthesis, MTHFD2L, MTHFD2, MTHFD1L and SHMT2 were upregulated, whereas transcripts of the cytosolic part of the one-carbon cycle, DHFR, SHMT1, TYMS and MTHFD1 were down-regulated in galactose in the patient. Mitochondrial folate metabolism is responsible for the supply of formate in the cytosol for purine and pyrimidine synthesis and for the synthesis of NADPH in mitochondria, which is needed to tackle increased amounts of reactive oxygen species (ROS) (Martinez-Reyes & Chandel, 2014, Zheng et al., 2018). The same tendency was observed in patient cells in glucose versus galactose, indicating a marked shift in one carbon metabolism in patient cells in galactose (Fig. S3.1C, D). Lastly, transcripts of the serine metabolism were downregulated in the 'Glucose' and 'Galactose' conditions, indicating that serine is not synthesized *de novo* from glucose but rather directly obtained from the culture media or through the conversion of glycine to serine (Fig. 3.2A).

Mitochondrial processes down-regulated in galactose included the catabolism of fatty acids, transcripts of respiratory chain complex assembly, in particular the assembly of complexes I and IV, and a number of mitochondrial transporters such as SLC25A27 (UCP4) and SLC25A14 (UCP5). These latter transporters were also down-regulated in glucose (Fig. 3.1C). Both have the highest level of expression in the brain, where they were suggested to uncouple oxidative phosphorylation, consequentially exerting a protective role in cells exposed to mitochondrial defects (Hoang et al., 2012, Ramsden et al., 2012). Another transporter

downregulated in patient cells in galactose is the aspartate/glutamate transporter SLC25A12, which catalyses the calcium-dependent exchange of cytoplasmic glutamate with mitochondrial aspartate (Thangaratnarajah et al., 2014).

In summary, patient cells upregulated transcripts of the mitochondrial respiratory chain, the TCA cycle and fatty acid beta-oxidation at the transcript level to compensate for the lack of mitochondrial energy production in glucose. In galactose on the other hand patient cells upregulated transcripts of mitochondrial translation and mitochondrial protein import to rescue the energy deficit. Transcripts of the one-carbon metabolism in mitochondria are upregulated to supply the cytosol with more formate to produce purines and pyrimidines and mitochondria with more NADPH to fight increased amounts of ROS. Interestingly, the mitochondrial aspartate/glutamate carrier was downregulated, which could lead to a deficiency of energy equivalents in mitochondria and a lack of mitochondrial aspartate in the cytosol. In both conditions transcripts of apoptotic processes are increased.

Metabolomic analysis reveals a high NADH/NAD$^+$ ratio which stalls the TCA cycle in patient cells

Metabolomic analyses were performed in the four groups described above on whole cells without subcellular fractionation. Using a targeted assay for 116 metabolites involved in bioenergetics, oxidative stress and mitochondrial function, absolute the levels of 85 metabolites were successfully determined across all samples. Analysis of the multi-variant data using orthogonal transformation through principal component analysis (PCA) or hierarchical clustering with heatmap analysis showed tight clustering of the replicates and clear differences among the four conditions analysed, demonstrating the quality of the data (Fig. 3.3A and S3.2A). The first component, which explains 55% of the variance in the dataset, showed that the treatment effect of glucose medium versus galactose medium was clearly separated, particularly for the patient cells. Moreover, through the second component, explaining 18% of the variance, we were able to separate the genotype effect in the two conditions galactose and glucose. The genotype difference was larger in galactose than in glucose (Fig. 3.3A). The fold-change distribution of differentially detected metabolites in the two conditions ‘glucose’ and ‘galactose’ was larger in the galactose condition showing log2 fold changes ranging from +3 to -2.5 in galactose versus +1 to -2.5 in glucose (Fig. 3.3B).

Redox imbalance caused by high levels of NADH in the patient

The NADH/NAD^+ ratio was significantly increased in both glucose and galactose condition in patient cells. Normally, when control cells are put in galactose the NADH/NAD^+ level decreases (Ryall et al., 2015), and this was evident in the rescued cell line (Fig. 3.3C, D). The complex I deficiency in the patient cells likely accounted for the increase in the NADH/NAD^+ ratio in galactose.

Additionally, the glutathione antioxidant defence pathway was activated in patient cells in galactose. Total levels of glutathione were increased (GSH + GSSG), and the GSH:GSSG ratio was decreased (Fig. 3.3C, D), potentially to deal with increased oxidative stress in galactose.

The TCA cycle is stalled in the patient

Analysis of the common up-regulated and down-regulated metabolites in glucose and galactose, revealed decreased levels of TCA-cycle intermediates, including cis-aconitic acid, succinate, fumarate, and citrate (Fig. 3.3C). However, the levels of metabolites entering the TCA cycle, pyruvate and acetyl-CoA, were increased or unchanged, respectively (Fig. 3.3C). The TCA cycle is regulated by ATP and NADH levels (Berg JM, 2002), which were decreased and increased, respectively (Fig. 3.3C). The conversion of pyruvate into acetyl-CoA, from acetyl-CoA into citrate and from ketoglutarate to succinate is NADH-dependent and likely inhibited in the patient, as NADH levels were high. Instead, ADP activates the conversion from pyruvate into acetyl-CoA, acetyl-CoA into citrate and isocitrate into ketoglutarate, and its levels were increased, producing counteracting signals (Fig. 3.3C, D). Overall, however, the data suggested that the TCA cycle was downregulated in both conditions.

Reduced energy equivalents in the patient in galactose

The metabolomic analysis revealed that nucleoside mono- and diphosphates (IMP, AMP/ADP and GMP/GDP) were the most highly increased metabolites in patient cells grown in galactose, resulting in a marked increase in the AMP/ATP and GMP/GTP ratios (Fig. 3.3C, D). Concomitantly, the metabolite adenylosuccinic acid, in the pathway for the conversion of IMP to AMP, was also markedly increased as well as two other metabolites involved in the biosynthesis of purines and pyrimidines, ADP-ribose and folate (Fig. 3.3C, D). Formyl folate is the precursor for inosine monophosphate, which itself is the precursor of GMP and AMP. Besides, levels of S-

Adenosylmethionine (SAM) a metabolite of the methionine cycle, which is linked to the folate cycle were increased; however, levels of its counterpart S-Adenosylhomocysteine (SAH) were below the detection limit (Fig. S3.2B). We conclude that increased folate levels lead to an increased generation of nucleic acids IMP, AMP, and GMP for subsequent ATP production primarily carried out in mitochondria, as major enzymes of the folate cycle in the cytosol were transcriptionally down-regulated (Fig. 3.2A, B). However, mitochondrial ATP production was hampered in patient cells due to a complex I deficiency.

High levels of aspartate do not rescue the stalled TCA cycle and subsequent mitochondrial energy production

With the exception of aspartate, all other detectable amino acids were not significantly altered in either glucose or galactose media (Fig. 3.3F). Aspartate plays a key role in mitochondrial metabolism and is involved in the shuttling of electrons across the inner mitochondrial membrane through the malate-aspartate shuttle (Fig. 3.3G) (Berg JM, 2002). The malate/aspartate ratio thus serves as an indirect indicator of the NADH/NAD^+ ratio and the energy state of the cell. A dysregulation of the malate/aspartate ratio was observed in both glucose and galactose; however, in opposite directions (Fig. 3.3D, F). The shuttle is responsible for transporting NADH into mitochondria where it is reoxidized to NAD^+ by respiratory chain complex I. The mitochondrial asparate/glutamate transporter SLC25A12 was downregulated in patient cells in galactose at the transcript level, which at the protein level would lead to diminished transport of aspartate outside of mitochondria and a lack of NADH inside of mitochondria (Fig. 3.1C). In the cytosol, aspartate is converted to malate by GOT1 and MDH1 (Birsoy et al., 2015). Interestingly, the enzyme GOT1 was increased at the transcript level in the patient in galactose. GOT1 normally metabolizes aspartate to oxalacetic acid, which is then converted by MDH1 into malate. This cycle allows the supply of electrons for the mitochondrial respiratory chain. When the electron transport chain is inhibited however, GOT1 produces aspartate, which serves as a substrate to synthesize purines and pyrimidines, compensating for the lack of mitochondrial aspartate synthesis (Birsoy et al., 2015, Lane & Fan, 2015) (Fig. 3G). The increased levels of aspartate and GOT1 therefore suggest that aspartate is produced by GOT1 in the cytosol to support the proliferation of patient cells. At the same time, the pyrimidine carrier SLC25A33 is markedly upregulated in patient cells in galactose (Fig. 1C).

The energy balance is tightly monitored in patient in galactose

Concomitant with the markedly disturbed AMP/ATP ratio, we detected an increase in phosphorylated AMP-activated protein kinase (pAMPK) at position Thr172, signaling low cellular energy levels (Herzig & Shaw, 2018) (Fig. 3.3E). Another sensor of energy balance in the cell is the mechanistic/mammalian target of rapamycin (mTOR) pathway. mTOR is a serine/threonine kinase that responds to a number of physiological inputs including nutrients (amino acids), oxygen levels, hormones and energy status (AMP/ATP ratio) (Bond, 2016). Generally, mTORC1 is activated when energy supply is sufficient, and negatively regulated by pAMPK. We observed the inhibition of the mTOR pathway through the downregulation of phosphorylated ribosomal protein S6 in patient cells in galactose (Fig. 3.3E).

In summary, in both glucose and galactose NADH/NAD^+ ratios are high but only in galactose media a lack of cellular energy could be observed in parallel. The glycolytic process in glucose rescued the inefficient energy supply from mitochondria, however in galactose glycolysis came almost entirely to a halt. High levels of NADH stalled the TCA cycle as the amounts of NADH produced could not be used by the respiratory chain to generate ATP. Subsequently, entry substrates of the TCA cycle, like pyruvate and aspartate accumulate. Aspartate was additionally generated by GOT1 in the cytosol to rescue the proliferation defect of the patient in galactose.

Integration of proteomics and metabolomics confirms reduction in TCA cycle activity at the protein level

Changes in the proteome of isolated crude mitochondria from patient and rescue cells were determined by quantitative proteomic analysis using TMT - technology. We identified 1901 unique proteins in all conditions, of which 414 proteins were mitochondrial based on MitoCarta2.0 (Calvo et al., 2016), accounting for 21.8% of the total proteins determined (Fig. 3.4A). Applying a significance level of 5% (FDR, False Discovery Rate), we identified differentially expressed proteins for each condition (Fig. 4B, S3). Confirming the results from our first study (Straub et al., 2018), several complex I subunits were downregulated in glucose (NDUFV1, NDUFS8, NDUFA7, NDUFB8) (Fig. S3.3). Among the most significantly up-

regulated proteins we observed four proteins in the glycolytic pathway, glyceraldehyde-3-phosphate dehydrogenase (GAPDHS), fructose-bisphosphate aldolase A (ALDOA), phosphopyruvate hydratase (ENO1), and phosphoglycerate kinase 1 (PGK1) again confirming the increased activity of the glycolytic pathway in patient cells in glucose. Phosphoserine aminotransferase 1 (PSAT1), responsible for the conversion of 3-phosphoglycerate, an intermediate of glycolysis, to serine (Fig. 3.2B), was also upregulated in glucose (Fig. S3.3). Serine is used through the folate cycle to produce purines and pyrimidines. Lastly, glutathione S-transferase P (GSTP1) and glutathione S-transferase omega 1 (GSTO1), two detoxification enzymes that catalyse the conjugation of glutathione to chemical mutagens and protect against products of oxidative stress, were upregulated (Fig. S3.3).

In galactose medium we observed the downregulation of several complex I subunits (NDUFS8, NDUFS7, NDUFB10, NDUFA5, NDUFS5, NDUFA10, NDUFS4, NDUFS2) as well as cytochrome c (CYCS) (Fig. 3.4B). Interestingly, many lysosomal proteins were downregulated as well (ASAH1, HEXB, CTSZ, CLTB, GNS, LAMP1, CTSL, NPC2, CTSK, PSAP, PPT1, DNASE2, CTSD, LGMN, CTSB, ATP6V1G1), in particular cathepsins with cysteine-type peptidase activity (unpublished data). The cytosolic serine hydroxy methyltransferase (SHMT1), which is responsible for converting serine to glycine and vice-versa, providing one-carbon units for the synthesis of methionine, thymidylate, and purines was downregulated in galactose at the protein level as well as the transcript level (Fig. 3.4B and 3.2A, B).

The most prominent group of proteins upregulated in galactose are implicated in endoplasmic reticulum stress (unpublished data). Furthermore, several transporters responsible for providing glycolysis and the TCA cycle with substrates, SLC2A1/A3 and SLC2A14 (glucose carrier) and SLC7A1/A2 (arginine, lysine and ornithine transporter) were upregulated. Lastly, we observed an increase in proteins of glutathione metabolism, GSTP1, microsomal glutathione S-transferase (MGST1), and thioredoxin domain containing 12 (TXNDC12) (Fig. 3.3B, unpublished data).

To improve the depth of the proteomic study, we used the ‘MetaboAnalyst’ tool for the integration of proteomic and metabolomic data, which allows one to perform pathway enrichment analysis based on differentially detected metabolites and expressed proteins (Fig. 3.4C). We used the degree of the node (number of nodal connections) to define our

enrichment analysis. Nodes with more connections, so-called hubs, have a higher impact in the pathway and, when affected, influence the enrichment more than a less connected node. Glycolysis (ALDOA, LDHA, ENO1, GAPDHS, PGK1, lactic acid, pyruvic acid), the synthesis and degradation of ketone bodies (ACAT2, 3-hydroxy-3-methylglutaryl-CoA), and pyruvate metabolism (LDHA, ACAT2, lactic acid, pyruvic acid) were the most highly induced pathways under glucose conditions (Fig. 3.4C, S3.3). The increase of 3-hydroxy-3-methyl-glutaryl-CoA (HMG-CoA) indicates a stalled mevalonate pathway, responsible for the synthesis of cholesterol and other isoprenoids (Fig. 3.3C). The rate limiting step of the mevalonate pathway is in the conversion of HMG-CoA to mevalonate by HMG reductase, which itself is inactivated by high levels of AMP. Therefore, in addition to TCA cycle stalling due to high levels of NADH, there was a reduction of anabolic cellular metabolism due to high levels of AMP. The integration of proteins with metabolites revealed a downregulation of the TCA cycle (DLD, OGDH, MDH2, cis-aconitic acid, succinic acid, citric acid), pyruvate metabolism (PKLR, MDH2, ALDH3A2, DLD, malonyl-CoA), and glyoxylate and dicarboxylate metabolism (MDH2, CAT, citric acid, cis-aconitic acid, glycine).

In galactose on the other hand we detected an up-regulation of alanine, aspartate and glutamate metabolism (ADSL, aspartic acid, adenylsuccinic acid, argininosuccinic acid, pyruvic acid, ureidosuccinic acid, gamma-aminobutyric acid), glutathione metabolism (ANPEP, TXNDC12, GSTP1, MGST1, oxidized glutathione, NADP) as well as glycolysis and gluconeogenesis (LDHAL6B, LDHA, ENO2, ENO3, PGAM1, PGAM4, TPI1, pyruvate). However, the absence of cellular lactate and other intermediates of glycolysis at the metabolite level in galactose (Fig. 3.3C) demonstrates that glycolysis does not occur in patient as well as rescue cells in galactose medium.

Integrating the downregulated metabolites and proteins revealed a downregulation of the TCA cycle (DLD, SUCLA2, SUCLG1, IDH3A, MDH2, PDHA1, PDHB, FH, fumaric acid, cis-aconitic acid). The TCA cycle and mitochondrial activity is normally upregulated in galactose condition in control cells (Aguer et al., 2011, Lane et al., 2015, Ostergaard et al., 2001).

In essence, the TCA cycle and the mitochondrial respiratory chain complex I were downregulated in both glucose and galactose This energy deficit could be compensated by high glycolytic activity in patient in glucose, but not in galactose. Furthermore, the synthesis of cholesterol was inhibited through high levels of AMP stalling the mevalonate pathway and

consequently accumulating HMG-CoA. And lastly glutathione related proteins were upregulated in both conditions, indicating an increased need to deal with mitochondrial oxidative stress.

Metabolic dysfunction leads to canonical ER stress response in patient in galactose

The upregulation of ATF6-mediated targets at the protein level (unpublished data) and the fact that mitochondria and the ER are tightly linked organelles led us to analyse the integrated stress response in both organelles. Coordinate expression of the mitochondrial unfolded protein response and the integrated stress response of the ER has been proposed previously (Melber & Haynes, 2018). The activation of the integrated stress response has also been described in control cells in galactose (Soustek et al., 2018). In response to unfolded protein in the ER protein kinases like PERK and IRE1/ERN1 release a folding chaperone called binding immunoglobulin protein (BiP/GRP78/HSPA5) and oligomerize. Other stresses are sensed by four different kinases such as amino acid stress (GCN2), hypoxia (HRI), and double-stranded RNA through viral infection (PKR) initiating the ISR through the phosphorylation of eukaryotic translation factor 2 alpha (eIF2alpha) (Pakos-Zebrucka et al., 2016). This results in the global attenuation of protein synthesis, and the selective translation of stress response proteins. Transcript levels of EIF2AK2 (PKR), and EIF2AK3 (PERK) were upregulated and as were the levels of the PERK and GCN2 proteins in patient cells in galactose (Fig. 3.5A). However, we did not observe a change in phosphorylated PERK, GCN2 or consequently eIF2alpha (Fig. 3.5B). The IRE1 pathway on the other hand is independent of eIF2alpha activation. IRE1 phosphorylates JUN N-terminal kinase (JNK), and also serves as an endonuclease splicing the mRNA of X-Box Binding Protein 1 (XBP1), removing a premature stop codon (Huang et al., 2019). Patient cells in galactose exhibit the integrated stress response through the activation of IRE1 and XBP1 and not through the phosphorylation of eIF2alpha (Fig. 3.5A, B). Consistent with this we observed an upregulation of transcripts involved in cytoplasmic and mitochondrial translation (Fig. 3.1C, 3.5C). The activation of IRE1 is often accompanied by the phosphorylation of JNK (Urano et al., 2000). However, the phosphorylation of both JNK isoforms p54 and p46 was completely abolished in patient cells in galactose (Fig. 3.5B). Concomitantly, many dual specific phosphatases responsible for the dephosphorylation of JNK were upregulated at the transcript level (Fig. 3.5D).

The activation of IRE1 was associated with the increased translation of several ER quality control genes including transcription factors ATF3 and ATF4, proteases, CHOP/DDIT3 and the cellular oxygen sensor EGLN3 (Fig. 3.5A, B, D). Interestingly, the enzyme recruiting the protein phosphatase PP1, which dephosphorylates eIF2alpha and therefore attenuates the ISR, protein phosphatase GADD34 (PPP1R15A), was upregulated at the transcript level but not the protein level, possibly indicating a transcriptional response for prolonged ISR signalling (Fig. 3.5A, B).

Two metabolic cytokines, fibroblast growth factor 21 (FGF21) and Growth Differentiation Factor 15 (GDF15), associated with mitochondrial disease and proposed as potential biomarkers, are often activated concomitantly with the integrated stress response (Lehtonen et al., 2016, Scholle et al., 2018). Protein levels of both FGF21 and GDF15 as well as transcript levels of GDF15 were upregulated (Fig. 3.5A, E). GDF15 transcript levels were upregulated even in glucose medium (Fig. 3.5A). Lastly, comparing the patient in galactose to the patient in glucose changed the transcripts in the same direction and has the tendency to have higher changes than the 'Galactose' condition (Fig. S3.4).

Metabolic dysfunction leads to an activation of the mitochondrial unfolded protein response and increase in cell death

The upregulation of the integrated stress response in the ER as well as the increase of FGF21 and GDF15 led us to analyse known players of the mitochondrial unfolded protein response in more detail (Fig. 3.6A). SIRT3, a mitochondrial NAD^+-dependent protein deacetylase that affects gene expression in the nucleus (Scher et al., 2007), interacts with FOXO3 to activate anti-oxidant genes like superoxide dismutase 2 (SOD2) and catalase (CAT) (Tseng et al., 2013). Although transcript levels of CAT and SOD2 were reduced in the patient (Fig. 3.6A), the level of CAT protein was increased (Fig. 3.6B). SIRT7 is another member of NAD^+-dependent protein deacetylases, which increases nuclear respiratory factor 1(NRF1) activity, and alleviating mitochondrial stress by reducing the expression of mitochondrial translation proteins (Mohrin et al., 2015), was also increased in our model. ATF4 and ATF5 are transcription factors that activate the mitochondrial unfolded protein response (Teske et al., 2013). Transcripts for ATF4 and ATF5 were increased in patient cells in galactose medium consistent with the activation of the mitochondrial stress response. We saw a marked increase in the transcript level for the transcription coactivator peroxisome proliferation-activated receptor

gamma, coactivator 1 alpha (PPARGC1A, also known as PGC-1α), which enhances oxidative phosphorylation, mitochondrial biogenesis, antioxidant enzyme expression, and mitochondrial fatty acid oxidation (Fig. 3.6A) (Austin & St-Pierre, 2012, Cheng et al., 2018), but components of fatty acid catabolic pathway were transcriptionally downregulated (Fig. 3.1C). Transcripts for the downstream targets of the mitochondrial unfolded protein response, proteases including CLPP, HTRA2 and LONP1 and the heat shock proteins HSP70 (HSPA9), HSP60 (HSPD1) and HSP10 (HSPE1) were upregulated at the transcript and/or the protein level. Here too, the comparison of the patient in galactose versus patient in glucose, changed in the same direction than the comparison 'Galactose', underlining the marked changes of the patient in galactose (Fig. S3.5). Processes like autophagy and apoptosis are generally upregulated during the cellular stress response. In our model we could also identify an upregulation of markers of autophagy SQSTM1 (p62) and LC3 (MAP1LC3A/B) at the transcript and the protein level for the patient in galactose (Fig. 3.6C). An increase, particularly in the levels of LC3B are characteristic for a higher autophagic flux, which clears damaged cells in the patient cells in galactose (Glick et al., 2010). Moreover, we could also observe increased PARP and caspase 3 cleavage in patient cells in galactose (Fig. 3.6D).

In summary, we identified the activation of the integrated stress response particularly through the IRE1/XBP1 axis and not through the phosphorylation of eIF2alpha in patient cells in galactose. We identified an upregulation at the transcript and protein level of specific downstream targets like CHOP, CLPP, HTRA2, HSP60, HSP10, FGF21 and GDF15 acting to rescue the patient cells in galactose and no overall downregulation of transcription. Lastly, we could identify increased autophagic and apoptotic flux possibly induced by CHOP, however independent from the JNK pathway.

Discussion

This study illustrates the metabolic consequences of nutrient stress in cells harbouring the CHCHD10 p.R15L pathogenic variant. This variant causes a fundamental metabolic reorganization with a nutrient-dependent energy deficit and an activation of the integrated stress response in both the endoplasmic reticulum and mitochondria. The integrated stress response in the ER is activated through IRE1 and not phosphorylated eIF2alpha. Our findings implicate an essential role of CHCHD10 in mitochondrial energy metabolism, directly affecting the mitochondrial respiratory chain, and subsequently resulting in a global change of cellular metabolism. To date, six families carrying the CHCHD10 p. R15L variant (caused b y c.44C>A mutation) have been reported, and all patients present with muscle wasting and progressive motor neuron disease, characteristic signs of pure ALS (Johnson et al., 2014, Khan et al., 2017, Muller et al., 2014, Zhang et al., 2015). Other CHCHD10 variants, such as p.S59L and G66V, cause a much broader range of disease phenotypes including frontotemporal dementia, mitochondrial myopathy and spinal muscular atrophy (Bannwarth et al., 2014, Chaussenot et al., 2014, Penttila et al., 2015, Rubino et al., 2017). In all reported variants but one (CHCHD10 p.Q108P), disease onset is late and slowly progressive (Lehmer et al., 2018). CHCHD10 variants present with unique features of mitochondrial disease, which are rarely linked to neurodegenerative diseases like ALS and PD (Gorman et al., 2016).

Previous work exploring the role of CHCHD10 showed that the CHCHD10 p.R15L patient fibroblasts were unable to rely on mitochondrial respiration for energy production due to a complex I defect and therefore showed an increased use of glycolysis (Straub et al., 2018). Mitochondrial respiration in these cells could be rescued by expression of the wild-type CHCHD10 protein, suggesting that the mutation is haploinsufficient. In this study, we used the same cellular model to investigate changes in metabolites, transcripts and proteins in patient and rescued cells grown in glucose- and galactose- containing medium.

Despite numerous functional studies, the physiological role of CHCHD10 remains unknown. The deletion of the yeast orthologue *Mic17* in *S. cerevisiae* results in the reduction of mitochondrial oxygen consumption (Longen et al., 2009), implicating it in some aspect of oxidative metabolism. A link between energy metabolism and ALS has long been established, and reduced oxidative phosphorylation has been described previously for other genetic models (Jung et al., 2002, Mattiazzi et al., 2002, Menzies et al., 2002, Wiedemann et al., 2002). In

human cells, siRNA mediated knockdown of CHCHD10 does not result in a destabilization of OXPHOS complexes (unpublished data); however, two CHCHD10 variants have been reported to alter the OXPHOS complex assembly/stability. The CHCHD10 p.S59L variant was shown to destabilize complex V and lead to its disassembly (Bannwarth et al., 2014), and we previously showed the complex I defect in p.R15L patient cells was phenocopied by the CRISPR-Cas9 mediated knockout of CHCHD10 (Straub et al., 2018). Here, our proteomics data confirmed the downregulation of complex I subunits in patient cells in both glucose and galactose conditions (Fig. 3.4B, S3.3). Moreover, the transcripts for several factors involved in the complex I and IV assembly were downregulated in patient cells in galactose (Fig. 3.1C).

Nicotinamide adenine dinucleotide (NAD^+) is an essential redox molecule, which enables mitochondrial respiration through the transport of electrons. The ratio between the oxidized and reduced form (NADH) influences many cellular and mitochondrial processes (Stein & Imai, 2012). Generally, balanced levels of NAD^+ protect and sustain basal metabolic function and health in neurons. The depletion of NAD^+ leads to the activation of poly (ADP-ribose) polymerases, which synthesize ADP-ribose. In our model, levels of the reducing agent NADH was upregulated in the patient, whereas NAD^+ levels were unchanged, resulting in an increased NADH/NAD^+ ratio in glucose as well as galactose. The NADH level and therefore the level of reducing equivalents in mitochondria is balanced by the malate/aspartate shuttle. In patient cells in galactose, we identified an upregulation of the metabolite aspartate, GOT1 transcript, and a downregulation at the transcript level of the mitochondrial aspartate/glutamate carrier SLC25A12, all related to the malate-aspartate shuttle (Fig. 3.3G). In a state of electron transport chain deficiency and compromised aspartate export from mitochondria, which was present in patient cells in galactose, aspartate is synthesized by reductive glutamine metabolism from glutamine, which depends on GOT1 (Metallo et al., 2011, Mullen et al., 2011) (Fig. 3.3G). The synthesis of aspartate, usually achieved through oxidative glutamine metabolism, is necessary for proliferation (Birsoy et al., 2015). We previously analysed the growth of patient fibroblasts of which 20%, when put in galactose media undergo cell death, the remaining cells remain alive but only start proliferating after an adaption phase (Straub et al., 2018). This phenotype is not uncommon for cells with compromised oxidative metabolism, and was described to be more prevalent for complex I deficiencies (Robinson et al., 1992, Soustek et al., 2018). The upregulation of GOT1 in the patient cells likely indicates increased aspartate synthesis to help

patient cells adapt and eventually proliferate. And lastly, an increase in mitochondrial folate metabolism could result from an increased need of formate in the cytosol, supplied by mitochondria for purine and pyrimidine synthesis for growth (Zheng et al., 2018).

As mentioned above, the change in the NADH/NAD^+ ratio leads to an increase in ADP-ribose, which connects the NAD pool with the AMP pool (Dolle et al., 2013). Patient cells showed changes in nucleotide levels and an energy deficit in galactose. ATP and GTP levels were decreased whereas monophosphates IMP, AMP and GMP were markedly increased. The inability of patient cells to generate sufficient energy under the nutrient stress conditions, hints at the severity of the mitochondrial dysfunction in this model. Moreover, the imbalanced AMP/ATP ratio resulted in an increase of phosphorylated AMPK, which positively regulates signalling pathways that replenish ATP supplies (Herzig & Shaw, 2018). Mitochondrial biogenesis, autophagy and folate metabolism were upregulated to counteract the ATP deficit in patient cells in galactose. Interestingly, AMPK was previously shown to be activated in TDP-43 mouse spinal cords, and reducing AMPK activity lead to an increase in survival of motor neurons (Lim et al., 2012). It could, therefore, be advantageous to inhibit AMPK activation in order to rescue the CHCHD10 p.R15L variant induced phenotypes.

The NADH/NAD^+ and the AMP/ATP ratios also regulate the TCA cycle (Berg JM, 2002). Depletion of ATP generally activates, whereas increased levels of NADH block the enzymatic activity of certain proteins of the cycle. We identified a downregulation of metabolites and enzymes of the TCA cycle in patient cells in both glucose and galactose media, with more enzymes being affected in the galactose condition. At the same time, potential entry substrates of the TCA cycle, aspartate and pyruvate accumulated, whereas levels of entry substrates of glycolysis, glucose-6-phosphate and fructose-6-phosphate were largely decreased in patient in galactose. The reintroduction of wild-type CHCHD10 in patient cells rescued the very low entry substrates, glucose-6-phosphate and fructose-6-phosphate; however, glycolytic activity was not detectable. Taken together, there was a tendency to decrease TCA cycle flux, aspartate and pyruvate were used for cell proliferation instead (Fig. 3.3G). Interestingly, the supplied glutamate in the culture media was not sufficient to upregulate the TCA cycle to normal levels.

Recent studies of two ALS mouse models have demonstrated fundamental shifts in energy metabolism. A study describing an SOD1 mouse model identified a metabolic switch from glycolysis toward the use of lipids in muscle (Palamiuc et al., 2015). This switch is regulated by

the pyruvate dehydrogenase kinase 4 (PDK4), which phosphorylates the PDH complex and thereby redirects the metabolic flux through the TCA cycle from lipids instead of glucose (Palamiuc et al., 2015). Another study in a mouse model of CHCHD10 p.S59L, found that white fat tissue was almost entirely lost coinciding with an increase of the lipid metabolism regulating protein FGF21 (Anderson et al., 2019a). In our model, we identified an upregulation of PDK4 at the transcript level as well as FGF21 at the protein level, consistent with the absence of glycolytic flux in galactose medium. What role the lipid catabolism plays in our model could not be determined as acetoacetyl-CoA levels were not determined. However, the synthesis of lipids was possibly slightly increased in the rescue cells as the compound malonyl-CoA was increased in galactose.

Cellular proliferation is tightly linked to cellular stress and regulated cell death. The activation of the integrated stress response can be initiated through one of the following sensors in the ER: (1) the inositol-requiring enzyme 1 (IRE1); (2) the extrinsic sensors PERK, PKR, GCN2, HRI, sensing unfolded protein, viral infection, amino acid deprivation and hypoxia, respectively; and (3) the activating transcription factor 6 (ATF6) (Pakos-Zebrucka et al., 2016). The activation of IRE1 leads to the splicing of XBP1, which renders the protein transcriptionally active and initiates the upregulation of stress target proteins. Moreover, IRE1 promotes a process called 'regulated IRE1-dependent decay' (RIDD), which degrades mRNAs of ER-targeted proteins to reduce the load of incoming proteins into the ER (Hollien & Weissman, 2006). And lastly, IRE1 activates the JNK pathway through the phosphorylation of JNK, which regulates gene expression and apoptosis (Urano et al., 2000). The phosphorylation of eiF2alpha through PERK, PKR, GCN2 or PERK on the other hand results in an overall decrease of global cellular protein synthesis, but a specific increase of proteins which are needed for the stress response and survival (Pakos-Zebrucka et al., 2016). Recently, two groups revealed the activation of the integrated stress response for the CHCHD10 variant p.S59L and the double knock-out of CHCHD10 and CHCHD2 in mouse (Anderson et al., 2019a, Liu et al., 2019). CHCHD10 p.S59L aggregated in a knock-in (KI) mouse model and thereby induced the activation of mTORC1, the increase of transcription factors specific for the stress response, the secretion of metabolic cytokines FGF21 and GDF15, the upregulation of the serine and one-carbon metabolism, and the downregulation of the respiratory chain complexes (Anderson et al., 2019a). Although the p.S59L CHCHD10 variant appeared to act through a dominant gain of function mechanism

(Anderson et al., 2019a), the p.R15L CHCHD10 variant through a haploinsufficient mechanism (Straub et al., 2018), and the double-knock-out presented a total lack of protein, in all three models the integrated stress response was upregulated. Our results show that the integrated stress response was activated through the IRE1/XBP1 axis and not through the phosphorylation of eIF2alpha in CHCHD10 p.R15L patient cells under nutrient stress conditions. This activation induced the transcription of characteristic ER stress survival proteins, however no general attenuation of translation. Moreover, we did not identify an activation of mTOR but rather an inhibition through the phosphorylation of AMPK. Furthermore, we observed increased autophagic and apoptotic flux, which was regulated through increased CHOP levels but not phosphorylated JNK. Phosphorylated JNK has been shown to be involved in apoptosis through the phosphorylation of BcL2 family of proteins (Tsuruta et al., 2004). The JNK1 and JNK2 double knock-out cells are resistant to apoptosis and interestingly CHCHD10 mutant cells have also been found to be less sensitive to apoptotic cell death (Genin et al., 2016, Tournier et al., 2000). Considering our results, we can speculate that CHCHD10 variants cause abnormalities in the homeostasis of healthy cells through the inhibition of JNK phosphorylation and the upregulation of XBP1. The knockdown of XBP1 led to an increase in macroautophagy in vivo in other ALS models, and could comprise a valuable starting point for future research studying CHCHD10 related disorders (Hetz et al., 2009).

In summary, our study describes how the CHCHD10 p.R15L variant affects mitochondrial metabolism, especially in nutrient stress conditions (Fig. 3.7). The complex I deficiency leads to an increased NADH/NAD^+ ratio, which is exacerbated in galactose, where the cell relies solely on mitochondria for energy production. The cell responds to the proliferation defect associated with the energy deficit, through the synthesis of aspartate from malate through GOT1 and the upregulation of the mitochondrial folate metabolism to supply formate to the cytosol. This process as well as the high levels of NADH result in diminished activity of the TCA cycle. High levels of AMP, and therefore the AMP/ATP ratio, result in increased phosphorylation of AMPK with the activation of catabolic processes on one hand and the deactivation of mTOR on the other hand. These metabolic changes activate the integrated stress response in the ER through the IRE1/XBP1 axis and the unfolded protein response in mitochondria. Finally, the patient cells either survive the existing nutrient stress by adapting their metabolism over time or undergo apoptosis, through a JNK independent mechanism as a result of the activation of the integrated

stress response. We can speculate, that in motor neurons, the specific cells affected by ALS, are more susceptible to mitochondrial dysfunction and potentially suffer damage much earlier in limited nutrient conditions than fibroblasts. It is known that ageing results in decreased neuronal uptake of glucose therefore rendering motor neurons harbouring CHCHD10 p.R15L variant more susceptible to cell death in the ageing individual (Yin et al., 2016). We therefore propose the careful consideration of targeting mitochondrial metabolism and the integrated stress response for potential treatments in ALS models of CHCHD10, and potentially Parkinson models of CHCHD2.

Materials and Methods

Human studies

The investigation of cell lines was approved by the institutional review board of the Montreal Neurological Institute, McGill University.

Cell lines and media

A primary fibroblast culture was previously established from a heterozygous carrier of c.44G>T (p.R15L) (patient DNA #8807) diagnosed with sporadic ALS at age 54 (involving his upper limb) and died at the age of 69 (Straub et al., 2018, Zhang et al., 2015). The variant CHCHD10 p.R15L, has been associated with ALS in several independent studies (Johnson et al., 2014, Muller et al., 2014, Zhang et al., 2015). Fibroblasts stably overexpressing *CHCHD10* in patient cells (rescue) were engineered using retroviral vectors as described previously (Lochmuller et al., 1999, Straub et al., 2018). Cells were cultivated in 4.5 g/l glucose DMEM supplemented with 10% fetal bovine serum (FBS) and 5% pen/strep, at 37 °C in an atmosphere of 5% CO_2. For carbon source-dependent experiments, fibroblasts were cultivated for two days in DMEM with 10% dialyzed FBS supplemented with either 4.5 g/l glucose or 4.5 g/l galactose before harvesting for 'omics' experiments.

Mitochondrial isolation

Fibroblasts were washed twice with phosphate buffered saline (PBS), resuspended in ice-cold buffer (250 mM sucrose,10 mM Tris–HCl, pH 7.4), and homogenized by nitrogen cavitation under 500 psi pressure for 5 min. A post-nuclear supernatant was obtained by centrifugation of the samples twice for 10 min at 600 × *g*. Mitochondria were pelleted by centrifugation for 10 min at 10 000 × *g* and washed once in the same buffer. Protein concentration was determined using the Bradford assay.

Antibodies

Antibodies directed against the following proteins were used in this study: CHCHD10 (Sigma, HPA003440), CHCHD2 (Sigma, HPA027407) SDHA (abcam, ab14715), AMPK (Cell Signaling, 2532), p-AMPK (Thr172) (Cell Signaling, 2535), AKT (Cell Signaling, 9272S), p-AKT (Cell Signaling, 4060S), mTOR (Cell Signaling, 2983P), p-mTOR (Cell Signaling, 5536P), S6 (Cell Signaling, 2217), p-S6 (Cell Signaling, 4858), SDHA (abcam, ab14715), CLPP (Proteintech, 15698-1-1AP), HTRA2 (Proteintech, 15775-1-AP), HSP60 (Santa Cruz, sc-136291), CAT (Abclonal, A11777), HSP10 (Santa Cruz, SC-376313), LC3 (Cell Signaling, D3U4C), SQSTM1 (Cell Signaling, 8025), PERK (Cell Signaling, 5683), p-eIF2α Ser 51 (SIGMA, SAB4504388), ERN1 (Cell Signaling, 3294), BIP (abcam, ab21685), XBP1 (Santa Cruz, sc-7160), FGF21 (abcam, ab171941), GDF15 (abcam, ab106006), GCN2 (Cell Signaling, 3302), p-JNK/SAPK (T183/Y185) (Cell Signaling, 9251), CHOP/DDIT3 (Cell Signaling, 5554), PARP (Cell Signaling, 9542), cleaved PARP (Cell Signaling, 9541), cleaved caspase 3 (Cell Signaling, 9661S).

SDS-PAGE and immunoblot analysis

Cells were pelleted and lysed with 1.5% *n*-dodecyl-D-maltoside (DDM) in PBS with cOmplete™ protease inhibitor (Roche) for 15 min on ice. Cells were centrifuged at 20,000 × g for 20 min at 4 °C. Protein concentration was determined using Bradford assay. 2x Laemmli buffer was added to 20-30 µg of protein and denatured at 55 °C for 15 min. The mixture was run on denaturing 8 % to 12.5 % polyacrylamide gels. Separated proteins were transferred onto a nitrocellulose membrane and immunoblot analysis was performed with the indicated antibodies in 5% milk in tris-buffered saline and Tween 20 (TBST).

RNA extraction and RNA sequencing

Total RNA from fibroblasts was extracted and purified by using RNeasy Mini kit (QIAGEN). RNA quality was tested on a 1% agarose gel and then RNA sequencing was performed by GENEWIZ on the Illumina HiSeq instrument.

Transcriptomic analysis

The sample analysis was done by GENEWIZ. The original read counts were normalized to adjust for various factors such as variations of sequencing yield between samples. These normalized read counts were used to accurately determine differentially expressed genes. Data quality assessments were performed to detect any samples that are not representative of their group, and thus, may affect the quality of the analysis. Using DESeq2, a comparison of gene expression between groups of samples was performed. Groups were defined as follows: (1) 'Glucose': patient in glucose versus rescue in glucose, (2) 'Galactose': patient in galactose versus rescue in glucose, (3) 'Patient': patient in galactose versus patient in glucose and (4) 'Rescue': rescue in galactose versus rescue in glucose. The Wald test was used to generate p-values and log2 fold changes. Genes with an adjusted p-value < 0.05 and absolute log2 fold change > 1 were considered as differentially expressed genes. RNA sequencing data was deposited to NCBI Gene Expression Omnibus (GEO), GSE144725.

Gene ontology analysis

Gene ontology (GO) analysis of significant differentially expressed transcripts was performed using the annotation tool ENRICHR (https://amp.pharm.mssm.edu/Enrichr/, GO_BP 2018), focusing on the GO term of biological processes (Chen et al., 2013, Kuleshov et al., 2016). As an input, gene symbols of genes passing the cut off of log2 fold change of $\gtrless \pm 0.3$ were used. A maximum p-value of 0.05 was chosen to select only significant enrichment.

Metabolite extraction and analysis

Metabolite extraction was performed according to the protocol of Human Metabolome Technologies, Inc. Briefly, 5 million cells where seeded in four replicates for each condition, one for counting and three for the collection of metabolites in three independent biological replicates. The culture medium was aspirated from each culture plate and cells were washed twice with washing buffer (5% w/w mannitol solution). The washing buffer was aspirated and methanol (LC/MS grade) together with an internal standard solution was added to extract metabolites. Cell extracts were centrifuged for 5 min at 2,300 × g at 4 °C. The supernatant was transferred into ultracentrifuge filter cups and centrifuged at 9,000 × at 4 °C for 3 hours. The tube was set up in a

centrifugal evaporator for 6 hours to evaporate the supernatant and obtain the metabolites as precipitate. Metabolites were quantified by Human Metabolome Technologies, Inc. Metabolic pathway analysis was performed using the integrative tool for joint pathway analysis in the MetaboAnalyst 4.0 platform (http://www.metaboanalyst.ca; (Chong et al., 2018)). Metabolites and proteins were selected with a cut-off of log2 fold change of $\gtrless \pm 0.2$ and a p-value < 0.05. Selected parameters were: hypergeometric test for enrichment analysis, degree centrality for topology analysis, metabolic pathways for pathway database and 'combine query' as the integration method. Metabolomic data sets will be deposited to 'MetaboLights'.

Proteome extraction and analysis

Fibroblasts were grown to 90% confluency in 15 cm dishes to lead to a minimum of 2×10^6 cells per condition. Cells were rinsed 2-3 times with 1x PBS to remove cell culture media and pelleted at 600 × g. Cells were lysed with lysis buffer (50 mM HEPES, 1% SDS, 150 mM NaCl). The lysate was centrifuged at 16,000 × g for 10 minutes at 4 °C. Protein concentration was determined in the supernatant by BCA Protein Assay Kit (Thermo Fisher Scientific, #23227). 100 µg of protein was transferred into a new tube and the final volume was adjusted to 100 µL with 100 mM triethylammonium bicarbonate (TEAB). 5 µL of 200 mM tris(2-carboxyethyl)phosphine) (TCEP) was added and samples were incubated at 55 °C for 1 hour. 5 µL of 375 mM iodoacetamide was added to the mix and let stand for 30 minutes protected from light at room temperature. 600 µL of pre-chilled acetone (-20 °C) was added and the mix was put at -20 °C over-night to precipitate. Samples were centrifuged at 8000 × g for 10 minutes at 4 °C. The tubes were carefully inverted to decant the acetone and let dry for 30 min at room temperature. Samples were digested, labelled and analysed by mass spectrometry on an Orbitrap (Thermo Scientific) at the Institute de Recherches Cliniques (IRCM) de Montreal. The isobaric labelling of the peptides was performed using 10-plex TMT reagents (Thermo Fisher Scientific). Differentially expressed proteins were identified by performing Welch's t-statistic test, comparing patient cells with rescue cells in glucose and galactose. Values were normalized by subtraction of the mean from the log2 values of the comparison ratios. The mass spectrometry proteomics data sets will be deposited to the ProteomeXchange Consortium.

Bioinformatic and statistical analysis

Pathways, transcripts and proteins selected in each condition were filtered after Benjamini-Hochberg correction at an adjusted p-value < 0.05 (FDR 5%). All data analysis and plots were generated using R and RStudio and modified using Adobe Illustrator CC. For the rest of the analysis, data were expressed as mean ± SEM, and p-values were calculated using two-tailed Welch's t-test for pairwise comparisons of metabolites and proteins and the Wald as well as the Wilcoxon test for transcripts. Statistical tests were performed using RStudio and GraphPad Prism 6.0 (*, $P < 0.05$; **, $P < 0.01$; ***, $P < 0.001$; $n \geq 3$).

Acknowledgements

We thank Hana Antonicka, Aurel Besse-Patin, for fruitful discussions and critique of the manuscript and Logan Walsh for the help with the analysis of the RNAseq data. This work was supported by grants from the CIHR, Parkinson Canada, and the Muscular Dystrophy Association to EAS.

Author contribution

IR planned and executed all the experiments. WW executed several immunoblot experiments. EAS guided the research and proof read the manuscript.

Conflict of interest statement: The authors report no conflict of interest.

References

Aguer C, Gambarotta D, Mailloux RJ, Moffat C, Dent R, McPherson R, Harper ME (2011) Galactose enhances oxidative metabolism and reveals mitochondrial dysfunction in human primary muscle cells. *PLoS One* 6: e28536

Anderson CJ, Bredvik K, Burstein SR, Davis C, Meadows SM, Dash J, Case L, Milner TA, Kawamata H, Zuberi A, Piersigilli A, Lutz C, Manfredi G (2019a) ALS/FTD mutant CHCHD10 mice reveal a tissue-specific toxic gain-of-function and mitochondrial stress response. *Acta Neuropathol* 138: 103-121

Austin S, St-Pierre J (2012) PGC1alpha and mitochondrial metabolism--emerging concepts and relevance in ageing and neurodegenerative disorders. *J Cell Sci* 125: 4963-71

Bannwarth S, Ait-El-Mkadem S, Chaussenot A, Genin EC, Lacas-Gervais S, Fragaki K, Berg-Alonso L, Kageyama Y, Serre V, Moore DG, Verschueren A, Rouzier C, Le Ber I, Auge G, Cochaud C, Lespinasse F, N'Guyen K, de Septenville A, Brice A, Yu-Wai-Man P et al. (2014) A mitochondrial origin for frontotemporal dementia and amyotrophic lateral sclerosis through CHCHD10 involvement. *Brain* 137: 2329-45

Berg JM TJ, Stryer L. (2002) Biochemistry. *New York: W H Freeman* 5th edition.

Birsoy K, Wang T, Chen WW, Freinkman E, Abu-Remaileh M, Sabatini DM (2015) An Essential Role of the Mitochondrial Electron Transport Chain in Cell Proliferation Is to Enable Aspartate Synthesis. *Cell* 162: 540-51

Bond P (2016) Regulation of mTORC1 by growth factors, energy status, amino acids and mechanical stimuli at a glance. *J Int Soc Sports Nutr* 13: 8

Brockmann SJ, Freischmidt A, Oeckl P, Muller K, Ponna SK, Helferich AM, Paone C, Reinders J, Kojer K, Orth M, Jokela M, Auranen M, Udd B, Hermann A, Danzer KM, Lichtner P, Walther P, Ludolph AC, Andersen PM, Otto M et al. (2018) CHCHD10 mutations p.R15L and p.G66V cause motoneuron disease by haploinsufficiency. *Hum Mol Genet* 27: 706-715

Calvo SE, Clauser KR, Mootha VK (2016) MitoCarta2.0: an updated inventory of mammalian mitochondrial proteins. *Nucleic Acids Res* 44: D1251-7

Chaussenot A, Le Ber I, Ait-El-Mkadem S, Camuzat A, de Septenville A, Bannwarth S, Genin EC, Serre V, Auge G, French research network on FTD, Ftd ALS, Brice A, Pouget J, Paquis-Flucklinger V (2014) Screening of CHCHD10 in a French cohort confirms the involvement of this gene in frontotemporal dementia with amyotrophic lateral sclerosis patients. *Neurobiol Aging* 35: 2884 e1-4

Chen EY, Tan CM, Kou Y, Duan Q, Wang Z, Meirelles GV, Clark NR, Ma'ayan A (2013) Enrichr: interactive and collaborative HTML5 gene list enrichment analysis tool. *BMC Bioinformatics* 14: 128

Cheng CF, Ku HC, Lin H (2018) PGC-1alpha as a Pivotal Factor in Lipid and Metabolic Regulation. *Int J Mol Sci* 19

Chio A, Mora G, Sabatelli M, Caponnetto C, Traynor BJ, Johnson JO, Nalls MA, Calvo A, Moglia C, Borghero G, Monsurro MR, La Bella V, Volanti P, Simone I, Salvi F, Logullo FO, Nilo R, Battistini S, Mandrioli J, Tanel R et al. (2015) CHCH10 mutations in an Italian cohort of familial and sporadic amyotrophic lateral sclerosis patients. *Neurobiol Aging* 36: 1767 e3-1767 e6

Chong J, Soufan O, Li C, Caraus I, Li S, Bourque G, Wishart DS, Xia J (2018) MetaboAnalyst 4.0: towards more transparent and integrative metabolomics analysis. *Nucleic Acids Res* 46: W486-W494

Dolle C, Rack JG, Ziegler M (2013) NAD and ADP-ribose metabolism in mitochondria. *FEBS J* 280: 3530-41

Dols-Icardo O, Nebot I, Gorostidi A, Ortega-Cubero S, Hernandez I, Rojas-Garcia R, Garcia-Redondo A, Povedano M, Llado A, Alvarez V, Sanchez-Juan P, Pardo J, Jerico I, Vazquez-Costa J, Sevilla T, Cardona F, Indakoechea B, Moreno F, Fernandez-Torron R, Munoz-Llahuna L et al. (2015) Analysis of the CHCHD10 gene in patients with frontotemporal dementia and amyotrophic lateral sclerosis from Spain. *Brain* 138: e400

Genin EC, Bannwarth S, Lespinasse F, Ortega-Vila B, Fragaki K, Itoh K, Villa E, Lacas-Gervais S, Jokela M, Auranen M, Ylikallio E, Mauri-Crouzet A, Tyynismaa H, Vihola A, Auge G, Cochaud C, Sesaki H, Ricci JE, Udd B, Vives-Bauza C et al. (2018) Loss of MICOS complex integrity and mitochondrial damage, but not TDP-43 mitochondrial localisation, are likely associated with severity of CHCHD10-related diseases. *Neurobiol Dis* 119: 159-171

Genin EC, Madji Hounoum B, Bannwarth S, Fragaki K, Lacas-Gervais S, Mauri-Crouzet A, Lespinasse F, Neveu J, Ropert B, Auge G, Cochaud C, Lefebvre-Omar C, Bigou S, Chiot A, Mochel F, Boillee S, Lobsiger CS, Bohl D, Ricci JE, Paquis-Flucklinger V (2019) Mitochondrial defect in muscle precedes neuromuscular junction degeneration and motor neuron death in CHCHD10(S59L/+) mouse. *Acta Neuropathol* 138: 123-145

Genin EC, Plutino M, Bannwarth S, Villa E, Cisneros-Barroso E, Roy M, Ortega-Vila B, Fragaki K, Lespinasse F, Pinero-Martos E, Auge G, Moore D, Burte F, Lacas-Gervais S, Kageyama Y, Itoh K, Yu-Wai-Man P, Sesaki H, Ricci JE, Vives-Bauza C et al. (2016) CHCHD10 mutations promote loss of mitochondrial cristae junctions with impaired mitochondrial genome maintenance and inhibition of apoptosis. *EMBO Mol Med* 8: 58-72

Glick D, Barth S, Macleod KF (2010) Autophagy: cellular and molecular mechanisms. *J Pathol* 221: 3-12

Gorman GS, Chinnery PF, DiMauro S, Hirano M, Koga Y, McFarland R, Suomalainen A, Thorburn DR, Zeviani M, Turnbull DM (2016) Mitochondrial diseases. *Nat Rev Dis Primers* 2: 16080

Herzig S, Shaw RJ (2018) AMPK: guardian of metabolism and mitochondrial homeostasis. *Nat Rev Mol Cell Biol* 19: 121-135

Hetz C, Mollereau B (2014) Disturbance of endoplasmic reticulum proteostasis in neurodegenerative diseases. *Nat Rev Neurosci* 15: 233-49

Hetz C, Thielen P, Matus S, Nassif M, Court F, Kiffin R, Martinez G, Cuervo AM, Brown RH, Glimcher LH (2009) XBP-1 deficiency in the nervous system protects against amyotrophic lateral sclerosis by increasing autophagy. *Genes Dev* 23: 2294-306

Hoang T, Smith MD, Jelokhani-Niaraki M (2012) Toward understanding the mechanism of ion transport activity of neuronal uncoupling proteins UCP2, UCP4, and UCP5. *Biochemistry* 51: 4004-14

Hollien J, Weissman JS (2006) Decay of endoplasmic reticulum-localized mRNAs during the unfolded protein response. *Science* 313: 104-7

Huang S, Xing Y, Liu Y (2019) Emerging roles for the ER stress sensor IRE1alpha in metabolic regulation and disease. *J Biol Chem* 294: 18726-18741

Huang X, Wu BP, Nguyen D, Liu YT, Marani M, Hench J, Benit P, Kozjak-Pavlovic V, Rustin P, Frank S, Narendra DP (2018) CHCHD2 accumulates in distressed mitochondria and facilitates oligomerization of CHCHD10. *Hum Mol Genet* 27: 3881-3900

Hughes D, Mallucci GR (2019) The unfolded protein response in neurodegenerative disorders - therapeutic modulation of the PERK pathway. *FEBS J* 286: 342-355

Ito Y, Yamada M, Tanaka H, Aida K, Tsuruma K, Shimazawa M, Hozumi I, Inuzuka T, Takahashi H, Hara H (2009) Involvement of CHOP, an ER-stress apoptotic mediator, in both human sporadic ALS and ALS model mice. *Neurobiol Dis* 36: 470-6

Jaronen M, Goldsteins G, Koistinaho J (2014) ER stress and unfolded protein response in amyotrophic lateral sclerosis-a controversial role of protein disulphide isomerase. *Front Cell Neurosci* 8: 402

Johnson JO, Glynn SM, Gibbs JR, Nalls MA, Sabatelli M, Restagno G, Drory VE, Chio A, Rogaeva E, Traynor BJ (2014) Mutations in the CHCHD10 gene are a common cause of familial amyotrophic lateral sclerosis. *Brain* 137: e311

Jung C, Higgins CM, Xu Z (2002) Mitochondrial electron transport chain complex dysfunction in a transgenic mouse model for amyotrophic lateral sclerosis. *J Neurochem* 83: 535-45

Khan NA, Nikkanen J, Yatsuga S, Jackson C, Wang L, Pradhan S, Kivela R, Pessia A, Velagapudi V, Suomalainen A (2017) mTORC1 Regulates Mitochondrial Integrated Stress Response and Mitochondrial Myopathy Progression. *Cell Metab* 26: 419-428 e5

Kuleshov MV, Jones MR, Rouillard AD, Fernandez NF, Duan Q, Wang Z, Koplev S, Jenkins SL, Jagodnik KM, Lachmann A, McDermott MG, Monteiro CD, Gundersen GW, Ma'ayan A (2016) Enrichr: a comprehensive gene set enrichment analysis web server 2016 update. *Nucleic Acids Res* 44: W90-7

Kurzwelly D, Kruger S, Biskup S, Heneka MT (2015) A distinct clinical phenotype in a German kindred with motor neuron disease carrying a CHCHD10 mutation. *Brain* 138: e376

Lane AN, Fan TW (2015) Regulation of mammalian nucleotide metabolism and biosynthesis. *Nucleic Acids Res* 43: 2466-85

Lane RS, Fu Y, Matsuzaki S, Kinter M, Humphries KM, Griffin TM (2015) Mitochondrial respiration and redox coupling in articular chondrocytes. *Arthritis Res Ther* 17: 54

Lehmer C, Schludi MH, Ransom L, Greiling J, Junghanel M, Exner N, Riemenschneider H, van der Zee J, Van Broeckhoven C, Weydt P, Heneka MT, Edbauer D (2018) A novel CHCHD10 mutation implicates a Mia40-dependent mitochondrial import deficit in ALS. *EMBO Mol Med* 10

Lehtonen JM, Forsstrom S, Bottani E, Viscomi C, Baris OR, Isoniemi H, Hockerstedt K, Osterlund P, Hurme M, Jylhava J, Leppa S, Markkula R, Helio T, Mombelli G, Uusimaa J, Laaksonen R, Laaksovirta H, Auranen M, Zeviani M, Smeitink J et al. (2016) FGF21 is a biomarker for mitochondrial translation and mtDNA maintenance disorders. *Neurology* 87: 2290-2299

Lim MA, Selak MA, Xiang Z, Krainc D, Neve RL, Kraemer BC, Watts JL, Kalb RG (2012) Reduced activity of AMP-activated protein kinase protects against genetic models of motor neuron disease. *J Neurosci* 32: 1123-41

Liu Y-T, Huang X, Nguyen D, Dombi E, Springer DA, Poulton J, Sekine S, Narendra DP (2019) Loss of CHCHD2 and CHCHD10 activates OMA1 peptidase to disrupt mitochondrial cristae phenocopying patient mutations. *bioRxiv*: 773135

Lochmuller H, Johns T, Shoubridge EA (1999) Expression of the E6 and E7 genes of human papillomavirus (HPV16) extends the life span of human myoblasts. *Exp Cell Res* 248: 186-93.

Longen S, Bien M, Bihlmaier K, Kloeppel C, Kauff F, Hammermeister M, Westermann B, Herrmann JM, Riemer J (2009) Systematic analysis of the twin cx(9)c protein family. *J Mol Biol* 393: 356-68

Martinez-Reyes I, Chandel NS (2014) Mitochondrial one-carbon metabolism maintains redox balance during hypoxia. *Cancer Discov* 4: 1371-3

Mattiazzi M, D'Aurelio M, Gajewski CD, Martushova K, Kiaei M, Beal MF, Manfredi G (2002) Mutated human SOD1 causes dysfunction of oxidative phosphorylation in mitochondria of transgenic mice. *J Biol Chem* 277: 29626-33

Medinas DB, Gonzalez JV, Falcon P, Hetz C (2017) Fine-Tuning ER Stress Signal Transducers to Treat Amyotrophic Lateral Sclerosis. *Front Mol Neurosci* 10: 216

Melber A, Haynes CM (2018) UPR(mt) regulation and output: a stress response mediated by mitochondrial-nuclear communication. *Cell Res* 28: 281-295

Menzies FM, Cookson MR, Taylor RW, Turnbull DM, Chrzanowska-Lightowlers ZM, Dong L, Figlewicz DA, Shaw PJ (2002) Mitochondrial dysfunction in a cell culture model of familial amyotrophic lateral sclerosis. *Brain* 125: 1522-33

Metallo CM, Gameiro PA, Bell EL, Mattaini KR, Yang J, Hiller K, Jewell CM, Johnson ZR, Irvine DJ, Guarente L, Kelleher JK, Vander Heiden MG, Iliopoulos O, Stephanopoulos G (2011) Reductive glutamine metabolism by IDH1 mediates lipogenesis under hypoxia. *Nature* 481: 380-4

Mohrin M, Shin J, Liu Y, Brown K, Luo H, Xi Y, Haynes CM, Chen D (2015) Stem cell aging. A mitochondrial UPR-mediated metabolic checkpoint regulates hematopoietic stem cell aging. *Science* 347: 1374-7

Mullen AR, Wheaton WW, Jin ES, Chen PH, Sullivan LB, Cheng T, Yang Y, Linehan WM, Chandel NS, DeBerardinis RJ (2011) Reductive carboxylation supports growth in tumour cells with defective mitochondria. *Nature* 481: 385-8

Muller K, Andersen PM, Hubers A, Marroquin N, Volk AE, Danzer KM, Meitinger T, Ludolph AC, Strom TM, Weishaupt JH (2014) Two novel mutations in conserved codons indicate that CHCHD10 is a gene associated with motor neuron disease. *Brain* 137: e309

Ostergaard S, Olsson L, Nielsen J (2001) In vivo dynamics of galactose metabolism in Saccharomyces cerevisiae: metabolic fluxes and metabolite levels. *Biotechnol Bioeng* 73: 412-25

Pakos-Zebrucka K, Koryga I, Mnich K, Ljujic M, Samali A, Gorman AM (2016) The integrated stress response. *EMBO Rep* 17: 1374-1395

Palamiuc L, Schlagowski A, Ngo ST, Vernay A, Dirrig-Grosch S, Henriques A, Boutillier AL, Zoll J, Echaniz-Laguna A, Loeffler JP, Rene F (2015) A metabolic switch toward lipid use in glycolytic muscle is an early pathologic event in a mouse model of amyotrophic lateral sclerosis. *EMBO Mol Med* 7: 526-46

Penttila S, Jokela M, Bouquin H, Saukkonen AM, Toivanen J, Udd B (2015) Late onset spinal motor neuronopathy is caused by mutation in CHCHD10. *Ann Neurol* 77: 163-72

Ramsden DB, Ho PW, Ho JW, Liu HF, So DH, Tse HM, Chan KH, Ho SL (2012) Human neuronal uncoupling proteins 4 and 5 (UCP4 and UCP5): structural properties, regulation, and physiological role in protection against oxidative stress and mitochondrial dysfunction. *Brain Behav* 2: 468-78

Robinson BH, Petrova-Benedict R, Buncic JR, Wallace DC (1992) Nonviability of cells with oxidative defects in galactose medium: a screening test for affected patient fibroblasts. *Biochem Med Metab Biol* 48: 122-6

Ronchi D, Riboldi G, Del Bo R, Ticozzi N, Scarlato M, Galimberti D, Corti S, Silani V, Bresolin N, Comi GP (2015) CHCHD10 mutations in Italian patients with sporadic amyotrophic lateral sclerosis. *Brain* 138: e372

Rubino E, Brusa L, Zhang M, Boschi S, Govone F, Vacca A, Gai A, Pinessi L, Lopiano L, Rogaeva E, Rainero I (2017) Genetic analysis of CHCHD2 and CHCHD10 in Italian patients with Parkinson's disease. *Neurobiol Aging* 53: 193 e7-193 e8

Ryall JG, Dell'Orso S, Derfoul A, Juan A, Zare H, Feng X, Clermont D, Koulnis M, Gutierrez-Cruz G, Fulco M, Sartorelli V (2015) The NAD(+)-dependent SIRT1 deacetylase translates a metabolic switch into regulatory epigenetics in skeletal muscle stem cells. *Cell Stem Cell* 16: 171-83

Ryan M, Zaldivar Vaillant T, McLaughlin RL, Doherty MA, Rooney J, Heverin M, Gutierrez J, Lara-Fernandez GE, Pita Rodriguez M, Hackembruch J, Perna A, Vazquez MC, Musio M, Ketzoian CN, Logroscino G, Hardiman O (2019) Comparison of the clinical and genetic features of amyotrophic lateral sclerosis across Cuban, Uruguayan and Irish clinic-based populations. *J Neurol Neurosurg Psychiatry* 90: 659-665

Scher MB, Vaquero A, Reinberg D (2007) SirT3 is a nuclear NAD+-dependent histone deacetylase that translocates to the mitochondria upon cellular stress. *Genes Dev* 21: 920-8

Scholle LM, Lehmann D, Deschauer M, Kraya T, Zierz S (2018) FGF-21 as a Potential Biomarker for Mitochondrial Diseases. *Curr Med Chem* 25: 2070-2081

Shen S, He J, Tang L, Zhang N, Fan D (2017) CHCHD10 mutations in patients with amyotrophic lateral sclerosis in Mainland China. *Neurobiol Aging* 54: 214 e7-214 e10

Soustek MS, Balsa E, Barrow JJ, Jedrychowski M, Vogel R, Jan S, Gygi SP, Puigserver P (2018) Inhibition of the ER stress IRE1alpha inflammatory pathway protects against cell death in mitochondrial complex I mutant cells. *Cell Death Dis* 9: 658

Stein LR, Imai S (2012) The dynamic regulation of NAD metabolism in mitochondria. *Trends Endocrinol Metab* 23: 420-8

Straub IR, Janer A, Weraarpachai W, Zinman L, Robertson J, Rogaeva E, Shoubridge EA (2018) Loss of CHCHD10-CHCHD2 complexes required for respiration underlies the pathogenicity of a CHCHD10 mutation in ALS. *Hum Mol Genet* 27: 178-189

Teske BF, Fusakio ME, Zhou D, Shan J, McClintick JN, Kilberg MS, Wek RC (2013) CHOP induces activating transcription factor 5 (ATF5) to trigger apoptosis in response to perturbations in protein homeostasis. *Mol Biol Cell* 24: 2477-90

Thangaratnarajah C, Ruprecht JJ, Kunji ER (2014) Calcium-induced conformational changes of the regulatory domain of human mitochondrial aspartate/glutamate carriers. *Nat Commun* 5: 5491

Tournier C, Hess P, Yang DD, Xu J, Turner TK, Nimnual A, Bar-Sagi D, Jones SN, Flavell RA, Davis RJ (2000) Requirement of JNK for stress-induced activation of the cytochrome c-mediated death pathway. *Science* 288: 870-4

Tseng AH, Shieh SS, Wang DL (2013) SIRT3 deacetylates FOXO3 to protect mitochondria against oxidative damage. *Free Radic Biol Med* 63: 222-34

Tsuruta F, Sunayama J, Mori Y, Hattori S, Shimizu S, Tsujimoto Y, Yoshioka K, Masuyama N, Gotoh Y (2004) JNK promotes Bax translocation to mitochondria through phosphorylation of 14-3-3 proteins. *EMBO J* 23: 1889-99

Urano F, Wang X, Bertolotti A, Zhang Y, Chung P, Harding HP, Ron D (2000) Coupling of stress in the ER to activation of JNK protein kinases by transmembrane protein kinase IRE1. *Science* 287: 664-6

Wiedemann FR, Manfredi G, Mawrin C, Beal MF, Schon EA (2002) Mitochondrial DNA and respiratory chain function in spinal cords of ALS patients. *J Neurochem* 80: 616-25

Yin F, Sancheti H, Patil I, Cadenas E (2016) Energy metabolism and inflammation in brain aging and Alzheimer's disease. *Free Radic Biol Med* 100: 108-122

Zhang M, Xi Z, Zinman L, Bruni AC, Maletta RG, Curcio SA, Rainero I, Rubino E, Pinessi L, Nacmias B, Sorbi S, Galimberti D, Lang AE, Fox S, Surace EI, Ghani M, Guo J, Sato C, Moreno D, Liang Y et al. (2015) Mutation analysis of CHCHD10 in different neurodegenerative diseases. *Brain* 138: e380

Zheng Y, Lin TY, Lee G, Paddock MN, Momb J, Cheng Z, Li Q, Fei DL, Stein BD, Ramsamooj S, Zhang G, Blenis J, Cantley LC (2018) Mitochondrial One-Carbon Pathway Supports Cytosolic Folate Integrity in Cancer Cells. *Cell* 175: 1546-1560 e17

Zhou Q, Chen Y, Wei Q, Cao B, Wu Y, Zhao B, Ou R, Yang J, Chen X, Hadano S, Shang HF (2017a) Mutation Screening of the CHCHD10 Gene in Chinese Patients with Amyotrophic Lateral Sclerosis. *Mol Neurobiol* 54: 3189-3194

Figures

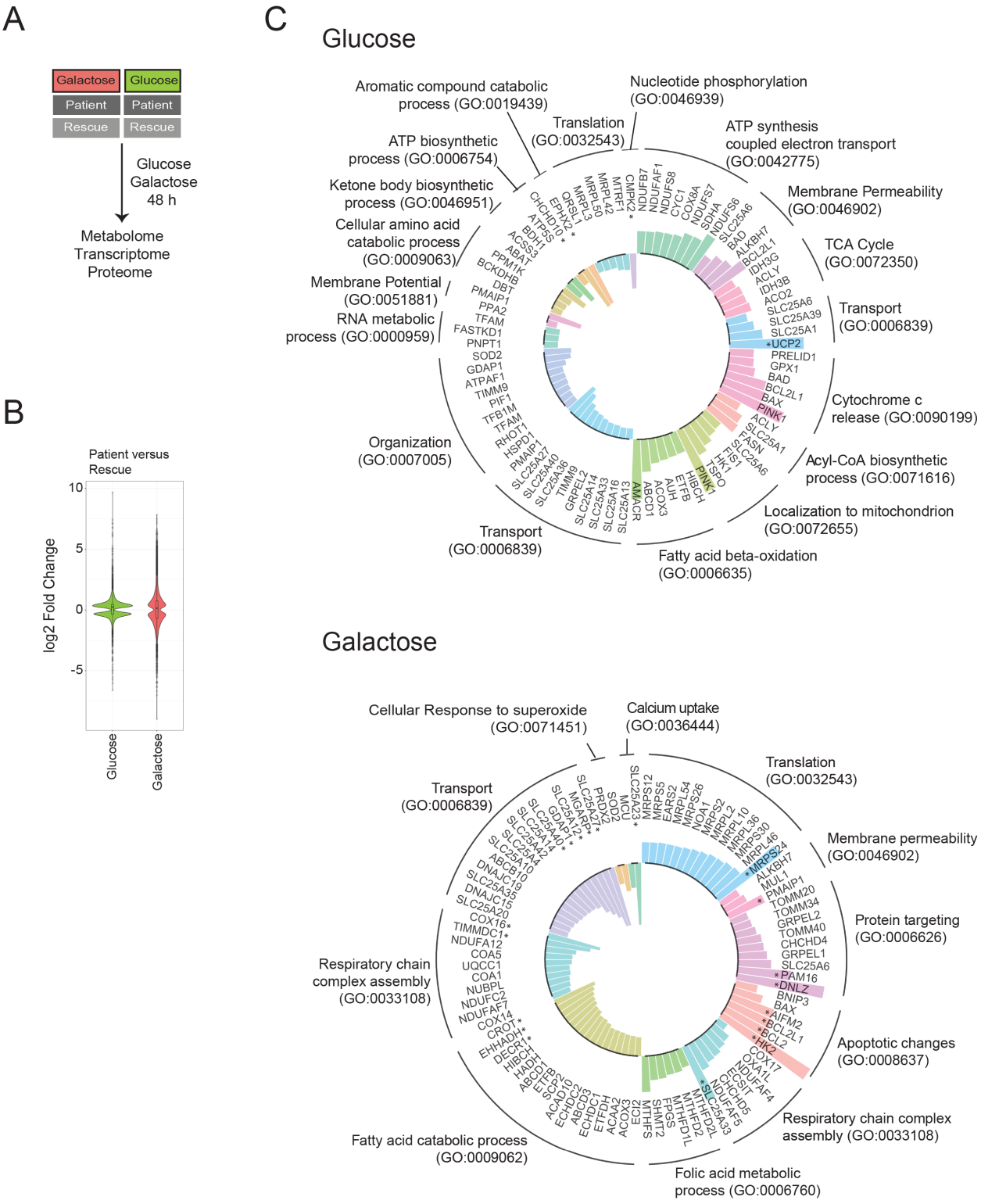

Figure 3.1 Disturbed biological processes revealed by RNAseq analysis.

(A) Schematic representation of the omics experiments. Patient and rescue cells were grown in glucose or galactose media for 48 h and subsequently, the metabolome, transcriptome and proteome were analysed.
(B) Violin Plot representing the distribution of log2 fold change of expression (patient vs rescue) in the two conditions ('Glucose' and 'Galactose') for significantly detected transcripts (FDR<0.05).
(C) Circular Bar Plot depicting mitochondrial transcripts with a minimum log2 fold change (patient vs rescue) of ±0.3 in 'Glucose' and 'Galactose', grouped based on the GO term: Biological Processes. Bars facing upwards from the inner circle represent the upregulated transcripts, and bars facing inwards represent the downregulated transcripts. Asterisk '*' indicates transcripts with a log2 fold change >1.

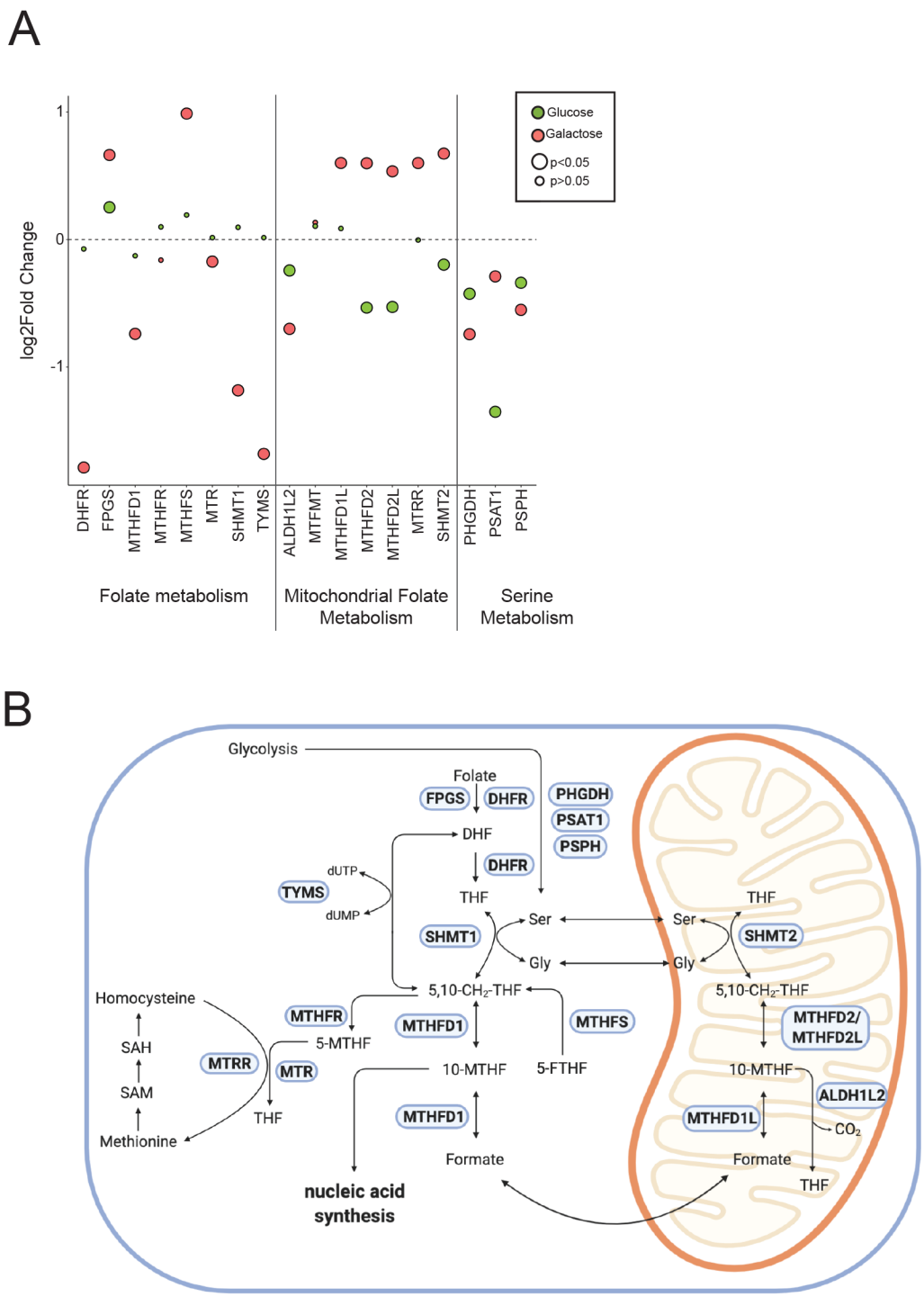

Figure 3.2 RNAseq analysis reveals changes in one-carbon metabolism.

(A) Dot plot representing the fold change of the transcripts of the folate and serine metabolism. Fold change is represented in log2 scale. Large circles represent significant values (FDR<0.05), small circles show non-significant values (FDR>0.05). 'Glucose' (green) represents the

comparison of patient versus rescue cells in glucose. ‘Galactose’ (red) represents the comparison of patient versus rescue cells in galactose.

(B) Graphical representation of enzymes and metabolites of the one-carbon metabolism. Selected enzymes are shown in blue boxes for cytosolic and mitochondrial folate metabolism as well as serine and methionine metabolism (created with *BioRender*).

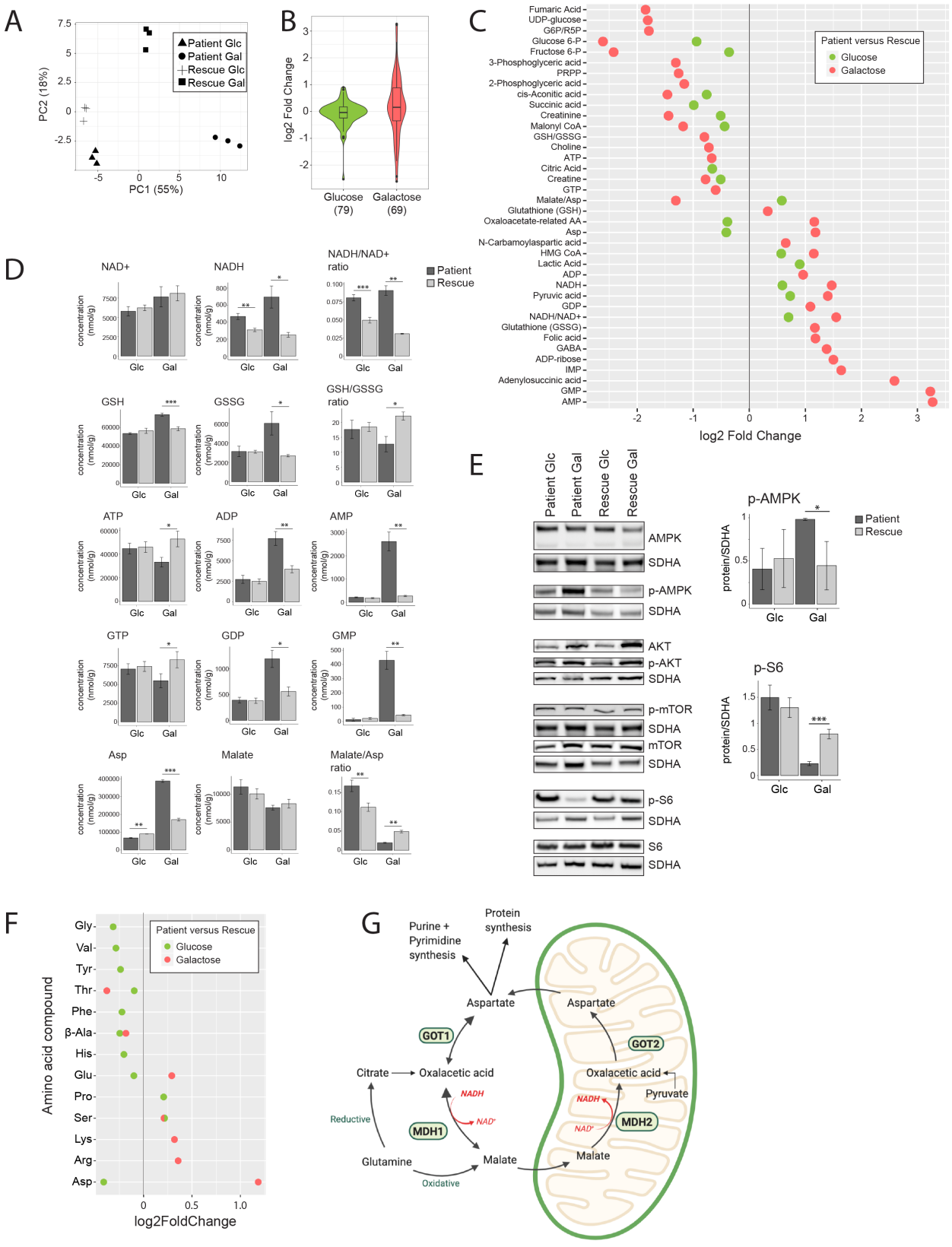
A
Patient Glc
Patient Gal
Rescue Glc
Rescue Gal
PC2 (18%)
PC1 (55%)
B
log2 Fold Change
Glucose (79)
Galactose (69)
C
Patient versus Rescue
Glucose
Galactose
log2 Fold Change
D
Patient
Rescue
NAD+
NADH
NADH/NAD+ ratio
GSH
GSSG
GSH/GSSG ratio
ATP
ADP
AMP
GTP
GDP
GMP
Asp
Malate
Malate/Asp ratio
concentration (nmol/g)
Glc
Gal
E
Patient Glc
Patient Gal
Rescue Glc
Rescue Gal
AMPK
SDHA
p-AMPK
AKT
p-AKT
p-mTOR
mTOR
p-S6
S6
p-AMPK
p-S6
protein/SDHA
F
Patient versus Rescue
Glucose
Galactose
Amino acid compound
log2FoldChange
G
Purine + Pyrimidine synthesis
Protein synthesis
Aspartate
GOT1
GOT2
Citrate
Oxalacetic acid
Pyruvate
NADH
NAD+
MDH1
MDH2
Reductive
Oxidative
Glutamine
Malate

Figure 3.3 Metabolomic analysis reveals a high NADH/NAD^+ ratio which stalls the TCA cycle in patient cells.

(A) Principal component analysis of the overall metabolomic profile. Symbols convey information about the four individual groups and their three replicates.

(B) Violin Plot representing the distribution of the log2 fold change (patient/rescue) for all measured metabolites. Box plots indicate the median and the first and third quartile. The number of metabolites in each group are indicated in parentheses below the graph.

(C) Dot plot representing the fold change of the most changed metabolites for each condition. Fold change is represented in log2 scale and the data show only metabolites with significant differences with a p-value <0.05. The p-value is computed by Welch's test.

(D) Bar plots representing the most significantly changed metabolites. Concentrations are depicted in nmol/g and ratios are pure ratios. Values for the patient cells are in dark grey and values for the rescue cells are in light grey. P-values were computed by Welch's test, *p<0.05, **p<0.01, ***p<0.001.

(E) Western blot analysis of proteins involved in the mTOR pathway. Whole cell extracts from patient and rescue fibroblasts grown in glucose and galactose for 2 days were separated by SDS-PAGE and probed with antibodies against indicated proteins. SDHA was used as a loading control. Bar plot indicates the quantification of the western blot analysis, where patient is depicted in dark grey and rescue in light grey, *p<0.05, **p<0.01, ***p<0.001.

(F) Dot plot representing the fold change of the most changed amino acid levels for each condition. Fold change is represented in log2 scale and data show only metabolites with significant differences with a p-value <0.05. The p-value is computed by Welch's test.

(G) Graphical representation of enzymes and metabolites of the malate aspartate shuttle. Selected enzymes are shown in green boxes for cytosolic and mitochondrial processes (created with *BioRender*).

A

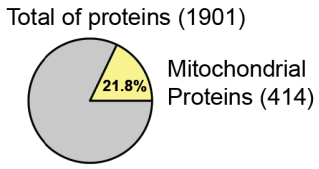
Total of proteins (1901)
21.8%
Mitochondrial
Proteins (414)

B

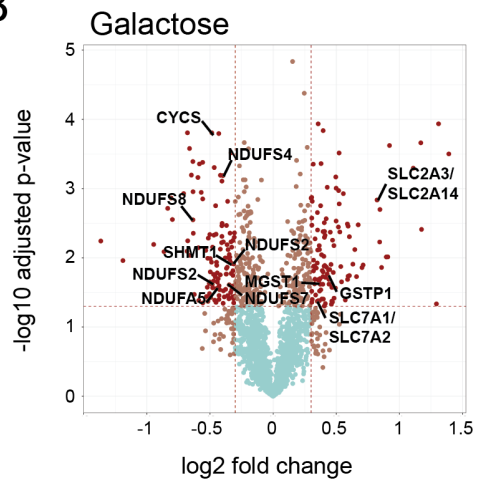
Galactose
-log10 adjusted p-value
log2 fold change
CYCS
NDUFS4
NDUFS8
SHMT1
NDUFS2
NDUFS2
NDUFA6
MGST1
NDUFS7
GSTP1
SLC2A3/
SLC2A14
SLC7A1/
SLC7A2

C

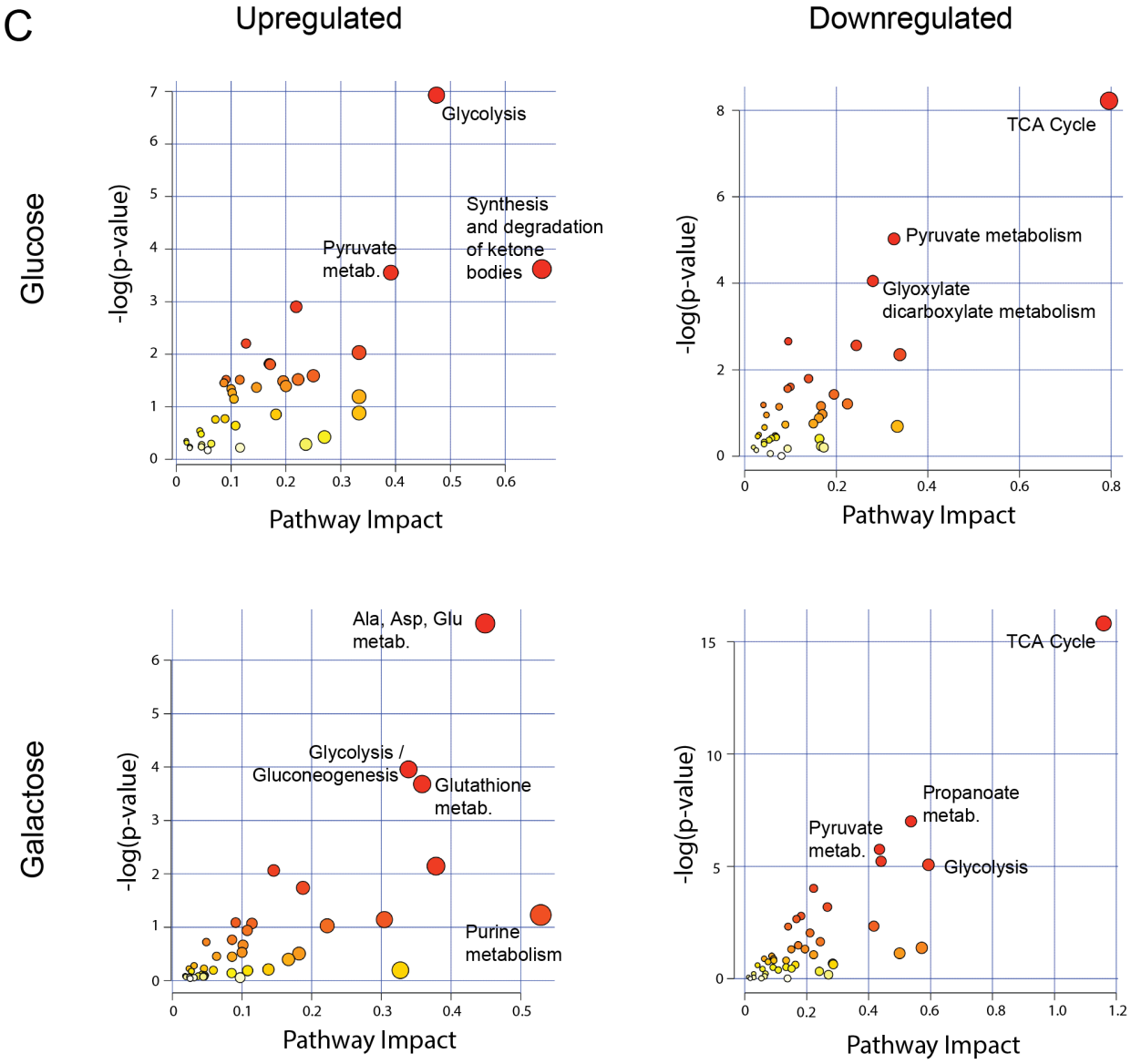
Upregulated
Downregulated
Glucose
Galactose
-log(p-value)
Pathway Impact
Glycolysis
Synthesis
and degradation
of ketone
bodies
Pyruvate
metab.
TCA Cycle
Pyruvate metabolism
Glyoxylate
dicarboxylate metabolism
Ala, Asp, Glu
metab.
Glycolysis /
Gluconeogenesis
Glutathione
metab.
Purine
metabolism
TCA Cycle
Propanoate
metab.
Pyruvate
metab.
Glycolysis

Figure 3.4 Integration of proteomics and metabolomics confirms insufficient TCA cycle at the protein level.

(A) Pie chart representing the total number of proteins identified in all conditions by TMT quantitative proteomics analysis. Number of nuclear encoded mitochondrial proteins (MitoCarta2.0) are indicated, as well as the percentage relative to the total.

(B) Volcano plot representing the results of differential protein expression analysis between patient and rescue cells in galactose. x-axis values represent the log2 fold change and y-axis values represent the -log10 of the adjusted p-value. Selected mitochondrial proteins of interest are labelled.

(C) Joint pathway enrichment analysis performed with the MetaboAnalyst tool of significant up- or down-regulated metabolites and proteins in glucose and galactose condition. Scatterplots represent p-values from integrated enrichment analysis and impact values from pathway topology analysis using KEGG metabolic pathways. The node colour represents the p-values and the node radius is based on the pathway impact values calculated with degree centrality.

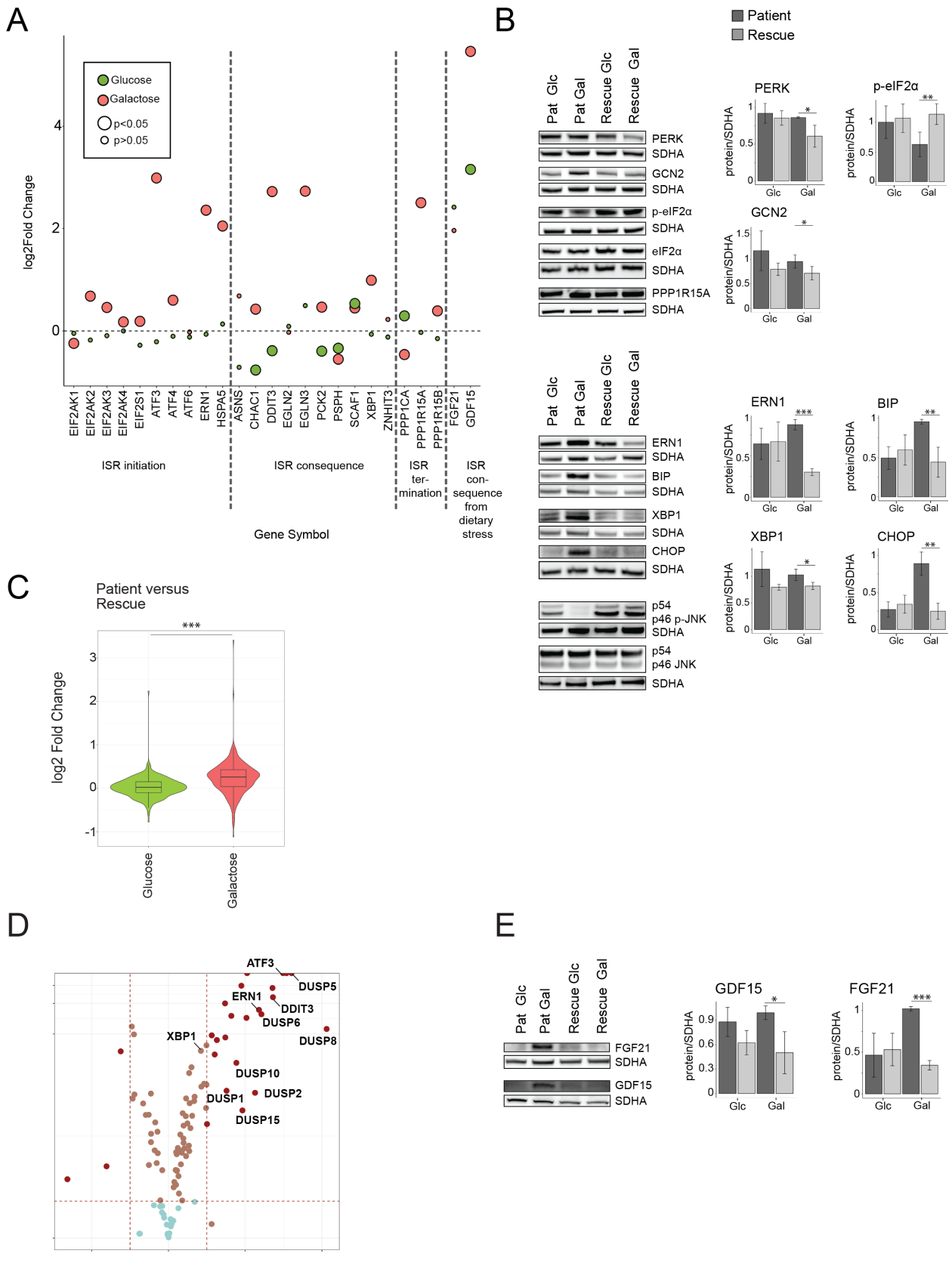

Figure 3.5 Metabolic dysfunction leads to canonical ER stress response in patient in galactose.

(A) Dot plot representing the fold change of the transcripts of ER integrated stress response. Fold change is represented in log2 scale. Large circles represent significant values (FDR<0.05), small circles show non-significant values (FDR>0.05). 'Glucose' (green) represents the comparison of patient versus rescue cells in glucose. 'Galactose' (red) represents the comparison of patient versus rescue cells in glucose.

(B) Western blot analysis of the proteins involved in the integrated stress response of the ER. Whole cell extracts from patient and rescue fibroblasts grown in glucose or galactose for 2 days were separated by SDS-PAGE and probed with antibodies against indicated proteins. SDHA was used as a loading control. Bar plot indicates the quantification of the western blot analysis normalized to SDHA, where patient is depicted in dark grey and rescue in light grey, *p<0.05, **p<0.01, ***p<0.001.

(C) Violin Plot representing the distribution of the log2 fold change (patient/rescue) for transcripts involved in translation for the glucose and galactose condition. Box plots indicate the median and the first and third quartile. Wilcoxon statistical test, ***p<0.001.

(D) Volcano plot representing the results of differential gene expression analysis between patient and rescue cells in galactose for proteins involved in the integrated stress response in the ER. x-axis values represent the log2 fold change and y-axis values represent the -log10 of the adjusted p-value. Selected genes of interested are labelled.

(E) Western blot analysis of GDF15 and FGF21. Whole cell extracts from patient and rescue fibroblasts grown in glucose or galactose for 2 days were separated by SDS-PAGE and probed with antibodies against GDF15 and FGF21. SDHA was used as a loading control. Bar plot indicates the quantification of the western blot analysis, where patient is depicted in dark grey and rescue in light grey, *p<0.05, **p<0.01, ***p<0.001.

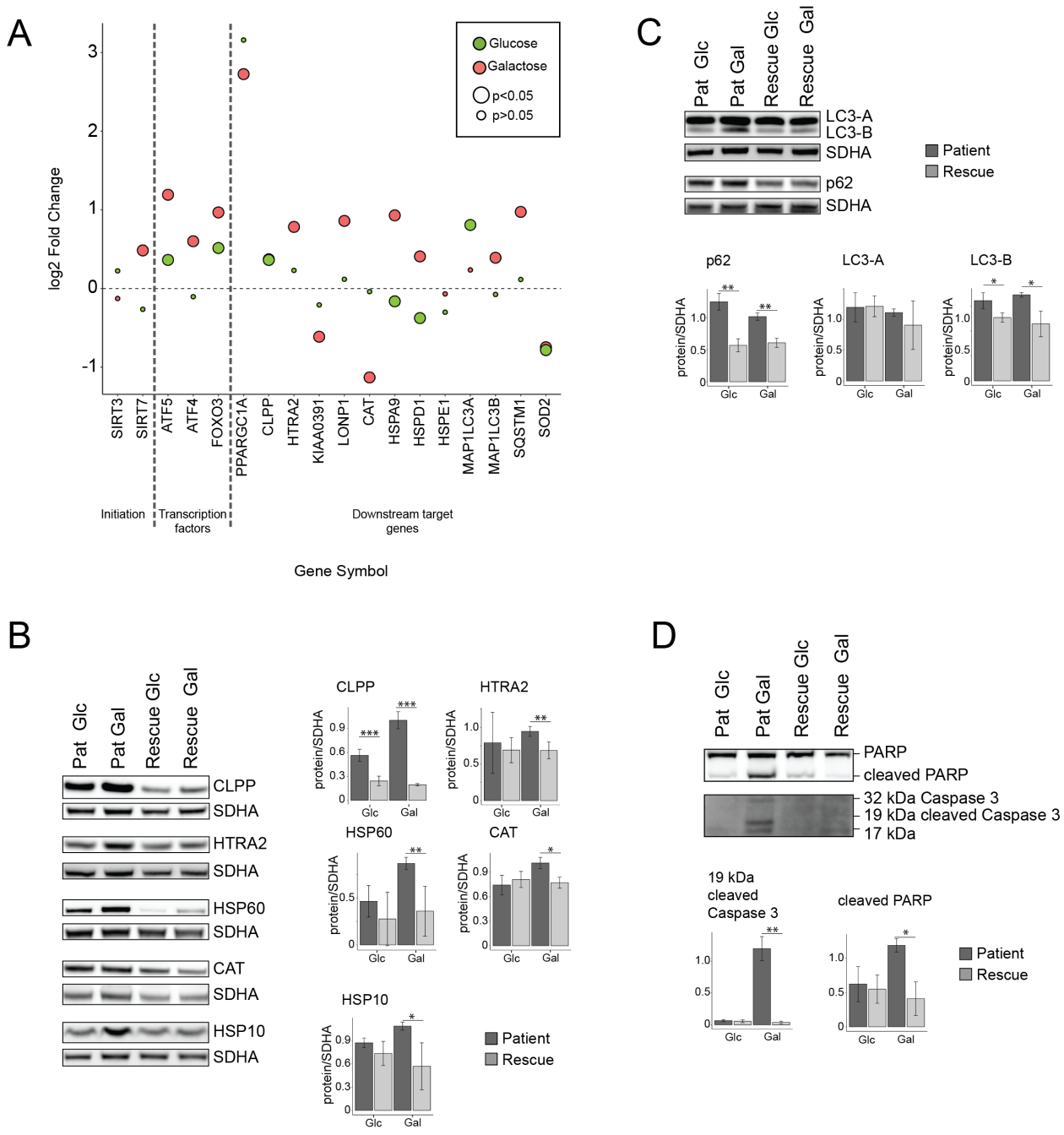

Figure 3.6 Metabolic dysfunction leads to an activation of the mitochondrial integrated stress response and increased autophagy.

(A) Dot plot representing the fold change of the transcripts of mitochondrial integrated protein response. Fold change is represented in log2 scale. Large circles represent significant values (FDR<0.05), small circles show non-significant values (FDR>0.05). 'Glucose' (green) represents

the comparison of patient versus rescue cells in glucose. ‘Galactose’ (red) represents the comparison of patient versus rescue cells in glucose.

(B) Western blot analysis of the proteins involved in mitochondrial integrated stress response. Whole cell extracts from patient and rescue fibroblasts grown in glucose or galactose for 2 days were separated by SDS-PAGE and probed with antibodies against indicated proteins. SDHA was used as a loading control. Bar plot indicates the quantification of the western blot analysis normalized to SDHA, where patient is depicted in dark grey and rescue in light grey, *$p<0.05$, **$p<0.01$, ***$p<0.001$.

(C) Western blot analysis of the proteins involved in autophagy. Whole cell extracts from patient and rescue fibroblasts grown in glucose or galactose for 2 days were separated by SDS-PAGE and probed with antibodies against indicated proteins. SDHA was used as a loading control. Bar plot indicates the quantification of the western blot analysis, where patient is depicted in dark grey and rescue in light grey, *$p<0.05$, **$p<0.01$, ***$p<0.001$.

(D) Western blot analysis of the proteins involved in apoptosis. Whole cell extracts from patient and rescue fibroblasts grown in glucose or galactose for 2 days were separated by SDS-PAGE and probed with antibodies against indicated proteins. SDHA was used as a loading control. Bar plot indicates the quantification of the western blot analysis, where patient is depicted in dark grey and rescue in light grey, *$p<0.05$, **$p<0.01$, ***$p<0.001$.

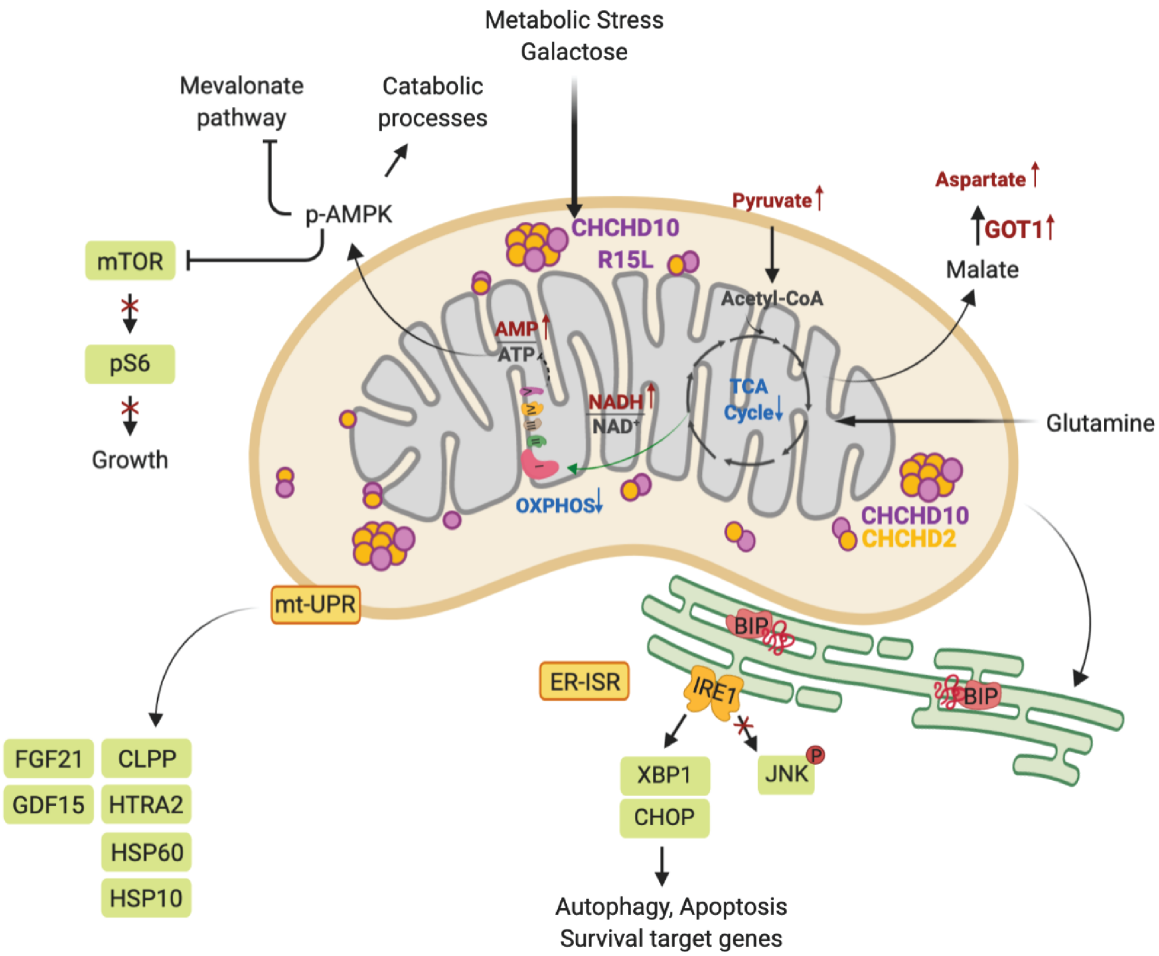

Figure 3.7 Synopsis (created with *BioRender*).

Mitochondrial metabolism and energy production plays a key role in cellular homeostasis. Here, disturbed metabolism can be related to the pathology of an ALS disease causing mutation in mitochondrial protein, CHCHD10. The variant CHCHD10 p.R15L leads to a complex I deficiency resulting in an increase in NADH/NAD^+ ratio and a downregulation of the TCA cycle. In stress condition (galactose), patient cells lack cellular energy and even with substitute use of glutamine have a highly upregulated AMP/ATP ratio, which leads to an increased phosphorylation of AMPK and the subsequent activation of catabolic pathways and the downregulation of the growth targeted mTOR pathway. The metabolic stress condition results in an activation of the integrated stress response of the ER through IRE1 and not through eIF2alpha. The upregulation of different proteases as well as heatshock proteins and the metabolic cytokines FGF21 and GDF15 points to a simultaneous activation of the unfolded protein response in mitochondria. Finally, patient cells show increased cell death through apoptotic processes independent of JNK.

Supplementary Materials

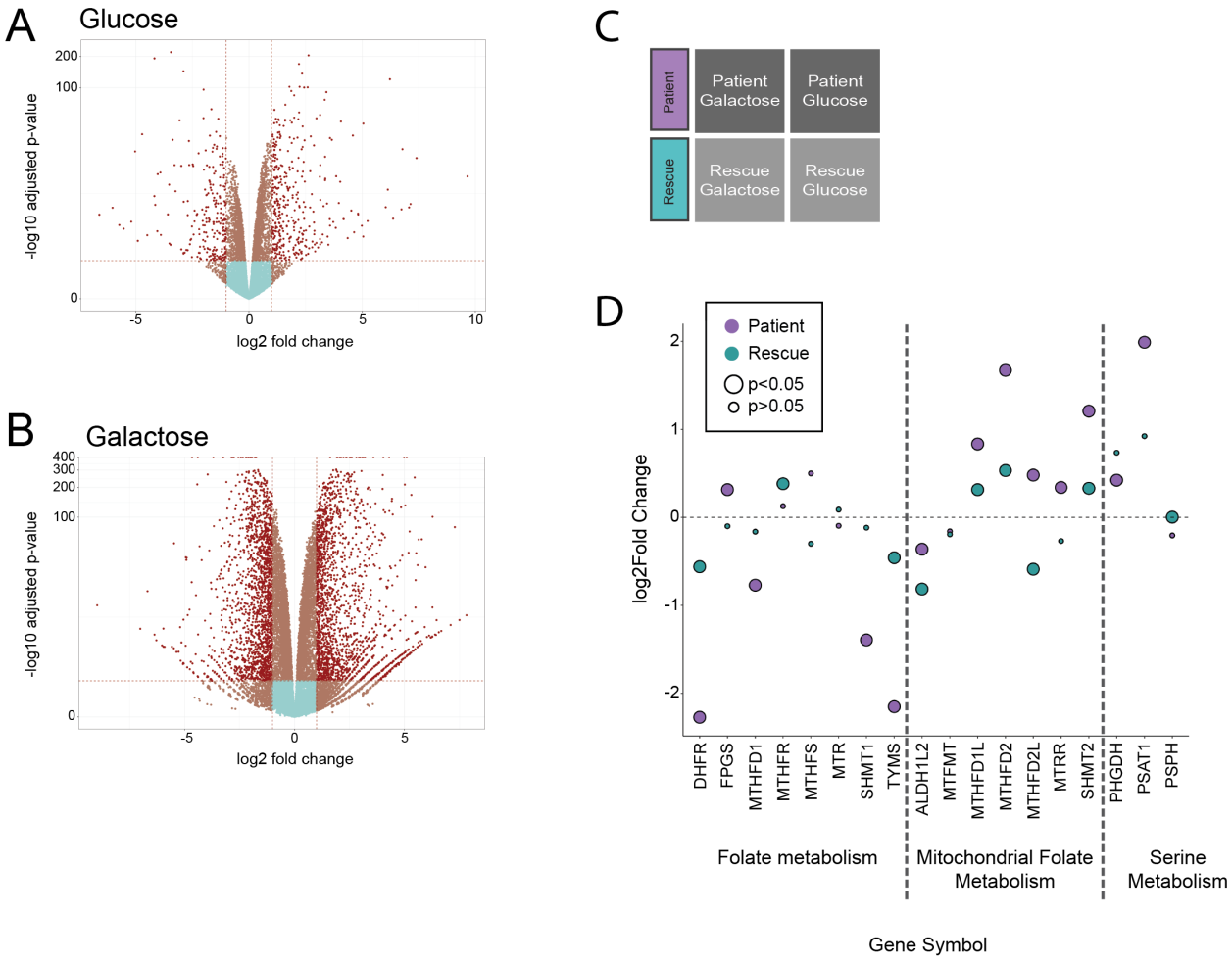

Figure S3.1 Analysis of the transcriptome.

(A) Volcano plot representing the results of differential transcript expression analysis between patient and rescue cells in glucose. x-axis values represent the log2 fold change and y-axis values represent the -log10 of the adjusted p-value.

(B) Volcano plot representing the results of differential transcripts expression analysis between patient and rescue cells in galactose. x-axis values represent the log2 fold change and y-axis values represent the -log10 of the adjusted p-value.

(C) Schematic representation of the treatment comparison. 'Patient' (purple) is defined as patient in galactose versus patient in glucose. 'Rescue' (blue) is defined as rescue in galactose versus rescue in glucose.

(D) Dot plot representing the fold change of the transcripts of the folate and serine metabolism in response to the treatment. Fold change is represented in log2 scale. Large circles represent significant values (FDR<0.05), small circles show non-significant values (FDR>0.05). 'Patient' (purple) represents the comparison of patient cells in galactose versus patient cells in glucose. 'Rescue' (blue) represents the comparison of rescue cells in galactose versus rescue cells in glucose.

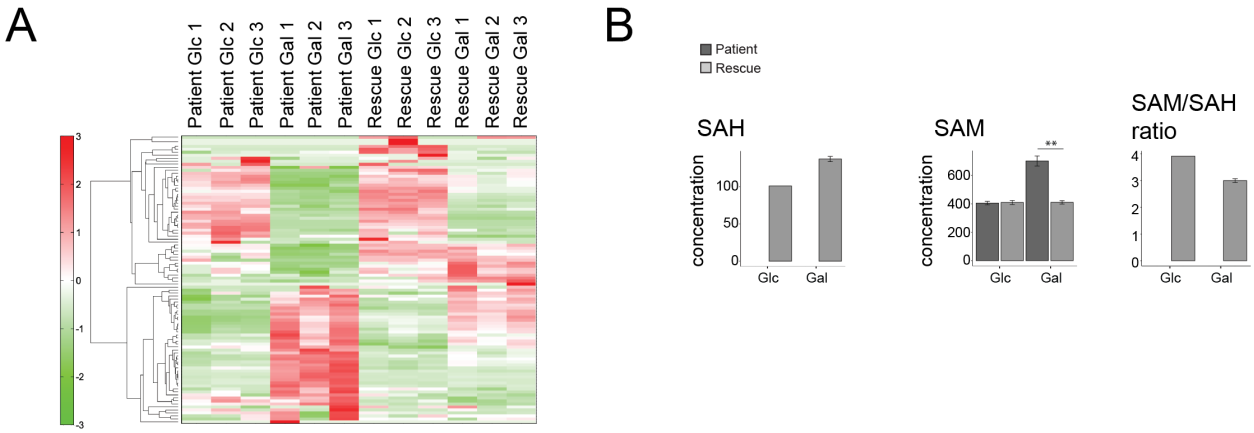

Figure S3.2 Analysis of the metabolome.

(A) Heat map analysis of the metabolome. Hierarchical clustering of samples (columns) and metabolites (rows) was based on the standardized value of relative area in detected peaks. Upregulated metabolites are shown in red, downregulated metabolites in green.

(B) Bar plots representing the change of SAH, SAM and their ratio. Concentrations are depicted in nmol/g and ratios are pure ratios. Values for the patient cells (dark grey), value for the rescue cells (light grey). The p-value is computed by Welch's test. SAH was not detected in patient cells.

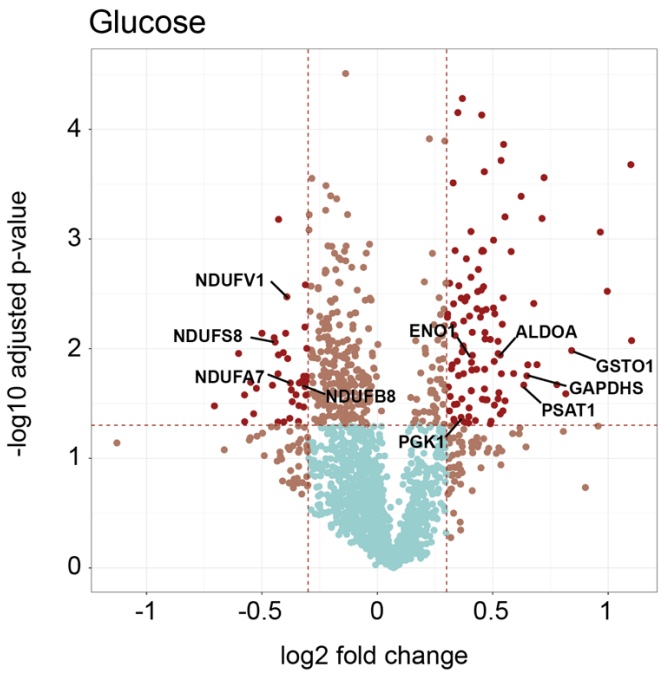

Figure S3.3 Proteome in glucose.

Volcano plot representing the results of differential protein expression analysis between patient and rescue cells in glucose. x-axis values represent the log2 fold change and y-axis values represent the -log10 of the adjusted p-value. Selected mitochondrial proteins of interested are labelled.

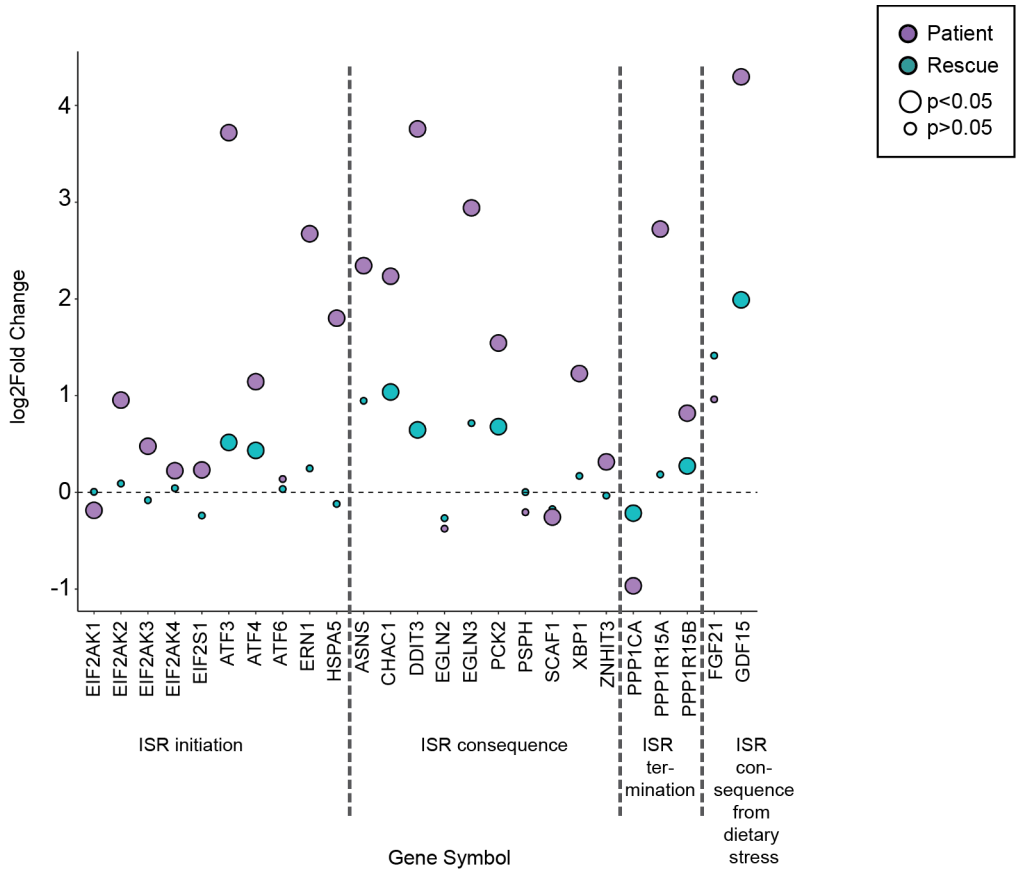

Figure S3.4 Canonical ER stress response in patient in galactose compared to patient in glucose.

Dot plot representing the fold change of the transcripts of the ER integrated stress response in response to treatment. Fold change is represented in log2 scale. Large circles represent significant values (FDR<0.05), small circles show non-significant values (FDR>0.05). 'Patient' (purple) represents the comparison of patient cells in galactose versus patient cells in glucose. 'Rescue' (blue) represents the comparison of rescue cells in galactose versus rescue cells in glucose.

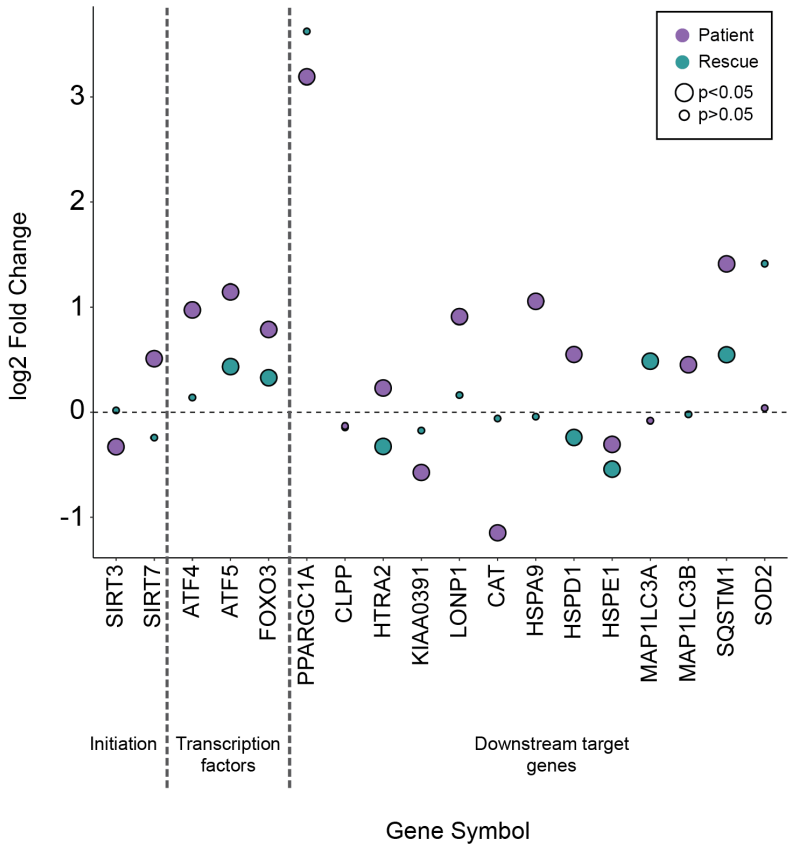

Figure S3.5 Canonical mtUPR in patient in galactose compared to patient in glucose.

Dot plot representing the fold change of the transcripts of mitochondrial integrated protein response in response to treatment. Fold change is represented in log2 scale. Large circles represent significant values (FDR<0.05), small circles show non-significant values (FDR>0.05). 'Patient' (purple) represents the comparison of patient cells in galactose versus patient cells in glucose. 'Rescue' (blue) represents the comparison of rescue cells in galactose versus rescue cells in glucose.

Preface to chapter 4

The first two studies dealt with the pathogenic effects of the CHCHD10 p.R15L variant, which had been associated with ALS in several patients. In the first chapter we identified CHCHD2 as the primary interaction partner of CHCHD10. CHCHD2 expression affected endogenous levels of CHCHD10, and CHCHD2 appeared to act upstream of CHCHD10, as CHCHD10 expression did not influence CHCHD2 levels. Both proteins are intermembrane space proteins with unknown function associated with neurodegenerative disease. Due to an amino acid sequence identity of 55% between the two proteins in H*omo sapiens* and their late duplication event in the evolutionary process only with metazoans, it is likely that both proteins have similar, but not completely overlapping functions. Moreover, levels of both proteins increased in various stress conditions. In the third study we analysed the effects of the loss of CHCHD2 in human fibroblasts as well as the influence of CHCHD2 disease variants p.T61I and p.R145Q on mitochondria. We also conducted transcriptomic and proteomic analysis of the variants compared to CHCHD2 knockout and control.

Chapter 4

CHAPTER 4

CHCHD2 interacts with RNA binding proteins outside of mitochondria and pathogenic variant p.T61I causes disturbed interaction with CHCHD10

Isabella R. Straub[1,2], Ziyang Chen[1,2,3], Diane Nakamura[1,2], Woranontee Weraarpachai[4], Alexandre Janer[1,2], Eric A. Shoubridge[1,2,*]

Affiliations:

[1]Department of Human Genetics, McGill University, Montreal, Quebec, Canada

[2]Montreal Neurological Institute, McGill University, Montreal, Quebec, Canada

[3]School of Life Science, Furan University, Shanghai, China

[4]Department of Biochemistry, Faculty of Medicine, Chiang Mai University, Chiang Mai, Thailand

*To whom correspondence should be addressed at: Eric A. Shoubridge, Montreal Neurological Institute, 3801 University Street, Montreal, Quebec, Canada H3A 2B4; Email: eric@ericpc.mni.mcgill.ca, Tel: 514-398-1997; FAX: 514-398-1509

Manuscript in preparation.

Abstract

Variants in CHCHD2 have been associated with Parkinson's disease, but the mechanisms of pathogenesis are not well understood. The wild-type protein forms a complex with its paralogue CHCHD10, and interacts with another predominantly mitochondrial protein C1QBP/p32. To investigate the role of the protein and the pathogenicity of CHCHD2 variants we generated a CHCHD2 knockout in fibroblasts in which we expressed the two most common variants p.T61I and p.R145Q. The loss of CHCHD2 resulted in decreased levels of OXPHOS complexes, mitochondrial fragmentation, and an increase of CHCHD10 in the high molecular weight complex. Expression of wild-type CHCHD2, but not the pathogenic variants, rescued the OXPHOS phenotype. Expression of the p.T61I variant led to an increased accumulation of the 230 kDa CHCHD2/CHCHD10 complex and additional complexes of CHCHD10. Although the majority of CHCHD2 localizes to mitochondria, analysis of its interactome showed that it also interacts with DNA/RNA binding proteins (ALYREF, YBX1, CHTOP, LBR) outside of mitochondria. The interaction with these proteins is absent or reduced with both pathogenic variants. Transcriptomic and proteomic analysis of knockout fibroblasts in which a wild-type or mutant CHCHD2 cDNAs was reintroduced, showed that transcripts and proteins involved in RNA binding were amongst those showing the largest changes when compared to the knockout. These findings suggest a role of CHCHD2 in RNA metabolism outside of mitochondria, a hypothesis which needs further validation.

Introduction

Parkinson's disease (PD) is the most prevalent neurodegenerative disease with loco-motor defects (Nussbaum & Ellis, 2003). Mitochondrial dysfunction has long been proposed to underlie the neuronal degeneration associated with PD, and over the last several years several genetic causes of PD have been identified, especially in early onset forms of the disease, confirming this suspicion (Henchcliffe & Beal, 2008). The PINK1-Parkin pathway implicates mitophagy - the turnover of defective mitochondria - as a centrepiece in the pathophysiology of familial PD. Variants in the mitochondrial protein CHCHD2 were suggested to cause late onset autosomal dominant PD as well as sporadic PD (Foo et al., 2015, Funayama et al., 2015, Ikeda et al., 2017, Jansen et al., 2015, Koschmidder et al., 2016, Lee et al., 2018, Li et al., 2016, Nicoletti et al., 2018, Ogaki et al., 2015, Shi et al., 2016, Wu et al., 2016). A *CHCHD2* missense mutation (c.182C>T, p.Thr61Ile) was identified in a family with dominantly inherited late-onset PD (8 cases), and further screening revealed another patient with the same mutation, and two potential splice site mutations in two additional families (c.424G>A, p.Arg145Gln; in intron: c.300+5G>A) (Funayama et al., 2015). Although multiple variants of CHCHD2 have been reported (Foo et al., 2015, Jansen et al., 2015, Koschmidder et al., 2016, Ogaki et al., 2015, Shi et al., 2016, Yang et al., 2016), there is sufficient evidence for pathogenicity in only two of them: p.T61I and p.R145Q (Imai et al., 2019b).

The CX_9C motif containing protein CHCHD2 is a mitochondrial intermembrane space protein that is imported via the Mia40 import pathway (Becker et al., 2012). CHCHD2 forms a high molecular weight complex with its paralogue CHCHD10, mutations in which have been associated with amyotrophic lateral sclerosis (ALS), frontotemporal dementia (FTD), mitochondrial myopathy and others (Ajroud-Driss et al., 2015, Auranen et al., 2015, Chio et al., 2015, Dols-Icardo et al., 2015, Johnson et al., 2014, Kurzwelly et al., 2015, Muller et al., 2014, Pasanen et al., 2016, Penttila et al., 2015, Ronchi et al., 2015, Rubino et al., 2018, Ryan et al., 2019, Shen et al., 2017, Straub et al., 2018, Zhang et al., 2015, Zhou et al., 2017a). CHCHD2 was reported to be a regulator of oxidative phosphorylation and cell migration (Baughman et al., 2009, Wei et al., 2015) and in a Drosophila model playing a role in regulating the function of cytochrome *c* in oxidative phosphorylation (Meng et al., 2017).

CHCHD2 has also been proposed to be a multifunctional protein with localization in cellular compartments other than mitochondria. Correlated gene expression for CHCHD2

suggested a role in cellular translation (Nayak et al., 2009), and several reports describe dual localization for CHCHD2 and/or CHCHD10 in mitochondria and the nucleus (Liu et al., 2015, Purandare et al., 2018, Wilson et al., 2020, Woo et al., 2017). CHCHD2 was also reported to regulate the expression of the nuclear-encoded COX4I2 subunit (Aras et al., 2015, Aras et al., 2013). In a recent paper, the same group described dual localization of CHCHD10, and suggested that its presence in the nucleus repressed the transcription of COX4I2 and CHCHD2 (Purandare et al., 2018). Furthermore, a CHCHD10 variant, with a mutation in the CHCH-domain (p.Q108*) was observed to localize to the nucleus (Lehmer et al., 2018). Lastly, the proposed interaction of CHCHD2 with Bcl-xL, suggested a localization to the outer mitochondrial membrane, where it inhibits apoptosis (Liu et al., 2015). It is evident that CHCHD2 may play a role in a multitude of cellular functions and understanding these is fundamental to understanding the pathogenicity of CHCHD2 mutations.

In this study, we extend our knowledge of the role of CHCHD2 and the effect of two pathogenic variants, p.T61I and p.R145Q using transcriptomic, proteomic and functional analyses. We used CHCHD2 knockout cells, and knockout cells where wild-type CHCHD2 or the pathogenic variants were reintroduced. Apart from the already established effect of CHCHD2 on respiratory function, our results suggest a role for CHCHD2 outside of the mitochondrial intermembrane space in RNA metabolism and translation.

Results

To investigate the function of CHCHD2 and its pathogenic variants associated with PD, we created a CRISPR-Cas9 mediated knockout cell line of *CHCHD2* in control fibroblasts (hereafter referred to as knockout, KO). Subsequently, wild-type *CHCHD2* and the two pathogenic disease variants p.T61I and p.R145Q were reintroduced into the knockout cell line on a retroviral expression vector (hereafter referred to as KO+WT, KO+T61I, and KO+R145Q) (Fig. 4.1A). CHCHD2 was undetectable in the knockout cell line by immunoblot analysis (Fig. 4.1B), and the transcript was decreased to 4.4% by qRT-PCR analysis (Fig. 4.1C). The *CHCHD2* KO was associated with a small decrease in *CHCHD10* transcript levels (73% of control) and CHCHD10 protein levels (60% of control). Expression of the wild-type *CHCHD2* cDNA in the knockout cell line, resulted in protein levels comparable to, or slightly higher than control (Fig. 4.1B). Interestingly, in these cells, transcripts for both *CHCHD2* and *CHCHD10* were decreased by 21% and 48%, respectively (Fig. 4.1C) and the levels of CHCHD10 protein were decreased (29% of control). The expression of CHCHD2 p.T61I, resulted in about 50% of protein compared to control and unchanged CHCHD10 levels (Fig. 4.1B). At the transcript level CHCHD2 p.T61I was 39% of control and *CHCHD10* transcript levels were unchanged (Fig. 4.1C). The CHCHD2 p.R145Q variant showed the lowest expression of the protein (25%) and transcript (43%) compared to control (Fig. 4.1B, C), and CHCHD10 protein and transcript levels are unchanged for this variant.

As shown previously, the disease variant CHCHD2 p.T61I amino acid substitution is located in the hydrophobic region of the protein, and the change from threonine to isoleucine renders the protein more lipophilic (Fig. S4.1A) (Huang et al., 2018). To assess the hydrophobicity of the *CHCHD2* pathogenic variants we tested their susceptibility to alkaline carbonate extraction. CHCHD2 wild-type protein was previously described as 89% soluble, whereas the CHCHD2 variant p.T61I only showed a 76% solubility (Huang et al., 2018). We found that 48% of the CHCHD2 p.T61I variant was found in the pellet, whereas only 18% and 20% of the wild-type or the CHCHD2 p.R145Q variant were detected in the insoluble fraction (Fig. 4.1D). The hydrophobicity of CHCHD10 did not change under any of the conditions tested.

CHCHD2 and CHCHD10 have been reported to increase in response to stress, and in particular under conditions where the mitochondrial membrane potential is dissipated (Huang et al., 2018, Meng et al., 2017). To test whether the stability of CHCHD2 variants depends on

membrane potential, we investigated their response to treatment with CCCP, which completely collapses the mitochondrial membrane potential (Fig. 4.1E). As expected, CCCP treatment resulted in increased levels of wild-type and CHCHD2 variants, as well as CHCHD10; however, we unexpectedly identified short forms of CHCHD2 which also increased in the stress condition. All these short forms were specific for CHCHD2 as they were absent in knockout cells. The nature of these short forms as well as the differences between wild-type and variants and their localization have to be validated in future experiments.

CHCHD2 knockout leads to altered mitochondrial morphology

To investigate the influence of CHCHD2 levels and variants on mitochondrial morphology we performed immunofluorescence analysis of the mitochondrial network. CHCHD2 knockout fibroblasts showed significantly smaller and less branched mitochondria (Fig. 4.2A, B). In addition, the branch length was significantly shorter. These data demonstrate that the mitochondrial network is more fragmented in CHCHD2 knockout fibroblasts. The reintroduction of CHCHD2 wild-type protein rescued all of these parameters (Fig. 4.2B). The expression of pathogenic disease variants p.T61I and p.R.145Q did not lead to any significant changes in mitochondrial morphology; however, the changes of the CHCHD2 p.T61I variant resembled the knockout more than the control (Fig. 4.2B). To see if the changes in mitochondrial morphology were reflected in the levels of the proteins involved in regulating fission or fusion, we next examined the integrity of the mitochondrial fission/fusion machinery. siRNA-mediated knockdown of CHCHD2 was previously shown to result in decreased levels of long OPA1 isoforms and increased levels of the short isoform, a phenomenon which correlates with mitochondrial fragmentation (Anand et al., 2014, Straub et al., 2018). In our knockout model, we also observed an accumulation of the short OPA1 isoform and a decrease of the long forms (Fig. 4.2C). These changes were rescued by the reintroduction of wild-type CHCHD2 protein. Introduction of the pathogenic variant p.T61I did not rescue OPA1 levels, but the degree of mitochondrial fragmentation was not substantially different than (Fig. 4.2B, C). The CHCHD2 p.R145Q variant almost fully restores OPA1 isoforms as seen in control and does not show signs of mitochondrial morphological alterations (Fig. 4.2B, C). The levels of MFN2 protein were insensitive to loss of CHCHD2 or the expression of either disease variant. These results suggest that the fragmentation phenotype is partially supported by an accumulation of short OPA1

isoforms; however, how CHCHD2 knockout influences OPA1 cleavage, or if this is a pleiotropic effect remains to be established.

CHCHD2 knockout and mutants affect mitochondrial respiratory chain assembly and the interaction with CHCHD10

Previous results from a study of CHCHD2 function suggested the protein to have dual localization, activating transcription of itself and complex IV subunit COX4I2 in the nucleus; however, this finding has not been confirmed (Aras et al., 2015). Another link to mitochondrial respiration was made in a knockout model of *CHCHD2* in *Drosophila*, where decreased mitochondrial ATP production and oxygen consumption was reported (Meng et al., 2017). Conversely, another recent study reported a normal oxygen consumption rate in CHCHD2 knockout fibroblasts (Liu et al., 2019). To investigate the assembly of the OXPHOS complexes in our model, we performed a Blue-Native polyacrylamide gel analysis (BN-PAGE). *CHCHD2* knockout cells showed significant decreases in the levels of complexes I, and IV, and complex I was fully rescued whereas complex IV was partially rescued by expression of the wild-type protein (Fig. 4.3A). These results were corroborated by immunoblot analyses of the steady-state levels of different subunits of the OXPHOS complexes (Fig. 4.3B). However, further experiments have to be conducted to fully quantify the decrease and the rescue. To test whether the assembly of respiratory supercomplexes was affected, we extracted the complexes with a mild detergent and subjected them to a BN-PAGE. The assembly of the supercomplexes correlated with the decrease in monomeric respiratory chain complexes (Fig. S4.1B). The defect of complex I and IV was partially rescued by the reintroduction of the wild-type and the CHCHD2 p.R145Q variant but not the CHCHD2 p.T61I variant. With this method we could also identify the unassembled complex V subunits, and assembly was partially rescued by the reintroduction of wild-type CHCHD2 protein but not the two pathogenic disease variants (Fig. S4.1B).

CHCHD2 forms stable complexes with its paralogue CHCHD10 (Fig. 4.3C, control) (Straub et al., 2018). These complexes are around ~230 kDa in size and their composition changes in patient fibroblasts with the CHCHD10 p.R15L variant (Straub et al., 2018). As these complexes could play a role in pathogenesis we investigated their composition in CHCHD2 knockout cells as well as cells expressing wild-type or the two pathogenic variants. Identical to

our previous results, in control cells we observed the majority of CHCHD2 and CHCHD10 as a low molecular weight entities (possibly in the monomeric form); and two high molecular weight complexes around 170-230 kDa in size (Fig. 4.3C, control) (Straub et al., 2018). The CHCHD2 knockout cell line showed an increased amount of CHCHD10 in the 230 kDa complex and less protein at the lower molecular weight (Fig. 4.3C, KO), which did not result from an increase in levels of total protein (Fig. 4.1B). The CHCHD2/CHCHD10 complex formation was fully rescued by the reintroduction of the wild-type cDNA (Fig. 4.3C, KO + WT). For the CHCHD2 p. T61I variant, CHCHD10 formed an additional complex of ~140 kDa and accumulated together with CHCHD2 p.T61I at 230 kDa, similar to the CHCHD2 p.T61I variant. Interestingly, the CHCHD2 p.T61I variant only accumulated in the higher molecular weight complex at ~230 kDa (Fig. 4.3C, KO + T61I). The complexes were similar to those in control cells in CHCHD2 p.R145Q expressing cells (Fig. 4.3C, KO + R145Q); however, the total amount of CHCHD2 was decreased, as seen previously (Fig. 4.1B).

To determine whether intermolecular disulfide bonds could form between CHCHD2 and CHCHD10 in these complexes, we analysed the redox state of the two proteins. The cysteines of other proteins of the CX_9C family have different redox states at steady-state and this relates to their function in the cell. An example of a partially reduced/oxidized protein is Mia40/CHCHD4, which is responsible for the import of twin CX_9C-containing proteins into the mitochondrial IMS. The oxidized form of Mia40 represents the form that mediates oxidative protein folding (Erdogan et al., 2018). Other examples are the metal binding chaperones SCO1 and SCO2, responsible for the insertion of the prosthetic copper atoms into the active site of cytochrome *c* oxidase. They only bind copper in the reduced state (Leary et al., 2009). And lastly, CHCHD3/Mic19 in the reduced state, forms an intermediate with TOMM40 and CHCHD4 (Ueda et al., 2019). Immunoblot analysis of isolated mitochondria from control fibroblasts on a non-reducing SDS-PAGE showed that both CHCHD10 and CHCHD2 are completely oxidized under normal physiological conditions in contrast to CHCHD3, CHCHD4 and SCO1 (Fig. 4.3D). The oxidation state did not change under nutrient stress (glucose-free galactose-containing medium), although as shown previously, the levels of CHCHD2 and CHCHD10 increased (Straub et al., 2018). We conclude that the four cysteines present in CHCHD2 or CHCHD10 serve an entirely structural purpose, and are not likely involved in metal or substrate-binding, or in forming intermolecular disulfide bonds. The bands observed for CHCHD2 and CHCHD10 at

~25 kDa are visible only at high temperature and with reducing agent dithiothreitol (DTT), hence the disulfide bonds of CHCHD2 and CHCHD10 are of structural nature and stable in physiological conditions (Fig. 4.3D).

CHCHD2 interacts with proteins of the RNA metabolism

We previously identified CHCHD10 and C1QBP as interacting partners of CHCHD2 (Straub et al., 2018). Several recent studies have conducted immunoprecipitation, affinity purification or proximity biotinylation assays to investigate the interactome of CHCHD2, C1QBP and CHCHD10 (Wei et al., 2015, Zhang et al., 2013). These proteins have also been identified as preys in multiple large-scale human interactome studies, most of which are gathered in BioGRID, a large interaction repository (Floyd et al., 2016, Hein et al., 2015, Huttlin et al., 2015). We compiled all of these studies and added our results from the C1QBP-BirA*-FLAG proximity biotinylation assay, as well as a C1QBP-HA immunoprecipitation (unpublished). We identified several new interaction partners of the already known interactome of CHCHD2, CHCHD10 and C1QBP (Fig. 4.4A): Aly/REF export factor (ALYREF), Y-box binding protein 1 (YBX1) and chromatin target of PRMT1 (CHTOP) are all proteins involved in mRNA processing as well as mRNA export from the nucleus to the cytosol. The lamin B receptor (LBR), which is a nuclear inner membrane protein has been shown to interact with DNA (Ye & Worman, 1994).

To confirm and investigate whether these, or other interaction partners of CHCHD2, change in the presence of the pathogenic variant proteins, we immunoprecipitated CHCHD2 from digitonized mitochondrial extracts and analysed the co-immunoprecipitated proteins by liquid chromatography-tandem mass spectrometry (LC-MS/MS). This analysis confirmed the interaction with C1QBP and CHCHD10, the previously identified partners of CHCHD2 (Fig. 4.4B) and validated the interactions of wild-type CHCHD2 with the RNA binding proteins ALYREF and CHTOP, as well as with LBR. Significantly, while the p.T61I and p.R145Q variants co-immunoprecipitated with both CHCHD10 and C1QBP, the interaction with ALYREF and LBR was decreased or lost completely, suggesting that these interactions might play a role in the pathogenicity of these variants.

CHCHD2 knockout and variants affect levels of RNA binding proteins

To investigate the impact of CHCHD2 knockout and disease mutations on cellular and mitochondrial biology, changes in the transcriptome and proteome were determined by RNA sequencing and tandem mass tag spectrometry (TMT). The overall number of significant differentially expressed transcripts and proteins was larger for the wild-type expression than the two pathogenic variants (compare Fig. 4.5A with C, E, and B with D, F), indicating the similarity between the knockout and cells harbouring pathogenic variants. The expression of wild-type CHCHD2 particularly increased transcripts and proteins involved in RNA binding (Fig. 4.5A, B). The reintroduction of the CHCHD2 variant p.T61I resulted in differentially expressed proteins involved in RNA binding, nuclease activity and DNA helicase activity (Fig. 4.5C, D). Interestingly, for this variant we found differential expression of transcripts involved in sodium voltage channel activity, a process crucial in neurons, the cell-type affected in PD (Fig. 4.5C). Differentially expressed proteins for the R145Q variant are involved in RNA binding, DNA helicase activity and aldehyde dehydrogenase activity (Fig. 4.5E, F).

To obtain further information about the importance of RNA binding proteins and their interaction with CHCHD2 and its variants, we took the hits from Figure 4.4B and cross-checked their regulation at the transcript and/or protein level. We identified increased expression of transcripts and protein of two metalloproteases, MMP1 and MMP3 only when KO cells were rescued with wild-type CHCHD2, but not the pathogenic variants (Fig. 4.5). The CHCHD2 p.R145Q variant even showed reduced protein levels of MMP1 (Fig. 4.5F). Our immunoprecipitation experiment identified these two metalloproteases as interactors of wild-type CHCHD2 but not of the two pathogenic variants (Fig. 4.4B). Interestingly, ALYREF protein levels were lower in cells in which wild-type CHCHD2 was reintroduced (Fig. 4.5B, S4.1C) and higher in cells with the CHCHD2 p.R145Q variant (Fig. 4.5F, S4.1C). The interaction with ALYREF however, is strongest for the wild-type CHCHD2 protein (Fig. 4.4B). Another example is the alanyl aminopeptidase (ANPEP), which was only upregulated at the protein level for the CHCHD2 variants (Fig. 4.5D, F). The variants, but not the wild-type CHCHD2 protein, interact with ANPEP (Fig. 4.4B). Lastly, the microtubule-dependent motor required for the distribution of mitochondria and lysosomes, kinesin family member 5B (KIF5B) is decreased in cells in which the wild-type CHCHD2 was reintroduced (Fig. 4.5B); however, it interacts with the CHCHD2 p.R145Q variant and not the wild-type (Fig. 4.4B).

We therefore identified altered gene and protein regulation for several interaction partners of CHCHD2 wild-type protein and the pathogenic variants. Most markedly affected are the metalloproteases MMP1 and MMP3, and further research has to be conducted to identify the significance of the interaction with CHCHD2.

Discussion

In this study, we investigated the role of CHCHD2 and the pathogenic mechanisms of two variants associated with PD in human fibroblasts. The loss of CHCHD2 altered mitochondrial morphology, and was associated with reduced levels of OXPHOS complexes I, and IV and an assembly defect of complex V. The two pathogenic variants p.T61I and p.R145Q did not significantly alter mitochondrial morphology, but showed a reduction in mitochondrial complex IV and a complex V defect similar to the knockout cells. Moreover, without CHCHD2, CHCHD10 formed different sized high molecular weight complexes and the p.T61I variant lead to an accumulation of CHCHD10 and CHCHD2 p.T61I at a high molecular weight. The analysis of differentially expressed transcripts and proteins and immunoprecipitation of CHCHD2 revealed an interaction of CHCHD2 with RNA-binding proteins. We therefore propose a new interactome of CHCHD2, which suggests that CHCHD2 is involved in cellular and mitochondrial RNA metabolism affecting mitochondrial biogenesis and morphology.

Changes in mitochondrial morphology have been identified for other genetic causes of PD, involving PINK1, parkin, DJ-1, and alpha-synuclein (Bueler, 2009, Morais et al., 2014, Pozo Devoto & Falzone, 2017, Walter et al., 2019, Winklhofer & Haass, 2010). Mitochondrial fragmentation has been reported in models of sporadic PD, driven by OPA1 cleavage in some of these (Santos et al., 2015). The mitochondrial network for homozygous CHCHD2 variant p.A71P has also been described as fragmented with the accumulation of granular bodies in patient cells (Lee et al., 2018). Very recently, a study claimed the involvement of CHCHD2 in the regulation of mitochondrial morphology through the interaction with C1QBP, which itself interacts with YME1L, a protease involved in OPA1 processing (Liu et al., 2020). Interestingly, we found an interaction of CHCHD2 with YME1L, which was increased with the CHCHD2 p.T61I variant (Fig. 4.4B). The complete loss of CHCHD2 lead to a more compact and branched mitochondrial network, which correlated with the increased expression of short OPA1 forms and decreased expression of long OPA1 forms (Fig. 4.2). Interestingly, a recent study reported no change in OPA1 distribution for the CHCHD2 knockout but found a decrease in long and an increase in short OPA1 forms for the double knockout of CHCHD2 and its paralogue CHCHD10 (Liu et al., 2019). In our model the disease variant p.T61I showed a phenotype similar to the knockout; however, the changes were not significant. Whether, indeed CHCHD2 directly affects

OPA1 function through the interaction with C1QBP or YME1L, and if the pathogenic variants alter these interactions, needs further experimental validation.

Apart from morphological changes, defects in mitochondrial respiration have also been associated with PD (Shoffner et al., 1991), and the first siRNA mediated knockdown of CHCHD2 revealed a destabilization of OXPHOS complexes (Baughman et al., 2009). Furthermore, the loss of CHCHD2 in *Drosophila* caused mitochondrial respiratory defects and lower ATP production, which were rescued by the wild-type CHCHD2 protein, but not the two pathogenic variants p.T61I and p.R145Q (Meng et al., 2017). In our model, CHCHD2 knockout cells showed a marked decrease in complex I and IV and partially unassembled complex V. Similar to the study in *Drosophila* the phenotype could be partially rescued with wild-type protein but not the two pathogenic disease variants.

The variants of CHCHD2 and CHCHD10 which are present in the hydrophobic stretch of the proteins (amino acids 55-68), have been described as having a more detrimental, dominant-gain of function mechanism compared to other variants through the formation of aggregates due to increased hydrophobicity (Anderson et al., 2019a, Huang et al., 2018). The CHCHD2 p.T61I variant, as well as CHCHD10 p.S59L and p.G66V variants render the protein more hydrophobic (Huang et al., 2018). We confirmed that the CHCHD2 p.T61I variant shows indeed a stronger association with the membrane when compared to wild-type CHCHD2 or p.R145Q (Fig. 4.1D). We also find that the presence of CHCHD2 p.T61I protein changes the complex formation between CHCHD2 and CHCHD10 and leads to an accumulation of CHCHD10 in different molecular weight complexes that are not present in control cells (Fig. 4.3C). A previous study showed that the CHCHD2 p.T61I variant interacts more with CHCHD10 and leads to decreased CHCHD10 levels in patient cells (Mao et al., 2019). In our study, the presence of the two pathogenic CHCHD2 variants did not lead to a decrease in the levels of CHCHD10 (Fig. 4.1B), despite the fact that the CHCHD2 protein levels of the two pathogenic variants were significantly decreased. It is possible that these variants are recognized as detrimental in the mitochondria and degraded by one of the mitochondrial proteases, as we observed an increased interaction between CHCHD2 p.T61I and YME1L1, and CHCHD2 p.R145Q and LONP1, respectively (Fig. 4.4B). We did however, identify a downregulation of CHCHD10 transcript and protein levels after reintroduction of CHCHD2 wild-type protein (Fig. 4.1B, C). The reduction could possibly stem from higher CHCHD2 protein levels compared to control, which affect CHCHD10 transcription.

CHCHD2 is a predominantly mitochondrial protein, which in stress condition (4% hypoxia) has been reported to localize to the nucleus and enhance transcription of COX4I2 and itself, and genes harbouring the oxygen-responsive element (ORE) in their promoters (Grossman et al., 2017). Interestingly, the known interacting partner of CHCHD2, CHCHD10, was also reported to localize to the nucleus under 8% hypoxic condition and downregulate genes with an ORE, therefore fine-tuning oxygen-sensing in the cell (Purandare et al., 2018). How CHCHD2 or CHCHD10 could translocate or act as transcriptional regulators remains unknown. Another study, reporting CHCHD2 outside of mitochondria, describes its anti-apoptotic role through the interaction with Bcl-xL at the outer mitochondrial membrane (Liu et al., 2015). Immunofluorescence analysis of control cells, as well as CHCHD2 expressing cell lines showed a clear and exclusive localization of CHCHD2 in mitochondria. However, we cannot exclude the possibility, that a small amount of CHCHD2 protein localizes to a different cellular compartment, or that it is capable of shuttling between mitochondria and cytosol. The appearance of a short form of CHCHD2, particularly in the presence of the uncoupler CCCP, gives rise to speculation that shorter forms of CHCHD2 could possibly shuttle across the outer mitochondrial membrane and act as a stress signal. The association between CHCHD2 (and also its partner CHCHD10) and cellular stress has been established previously, and the levels of both proteins increase in stress conditions including dissipation of mitochondrial membrane potential, nutrient stress (glucose-free medium), mitochondrial genomic stress or the mitochondrial unfolded protein response (Huang et al., 2018, Meng et al., 2017, Straub et al., 2018). Further studies are needed to decipher where these short forms localize, what proteases are involved in the processing of CHCHD2, and which part of the CHCHD2 protein they comprise.

CHCHD2 and CHCHD2 have previously been described to interact with each other as well as C1QBP/p32 (Burstein et al., 2018, Straub et al., 2018, Wei et al., 2015). C1QBP is a predominantly mitochondrial protein, where it localizes to the matrix and is involved in translation (Muta et al., 1997, Yagi et al., 2012). With a milder extraction method, we have now identified additional interacting partners, suggesting that CHCHD2 also interacts with proteins involved in RNA processing and cytoplasmic translation (Fig. 4.4B). In particular, the proteins ALYREF, LBR, DDX6, CHTOP, FUBP3 and FARSA were identified in immunoprecipitation experiments with wild-type CHCHD2, but not with the two pathogenic variants we studied. A comparison of our data with the literature led to the identification of an interactome of CHCHD2,

CHCHD10, C1QBP with proteins involved in RNA metabolism, ALYREF, YBX1 and CHTOP (Fig. 4.4A). Of these, ALYREF is an export adapter of the THO transcription elongation complex (TREX) complex which is responsible for nuclear mRNA export (Katahira, 2012). ALYREF has been reported to bind the 5' end of mRNA and together with CHTOP to activate ATPases and RNA helicases to recruit ALYREF and CHTOP to mRNA for export (Chang et al., 2013, Shi et al., 2017). Our study showed that the interaction between CHCHD2 and ALYREF was lost when CHCHD2 was mutated. Interestingly, another identified interactor of CHCHD2, YBX1 has been reported to interact with mitochondrial tRNAs outside of mitochondria (Jady et al., 2018). For several other newly identified interaction partners transcript and protein levels changed upon CHCHD2 wild-type and variant expression. Among these are MMP1, MMP3, ANPEP and KIF5B. Whether increased protein expression was responsible for the interaction or if endogenous CHCHD2 protein also interacts with these proteins remains to be validated in future experiments. Only then we can discuss a potential significance of these interactions.

The newly discovered interactors open a novel path for research into the function of CHCHD2. Previous studies have established a strong link between RNA interacting proteins like TDP43, FUS and DJ-1 in ALS and Parkinson's disease (Lu et al., 2014). Variants in these proteins cause dysregulation of RNA metabolism, cytoplasmic aggregation and dysfunction in stress granules (Zhao et al., 2018). The role that CHCHD2 might play in one of these processes is fertile ground for future research.

Materials and Methods

Human studies

The analysis of cell lines was approved by the institutional review board of the Montreal Neurological Institute, McGill University.

Cell lines and media

Fibroblasts stably expressing *CHCHD2* in CRISPR-Cas9 knockout cells were engineered using retroviral vectors as described previously (Lochmuller et al., 1999, Straub et al., 2018). Cells were cultivated in 4.5 g/l glucose DMEM supplemented with 10% fetal bovine serum (FBS) and 5% pen/strep, at 37 °C in an atmosphere of 5% CO_2. For carbon source-dependent experiments, fibroblasts were cultivated for two days in DMEM with 10% dialyzed FBS supplemented with 4.5 g/l galactose.

Generation of CRISPR-Cas9 CHCHD2 knockout cell line

The sgRNA oligomers for *CHCHD2* targeting exon 1 and exon 3 were annealed and inserted into plasmid pSpCas9(BB)-2A-Puro (PX459) V2.0 from Addgene (62988) via combined ligation (T7 ligase NEB) and restriction enzyme (BpiI, NEB) reaction.

Sequence for sgRNA targeting exon 1 of *CHCHD2*:
5′-caccCCCGCATGGCCCCTCCGGCC-3′
3′-GGGCGTACCGGGGAGGCCGGcaaa-5′

Sequence for sgRNA targeting exon 3 of *CHCHD2*:
5′-caccCTGTTTGATCTCATAGAGGCA-3′
3′-GACAAACTAGAGTATCTCCGTcaaa-5′

The two plasmids (1.5 μg) were transfected into a control fibroblasts cell line with the jetPRIME reagent. Twenty-four hours after transfection, puromycin was added for 48 hours at a concentration of 5 μg/mL. Cells were than expanded and single clones were selected and analysed by immunoblot and sequencing for positive *CHCHD10* knockout cell lines.

Mitochondrial isolation

Fibroblasts were washed twice with phosphate buffered saline (PBS), resuspended in ice-cold buffer (250 mM sucrose,10 mM Tris–HCl, pH 7.4), and homogenized by nitrogen cavitation under 500 psi pressure for 5 min. A post-nuclear supernatant was obtained by centrifugation of the samples twice for 10 min at 600 × *g*. Mitochondria were pelleted by centrifugation for 10 min at 10 000 × *g* and washed once in the same buffer. Protein concentration was determined using the Bradford assay.

Antibodies

Antibodies directed against the following proteins were used in this study: CHCHD10 (Sigma, HPA003440), CHCHD2 (Sigma, HPA027407), CHCHD2 Nter, SDHA (Abcam, ab14715), ATP5A1 (Abcam, ab14748), NDUFA9 (Abcam, ab14713), COXI (Abcam, ab14705) and COXII (Abcam, ab110258), COXIV (Abcam, ab110261), IMMT/MIC60 (Proteintech, 10179-1-AP), CHCHD3/MIC19 (Proteintech, 25625-1-AP), GRSF1 (Sigma, HPA036984), OPA1 (BD BioSciences, 612606), MFN2 (Cell Signaling, 11925S), porin/VDAC (Calbiochem, 529534), ATP6 (Proteintech, 55313-1-AP), NDUFA10 (Santa Cruz, sc-376357), SCO1 (made in house), CHCHD4 (Proteintech, 21090-1-AP).

SDS-PAGE and immunoblot analysis

Cells were pelleted and lysed with 1.5% *n*-dodecyl-D-maltoside (DDM) in PBS with cOmplete™ protease inhibitor (Roche) for 15 min on ice. Cells were centrifuged at 20,000 × g for 20 min at 4 °C. Protein concentration was determined using Bradford assay. 2x Laemmli buffer was added to 20-30 µg of protein and denatured at 55 °C for 15 min. The mixture was run on denaturing 8 % to 12.5 % polyacrylamide gels. Separated proteins were transferred onto a nitrocellulose membrane and immunoblot analysis was performed with the indicated antibodies in 5% milk in tris-buffered saline and Tween 20 (TBST).

Non-reducing denaturing SDS-PAGE

50 μg isolated mitochondria were resuspended in 50 μL buffer (250 mM sucrose,10 mM Tris–HCl, pH 7.4) with 50 mM dithiothreitol (DTT) and set up at different temperatures for 15 minutes. The suspension was centrifuged at 10,000 × g for 8 min. The pellet was resuspended in 1X Laemmli buffer with 15mM 4-Acetamido-4'-Maleimidylstilbene-2,2'-Disulfonic Acid, Disodium salt (AMS, Sigma A485) and left for one hour at room temperature before loading on a 15 % SDS-PAGE gel.

Blue native (BN) PAGE and 2D-PAGE analysis

BN-PAGE was used to separate individual OXPHOS complexes. Isolated mitochondria were solubilized with 1% DDM (for standard OXPHOS extraction) or 4mg/mg protein digitonin (for supercomplexes), and 20 μg of solubilized samples were run in the first dimension on 6–15% or 8–15% polyacrylamide gradient gels as previously described (Straub et al., 2018). Two-dimensional (2D)-BN-PAGE/SDS-PAGE was carried out as detailed previously (Straub et al., 2018). The separated proteins were transferred to a nitrocellulose membrane and immunoblot analysis was performed with the indicated antibodies.

Immunofluorescence analysis

Immunofluorescence analyses were performed by fixing cells grown on glass coverslips with 4% formaldehyde in PBS at room temperature for 20 min, permeabilization in 0.1% Triton X-100 in PBS, blocking with 5% bovine serum albumin (BSA) in PBS, followed by incubation with primary antibodies in 5% BSA in PBS, for 1 h at RT. The appropriate anti-species secondary antibodies coupled to Alexa fluorochromes (Invitrogen) (1:1000) were further used for 30 min at RT. Coverslips were mounted onto slides using fluorescence mounting medium (Dako).

Stained cells were imaged using a 100× objective lenses (NA1.4) on an Olympus IX81 inverted microscope with appropriate lasers using an Andor/Yokogawa spinning disk system (CSU-X), with a sCMOS camera. For each condition, 31 cells were analysed. Error bars represent mean ± SD and *P*-values were calculated using an unpaired *t*-test.

For the analysis of mitochondrial morphology, all images were analysed in FIJI using a custom made macro (Schindelin et al., 2012). In short, after background subtraction using the Rolling Ball algorithm, a white top hat 3D filter was applied to the z-stacks (https://github.com/ijpb/MorphoLibJ, (Legland et al., 2016)). Next, a 2D rendering was created using a standard deviation projection of the z-stacks. After further filtering using a Bandpass filter and background subtraction, the contrast was enhanced using the "Enhance local contrast (CLAHE)" algorithm (https://imagej.net/Enhance_Local_Contrast_(CLAHE). The mitochondria were segmented using an Adaptive Threshold (https://sites.google.com/site/qingzongtseng/adaptivethreshold), and further processed using the built-in "Despeckle" and "Close" functions in FIJI. Finally, the mitochondrial morphology and network were analysed using the "Analyze Particles" and the "Skeletonize" functions.

Immunoprecipitation

Mitochondria (200 µg) isolated from fibroblasts were pelleted, rinsed once with PBS, and extracted in 200 µL of lysis buffer (10 mM Tris–HCl pH 7.5, 150 mM NaCl, 4mg digitonin/mg protein final concentration, and complete protease inhibitors (Roche)) on ice for 30 min. The extract was centrifuged at 20,000 *g* at 4°C for 20 min, and the supernatant was pre-cleared overnight with non-coated Dynabeads Protein A (Invitrogen) to reduce non-specific protein binding to the beads. Binding of indicated antibodies to Dynabeads Protein A (Invitrogen) was performed overnight. Antibodies were then cross-linked to the beads using 20 mM dimethyl pimelimidate (DMP) (Sigma). The immunoprecipitation reaction was performed overnight at 4°C. Samples were eluted using 0.1 M glycine pH 2.5/0.5% DDM, trichloroacetic acid precipitated, and analysed by mass spectrometry on an Orbitrap (Thermo Scientific) at the Institute de Recherches Cliniques (IRCM) de Montreal. The false discovery rate is < 5% with a Mascot score of 50.

RNA extraction and RNA sequencing

Total RNA from fibroblasts was extracted and purified by using RNeasy Mini kit (QIAGEN). RNA quality was tested on a 1% agarose gel and then RNA sequencing was performed by GENEWIZ on an Illumina HiSeq instrument.

Transcriptomic analysis

Transcriptomic analysis was performed by GENEWIZ. Briefly, the original read counts were normalized to adjust for various factors such as variations of sequencing yield between samples. These normalized read counts were used to accurately determine differentially expressed genes. Data quality assessments were performed to detect any samples that are not representative of their group, and thus, may affect the quality of the analysis. Using DESeq2, a comparison of gene expression between groups of samples was performed. The Wald test was used to generate p-values and log2 fold changes. Genes with an adjusted p-value < 0.05 and absolute log2 fold change > 1 were considered as differentially expressed genes. RNA sequencing data will be deposited to NCBI Gene Expression Omnibus (GEO).

Gene ontology analysis

Gene ontology (GO) analysis of significant differentially expressed transcripts was performed using the annotation tool ENRICHR (https://amp.pharm.mssm.edu/Enrichr/, GO_MF 2019), focusing on the GO term of biological processes (Chen et al., 2013, Kuleshov et al., 2016). As an input, gene symbols of genes passing the cut off of log2 fold change of $\gtrless \pm 0.3$ were used. A maximum p-value of 0.05 was chosen to select only significant enrichment.

Proteome extraction and analysis

Fibroblasts were grown to 90% confluency in 15 cm dishes (minimum of 2×10^6 cells per condition). Cells were rinsed 2-3 times with 1x PBS to remove cell culture media and pelleted at 600 × g. Cells were lysed with lysis buffer (50 mM HEPES, 1% SDS, 150 mM NaCl). The lysate was centrifuged at 16,000 × g for 10 minutes at 4 °C. Protein concentration was determined in the supernatant by BCA Protein Assay Kit (Thermo Fisher Scientific, #23227). 100 μg of protein was transferred into a new tube and the final volume was adjusted to 100 μL with 100 mM triethylammonium bicarbonate (TEAB). 5 μL of 200 mM tris(2-carboxyethyl)phosphine) (TCEP) was added and samples were incubated at 55 °C for 1 hour. 5 μL of 375 mM iodoacetamide was added to the mix and let stand for 30 minutes protected from light at room temperature. 600 μL of pre-chilled acetone (-20 °C) was added and the mix was put at -20 °C

over-night to precipitate. Samples were centrifuged at 8000 × g for 10 minutes at 4 °C. The tubes were carefully inverted to decant the acetone and dried for 30 min at room temperature. Samples were digested, labelled and analysed by mass spectrometry on an Orbitrap (Thermo Scientific) at the Institute de Recherches Cliniques de Montreal (IRCM). The isobaric labelling of the peptides was performed using 10-plex TMT reagents (Thermo Fisher Scientific).
Differentially expressed proteins were identified by performing Welch's t-statistic test, comparing patient cells with rescue cells in glucose and galactose. Values were normalized by subtraction of the mean from the log2 values of the comparison ratios. The mass spectrometry proteomics data sets will be deposited to ProteomeXchange Consortium.

Bioinformatic and statistical analysis

Pathways, transcripts and proteins selected in each condition were filtered after Benjamini-Hochberg correction at an adjusted p-value < 0.05 (FDR 5%). All data analysis and plots were generated using R and RStudio and modified using Adobe Illustrator CC. For the rest of the analysis, data were expressed as mean ± SEM, and p-values were calculated using two-tailed Welch's t-test for pairwise comparisons of metabolites and proteins and the Wald test for transcripts. Statistical tests were performed using RStudio and GraphPad Prism 6.0 (*, $P < 0.05$; **, $P < 0.01$; ***, $P < 0.001$; $n \geq 3$).

Acknowledgements

We thank Hana Antonicka for fruitful discussions and thorough critique of the manuscript. This work was supported by grants from the CIHR, Parkinson Canada, and the Muscular Dystrophy Association to EAS, and by the James Hunter ALS Initiative (JR, LZ). IS was supported by a scholarship from Parkinson Canada.

Conflict of interest statement: The authors report no conflict of interest.

References

Ajroud-Driss S, Fecto F, Ajroud K, Lalani I, Calvo SE, Mootha VK, Deng HX, Siddique N, Tahmoush AJ, Heiman-Patterson TD, Siddique T (2015) Mutation in the novel nuclear-encoded mitochondrial protein CHCHD10 in a family with autosomal dominant mitochondrial myopathy. *Neurogenetics* 16: 1-9

Anand R, Wai T, Baker MJ, Kladt N, Schauss AC, Rugarli E, Langer T (2014) The i-AAA protease YME1L and OMA1 cleave OPA1 to balance mitochondrial fusion and fission. *J Cell Biol* 204: 919-29

Anderson CJ, Bredvik K, Burstein SR, Davis C, Meadows SM, Dash J, Case L, Milner TA, Kawamata H, Zuberi A, Piersigilli A, Lutz C, Manfredi G (2019) ALS/FTD mutant CHCHD10 mice reveal a tissue-specific toxic gain-of-function and mitochondrial stress response. *Acta Neuropathol* 138: 103-121

Aras S, Bai M, Lee I, Springett R, Huttemann M, Grossman LI (2015) MNRR1 (formerly CHCHD2) is a bi-organellar regulator of mitochondrial metabolism. *Mitochondrion* 20: 43-51

Aras S, Pak O, Sommer N, Finley R, Jr., Huttemann M, Weissmann N, Grossman LI (2013) Oxygen-dependent expression of cytochrome c oxidase subunit 4-2 gene expression is mediated by transcription factors RBPJ, CXXC5 and CHCHD2. *Nucleic Acids Res* 41: 2255-66

Auranen M, Ylikallio E, Shcherbii M, Paetau A, Kiuru-Enari S, Toppila JP, Tyynismaa H (2015) CHCHD10 variant p.(Gly66Val) causes axonal Charcot-Marie-Tooth disease. *Neurol Genet* 1: e1

Baughman JM, Nilsson R, Gohil VM, Arlow DH, Gauhar Z, Mootha VK (2009) A computational screen for regulators of oxidative phosphorylation implicates SLIRP in mitochondrial RNA homeostasis. *PLoS Genet* 5: e1000590

Becker T, Bottinger L, Pfanner N (2012) Mitochondrial protein import: from transport pathways to an integrated network. *Trends Biochem Sci* 37: 85-91

Bueler H (2009) Impaired mitochondrial dynamics and function in the pathogenesis of Parkinson's disease. *Exp Neurol* 218: 235-46

Burstein SR, Valsecchi F, Kawamata H, Bourens M, Zeng R, Zuberi A, Milner TA, Cloonan SM, Lutz C, Barrientos A, Manfredi G (2018) In vitro and in vivo studies of the ALS-FTLD protein CHCHD10 reveal novel mitochondrial topology and protein interactions. *Hum Mol Genet* 27: 160-177

Calvo SE, Clauser KR, Mootha VK (2016) MitoCarta2.0: an updated inventory of mammalian mitochondrial proteins. *Nucleic Acids Res* 44: D1251-7

Chang CT, Hautbergue GM, Walsh MJ, Viphakone N, van Dijk TB, Philipsen S, Wilson SA (2013) Chtop is a component of the dynamic TREX mRNA export complex. *EMBO J* 32: 473-86

Chen EY, Tan CM, Kou Y, Duan Q, Wang Z, Meirelles GV, Clark NR, Ma'ayan A (2013) Enrichr: interactive and collaborative HTML5 gene list enrichment analysis tool. *BMC Bioinformatics* 14: 128

Chio A, Mora G, Sabatelli M, Caponnetto C, Traynor BJ, Johnson JO, Nalls MA, Calvo A, Moglia C, Borghero G, Monsurro MR, La Bella V, Volanti P, Simone I, Salvi F, Logullo FO, Nilo R, Battistini S, Mandrioli J, Tanel R et al. (2015) CHCH10 mutations in an Italian cohort of familial and sporadic amyotrophic lateral sclerosis patients. *Neurobiol Aging* 36: 1767 e3-1767 e6

Dols-Icardo O, Nebot I, Gorostidi A, Ortega-Cubero S, Hernandez I, Rojas-Garcia R, Garcia-Redondo A, Povedano M, Llado A, Alvarez V, Sanchez-Juan P, Pardo J, Jerico I, Vazquez-Costa J, Sevilla T, Cardona F, Indakoechea B, Moreno F, Fernandez-Torron R, Munoz-Llahuna L et al. (2015) Analysis of the CHCHD10 gene in patients with frontotemporal dementia and amyotrophic lateral sclerosis from Spain. *Brain* 138: e400

Erdogan AJ, Ali M, Habich M, Salscheider SL, Schu L, Petrungaro C, Thomas LW, Ashcroft M, Leichert LI, Roma LP, Riemer J (2018) The mitochondrial oxidoreductase CHCHD4 is present in a semi-oxidized state in vivo. *Redox Biol* 17: 200-206

Floyd BJ, Wilkerson EM, Veling MT, Minogue CE, Xia C, Beebe ET, Wrobel RL, Cho H, Kremer LS, Alston CL, Gromek KA, Dolan BK, Ulbrich A, Stefely JA, Bohl SL, Werner KM, Jochem A,

Westphall MS, Rensvold JW, Taylor RW et al. (2016) Mitochondrial Protein Interaction Mapping Identifies Regulators of Respiratory Chain Function. *Mol Cell* 63: 621-632

Foo JN, Liu J, Tan EK (2015) CHCHD2 and Parkinson's disease. *Lancet Neurol* 14: 681-2

Funayama M, Ohe K, Amo T, Furuya N, Yamaguchi J, Saiki S, Li Y, Ogaki K, Ando M, Yoshino H, Tomiyama H, Nishioka K, Hasegawa K, Saiki H, Satake W, Mogushi K, Sasaki R, Kokubo Y, Kuzuhara S, Toda T et al. (2015) CHCHD2 mutations in autosomal dominant late-onset Parkinson's disease: a genome-wide linkage and sequencing study. *Lancet Neurol* 14: 274-82

Hein MY, Hubner NC, Poser I, Cox J, Nagaraj N, Toyoda Y, Gak IA, Weisswange I, Mansfeld J, Buchholz F, Hyman AA, Mann M (2015) A human interactome in three quantitative dimensions organized by stoichiometries and abundances. *Cell* 163: 712-23

Henchcliffe C, Beal MF (2008) Mitochondrial biology and oxidative stress in Parkinson disease pathogenesis. *Nat Clin Pract Neurol* 4: 600-9

Huang X, Wu BP, Nguyen D, Liu YT, Marani M, Hench J, Benit P, Kozjak-Pavlovic V, Rustin P, Frank S, Narendra DP (2018) CHCHD2 accumulates in distressed mitochondria and facilitates oligomerization of CHCHD10. *Hum Mol Genet* 27: 3881-3900

Huttlin EL, Ting L, Bruckner RJ, Gebreab F, Gygi MP, Szpyt J, Tam S, Zarraga G, Colby G, Baltier K, Dong R, Guarani V, Vaites LP, Ordureau A, Rad R, Erickson BK, Wuhr M, Chick J, Zhai B, Kolippakkam D et al. (2015) The BioPlex Network: A Systematic Exploration of the Human Interactome. *Cell* 162: 425-440

Ikeda A, Matsushima T, Daida K, Nakajima S, Conedera S, Li Y, Yoshino H, Oyama G, Funayama M, Nishioka K, Hattori N (2017) A novel mutation of CHCHD2 p.R8H in a sporadic case of Parkinson's disease. *Parkinsonism Relat Disord* 34: 66-68

Imai Y, Meng H, Shiba-Fukushima K, Hattori N (2019) Twin CHCH Proteins, CHCHD2, and CHCHD10: Key Molecules of Parkinson's Disease, Amyotrophic Lateral Sclerosis, and Frontotemporal Dementia. *Int J Mol Sci* 20

Jady BE, Ketele A, Kiss T (2018) Dynamic association of human mRNP proteins with mitochondrial tRNAs in the cytosol. *RNA* 24: 1706-1720

Jansen IE, Bras JM, Lesage S, Schulte C, Gibbs JR, Nalls MA, Brice A, Wood NW, Morris H, Hardy JA, Singleton AB, Gasser T, Heutink P, Sharma M, Ipdgc (2015) CHCHD2 and Parkinson's disease. *Lancet Neurol* 14: 678-9

Johnson JO, Glynn SM, Gibbs JR, Nalls MA, Sabatelli M, Restagno G, Drory VE, Chio A, Rogaeva E, Traynor BJ (2014) Mutations in the CHCHD10 gene are a common cause of familial amyotrophic lateral sclerosis. *Brain* 137: e311

Katahira J (2012) mRNA export and the TREX complex. *Biochim Biophys Acta* 1819: 507-13

Koschmidder E, Weissbach A, Bruggemann N, Kasten M, Klein C, Lohmann K (2016) A nonsense mutation in CHCHD2 in a patient with Parkinson disease. *Neurology* 86: 577-9

Kuleshov MV, Jones MR, Rouillard AD, Fernandez NF, Duan Q, Wang Z, Koplev S, Jenkins SL, Jagodnik KM, Lachmann A, McDermott MG, Monteiro CD, Gundersen GW, Ma'ayan A (2016) Enrichr: a comprehensive gene set enrichment analysis web server 2016 update. *Nucleic Acids Res* 44: W90-7

Kurzwelly D, Kruger S, Biskup S, Heneka MT (2015) A distinct clinical phenotype in a German kindred with motor neuron disease carrying a CHCHD10 mutation. *Brain* 138: e376

Kyte J, Doolittle RF (1982) A simple method for displaying the hydropathic character of a protein. *J Mol Biol* 157: 105-32

Leary SC, Sasarman F, Nishimura T, Shoubridge EA (2009) Human SCO2 is required for the synthesis of CO II and as a thiol-disulphide oxidoreductase for SCO1. *Hum Mol Genet* 18: 2230-40

Lee RG, Sedghi M, Salari M, Shearwood AJ, Stentenbach M, Kariminejad A, Goullee H, Rackham O, Laing NG, Tajsharghi H, Filipovska A (2018) Early-onset Parkinson disease caused by a mutation in CHCHD2 and mitochondrial dysfunction. *Neurol Genet* 4: e276

Legland D, Arganda-Carreras I, Andrey P (2016) MorphoLibJ: integrated library and plugins for mathematical morphology with ImageJ. *Bioinformatics* 32: 3532-3534

Lehmer C, Schludi MH, Ransom L, Greiling J, Junghanel M, Exner N, Riemenschneider H, van der Zee J, Van Broeckhoven C, Weydt P, Heneka MT, Edbauer D (2018) A novel CHCHD10 mutation implicates a Mia40-dependent mitochondrial import deficit in ALS. *EMBO Mol Med* 10

Li NN, Wang L, Tan EK, Cheng L, Sun XY, Lu ZJ, Li JY, Zhang JH, Peng R (2016) Genetic analysis of CHCHD2 gene in Chinese Parkinson's disease. *Am J Med Genet B Neuropsychiatr Genet* 171: 1148-1152

Liu Y, Clegg HV, Leslie PL, Di J, Tollini LA, He Y, Kim TH, Jin A, Graves LM, Zheng J, Zhang Y (2015) CHCHD2 inhibits apoptosis by interacting with Bcl-x L to regulate Bax activation. *Cell Death Differ* 22: 1035-46

Liu Y-T, Huang X, Nguyen D, Dombi E, Springer DA, Poulton J, Sekine S, Narendra DP (2019) Loss of CHCHD2 and CHCHD10 activates OMA1 peptidase to disrupt mitochondrial cristae phenocopying patient mutations. *bioRxiv*: 773135

Lochmuller H, Johns T, Shoubridge EA (1999) Expression of the E6 and E7 genes of human papillomavirus (HPV16) extends the life span of human myoblasts. *Exp Cell Res* 248: 186-93.

Lu B, Gehrke S, Wu Z (2014) RNA metabolism in the pathogenesis of Parkinsons disease. *Brain Res* 1584: 105-15

Mao C, Wang H, Luo H, Zhang S, Xu H, Zhang S, Rosenblum J, Wang Z, Zhang Q, Tang M, Shepard MJ, Wang X, Wang Y, Zhuang Z, Shi C, Xu Y (2019) CHCHD10 is involved in the development of Parkinson's disease caused by CHCHD2 loss-of-function mutation p.T61I. *Neurobiol Aging* 75: 38-41

Meng H, Yamashita C, Shiba-Fukushima K, Inoshita T, Funayama M, Sato S, Hatta T, Natsume T, Umitsu M, Takagi J, Imai Y, Hattori N (2017) Loss of Parkinson's disease-associated protein CHCHD2 affects mitochondrial crista structure and destabilizes cytochrome c. *Nat Commun* 8: 15500

Morais VA, Haddad D, Craessaerts K, De Bock PJ, Swerts J, Vilain S, Aerts L, Overbergh L, Grunewald A, Seibler P, Klein C, Gevaert K, Verstreken P, De Strooper B (2014) PINK1 loss-of-function mutations affect mitochondrial complex I activity via NdufA10 ubiquinone uncoupling. *Science* 344: 203-7

Muller K, Andersen PM, Hubers A, Marroquin N, Volk AE, Danzer KM, Meitinger T, Ludolph AC, Strom TM, Weishaupt JH (2014) Two novel mutations in conserved codons indicate that CHCHD10 is a gene associated with motor neuron disease. *Brain* 137: e309

Muta T, Kang D, Kitajima S, Fujiwara T, Hamasaki N (1997) p32 protein, a splicing factor 2-associated protein, is localized in mitochondrial matrix and is functionally important in maintaining oxidative phosphorylation. *J Biol Chem* 272: 24363-70

Nayak RR, Kearns M, Spielman RS, Cheung VG (2009) Coexpression network based on natural variation in human gene expression reveals gene interactions and functions. *Genome Res* 19: 1953-62

Nicoletti G, Gagliardi M, Procopio R, Iannello G, Morelli M, Annesi G, Quattrone A (2018) A new CHCHD2 mutation identified in a southern italy patient with multiple system atrophy. *Parkinsonism Relat Disord* 47: 91-93

Nussbaum RL, Ellis CE (2003) Alzheimer's disease and Parkinson's disease. *N Engl J Med* 348: 1356-64

Ogaki K, Koga S, Heckman MG, Fiesel FC, Ando M, Labbe C, Lorenzo-Betancor O, Moussaud-Lamodiere EL, Soto-Ortolaza AI, Walton RL, Strongosky AJ, Uitti RJ, McCarthy A, Lynch T, Siuda J, Opala G, Rudzinska M, Krygowska-Wajs A, Barcikowska M, Czyzewski K et al. (2015) Mitochondrial targeting sequence variants of the CHCHD2 gene are a risk for Lewy body disorders. *Neurology* 85: 2016-25

Pasanen P, Myllykangas L, Poyhonen M, Kiuru-Enari S, Tienari PJ, Laaksovirta H, Toppila J, Ylikallio E, Tyynismaa H, Auranen M (2016) Intrafamilial clinical variability in individuals carrying the CHCHD10 mutation Gly66Val. *Acta Neurol Scand* 133: 361-6

Penttila S, Jokela M, Bouquin H, Saukkonen AM, Toivanen J, Udd B (2015) Late onset spinal motor neuronopathy is caused by mutation in CHCHD10. *Ann Neurol* 77: 163-72

Pozo Devoto VM, Falzone TL (2017) Mitochondrial dynamics in Parkinson's disease: a role for alpha-synuclein? *Dis Model Mech* 10: 1075-1087

Purandare N, Somayajulu M, Huttemann M, Grossman LI, Aras S (2018) The cellular stress proteins CHCHD10 and MNRR1 (CHCHD2): Partners in mitochondrial and nuclear function and dysfunction. *J Biol Chem* 293: 6517-6529

Ronchi D, Riboldi G, Del Bo R, Ticozzi N, Scarlato M, Galimberti D, Corti S, Silani V, Bresolin N, Comi GP (2015) CHCHD10 mutations in Italian patients with sporadic amyotrophic lateral sclerosis. *Brain* 138: e372

Rubino E, Zhang M, Mongini T, Boschi S, Vercelli L, Vacca A, Govone F, Gai A, Giordana MT, Grinberg M, Rogaeva E, Rainero I (2018) Mutation analysis of CHCHD2 and CHCHD10 in Italian patients with mitochondrial myopathy. *Neurobiol Aging* 66: 181 e1-181 e2

Ryan M, Zaldivar Vaillant T, McLaughlin RL, Doherty MA, Rooney J, Heverin M, Gutierrez J, Lara-Fernandez GE, Pita Rodriguez M, Hackembruch J, Perna A, Vazquez MC, Musio M, Ketzoian CN, Logroscino G, Hardiman O (2019) Comparison of the clinical and genetic features of amyotrophic lateral sclerosis across Cuban, Uruguayan and Irish clinic-based populations. *J Neurol Neurosurg Psychiatry* 90: 659-665

Santos D, Esteves AR, Silva DF, Januario C, Cardoso SM (2015) The Impact of Mitochondrial Fusion and Fission Modulation in Sporadic Parkinson's Disease. *Mol Neurobiol* 52: 573-86

Schindelin J, Arganda-Carreras I, Frise E, Kaynig V, Longair M, Pietzsch T, Preibisch S, Rueden C, Saalfeld S, Schmid B, Tinevez JY, White DJ, Hartenstein V, Eliceiri K, Tomancak P, Cardona A (2012) Fiji: an open-source platform for biological-image analysis. *Nat Methods* 9: 676-82

Shen S, He J, Tang L, Zhang N, Fan D (2017) CHCHD10 mutations in patients with amyotrophic lateral sclerosis in Mainland China. *Neurobiol Aging* 54: 214 e7-214 e10

Shi CH, Mao CY, Zhang SY, Yang J, Song B, Wu P, Zuo CT, Liu YT, Ji Y, Yang ZH, Wu J, Zhuang ZP, Xu YM (2016) CHCHD2 gene mutations in familial and sporadic Parkinson's disease. *Neurobiol Aging* 38: 217 e9-217 e13

Shi M, Zhang H, Wu X, He Z, Wang L, Yin S, Tian B, Li G, Cheng H (2017) ALYREF mainly binds to the 5' and the 3' regions of the mRNA in vivo. *Nucleic Acids Res* 45: 9640-9653

Shoffner JM, Watts RL, Juncos JL, Torroni A, Wallace DC (1991) Mitochondrial oxidative phosphorylation defects in Parkinson's disease. *Ann Neurol* 30: 332-9

Straub IR, Janer A, Weraarpachai W, Zinman L, Robertson J, Rogaeva E, Shoubridge EA (2018) Loss of CHCHD10-CHCHD2 complexes required for respiration underlies the pathogenicity of a CHCHD10 mutation in ALS. *Hum Mol Genet* 27: 178-189

Ueda E, Tamura Y, Sakaue H, Kawano S, Kakuta C, Matsumoto S, Endo T (2019) Myristoyl group-aided protein import into the mitochondrial intermembrane space. *Sci Rep* 9: 1185

Walter J, Bolognin S, Antony PMA, Nickels SL, Poovathingal SK, Salamanca L, Magni S, Perfeito R, Hoel F, Qing X, Jarazo J, Arias-Fuenzalida J, Ignac T, Monzel AS, Gonzalez-Cano L, Pereira de Almeida L, Skupin A, Tronstad KJ, Schwamborn JC (2019) Neural Stem Cells of Parkinson's Disease Patients Exhibit Aberrant Mitochondrial Morphology and Functionality. *Stem Cell Reports* 12: 878-889

Wei Y, Vellanki RN, Coyaud E, Ignatchenko V, Li L, Krieger JR, Taylor P, Tong J, Pham NA, Liu G, Raught B, Wouters BG, Kislinger T, Tsao MS, Moran MF (2015) CHCHD2 Is Coamplified with EGFR in NSCLC and Regulates Mitochondrial Function and Cell Migration. *Mol Cancer Res* 13: 1119-29

Wilson R, Gundamaraju R, Vemuri R, Angelucci C, Geraghty D, Gueven N, Eri RD (2020) Identification of Key Pro-Survival Proteins in Isolated Colonic Goblet Cells of Winnie, a Murine Model of Spontaneous Colitis. *Inflamm Bowel Dis* 26: 80-92

Winklhofer KF, Haass C (2010) Mitochondrial dysfunction in Parkinson's disease. *Biochim Biophys Acta* 1802: 29-44

Woo JA, Liu T, Trotter C, Fang CC, De Narvaez E, LePochat P, Maslar D, Bukhari A, Zhao X, Deonarine A, Westerheide SD, Kang DE (2017) Loss of function CHCHD10 mutations in cytoplasmic TDP-43 accumulation and synaptic integrity. *Nat Commun* 8: 15558

Wu H, Lu X, Cen Z, Xie F, Zheng X, Chen Y, Luo W (2016) Genetic analysis of the CHCHD2 gene in Chinese patients with familial essential tremor. *Neurosci Lett* 634: 104-106

Yagi M, Uchiumi T, Takazaki S, Okuno B, Nomura M, Yoshida S, Kanki T, Kang D (2012) p32/gC1qR is indispensable for fetal development and mitochondrial translation: importance of its RNA-binding ability. *Nucleic Acids Res* 40: 9717-37

Yang X, Zhao Q, An R, Zheng J, Tian S, Chen Y, Xu Y (2016) Mutational scanning of the CHCHD2 gene in Han Chinese patients with Parkinson's disease and meta-analysis of the literature. *Parkinsonism Relat Disord* 29: 42-6

Ye Q, Worman HJ (1994) Primary structure analysis and lamin B and DNA binding of human LBR, an integral protein of the nuclear envelope inner membrane. *J Biol Chem* 269: 11306-11

Zhang M, Xi Z, Zinman L, Bruni AC, Maletta RG, Curcio SA, Rainero I, Rubino E, Pinessi L, Nacmias B, Sorbi S, Galimberti D, Lang AE, Fox S, Surace EI, Ghani M, Guo J, Sato C, Moreno D, Liang Y et al. (2015) Mutation analysis of CHCHD10 in different neurodegenerative diseases. *Brain* 138: e380

Zhang X, Zhang F, Guo L, Wang Y, Zhang P, Wang R, Zhang N, Chen R (2013) Interactome analysis reveals that C1QBP (complement component 1, q subcomponent binding protein) is associated with cancer cell chemotaxis and metastasis. *Mol Cell Proteomics* 12: 3199-209

Zhao M, Kim JR, van Bruggen R, Park J (2018) RNA-Binding Proteins in Amyotrophic Lateral Sclerosis. *Mol Cells* 41: 818-829

Zhou Q, Chen Y, Wei Q, Cao B, Wu Y, Zhao B, Ou R, Yang J, Chen X, Hadano S, Shang HF (2017) Mutation Screening of the CHCHD10 Gene in Chinese Patients with Amyotrophic Lateral Sclerosis. *Mol Neurobiol* 54: 3189-3194

Figures

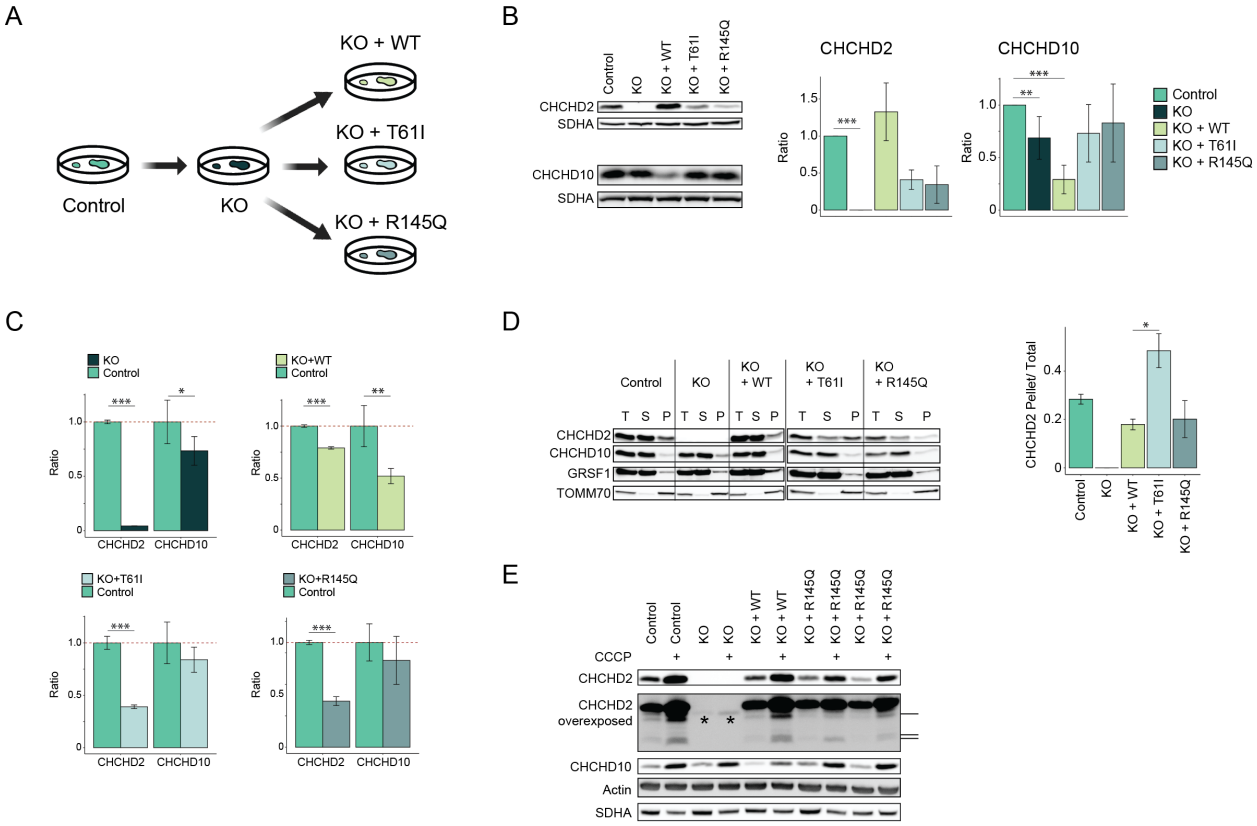

Figure 4.1 Characterization of the CHCHD2 knock out cell and cells expressing wild-type CHCHD2 or the pathogenic CHCHD2 variants p.T61I and p.R145Q.

(A) Schematic representation of the experimental set up. Control fibroblasts (Control) were used to generate a CRISPR-Cas9 mediated knockout of CHCHD2 (KO). Subsequently, expression from a retroviral vector was used to reintroduce wild-type CHCHD2 (KO+WT) or one of the two pathogenic disease variants p.T61I (KO+T61I) or p.R145Q (KO+R145Q).

(B) Immunoblot analysis of protein levels of CHCHD2 and CHCHD10. Whole cell extracts were separated by SDS-PAGE and probed with antibodies against the indicated proteins. SDHA was used as a loading control. Bar plot indicates the quantification of the western blot analysis.

(C) mRNA levels of CHCHD2 and CHCHD10 in respective cell lines determined by RNAseq analysis in triplicates. An unpaired student's t-test, was used to test for significance *p<0.05, **p<0.01, ***p<0.001.

(D) Western blot analysis of alkaline carbonate extraction of mitochondria from control, knockout and rescued cell lines. TOMM70 (membrane protein with one transmembrane domain) and GRSF1 (soluble matrix protein) were used as controls. Bar plot indicates the quantification of the amount of CHCHD2 in the pellet in percent. T=total, S=soluble, P=pellet.
(E) Western blot analysis of proteins levels of CHCHD2 and CHCHD10 in CCCP treated cell lines. Whole cell extracts separated by SDS-PAGE and probed with antibodies against indicated proteins. Asterisks indicates leftover CHCHD10 staining from previous revelation. Lines on the right-hand side indicate positions of CHCHD2 short forms.

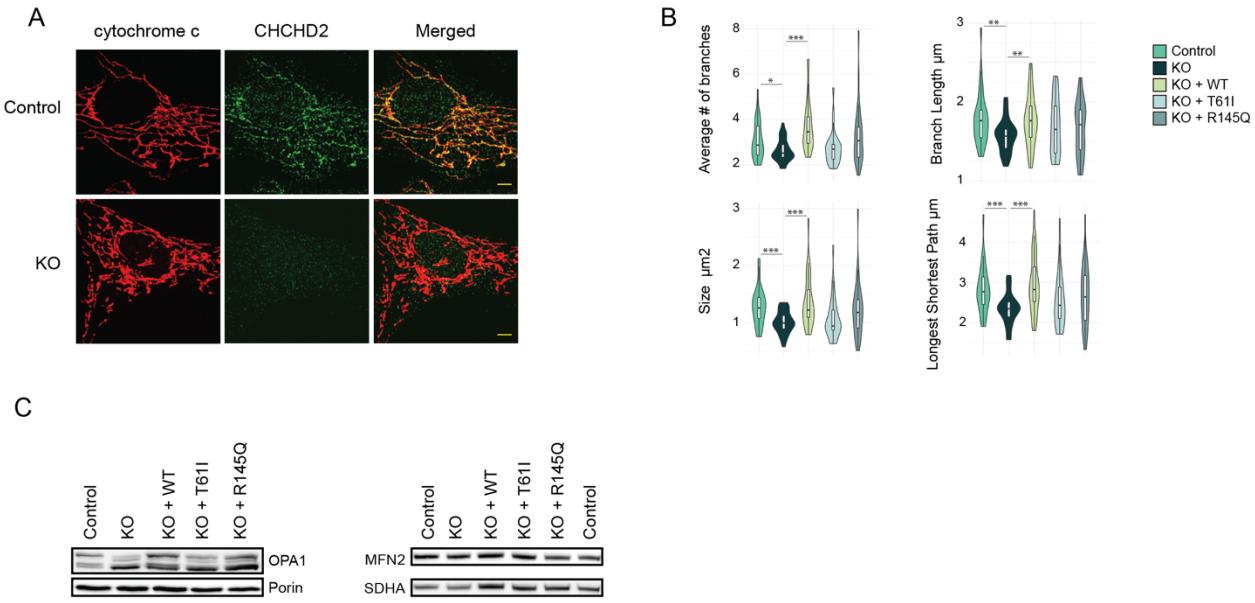

Figure 4.2 CHCHD2 knockout leads to altered mitochondrial morphology.

(A) Mitochondrial morphology of control and knockout fibroblasts. Immunofluorescence analysis of control and *CHCHD2* knockout fibroblasts. Endogenous CHCHD2 staining is shown in green, the mitochondrial marker cytochrome *c* is shown in red. Scale bar: 10 µm.

(B) Violin Plot representing the distribution of different parameters of mitochondrial morphology. The analysis was conducted with an Image J macros as described in Materials and Methods. Box plots indicate the median and the first and third quartile. Significance was tested using an unpaired student's t-test, *p<0.05, **p<0.01, ***p<0.001.

(C) Immunoblot analysis of protein components of the mitochondrial fission and fusion machinery and cristae organization. Whole cell extracts were separated by SDS-PAGE and probed with antibodies against the indicated proteins. SDHA and porin (VDAC) were used as loading controls. Bar plot indicates the quantification of the immunoblot analysis and the colour code is indicated in the legend.

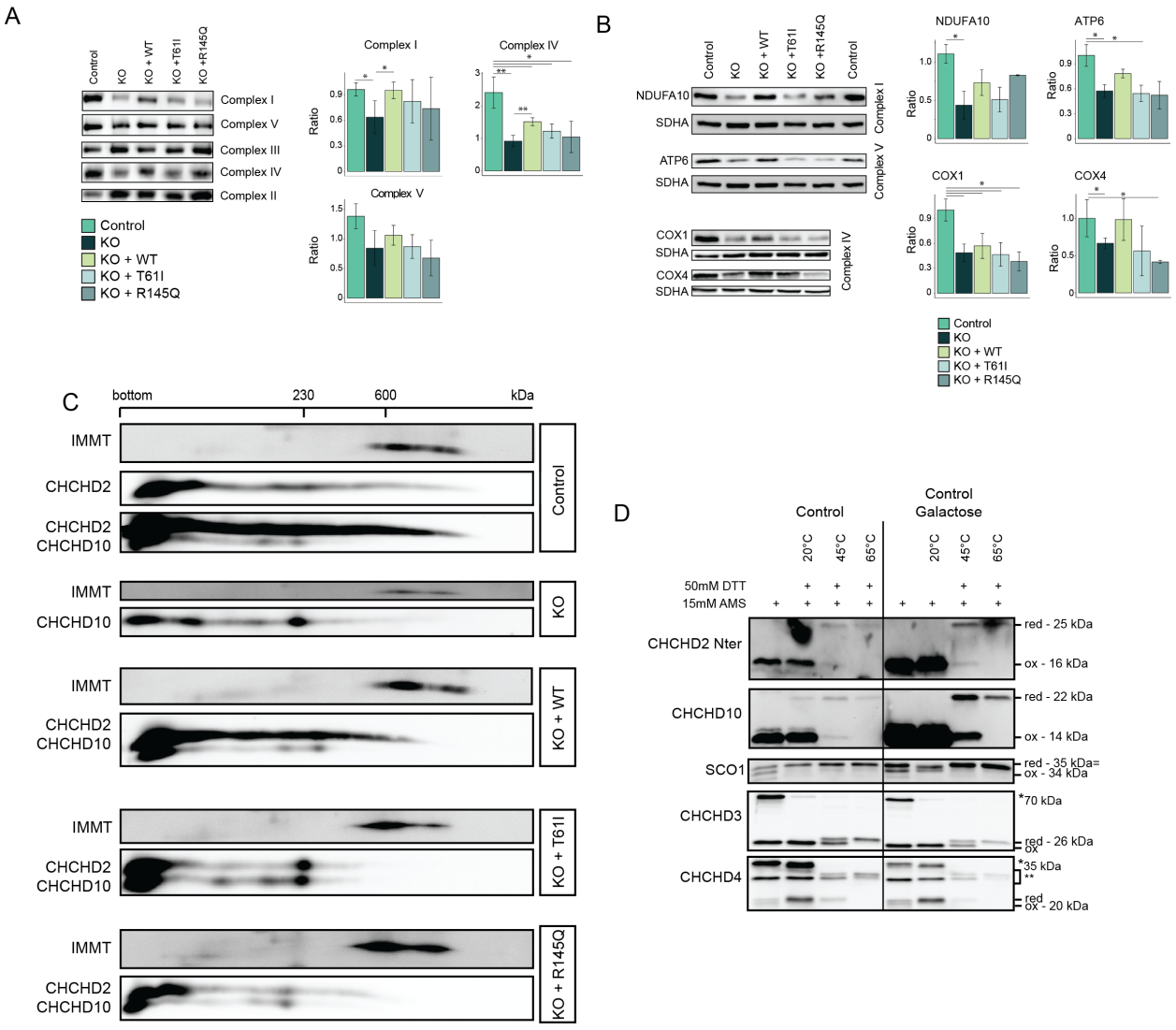

Figure 4.3 CHCHD2 knockout and mutants affect mitochondrial respiratory chain assembly and the interaction with CHCHD10.

(A) BN-PAGE analysis of knockout, disease variants and control fibroblasts. The assembly of individual OXPHOS complexes is revealed by subunit-specific antibodies. Quantification from three independent experiments normalized to Complex III, data represent mean ± SEM. *P*-values were calculated using a two-tailed, unpaired t-test $*p < 0.05$.

(B) Inmmunoblot analysis of components of the OXPHOS complexes. Whole cell extracts were separated by SDS-PAGE and probed with antibodies against subunits of OXPHOS complexes. SDHA was used as a loading control. Quantification from three independent

experiments, data represent mean ± SEM. *P*-values were calculated using a two-tailed, unpaired t-test *$p < 0.05$.

(C) Two-dimensional BN-PAGE/SDS-PAGE electrophoresis analysis of mitochondria from generated cell lines. The positions and molecular weight of identified CHCHD2/CHCHD10 containing complexes are indicated in kDa. Mitofilin (IMMT) was used for size reference.

(D) Non-reducing SDS-PAGE analysis of the cysteine bonds formed by CX_9C motif-containing proteins in glucose and galactose media. Isolated mitochondria from control fibroblasts as well as control fibroblasts grown in galactose were treated at different temperatures with the reducing agent DTT and alkylating reagent, AMS. Antibodies against the indicated proteins where used to determine their redox state in different conditions (reduced/oxidized: red/ox). * asterisks indicate higher molecular weight intermolecular disulfide bonds between potentially two different proteins. For CHCHD3: at 70 kDa it is an interaction between CHCHD3 and CHCHD4.

A

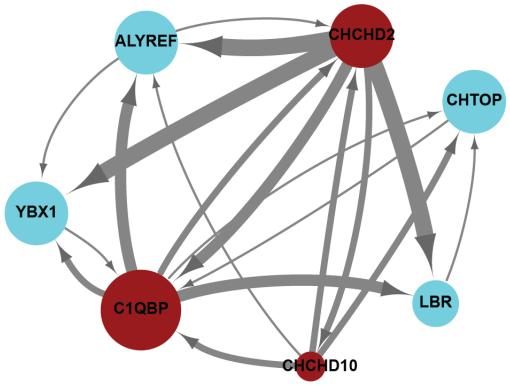

B

Total Spectral Counts			
Prey \ Bait	CHCHD2-WT	CHCHD2-T61I	CHCHD2-R145Q
CHCHD2	26 (0)	15 (0)	17 (0)
C1QBP	51 (0)	26 (0)	20 (0)
CHCHD10	5 (4)	4 (3)	6 (3)
ALYREF	15 (0)	1 (0)	2 (0)
MMP3	12 (0)		
MMP1	49 (2)		
EHD2	12 (0)	4 (0)	7 (0)
CTNND1	11 (0)	3 (0)	7 (0)
MTHFD1	10 (0)		10 (0)
FLNC	8 (0)	1 (0)	1 (0)
LONP1	6 (0)	2 (0)	12 (0)
DDX6	4 (0)		
LBR	4 (0)		
MYL12A	4 (0)	2 (0)	
YME1L1	3 (0)	15 (0)	6 (0)
FARSA	3 (0)		
FUBP3	3 (0)		
MVP			8 (0)
KIF5B			6 (0)
ANPEP		4 (0)	5 (0)
PICALM	3 (0)	2 (0)	5 (0)
CHTOP	2 (0)	3 (0)	2 (0)

Figure 4.4 CHCHD2 interacts with proteins of the RNA metabolism.

(A) Interactome of CHCHD2, CHCHD10 and C1QBP with proteins handling cellular mRNA. The interactome was created with datasets from BioGRID as well as data from previously published studies (Floyd et al., 2016, Hein et al., 2015, Huttlin et al., 2015, Wei et al., 2015, Zhang et al., 2013). Red nodes represent known mitochondrial proteins, according to Mitocarta2.0 (Calvo et al., 2016). Blue nodes represent proteins of non- mitochondrial localization and predominantly nuclear localization. The size of the node represents how many times the protein was interacting in one of the assays with another protein. The thickness of the edges is determined by the number of interactions detected (1-4). The arrowheads point in the direction of the detected interaction (from bait to prey).

(B) Co-immunoprecipitation experiment of CHCHD2 in cells expressing CHCHD2 wild-type and two pathogenic variants. Total spectral counts are shown for antibody-specific interactions, versus knockout (number in parentheses).

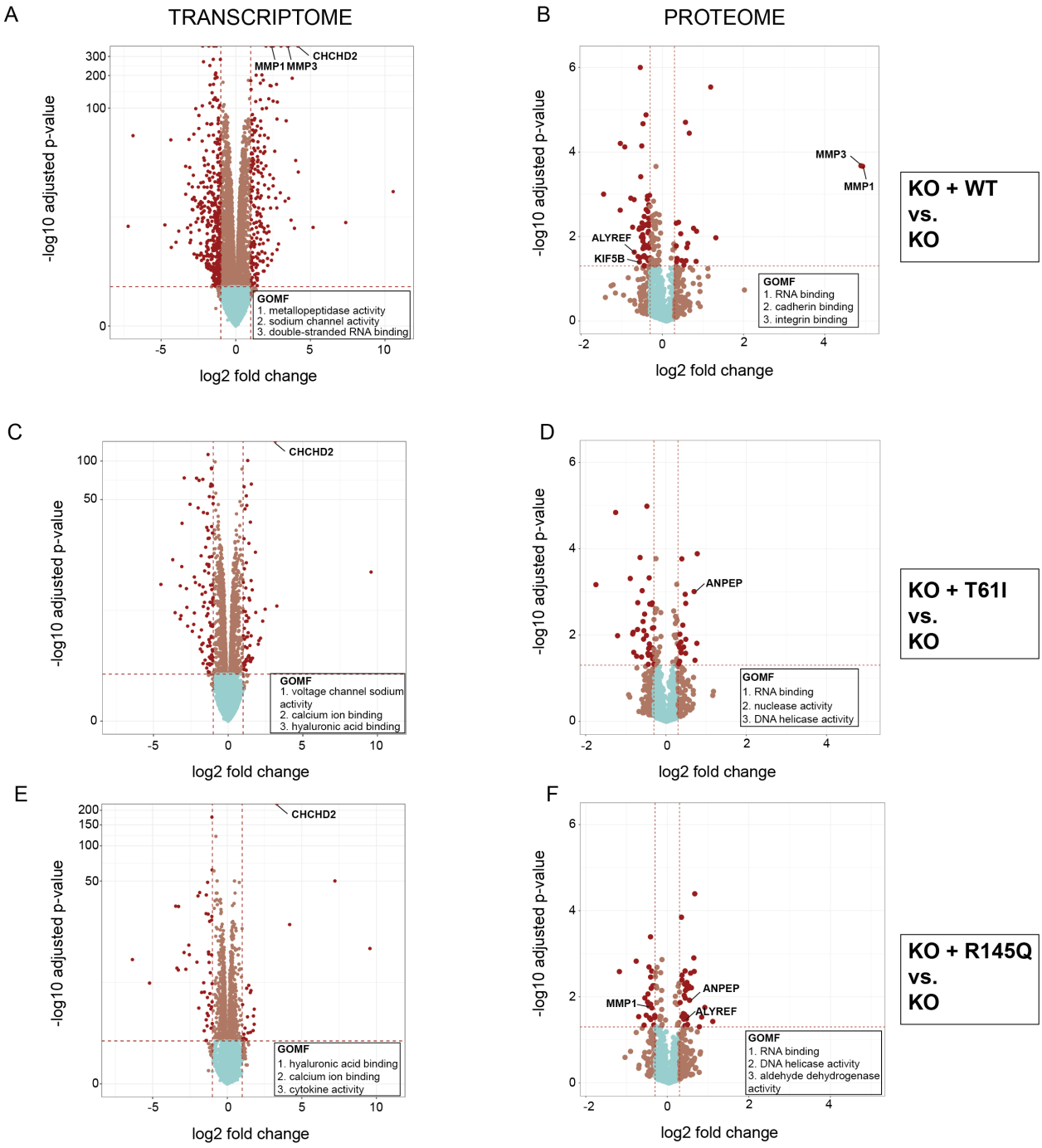

Figure 4.5 CHCHD2 knockout and variants affect levels of RNA binding proteins.

(A-F) Volcano plots showing differentially expressed transcripts (A, C, E) and proteins (B, D, F) in CHCHD2 knockout cells versus those rescued with wild-type CHCHD2 (A, B) or the pathogenic variants p.T61I (C, D) and p.R145Q (E, F) variant. Changes are depicted as log2 fold change of the respective ratio. x-axis values represent the log2 fold change (log2FC) and y-axis

values represent the -log10 of the adjusted p-value (false discovery rate, FDR<0.05). Deep red dots represent hits passing the two thresholds set for the experiment (transcriptome: log2FC<±1, FDR<0.05: proteome: log2FC<±0.3, FDR<0.05). Light red dots are significant but do not pass the log2FC threshold. Light blue dots represent values below the two thresholds. Labels for transcripts and proteins were used for hits from the immunoprecipitation experiment passing both thresholds (Fig. 4B). Insets represent the most enriched molecular functions after enrichment analysis of differentially expressed transcript or proteins using the GO term for molecular function (GOMF).

Supplementary Material

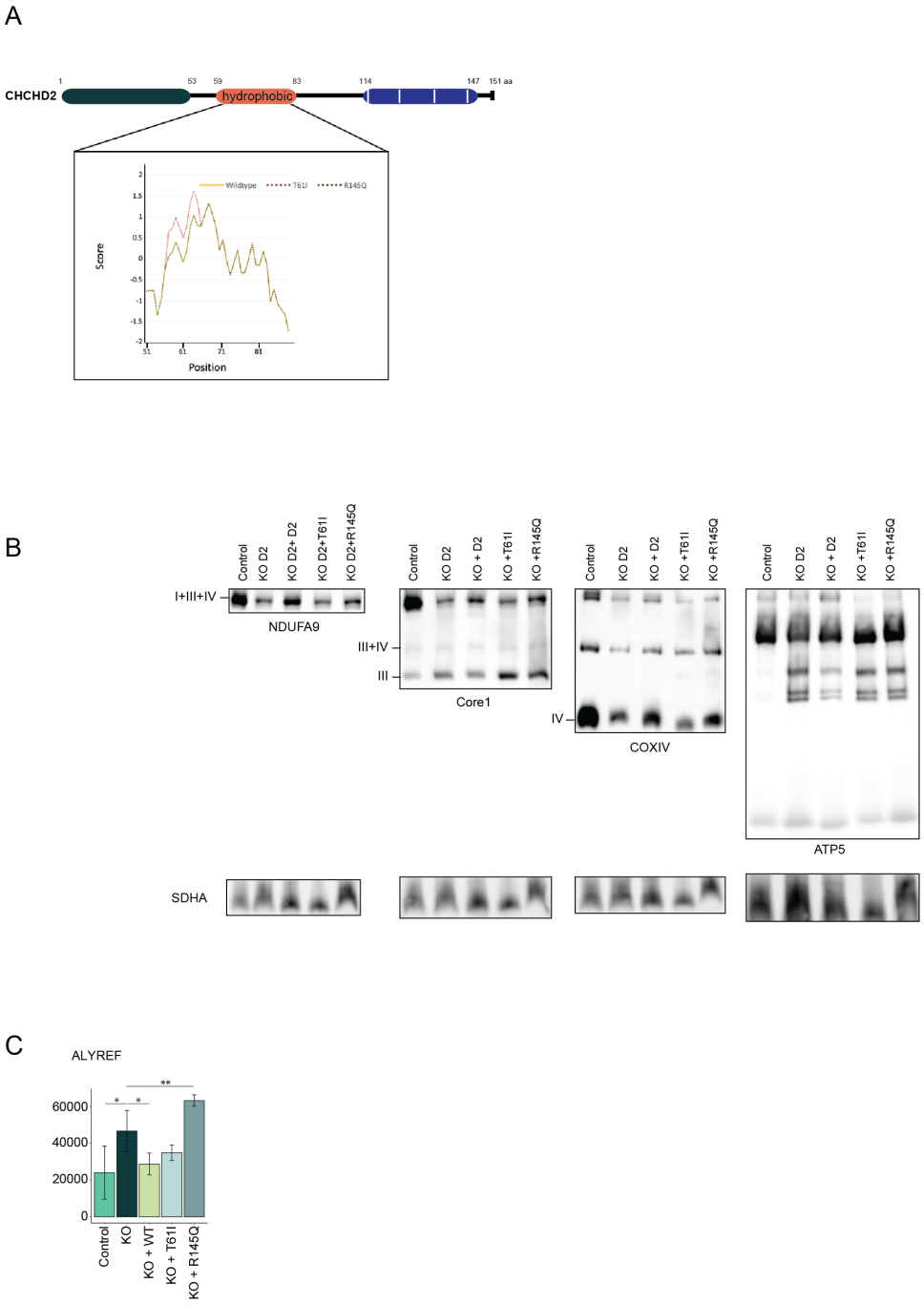

Figure S4.1 Supplementary data.

(A) Scheme of CHCHD2 with hydrophobicity plot and scores according to Kyte & Doolittle (Kyte & Doolittle, 1982). Wild-type CHCHD2 protein is shown in yellow, CHCHD2 p.T61I with a dotted red line, and CHCHD2 p.R145Q with a dotted green line.
(B) BN-PAGE electrophoresis showing OXPHOS supercomplexes. The assembly of individual OXPHOS complexes is revealed by subunit-specific antibodies and the type of supercomplexes are indicated.
(C) Protein levels of ALYREF determined by TMT-labelled LC/MS in respective cell lines in triplicates. An unpaired student's t-test, was used to test for significance *p<0.05, **p<0.01, ***p<0.001.

Chapter 5: General Discussion

5. General Discussion

CHCHD2 and *CHCHD10* code for two paralogous, predominately mitochondrial proteins that have been implicated in neurodegenerative disease (Imai et al., 2019b, Kim et al., 2018). Despite a shared sequence identity of 55 % (amino acids), the association with disease is distinctly different: CHCHD2 is predominantly associated with Parkinson's Disease, and CHCHD10 with ALS/FTD (Imai et al., 2019b). This thesis addressed the influence of CHCHD10 and CHCHD2 on mitochondrial function. We identified a complex between CHCHD10 and CHCHD2 in control cells, that is not formed in CHCHD10 p.R15L patient cells, which exhibit a respiratory chain defect. Although CHCHD10 has a role in mitochondrial complex I function, as demonstrated by a reduction in the levels of the fully assembled complex in patient cells and the decrease in oxygen consumption by the respiratory chain, its precise molecular remains unknown. Moreover, patient cells are less likely to survive during nutrient stress and respond by activating the universal integrated stress response, and concomitantly the release of two mitochondrial disease markers GDF15 and FGF21.

Loss of CHCHD2, as well as the presence of CHCHD2 pathogenic variants also influence the CHCHD10/CHCHD2 complex formation. In particular the more hydrophobic variant CHCHD2 p.T61I alters the complex and more CHCHD2 protein accumulated in the high molecular weight complex. We discovered that the CHCHD2 knockout affected the integrity of the oxidative phosphorylation complexes, specifically by affecting complex I, IV and V. The reintroduction of the wild-type CHCHD2 could rescue the complex I defect and partially rescue the complex IV defect as well as the disassembly of complex V. Furthermore, we established the existence of short forms of CHCHD2. Lastly, we identified a new interactome of CHCHD10 and CHCHD2 with proteins involved in RNA metabolism outside of mitochondria. In the next few paragraphs the contribution of this thesis is highlighted and brought into context with the literature.

5.1 Localization of CHCHD10 and CHCHD2

We started our investigation by exploring the localization of CHCHD10 and CHCHD2 as well as their pathogenic variants. Two earlier studies identified the yeast homologue of

CHCHD10 and CHCHD2, Mic17 (YMR002W) as a mitochondrial as well as a cytoplasmic and nuclear protein (Gabriel et al., 2007, Huh et al., 2003). CHCHD10 and CHCHD2 are classical twin CX_9C-motif proteins with a putative MTS, and are therefore predicted to predominantly localize to mitochondria. Many proteins in the IMS are imported through the translocases of the inner and outer membrane with a characteristic N-terminal MTS sequence, others are targeted by the twin CX_3C or CX_9C motif (Longen et al., 2009) (Fig. 5.1). It has been shown that the CHCH-motif of CHCHD10, and not the MTS, is crucial for mitochondrial localization, and this is likely also the case for CHCHD2 (Lehmer et al., 2018). SDS-PAGE analysis demonstrated that CHCHD10 and CHCHD2 run at their predicted molecular masses, suggesting that the putative MTS is not processed under normal physiological conditions. However, we identified several short forms of CHCHD2, which could be the result of the processing of CHCHD2 by an inner membrane or intermembrane space protease (Fig. 5.1).

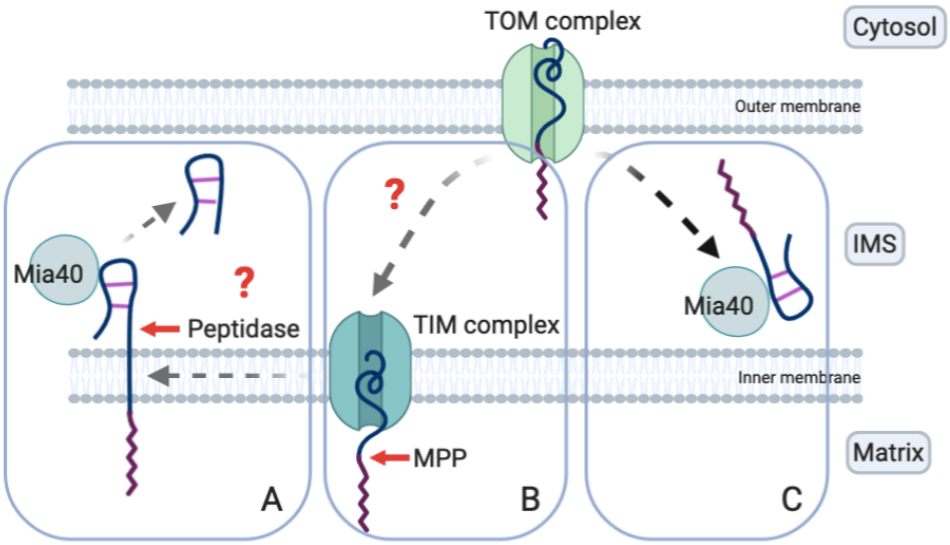

Figure 5.1 Potential import pathways of CHCHD10 and CHCHD2 (created with *BioRender*).

(A) Import through the STOP-transfer pathway, where the mitochondrial processing peptidase (MMP) cleaves the mitochondrial targeting sequence (MTS) in the matrix and the protein is then cleaved by another peptidase to give rise to a soluble protein in the IMS.

(B) Import into the mitochondrial matrix and classical processing of the MTS.

(C) Experimentally validated import pathway for CHCHD10 and CHCHD2: import into the IMS through the oxidation of Mia40 without processing of the MTS.

CHCHD2 contains classical features of a protein with a bipartite presequence (MTS + hydrophobic domain) imported into mitochondria by the so-called STOP-transfer pathway (Gasser et al., 1982). Hence, the protein has a probability for a processing event in or nearby the hydrophobic domain by one of the proteases PARL, IMMP1L, IMMP2L or with lower probability OMA1, YME1L, HTRA2 or XRCCBP6/KUB3. The sequence for CHCHD2 contains several conserved features including a possible MPP cleavage site after aa52, a possible PARL cleavage site after aa63, and a possible signal peptidase cleavage site after aa79 predicted by SignalP4.1 (Nielsen, 2017). It is therefore possible that a small amount of CHCHD2 is matured by one of these proteases and results in a soluble IMS protein of smaller size. Other IMS proteins that follow the stop-transfer pathway are cytochrome b_2 (Glick et al., 1992), apoptosis-inducing factor (AIF) (Hasson et al., 2010), and DIABLO (Burri et al., 2005).

In our study we analysed five different CHCHD10 variants (p.R15L, p.G58R, p.S59L, p.G66V and p.P80L) by immunofluorescence, all of which localized to mitochondria (unpublished data). Likewise, CHCHD2 wild-type as well as the p.T61I an p.R145Q localized to mitochondria. Analysing the localization of a protein by immunofluorescence, however, has the caveat that the experiment depends on the quality of the antibody, as well as the fact, that small amounts of a protein in a different compartment might not be detectable due to the very strong signal in mitochondria. Other studies reported a localization of CHCHD10 and CHCHD2 outside of mitochondria by immunofluorescence in stress conditions like hypoxia or the overexpression of TDP43 (Purandare et al., 2018, Woo et al., 2017). Another approach for the analysis of protein localization is cellular fractionation; however, the inevitable small amounts of contamination from other cellular compartments hampers the ability to provide conclusive evidence for multiple localizations. The majority of the endogenous CHCHD10 and CHCHD2 proteins localized to the mitochondrial intermembrane space by cellular fractionation; however, a small proportion of the CHCHD10, and even more so CHCHD2, also localized to the cytosol (unpublished data). In stress conditions, like hypoxia, treatment with CCCP or galactose we could not detect any significant amount of CHCHD10 or CHCHD2 outside of mitochondria by immunofluorescence (unpublished data); however, it would be valuable to test this by cellular fractionation.

In conclusion, we suggest CHCHD10 and CHCHD2 are predominantly mitochondrial proteins; however, our data cannot exclude a partial localization outside of mitochondria.

5.2 Protein expression of CHCHD10 and CHCHD2

CHCHD10 and CHCHD2 expression was highly variable in control cells and in different cell types. Cancer cell lines like 143B cells (osteosarcoma), HeLa and HEK showed high levels, whereas fibroblasts have rather low protein expression (unpublished results). Different types of neurons showed very different expression as well, and astrocytes, the motor neuron supporting cells, have a particularly high expression of CHCHD10 (unpublished results) (Sharma et al., 2015). Lastly, CHCHD10 and CHCHD2 proteins have a short half-life time of only 1.5 hours (unpublished results) (Burstein et al., 2018). In our studies we observed an increase of CHCHD10 and CHCHD2 in different stress conditions and a longer half-life time. The switch from glucose to galactose medium (glucose-free) led to a general increase of mitochondrial mass (Straub et al., 2018), yet, the increase in CHCHD10 and CHCHD2 levels surpassed that. Two variants of CHCHD10, CHCHD10 p.Q108P and CHCHD10 p.R15L have been shown to be less stable than wildtype protein (Lehmer et al., 2018). Previous studies have also shown an increase in the levels of CHCHD10 and CHCHD2 when the mitochondrial membrane potential was dissipated (Huang et al., 2018, Meng et al., 2017, Quiros et al., 2017). We found the same marked increase of CHCHD2 and CHCHD10; however, we also identified several short forms of CHCHD2, in stress and non-stress condition, which do not seem to be present for CHCHD10. It remains to be elucidated, whether these short forms result from an alternative transcription start site or a posttranslational processing by protease cleavage.

5.3 Mitochondrial morphological changes for CHCHD10 and CHCHD2 variants and knockouts

Changes in mitochondrial morphology have been linked to different neurodegenerative diseases and are a sign of mitochondrial stress (Martin, 2012). The mitochondrial network in patient CHCHD10 p.R15L fibroblasts was hyperfused (Straub et al., 2018), whereas other CHCHD10 variants, like CHCHD10 p.S59L, p.G58R or p.G66V, led to a fragmentation of the mitochondrial network (Baek et al., 2019, Genin et al., 2018, Lehmer et al., 2018) (and our unpublished results). The knockout of CHCHD2 led to a fragmentation of the mitochondrial network whereas the two CHCHD2 variants (p.T61I and p.R145Q) did not influence mitochondrial morphology significantly. CHCHD2 p.T61I however, did not fully rescue the observed alterations. Changes in mitochondrial morphology are orchestrated by proteins of the

fission and fusion machinery which include DRP1, MFN1/2 and OPA1. These proteins were largely unaffected by CHCHD10 and CHCHD2 variants; however, siRNA-mediated knockdown of CHCHD2, as well as the knockout of CHCHD2, led to a shift from long to short OPA1 forms (Straub et al., 2018), which is a hallmark of mitochondrial fragmentation. Similar changes in OPA1 were reported in a double knockout of CHCHD10 and CHCHD2 in mammalian cells, connecting OPA1 cleavage by the OMA1 protease to cristae abnormalities (Liu et al., 2019). A previous study suggested the interaction of CHCHD2 with p32 influences the interaction of p32 with YME1L and therefore OPA1 processing (Liu et al., 2020). In our study we identified increased interaction of CHCHD2 p.T61I with YME1L. Whether CHCHD2 interacts with YME1L endogenously and has a direct effect on OPA1 processing needs to be validated in further experiments.

CHCHD10 and CHCHD2 were reported to play a role in cristae structure formation through their interaction with MICOS subunits (Genin et al., 2018, Genin et al., 2015, Meng et al., 2017, Zhou et al., 2019). However, our study, and those of other groups failed to identify an interaction between CHCHD10 or CHCHD2 and the MICOS subunits (Burstein et al., 2018, Huang et al., 2018, Straub et al., 2018). Furthermore, we did not find any cristae abnormalities in mitochondria in patient fibroblasts harbouring the CHCHD10 p.R15L variant. The only CHCHD10 variant showing abnormal cristae structure is CHCHD10 p.S59L, which is thought to produce a toxic gain of function (Genin et al., 2015). The complete loss of the *Drosophila* orthologue of CHCHD10 and CHCHD2, CG5010, as well as the double knockout in human cells, also lead to a cristae morphology defect (Liu et al., 2019, Meng et al., 2017).

In conclusion, CHCHD10 and CHCHD2 variants result in the disturbance of mitochondrial morphology, most probably the result of mitochondrial respiration deficiencies.

5.4 CHCHD10 and CHCHD2 are involved in mitochondrial energy production

ALS and Parkinson's Disease primarily affect motor neurons and dopaminergic neurons, respectively. Neuronal metabolism depends largely on mitochondrial ATP production and neurons are more susceptible to low energy supply than other cell types, i.e. neuron-supporting astrocytes (Ames, 2000, Fernandez-Fernandez et al., 2012). The first indications that CHCHD2 or CHCHD10 could be involved in mitochondrial respiratory function came from a study in *Saccharomyces Cerevisiae*, where the deletion of Mic17 (the orthologue in yeast) resulted in

reduced oxygen consumption (Longen et al., 2009). We showed that CHCHD10 p.R15L patient fibroblasts had reduced oxygen consumption and increased lactate production compared to controls due to a complex I deficiency (Straub et al., 2018). CRISPR-Cas9 mediated CHCHD10 knockout cells phenocopied the patient, and in both models the phenotype could be rescued by the reintroduction of the wild-type protein. Similarly, overexpression of the CHCHD10 p.S59L and p.G58R variants resulted in a decreased ATP production and maximal respiratory capacity (Baek et al., 2019, Burstein et al., 2018). It was proposed that the knockdown of CHCHD10 also alters mitochondrial oxygen consumption (Lehmer et al., 2018, Purandare et al., 2018); however, siRNA mediated knockdown in fibroblasts cells in our hands and in another study does not support these findings (unpublished results) (Burstein et al., 2018).

The loss of CHCHD2 had an even more profound impact on mitochondrial oxygen consumption. An early computational study suggested an association of CHCHD2 with proteins involved in mitochondrial respiratory function (Baughman et al., 2009). The knockdown as well as the introduction of the disease variants p.R145Q and p.Q126X in isogenic human embryonic stem cells resulted in reduced oxygen consumption (Zhou et al., 2019). Similarly, a *Drosophila* CHCHD2 knockout model showed reduced maximal respiratory capacity (Meng et al., 2017). Our model representing the pathogenic variants p.T61I and p.R145Q in fibroblasts and the CHCHD2 knockout showed reduced levels of mitochondrial OXPHOS complexes I, IV and the disassembly of complex V. The analysis of oxygen consumption in CHCHD2 knockout cells, would be a valuable experiment to identify the extent of the deficiency of the respiratory chain. Interestingly, CHCHD10 levels were affected by short term siRNA mediated knockdown of CHCHD2; however, not by long term knockout of CHCHD2 (Straub et al., 2018). Moreover, CHCHD10 transcript and protein levels where significantly decreased when expressing CHCHD2 wildtype protein from cDNA. The overall reduction of OXPHOS complexes by the loss of CHCHD2, and the effect on CHCHD10 protein levels, indicate a role of CHCHD2 upstream of CHCHD10, and suggest regulation of CHCHD10 by CHCHD2.

5.5 CHCHD10 and its influence on mitochondrial and cellular metabolism

Growing cells in medium in which galactose is substituted for glucose forces cells to rely entirely on ATP production from mitochondria. Cells with mitochondrial deficiencies vary in their response to galactose as a nutrient stress. Some of them become more vulnerable to cell

death, because they are reliant on glycolysis to maintain survival and cell growth (Ghelli et al., 2003, Robinson et al., 1992, Soustek et al., 2018). Interestingly, only CHCHD10 p.R15L patient cells and CRISPR-Cas9 mediated CHCHD10 knockout cells exhibited cell death in galactose in our hands (Straub et al., 2018). The knockout of CHCHD2, as well as the expression of different disease variants of CHCHD10 or CHCHD2 did not result in any obvious growth defect (unpublished results). The metabolic switch from glucose to galactose leads to an increase of steady-state levels of mitochondrial proteins in general (Aguer et al., 2011), and this increase was even greater in CHCHD10 p.R15L patient cells compared to control cells (Straub et al., 2018). The $NADH/NAD^+$ ratio decreased in control cells in galactose, due to an increase in the use of mitochondrial respiration as the main energy source (Ryall et al., 2015). In CHCHD10 p.R15L patient cells, despite the increase in mitochondrial mass, the $NADH/NAD^+$ ratio increased.

The severe defect in complex I is most probably the cause of all the changes we observed, (1) increased $NADH/NAD^+$ ratio, (2) decreased ATP/AMP ratio, (3) increased activation of the one-carbon metabolism in mitochondria and decrease in the cytosol (4) inhibition of mTOR and (5) the activation of the integrated stress response in mitochondria and ER. Similar changes were observed in heart tissue in two different mouse models of CHCHD10 p.S59L as well as the double knockout of CHCHD10 and CHCHD2 (Anderson et al., 2019b, Liu et al., 2019). However, the CHCHD10 p.S59L variant caused an overall decrease in transcripts of the subunits of the mitochondrial OXPHOS complexes, formed punctuate aggregates in mitochondria, and acted as a dominant negative (Anderson et al., 2019b). It is therefore interesting that very different CHCHD10 variants caused a similar metabolic phenotype, although the haploinsufficient variant CHCHD10 p.R15L only exhibited these changes in galactose medium, suggesting that the latter is less severe than variant CHCHD10 p.S59L. Other models of ALS with mutant SOD1 or mutant aggregated TDP43 have been shown to be prone to ER stress (Das et al., 2015, Kim et al., 2014).

With the activation of the integrated stress response we identified a release of FGF21 and GDF15. FGF21 regulates lipid and glucose metabolism and was previously described as a specific response to diseases caused by mutations in mitochondrial DNA (mtDNA), and not respiratory chain deficiencies per se (Forsstrom et al., 2019, Lehtonen et al., 2016). Both myokines have been proposed as biomarkers for mitochondrial disease (Nohara et al., 2019,

Suomalainen et al., 2011). The CHCHD10 p.S59L variant induced high levels of FGF21 and GDF15, but also showed lower mtDNA copy numbers (Anderson et al., 2019b, Genin et al., 2019). The CHCHD10 p.R15L variant in our model did not show any obvious differences in mtDNA copy number by immunofluorescence analysis (unpublished results), but showed nonetheless a marked increase in FGF21 and GDF15. Also remarkable, is the universal response of FGF21 to metabolic stress in seemingly many cell types. FGF21 is mainly considered a hepatokine, secreted by the liver to regulate sugar intake (Tezze et al., 2019). The mouse model of variant CHCHD10 p.S59L had a reduced fat tissue mass and high levels of FGF21 (Anderson et al., 2019b). To date, there is no mouse model of the CHCHD10 p.R15L variant, but our data predict that a similar phenotype would be observed, at least in stress conditions.

5.6 Interaction of CHCHD10 and CHCHD2 with each other and other cellular proteins

Analysis of the CHCHD10 and CHCHD2 interaction revealed a complex between the two proteins of around 220 kDa (Straub et al., 2018), but most of the proteins appeared in the low molecular weight range, likely in monomeric form. The precise composition of the high molecular complexes seen on BN-PAGE gels remains unknown; however, it is altered, or non-existent in patient cells with CHCHD10 p.R15L variant as well as for the cells with a CHCHD2 knockout cells or those harbouring the p.T61I variant.

The CHCH-domain can form intermolecular disulfide bonds and it being the only known functional domain in CHCHD2 and CHCHD10, it becomes valuable to determine the redox state of the cysteines in these proteins. Like many other twin CX_9C motif containing proteins which form intermolecular disulfide bonds with other cysteine bearing proteins or bind metals (e.g. COX17 (Glerum et al., 1996)), CHCHD10 and CHCHD2 could form intermolecular disulfide bonds between each other to form the high molecular weight complex. However, our study established that the disulfide bonds of CHCHD2 and CHCHD10 are very stable and solely structural at steady state. Furthermore, we could not identify other proteins in the high molecular weight complex, suggesting that the complex is an assembly of multiple CHCHD2 and CHCHD10 proteins without intermolecular disulfide bonds. At the moment we do not know the function of this complex or its exact localization. Two other groups identified CHCHD2/CHCHD10 heterodimers or CHCHD2 dimers, but only when crosslinked with

disuccinimidyl glutarate (DSG) or dithiobis (succinimidyl propionate) (DSP) (Huang et al., 2018, Meng et al., 2017).

CHCHD10 and CHCHD2 have been shown to interact strongly with each other and another cellular protein C1QBP/p32 using different pull-down approaches (Burstein et al., 2018, Floyd et al., 2016, Liu et al., 2020, Straub et al., 2018, Wei et al., 2015, Zhang et al., 2013). However, all of our studies failed to support previously claimed interactions of CHCHD2 with MICS1, cytochrome *c* or BcL-xL (Liu et al., 2015, Meng et al., 2017, Oka et al., 2008). C1QBP/p32 was shown to be predominantly a mitochondrial matrix protein responsible for mitochondrial translation (Yagi et al., 2012). The knockdown or knockout of p32 resulted in severe defects of the mitochondrial respiratory chain and its function (unpublished results) (Gotoh et al., 2018). Protein levels of CHCHD2 and CHCHD10 were greatly diminished when p32 was knocked down (unpublished results). We therefore suggest that p32 has a role upstream of CHCHD2 and CHCHD10. This interaction is difficult to explain as p32 is a protein which mainly resides in the mitochondrial matrix and CHCHD10 and CHCHD2 are present largely in the intermembrane space. However, other subcellular localizations of p32, like the ER, the nucleus and the cell surface, have been described (Ghebrehiwet et al., 2001, Matthews & Russell, 1998, Strong & Hodges, 1976). Hence the question is how and where are p32 and CHCHD2 and CHCHD10 proteins interacting. In 2D-PAGE analysis we found that p32 behaves as a monomer and it did not co-migrate with the higher molecular weight complex of CHCHD10 and CHCHD2 (Straub et al., 2018). One idea is that CHCHD10/2 and p32 interact while p32 is being imported into mitochondria on its way through the intermembrane space into the matrix. Another possibility is that CHCHD10/2 are cleaved and imported into the matrix where the interaction with p32 occurs with shorter forms of CHCHD10 and CHCHD2. Lastly, it cannot be ruled out that an interaction could also take place in the cytosol or in the nucleus.

Using a relatively mild detergent like digitonin to extract proteins for immunoprecipitation experiments enables one to maintain stability of certain complexes (Niklas et al., 2011). With this approach, we identified additional interaction partners of ectopically expressed CHCHD2 which are involved in RNA metabolism outside of mitochondria. New interaction partners included ALYREF and CHTOP, two nuclear proteins important for exporting mRNAs from the nucleus into the cytosol (Chang et al., 2013, Shi et al., 2017). Although we do not understand the functional relevance or the localization of this interaction, we consider it significant, as the

interaction of CHCHD10 with ALYREF and with CHTOP, and CHCHD2 with ALYREF was independently reported in two other studies (Floyd et al., 2016, Wei et al., 2015). Moreover, p32 also interacted with ALYREF (unpublished results) (Zhang et al., 2013). As either ALYREF or CHTOP have never been shown to be present in mitochondria, the interaction with CHCHD10, CHCHD2 and p32 is most likely localized to the nucleus or the cytosol and not mitochondria.

In summary, using our data as well as previously published data we created an interactome of CHCHD2 and CHCHD10. The interaction with p32 and ALYREF as well as CHTOP, potentially occurs in the mitochondrial matrix, the cytosol or the nucleus. CHCHD2 and CHCHD10 do not possess an RNA-binding domain; nonetheless, they could support the RNA-bound proteins and thus facilitate RNA stability and/or translation. The overall reduction of cellular mRNA in CHCHD2 knockout cells is one indication for this hypothesis. However, the overexpression of CHCHD2 did not rescue this phenotype, suggesting crucial fine tuning of CHCHD2 levels to ensure its proper function, similarly another study showed that overexpression of wild-type CHCHD2 resulted in neuromuscular phenotype in flies (Tio et al., 2017).

Chapter 6: Conclusions and future directions

6. Conclusions and future directions

CHCHD10 and CHCHD2 are predominately mitochondrial intermembrane-space proteins, whose levels and whose half-life times are increased upon stress to support mitochondrial biogenesis and function. They interact with each other and form a high molecular weight complex of 220 kDa. The importance of this complex is highlighted by the fact that its composition changes in cells with different pathological variants of CHCHD10 or CHCHD2. Both CHCHD10 and CHCHD2 play an important role in mitochondrial respiratory function. The abnormalities in cristae and mitochondrial morphology seem to be secondary to the primary mitochondrial respiratory defect caused by the loss of functional CHCHD10 or CHCHD2. The CHCHD10/CHCHD2 complex is more likely involved in regulating the activity of the respiratory chain than in the assembly of the OXPHOS complexes *per se*. It could function as a relay to transmit signals to the respiratory chain to fine tune the demand for energy. Further studies will be necessary to determine the precise molecular function of CHCHD2 and CHCHD10, as well as the role of the high molecular weight complex formed by these proteins. What is the role of the shorter forms of CHCHD2? Is CHCHD2 processed by one of the inner membrane proteases only upon stress? Do they act as signalling molecules inside or outside of mitochondria?

Our results, together with those from other studies, established the differences in phenotypes between variants of CHCHD10 and CHCHD2 (Fig. 6.1). The variants present in the hydrophobic domain of the proteins are associated with the most severe phenotypes, with the formation of aggregates in mitochondria, an effect on mitochondrial cristae structure, as well as functional defects in the respiratory chain. These variants result in a toxic gain of function through the increase in hydrophobicity and consequent aggregation in the IMS. On the other hand, CHCHD10 p.R15L, CHCHD10 p.P80L and CHCHD2 p.R145Q appear haploinsufficient, with lower protein levels and a milder overall phenotype, and no effect on cristae structure. Lastly, some of the variants in the CHCH-domain do not localize to mitochondria and have been shown to cause very early disease onset (Lehmer et al., 2018). In summary, CHCHD10 and CHCHD2 variants show different phenotypes but have one in common, they all affect

mitochondrial respiration. We therefore suggest therein lies the primary function of these proteins.

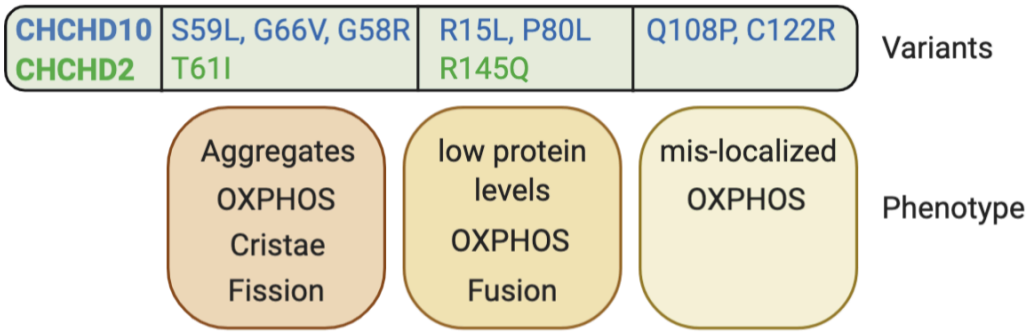

Figure 6.1 Scheme of selected variants of CHCHD10 and CHCHD2 and their most established phenotypes (created with *BioRender*). Aggregates: CHCHD10/CHCHD2 protein aggregates; OXPHOS: respiratory chain malfunctioning; Cristae: abnormal cristae structure; fission/fusion: alterations in mitochondrial morphology; mis-localized: localization of CHCHD10 variant outside of mitochondria. Aminoacid changes and positions of variants are abbreviated. CHCHD2 variants are depicted in green and CHCHD10 variants in blue.

Multi-omics studies of the CHCHD10 pathological variant p.R15L showed a marked cellular energy deficit under nutrient stress, induced by growth in galactose. The increased AMP/ATP ratio as well as NADH/NAD^+ ratio and the production of the metabolic cytokines FGF21 and GDF15 all suggested that the energy deficit might be the cause of motor neuron death in this ALS model. Potentially, restoring NAD^+ levels through the supplementation of precursors for *de novo* biosynthesis or manipulation of the enzymes involved in biosynthesis would be interesting possibilities for treatment. Moreover, the induction of the integrated stress response could serve as a point of drug targeting to treat CHCHD10 and CHCHD2 related disorders, a strategy that has previously been successfully implemented to reduce toxicity mediated by TDP43 aggregates in flies (Kim et al., 2014). Future experiments could include the study of metabolic changes of other CHCHD10 and CHCHD2 variants. Identifying an underlying common pattern for metabolic dysfunction could give further clarification on how to treat CHCHD10 and CHCHD2 related disorders.

CHCHD2 and CHCHD10 interact with C1QBP/p32 protein, as well as other proteins involved in cellular RNA metabolism. The involvement of commonly mutated genes in ALS and PD in RNA metabolism is an area of intense investigation. It has become clear that RNA

dysregulation in ALS (TDP43, FUS, and C9orf72) and PD (LRKK2 and DJ-1) is a key contributor to disease pathogenesis (Liu et al., 2017, Lu et al., 2014). Many processes, like RNA splicing, biogenesis, exo-nuclear transport, stability and regulation could potentially be affected. The interaction of CHCHD10 and CHCHD2 with ALYREF and CHTOP, RNA export factors, is therefore an area that links different disease-causing proteins, with potentially a common underlying mechanism for disease pathogenesis. The high expression of CHCHD2 in many cancers is another indication of its involvement in cell growth and biogenesis, and potentially translation. The investigation of the interaction with ALYREF is therefore of particular interest.

Chapter 7: Master reference list

7. Master reference list

Aasen T, Raya A, Barrero MJ, Garreta E, Consiglio A, Gonzalez F, Vassena R, Bilic J, Pekarik V, Tiscornia G, Edel M, Boue S, Belmonte JC (2008) Efficient and rapid generation of induced pluripotent stem cells from human keratinocytes. *Nat Biotechnol* 26: 1276-84

Abajian C, Yatsunyk LA, Ramirez BE, Rosenzweig AC (2004) Yeast cox17 solution structure and Copper(I) binding. *J Biol Chem* 279: 53584-92

Aguer C, Gambarotta D, Mailloux RJ, Moffat C, Dent R, McPherson R, Harper ME (2011) Galactose enhances oxidative metabolism and reveals mitochondrial dysfunction in human primary muscle cells. *PLoS One* 6: e28536

Ajroud-Driss S, Fecto F, Ajroud K, Lalani I, Calvo SE, Mootha VK, Deng HX, Siddique N, Tahmoush AJ, Heiman-Patterson TD, Siddique T (2015) Mutation in the novel nuclear-encoded mitochondrial protein CHCHD10 in a family with autosomal dominant mitochondrial myopathy. *Neurogenetics* 16: 1-9

Ames A, 3rd (2000) CNS energy metabolism as related to function. *Brain Res Brain Res Rev* 34: 42-68

Anand R, Wai T, Baker MJ, Kladt N, Schauss AC, Rugarli E, Langer T (2014) The i-AAA protease YME1L and OMA1 cleave OPA1 to balance mitochondrial fusion and fission. *J Cell Biol* 204: 919-29

Anderson CJ, Bredvik K, Burstein SR, Davis C, Meadows SM, Dash J, Case L, Milner TA, Kawamata H, Zuberi A, Piersigilli A, Lutz C, Manfredi G (2019a) ALS/FTD mutant CHCHD10 mice reveal a tissue-specific toxic gain-of-function and mitochondrial stress response. *Acta Neuropathol* 138: 103-121

Anderson CJ, Bredvik K, Burstein SR, Davis C, Meadows SM, Dash J, Case L, Milner TA, Kawamata H, Zuberi A, Piersigilli A, Lutz C, Manfredi G (2019b) ALS/FTD mutant CHCHD10

mice reveal a tissue-specific toxic gain-of-function and mitochondrial stress response. *Acta Neuropathol*

Antonicka H, Ogilvie I, Taivassalo T, Anitori RP, Haller RG, Vissing J, Kennaway NG, Shoubridge EA (2003) Identification and characterization of a common set of complex I assembly intermediates in mitochondria from patients with complex I deficiency. *J Biol Chem* 278: 43081-8

Aras S, Bai M, Lee I, Springett R, Huttemann M, Grossman LI (2015) MNRR1 (formerly CHCHD2) is a bi-organellar regulator of mitochondrial metabolism. *Mitochondrion* 20: 43-51

Aras S, Pak O, Sommer N, Finley R, Jr., Huttemann M, Weissmann N, Grossman LI (2013) Oxygen-dependent expression of cytochrome c oxidase subunit 4-2 gene expression is mediated by transcription factors RBPJ, CXXC5 and CHCHD2. *Nucleic Acids Res* 41: 2255-66

Auranen M, Ylikallio E, Shcherbii M, Paetau A, Kiuru-Enari S, Toppila JP, Tyynismaa H (2015) CHCHD10 variant p.(Gly66Val) causes axonal Charcot-Marie-Tooth disease. *Neurol Genet* 1: e1

Austin S, St-Pierre J (2012) PGC1alpha and mitochondrial metabolism--emerging concepts and relevance in ageing and neurodegenerative disorders. *J Cell Sci* 125: 4963-71

Baek M, Choe Y-J, Dorn GW, Taylor JP, Kim NC (2019) Dominant toxicity of ALS–FTD-associated CHCHD10 p.S59L is mediated by TDP-43 and PINK1. 753558

Banci L, Bertini I, Cefaro C, Ciofi-Baffoni S, Gallo A, Martinelli M, Sideris DP, Katrakili N, Tokatlidis K (2009) MIA40 is an oxidoreductase that catalyzes oxidative protein folding in mitochondria. *Nat Struct Mol Biol* 16: 198-206

Banci L, Bertini I, Ciofi-Baffoni S, Jaiswal D, Neri S, Peruzzini R, Winkelmann J (2012) Structural characterization of CHCHD5 and CHCHD7: two atypical human twin CX9C proteins. *J Struct Biol* 180: 190-200

Bannwarth S, Ait-El-Mkadem S, Chaussenot A, Genin EC, Lacas-Gervais S, Fragaki K, Berg-Alonso L, Kageyama Y, Serre V, Moore DG, Verschueren A, Rouzier C, Le Ber I, Auge G, Cochaud C, Lespinasse F, N'Guyen K, de Septenville A, Brice A, Yu-Wai-Man P et al. (2014) A

mitochondrial origin for frontotemporal dementia and amyotrophic lateral sclerosis through CHCHD10 involvement. *Brain* 137: 2329-45

Baughman JM, Nilsson R, Gohil VM, Arlow DH, Gauhar Z, Mootha VK (2009) A computational screen for regulators of oxidative phosphorylation implicates SLIRP in mitochondrial RNA homeostasis. *PLoS Genet* 5: e1000590

Becker T, Bottinger L, Pfanner N (2012) Mitochondrial protein import: from transport pathways to an integrated network. *Trends Biochem Sci* 37: 85-91

Berg JM TJ, Stryer L. (2002) Biochemistry. *New York: W H Freeman* 5th edition.

Birsoy K, Wang T, Chen WW, Freinkman E, Abu-Remaileh M, Sabatini DM (2015) An Essential Role of the Mitochondrial Electron Transport Chain in Cell Proliferation Is to Enable Aspartate Synthesis. *Cell* 162: 540-51

Bond P (2016) Regulation of mTORC1 by growth factors, energy status, amino acids and mechanical stimuli at a glance. *J Int Soc Sports Nutr* 13: 8

Brockmann SJ, Freischmidt A, Oeckl P, Muller K, Ponna SK, Helferich AM, Paone C, Reinders J, Kojer K, Orth M, Jokela M, Auranen M, Udd B, Hermann A, Danzer KM, Lichtner P, Walther P, Ludolph AC, Andersen PM, Otto M et al. (2018) CHCHD10 mutations p.R15L and p.G66V cause motoneuron disease by haploinsufficiency. *Hum Mol Genet* 27: 706-715

Bueler H (2009) Impaired mitochondrial dynamics and function in the pathogenesis of Parkinson's disease. *Exp Neurol* 218: 235-46

Burri L, Strahm Y, Hawkins CJ, Gentle IE, Puryer MA, Verhagen A, Callus B, Vaux D, Lithgow T (2005) Mature DIABLO/Smac is produced by the IMP protease complex on the mitochondrial inner membrane. *Mol Biol Cell* 16: 2926-33

Burstein SR, Valsecchi F, Kawamata H, Bourens M, Zeng R, Zuberi A, Milner TA, Cloonan SM, Lutz C, Barrientos A, Manfredi G (2018) In vitro and in vivo studies of the ALS-FTLD protein CHCHD10 reveal novel mitochondrial topology and protein interactions. *Hum Mol Genet* 27: 160-177

Calvo SE, Clauser KR, Mootha VK (2016) MitoCarta2.0: an updated inventory of mammalian mitochondrial proteins. *Nucleic Acids Res* 44: D1251-7

Calvo SE, Julien O, Clauser KR, Shen H, Kamer KJ, Wells JA, Mootha VK (2017) Comparative Analysis of Mitochondrial N-Termini from Mouse, Human, and Yeast. *Mol Cell Proteomics* 16: 512-523

Cavallaro G (2010) Genome-wide analysis of eukaryotic twin CX9C proteins. *Mol Biosyst* 6: 2459-70

Chang CT, Hautbergue GM, Walsh MJ, Viphakone N, van Dijk TB, Philipsen S, Wilson SA (2013) Chtop is a component of the dynamic TREX mRNA export complex. *EMBO J* 32: 473-86

Chaussenot A, Le Ber I, Ait-El-Mkadem S, Camuzat A, de Septenville A, Bannwarth S, Genin EC, Serre V, Auge G, French research network on FTD, Ftd ALS, Brice A, Pouget J, Paquis-Flucklinger V (2014) Screening of CHCHD10 in a French cohort confirms the involvement of this gene in frontotemporal dementia with amyotrophic lateral sclerosis patients. *Neurobiol Aging* 35: 2884 e1-4

Che XQ, Zhao QH, Huang Y, Li X, Ren RJ, Chen SD, Guo QH, Wang G (2018) Mutation Screening of the CHCHD2 Gene for Alzheimer's Disease and Frontotemporal Dementia in Chinese Mainland Population. *J Alzheimers Dis* 61: 1283-1288

Che XQ, Zhao QH, Huang Y, Li X, Ren RJ, Chen SD, Wang G, Guo QH (2017) Genetic Features of MAPT, GRN, C9orf72 and CHCHD10 Gene Mutations in Chinese Patients with Frontotemporal Dementia. *Curr Alzheimer Res* 14: 1102-1108

Chen EY, Tan CM, Kou Y, Duan Q, Wang Z, Meirelles GV, Clark NR, Ma'ayan A (2013) Enrichr: interactive and collaborative HTML5 gene list enrichment analysis tool. *BMC Bioinformatics* 14: 128

Cheng CF, Ku HC, Lin H (2018) PGC-1alpha as a Pivotal Factor in Lipid and Metabolic Regulation. *Int J Mol Sci* 19

Chio A, Mora G, Sabatelli M, Caponnetto C, Traynor BJ, Johnson JO, Nalls MA, Calvo A, Moglia C, Borghero G, Monsurro MR, La Bella V, Volanti P, Simone I, Salvi F, Logullo FO, Nilo R, Battistini S, Mandrioli J, Tanel R et al. (2015) CHCH10 mutations in an Italian cohort of familial and sporadic amyotrophic lateral sclerosis patients. *Neurobiol Aging* 36: 1767 e3-1767 e6

Chong J, Soufan O, Li C, Caraus I, Li S, Bourque G, Wishart DS, Xia J (2018) MetaboAnalyst 4.0: towards more transparent and integrative metabolomics analysis. *Nucleic Acids Res* 46: W486-W494

Das I, Krzyzosiak A, Schneider K, Wrabetz L, D'Antonio M, Barry N, Sigurdardottir A, Bertolotti A (2015) Preventing proteostasis diseases by selective inhibition of a phosphatase regulatory subunit. *Science* 348: 239-42

Dolle C, Rack JG, Ziegler M (2013) NAD and ADP-ribose metabolism in mitochondria. *FEBS J* 280: 3530-41

Dols-Icardo O, Nebot I, Gorostidi A, Ortega-Cubero S, Hernandez I, Rojas-Garcia R, Garcia-Redondo A, Povedano M, Llado A, Alvarez V, Sanchez-Juan P, Pardo J, Jerico I, Vazquez-Costa J, Sevilla T, Cardona F, Indakoechea B, Moreno F, Fernandez-Torron R, Munoz-Llahuna L et al. (2015) Analysis of the CHCHD10 gene in patients with frontotemporal dementia and amyotrophic lateral sclerosis from Spain. *Brain* 138: e400

Erdogan AJ, Ali M, Habich M, Salscheider SL, Schu L, Petrungaro C, Thomas LW, Ashcroft M, Leichert LI, Roma LP, Riemer J (2018) The mitochondrial oxidoreductase CHCHD4 is present in a semi-oxidized state in vivo. *Redox Biol* 17: 200-206

Fernandez-Fernandez S, Almeida A, Bolanos JP (2012) Antioxidant and bioenergetic coupling between neurons and astrocytes. *Biochem J* 443: 3-11

Floyd BJ, Wilkerson EM, Veling MT, Minogue CE, Xia C, Beebe ET, Wrobel RL, Cho H, Kremer LS, Alston CL, Gromek KA, Dolan BK, Ulbrich A, Stefely JA, Bohl SL, Werner KM, Jochem A, Westphall MS, Rensvold JW, Taylor RW et al. (2016) Mitochondrial Protein Interaction Mapping Identifies Regulators of Respiratory Chain Function. *Mol Cell* 63: 621-632

Foo JN, Liu J, Tan EK (2015) CHCHD2 and Parkinson's disease. *Lancet Neurol* 14: 681-2

Forsstrom S, Jackson CB, Carroll CJ, Kuronen M, Pirinen E, Pradhan S, Marmyleva A, Auranen M, Kleine IM, Khan NA, Roivainen A, Marjamaki P, Liljenback H, Wang L, Battersby BJ, Richter U, Velagapudi V, Nikkanen J, Euro L, Suomalainen A (2019) Fibroblast Growth Factor 21 Drives Dynamics of Local and Systemic Stress Responses in Mitochondrial Myopathy with mtDNA Deletions. *Cell Metab* 30: 1040-1054 e7

Funayama M, Ohe K, Amo T, Furuya N, Yamaguchi J, Saiki S, Li Y, Ogaki K, Ando M, Yoshino H, Tomiyama H, Nishioka K, Hasegawa K, Saiki H, Satake W, Mogushi K, Sasaki R, Kokubo Y, Kuzuhara S, Toda T et al. (2015) CHCHD2 mutations in autosomal dominant late-onset Parkinson's disease: a genome-wide linkage and sequencing study. *Lancet Neurol* 14: 274-82

Gabriel K, Milenkovic D, Chacinska A, Muller J, Guiard B, Pfanner N, Meisinger C (2007) Novel mitochondrial intermembrane space proteins as substrates of the MIA import pathway. *J Mol Biol* 365: 612-20

Gasser SM, Ohashi A, Daum G, Bohni PC, Gibson J, Reid GA, Yonetani T, Schatz G (1982) Imported mitochondrial proteins cytochrome b2 and cytochrome c1 are processed in two steps. *Proc Natl Acad Sci U S A* 79: 267-71

Genin EC, Bannwarth S, Lespinasse F, Ortega-Vila B, Fragaki K, Itoh K, Villa E, Lacas-Gervais S, Jokela M, Auranen M, Ylikallio E, Mauri-Crouzet A, Tyynismaa H, Vihola A, Auge G, Cochaud C, Sesaki H, Ricci JE, Udd B, Vives-Bauza C et al. (2018) Loss of MICOS complex integrity and mitochondrial damage, but not TDP-43 mitochondrial localisation, are likely associated with severity of CHCHD10-related diseases. *Neurobiol Dis* 119: 159-171

Genin EC, Madji Hounoum B, Bannwarth S, Fragaki K, Lacas-Gervais S, Mauri-Crouzet A, Lespinasse F, Neveu J, Ropert B, Auge G, Cochaud C, Lefebvre-Omar C, Bigou S, Chiot A, Mochel F, Boillee S, Lobsiger CS, Bohl D, Ricci JE, Paquis-Flucklinger V (2019) Mitochondrial defect in muscle precedes neuromuscular junction degeneration and motor neuron death in CHCHD10(S59L/+) mouse. *Acta Neuropathol* 138: 123-145

Genin EC, Plutino M, Bannwarth S, Villa E, Cisneros-Barroso E, Roy M, Ortega-Vila B, Fragaki K, Lespinasse F, Pinero-Martos E, Auge G, Moore D, Burte F, Lacas-Gervais S, Kageyama Y, Itoh K, Yu-Wai-Man P, Sesaki H, Ricci JE, Vives-Bauza C et al. (2015) CHCHD10 mutations

promote loss of mitochondrial cristae junctions with impaired mitochondrial genome maintenance and inhibition of apoptosis. *EMBO Mol Med* 8: 58-72

Genin EC, Plutino M, Bannwarth S, Villa E, Cisneros-Barroso E, Roy M, Ortega-Vila B, Fragaki K, Lespinasse F, Pinero-Martos E, Auge G, Moore D, Burte F, Lacas-Gervais S, Kageyama Y, Itoh K, Yu-Wai-Man P, Sesaki H, Ricci JE, Vives-Bauza C et al. (2016) CHCHD10 mutations promote loss of mitochondrial cristae junctions with impaired mitochondrial genome maintenance and inhibition of apoptosis. *EMBO Mol Med* 8: 58-72

Ghebrehiwet B, Lim BL, Kumar R, Feng X, Peerschke EI (2001) gC1q-R/p33, a member of a new class of multifunctional and multicompartmental cellular proteins, is involved in inflammation and infection. *Immunol Rev* 180: 65-77

Ghelli A, Zanna C, Porcelli AM, Schapira AH, Martinuzzi A, Carelli V, Rugolo M (2003) Leber's hereditary optic neuropathy (LHON) pathogenic mutations induce mitochondrial-dependent apoptotic death in transmitochondrial cells incubated with galactose medium. *J Biol Chem* 278: 4145-50

Glerum DM, Shtanko A, Tzagoloff A (1996) Characterization of COX17, a yeast gene involved in copper metabolism and assembly of cytochrome oxidase. *J Biol Chem* 271: 14504-9

Glick BS, Brandt A, Cunningham K, Muller S, Hallberg RL, Schatz G (1992) Cytochromes c1 and b2 are sorted to the intermembrane space of yeast mitochondria by a stop-transfer mechanism. *Cell* 69: 809-22

Glick D, Barth S, Macleod KF (2010) Autophagy: cellular and molecular mechanisms. *J Pathol* 221: 3-12

Gorman GS, Chinnery PF, DiMauro S, Hirano M, Koga Y, McFarland R, Suomalainen A, Thorburn DR, Zeviani M, Turnbull DM (2016) Mitochondrial diseases. *Nat Rev Dis Primers* 2: 16080

Gotoh K, Morisaki T, Setoyama D, Sasaki K, Yagi M, Igami K, Mizuguchi S, Uchiumi T, Fukui Y, Kang D (2018) Mitochondrial p32/C1qbp Is a Critical Regulator of Dendritic Cell Metabolism and Maturation. *Cell reports* 25: 1800-1815 e4

Grossman LI, Purandare N, Arshad R, Gladyck S, Somayajulu M, Huttemann M, Aras S (2017) MNRR1, a Biorganellar Regulator of Mitochondria. *Oxid Med Cell Longev* 2017: 6739236

Harner M, Korner C, Walther D, Mokranjac D, Kaesmacher J, Welsch U, Griffith J, Mann M, Reggiori F, Neupert W (2011) The mitochondrial contact site complex, a determinant of mitochondrial architecture. *EMBO J* 30: 4356-70

Hasson SA, Damoiseaux R, Glavin JD, Dabir DV, Walker SS, Koehler CM (2010) Substrate specificity of the TIM22 mitochondrial import pathway revealed with small molecule inhibitor of protein translocation. *Proc Natl Acad Sci U S A* 107: 9578-83

Heiman-Patterson TD, Argov Z, Chavin JM, Kalman B, Alder H, DiMauro S, Bank W, Tahmoush AJ (1997) Biochemical and genetic studies in a family with mitochondrial myopathy. *Muscle Nerve* 20: 1219-24

Hein MY, Hubner NC, Poser I, Cox J, Nagaraj N, Toyoda Y, Gak IA, Weisswange I, Mansfeld J, Buchholz F, Hyman AA, Mann M (2015) A human interactome in three quantitative dimensions organized by stoichiometries and abundances. *Cell* 163: 712-23

Henchcliffe C, Beal MF (2008) Mitochondrial biology and oxidative stress in Parkinson disease pathogenesis. *Nat Clin Pract Neurol* 4: 600-9

Herzig S, Shaw RJ (2018) AMPK: guardian of metabolism and mitochondrial homeostasis. *Nat Rev Mol Cell Biol* 19: 121-135

Hetz C, Mollereau B (2014) Disturbance of endoplasmic reticulum proteostasis in neurodegenerative diseases. *Nat Rev Neurosci* 15: 233-49

Hetz C, Thielen P, Matus S, Nassif M, Court F, Kiffin R, Martinez G, Cuervo AM, Brown RH, Glimcher LH (2009) XBP-1 deficiency in the nervous system protects against amyotrophic lateral sclerosis by increasing autophagy. *Genes Dev* 23: 2294-306

Hoang T, Smith MD, Jelokhani-Niaraki M (2012) Toward understanding the mechanism of ion transport activity of neuronal uncoupling proteins UCP2, UCP4, and UCP5. *Biochemistry* 51: 4004-14

Hollien J, Weissman JS (2006) Decay of endoplasmic reticulum-localized mRNAs during the unfolded protein response. *Science* 313: 104-7

Huang S, Xing Y, Liu Y (2019) Emerging roles for the ER stress sensor IRE1alpha in metabolic regulation and disease. *J Biol Chem* 294: 18726-18741

Huang X, Wu BP, Nguyen D, Liu YT, Marani M, Hench J, Benit P, Kozjak-Pavlovic V, Rustin P, Frank S, Narendra DP (2018) CHCHD2 accumulates in distressed mitochondria and facilitates oligomerization of CHCHD10. *Hum Mol Genet* 27: 3881-3900

Hughes D, Mallucci GR (2019) The unfolded protein response in neurodegenerative disorders - therapeutic modulation of the PERK pathway. *FEBS J* 286: 342-355

Huh WK, Falvo JV, Gerke LC, Carroll AS, Howson RW, Weissman JS, O'Shea EK (2003) Global analysis of protein localization in budding yeast. *Nature* 425: 686-91

Huttlin EL, Ting L, Bruckner RJ, Gebreab F, Gygi MP, Szpyt J, Tam S, Zarraga G, Colby G, Baltier K, Dong R, Guarani V, Vaites LP, Ordureau A, Rad R, Erickson BK, Wuhr M, Chick J, Zhai B, Kolippakkam D et al. (2015) The BioPlex Network: A Systematic Exploration of the Human Interactome. *Cell* 162: 425-440

Huynen MA, Muhlmeister M, Gotthardt K, Guerrero-Castillo S, Brandt U (2016) Evolution and structural organization of the mitochondrial contact site (MICOS) complex and the mitochondrial intermembrane space bridging (MIB) complex. *Biochim Biophys Acta* 1863: 91-101

Ikeda A, Matsushima T, Daida K, Nakajima S, Conedera S, Li Y, Yoshino H, Oyama G, Funayama M, Nishioka K, Hattori N (2017) A novel mutation of CHCHD2 p.R8H in a sporadic case of Parkinson's disease. *Parkinsonism Relat Disord* 34: 66-68

Ikeda A, Nishioka K, Meng H, Takanashi M, Hasegawa I, Inoshita T, Shiba-Fukushima K, Li Y, Yoshino H, Mori A, Okuzumi A, Yamaguchi A, Nonaka R, Izawa N, Ishikawa KI, Saiki H, Morita M, Hasegawa M, Hasegawa K, Elahi M et al. (2019) Mutations in CHCHD2 cause alpha-synuclein aggregation. *Hum Mol Genet* 28: 3895-3911

Imai Y, Inoshita T, Meng H, Shiba-Fukushima K, Hara KY, Sawamura N, Hattori N (2019a) Light-driven activation of mitochondrial proton-motive force improves motor behaviors in a Drosophila model of Parkinson's disease. *Commun Biol* 2: 424

Imai Y, Meng H, Shiba-Fukushima K, Hattori N (2019b) Twin CHCH Proteins, CHCHD2, and CHCHD10: Key Molecules of Parkinson's Disease, Amyotrophic Lateral Sclerosis, and Frontotemporal Dementia. *Int J Mol Sci* 20

Ito Y, Yamada M, Tanaka H, Aida K, Tsuruma K, Shimazawa M, Hozumi I, Inuzuka T, Takahashi H, Hara H (2009) Involvement of CHOP, an ER-stress apoptotic mediator, in both human sporadic ALS and ALS model mice. *Neurobiol Dis* 36: 470-6

Jady BE, Ketele A, Kiss T (2018) Dynamic association of human mRNP proteins with mitochondrial tRNAs in the cytosol. *RNA* 24: 1706-1720

Janer A, Prudent J, Paupe V, Fahiminiya S, Majewski J, Sgarioto N, Des Rosiers C, Forest A, Lin ZY, Gingras AC, Mitchell G, McBride HM, Shoubridge EA (2016) SLC25A46 is required for mitochondrial lipid homeostasis and cristae maintenance and is responsible for Leigh syndrome. *EMBO Mol Med*

Jansen IE, Bras JM, Lesage S, Schulte C, Gibbs JR, Nalls MA, Brice A, Wood NW, Morris H, Hardy JA, Singleton AB, Gasser T, Heutink P, Sharma M, Ipdgc (2015) CHCHD2 and Parkinson's disease. *Lancet Neurol* 14: 678-9

Jaronen M, Goldsteins G, Koistinaho J (2014) ER stress and unfolded protein response in amyotrophic lateral sclerosis-a controversial role of protein disulphide isomerase. *Front Cell Neurosci* 8: 402

Jiao B, Xiao T, Hou L, Gu X, Zhou Y, Zhou L, Tang B, Xu J, Shen L (2016) High prevalence of CHCHD10 mutation in patients with frontotemporal dementia from China. *Brain : a journal of neurology* 139: e21

Johnson JO, Glynn SM, Gibbs JR, Nalls MA, Sabatelli M, Restagno G, Drory VE, Chio A, Rogaeva E, Traynor BJ (2014) Mutations in the CHCHD10 gene are a common cause of familial amyotrophic lateral sclerosis. *Brain* 137: e311

Julia L. Keith ES, Andrew Gao, Samira Alminawi, Ming Zhang, Philip McGoldrick, Paul McKeever, Janice Robertson, Ekaterina Rogaeva, Lorne Zinman (2020) Neuropathologic description of CHCHD10 mutated amyotrophic lateral sclerosis. *Neurol Genet*

Jung C, Higgins CM, Xu Z (2002) Mitochondrial electron transport chain complex dysfunction in a transgenic mouse model for amyotrophic lateral sclerosis. *J Neurochem* 83: 535-45

Katahira J (2012) mRNA export and the TREX complex. *Biochim Biophys Acta* 1819: 507-13

Khan NA, Nikkanen J, Yatsuga S, Jackson C, Wang L, Pradhan S, Kivela R, Pessia A, Velagapudi V, Suomalainen A (2017) mTORC1 Regulates Mitochondrial Integrated Stress Response and Mitochondrial Myopathy Progression. *Cell Metab* 26: 419-428 e5

Kim HJ, Raphael AR, LaDow ES, McGurk L, Weber RA, Trojanowski JQ, Lee VM, Finkbeiner S, Gitler AD, Bonini NM (2014) Therapeutic modulation of eIF2alpha phosphorylation rescues TDP-43 toxicity in amyotrophic lateral sclerosis disease models. *Nat Genet* 46: 152-60

Kim Y, Zheng X, Ansari Z, Bunnell MC, Herdy JR, Traxler L, Lee H, Paquola ACM, Blithikioti C, Ku M, Schlachetzki JCM, Winkler J, Edenhofer F, Glass CK, Paucar AA, Jaeger BN, Pham S, Boyer L, Campbell BC, Hunter T et al. (2018) Mitochondrial Aging Defects Emerge in Directly Reprogrammed Human Neurons due to Their Metabolic Profile. *Cell reports* 23: 2550-2558

Koschmidder E, Weissbach A, Bruggemann N, Kasten M, Klein C, Lohmann K (2016) A nonsense mutation in CHCHD2 in a patient with Parkinson disease. *Neurology* 86: 577-9

Kozjak-Pavlovic V (2017) The MICOS complex of human mitochondria. *Cell Tissue Res* 367: 83-93

Kuleshov MV, Jones MR, Rouillard AD, Fernandez NF, Duan Q, Wang Z, Koplev S, Jenkins SL, Jagodnik KM, Lachmann A, McDermott MG, Monteiro CD, Gundersen GW, Ma'ayan A (2016) Enrichr: a comprehensive gene set enrichment analysis web server 2016 update. *Nucleic Acids Res* 44: W90-7

Kurzwelly D, Kruger S, Biskup S, Heneka MT (2015) A distinct clinical phenotype in a German kindred with motor neuron disease carrying a CHCHD10 mutation. *Brain* 138: e376

Kyte J, Doolittle RF (1982) A simple method for displaying the hydropathic character of a protein. *J Mol Biol* 157: 105-32

Lane AN, Fan TW (2015) Regulation of mammalian nucleotide metabolism and biosynthesis. *Nucleic Acids Res* 43: 2466-85

Lane RS, Fu Y, Matsuzaki S, Kinter M, Humphries KM, Griffin TM (2015) Mitochondrial respiration and redox coupling in articular chondrocytes. *Arthritis Res Ther* 17: 54

Leary SC (2012) Blue native polyacrylamide gel electrophoresis: a powerful diagnostic tool for the detection of assembly defects in the enzyme complexes of oxidative phosphorylation. *Methods Mol Biol* 837: 195-206

Leary SC, Sasarman F, Nishimura T, Shoubridge EA (2009) Human SCO2 is required for the synthesis of CO II and as a thiol-disulphide oxidoreductase for SCO1. *Hum Mol Genet* 18: 2230-40

Lee RG, Sedghi M, Salari M, Shearwood AJ, Stentenbach M, Kariminejad A, Goullee H, Rackham O, Laing NG, Tajsharghi H, Filipovska A (2018) Early-onset Parkinson disease caused by a mutation in CHCHD2 and mitochondrial dysfunction. *Neurol Genet* 4: e276

Legland D, Arganda-Carreras I, Andrey P (2016) MorphoLibJ: integrated library and plugins for mathematical morphology with ImageJ. *Bioinformatics* 32: 3532-3534

Lehmer C, Schludi MH, Ransom L, Greiling J, Junghanel M, Exner N, Riemenschneider H, van der Zee J, Van Broeckhoven C, Weydt P, Heneka MT, Edbauer D (2018) A novel CHCHD10 mutation implicates a Mia40-dependent mitochondrial import deficit in ALS. *EMBO Mol Med* 10

Lehtonen JM, Forsstrom S, Bottani E, Viscomi C, Baris OR, Isoniemi H, Hockerstedt K, Osterlund P, Hurme M, Jylhava J, Leppa S, Markkula R, Helio T, Mombelli G, Uusimaa J, Laaksonen R, Laaksovirta H, Auranen M, Zeviani M, Smeitink J et al. (2016) FGF21 is a biomarker for mitochondrial translation and mtDNA maintenance disorders. *Neurology* 87: 2290-2299

Li NN, Wang L, Tan EK, Cheng L, Sun XY, Lu ZJ, Li JY, Zhang JH, Peng R (2016) Genetic analysis of CHCHD2 gene in Chinese Parkinson's disease. *Am J Med Genet B Neuropsychiatr Genet* 171: 1148-1152

Lim MA, Selak MA, Xiang Z, Krainc D, Neve RL, Kraemer BC, Watts JL, Kalb RG (2012) Reduced activity of AMP-activated protein kinase protects against genetic models of motor neuron disease. *J Neurosci* 32: 1123-41

Liu EY, Cali CP, Lee EB (2017) RNA metabolism in neurodegenerative disease. *Dis Model Mech* 10: 509-518

Liu W, Duan X, Xu L, Shang W, Zhao J, Wang L, Li JC, Chen CH, Liu JP, Tong C (2020) Chchd2 regulates mitochondrial morphology by modulating the levels of Opa1. *Cell Death Differ*

Liu Y, Clegg HV, Leslie PL, Di J, Tollini LA, He Y, Kim TH, Jin A, Graves LM, Zheng J, Zhang Y (2015) CHCHD2 inhibits apoptosis by interacting with Bcl-x L to regulate Bax activation. *Cell Death Differ* 22: 1035-46

Liu Y-T, Huang X, Nguyen D, Dombi E, Springer DA, Poulton J, Sekine S, Narendra DP (2019) Loss of CHCHD2 and CHCHD10 activates OMA1 peptidase to disrupt mitochondrial cristae phenocopying patient mutations. *bioRxiv*: 773135

Lochmuller H, Johns T, Shoubridge EA (1999) Expression of the E6 and E7 genes of human papillomavirus (HPV16) extends the life span of human myoblasts. *Exp Cell Res* 248: 186-93.

Longen S, Bien M, Bihlmaier K, Kloeppel C, Kauff F, Hammermeister M, Westermann B, Herrmann JM, Riemer J (2009) Systematic analysis of the twin cx(9)c protein family. *J Mol Biol* 393: 356-68

Lu B, Gehrke S, Wu Z (2014) RNA metabolism in the pathogenesis of Parkinsons disease. *Brain Res* 1584: 105-15

Mao C, Wang H, Luo H, Zhang S, Xu H, Zhang S, Rosenblum J, Wang Z, Zhang Q, Tang M, Shepard MJ, Wang X, Wang Y, Zhuang Z, Shi C, Xu Y (2019) CHCHD10 is involved in the

development of Parkinson's disease caused by CHCHD2 loss-of-function mutation p.T61I. *Neurobiol Aging* 75: 38-41

Martin LJ (2012) Biology of mitochondria in neurodegenerative diseases. *Prog Mol Biol Transl Sci* 107: 355-415

Martinez-Reyes I, Chandel NS (2014) Mitochondrial one-carbon metabolism maintains redox balance during hypoxia. *Cancer Discov* 4: 1371-3

Mathis S, Goizet C, Soulages A, Vallat JM, Masson GL (2019) Genetics of amyotrophic lateral sclerosis: A review. *J Neurol Sci* 399: 217-226

Matthews DA, Russell WC (1998) Adenovirus core protein V interacts with p32--a protein which is associated with both the mitochondria and the nucleus. *J Gen Virol* 79 (Pt 7): 1677-85

Mattiazzi M, D'Aurelio M, Gajewski CD, Martushova K, Kiaei M, Beal MF, Manfredi G (2002) Mutated human SOD1 causes dysfunction of oxidative phosphorylation in mitochondria of transgenic mice. *J Biol Chem* 277: 29626-33

Medinas DB, Gonzalez JV, Falcon P, Hetz C (2017) Fine-Tuning ER Stress Signal Transducers to Treat Amyotrophic Lateral Sclerosis. *Front Mol Neurosci* 10: 216

Melber A, Haynes CM (2018) UPR(mt) regulation and output: a stress response mediated by mitochondrial-nuclear communication. *Cell Res* 28: 281-295

Meng H, Yamashita C, Shiba-Fukushima K, Inoshita T, Funayama M, Sato S, Hatta T, Natsume T, Umitsu M, Takagi J, Imai Y, Hattori N (2017) Loss of Parkinson's disease-associated protein CHCHD2 affects mitochondrial crista structure and destabilizes cytochrome c. *Nat Commun* 8: 15500

Menzies FM, Cookson MR, Taylor RW, Turnbull DM, Chrzanowska-Lightowlers ZM, Dong L, Figlewicz DA, Shaw PJ (2002) Mitochondrial dysfunction in a cell culture model of familial amyotrophic lateral sclerosis. *Brain* 125: 1522-33

Metallo CM, Gameiro PA, Bell EL, Mattaini KR, Yang J, Hiller K, Jewell CM, Johnson ZR, Irvine DJ, Guarente L, Kelleher JK, Vander Heiden MG, Iliopoulos O, Stephanopoulos G (2011) Reductive glutamine metabolism by IDH1 mediates lipogenesis under hypoxia. *Nature* 481: 380-4

Mohrin M, Shin J, Liu Y, Brown K, Luo H, Xi Y, Haynes CM, Chen D (2015) Stem cell aging. A mitochondrial UPR-mediated metabolic checkpoint regulates hematopoietic stem cell aging. *Science* 347: 1374-7

Morais VA, Haddad D, Craessaerts K, De Bock PJ, Swerts J, Vilain S, Aerts L, Overbergh L, Grunewald A, Seibler P, Klein C, Gevaert K, Verstreken P, De Strooper B (2014) PINK1 loss-of-function mutations affect mitochondrial complex I activity via NdufA10 ubiquinone uncoupling. *Science* 344: 203-7

Mullen AR, Wheaton WW, Jin ES, Chen PH, Sullivan LB, Cheng T, Yang Y, Linehan WM, Chandel NS, DeBerardinis RJ (2011) Reductive carboxylation supports growth in tumour cells with defective mitochondria. *Nature* 481: 385-8

Muller K, Andersen PM, Hubers A, Marroquin N, Volk AE, Danzer KM, Meitinger T, Ludolph AC, Strom TM, Weishaupt JH (2014) Two novel mutations in conserved codons indicate that CHCHD10 is a gene associated with motor neuron disease. *Brain* 137: e309

Munoz-Gomez SA, Slamovits CH, Dacks JB, Baier KA, Spencer KD, Wideman JG (2015) Ancient homology of the mitochondrial contact site and cristae organizing system points to an endosymbiotic origin of mitochondrial cristae. *Curr Biol* 25: 1489-95

Muta T, Kang D, Kitajima S, Fujiwara T, Hamasaki N (1997) p32 protein, a splicing factor 2-associated protein, is localized in mitochondrial matrix and is functionally important in maintaining oxidative phosphorylation. *J Biol Chem* 272: 24363-70

Nayak RR, Kearns M, Spielman RS, Cheung VG (2009) Coexpression network based on natural variation in human gene expression reveals gene interactions and functions. *Genome Res* 19: 1953-62

Nicoletti G, Gagliardi M, Procopio R, Iannello G, Morelli M, Annesi G, Quattrone A (2018) A new CHCHD2 mutation identified in a southern italy patient with multiple system atrophy. *Parkinsonism Relat Disord* 47: 91-93

Nielsen H (2017) Predicting Secretory Proteins with SignalP. *Methods Mol Biol* 1611: 59-73

Niklas J, Melnyk A, Yuan Y, Heinzle E (2011) Selective permeabilization for the high-throughput measurement of compartmented enzyme activities in mammalian cells. *Anal Biochem* 416: 218-27

Nohara S, Ishii A, Yamamoto F, Yanagiha K, Moriyama T, Tozaka N, Miyake Z, Yatsuga S, Koga Y, Hosaka T, Terada M, Yamaguchi T, Aizawa S, Mamada N, Tsuji H, Tomidokoro Y, Nakamagoe K, Ishii K, Watanabe M, Tamaoka A (2019) GDF-15, a mitochondrial disease biomarker, is associated with the severity of multiple sclerosis. *J Neurol Sci* 405: 116429

Nussbaum RL, Ellis CE (2003) Alzheimer's disease and Parkinson's disease. *N Engl J Med* 348: 1356-64

Ogaki K, Koga S, Heckman MG, Fiesel FC, Ando M, Labbe C, Lorenzo-Betancor O, Moussaud-Lamodiere EL, Soto-Ortolaza AI, Walton RL, Strongosky AJ, Uitti RJ, McCarthy A, Lynch T, Siuda J, Opala G, Rudzinska M, Krygowska-Wajs A, Barcikowska M, Czyzewski K et al. (2015) Mitochondrial targeting sequence variants of the CHCHD2 gene are a risk for Lewy body disorders. *Neurology* 85: 2016-25

Oka T, Sayano T, Tamai S, Yokota S, Kato H, Fujii G, Mihara K (2008) Identification of a novel protein MICS1 that is involved in maintenance of mitochondrial morphology and apoptotic release of cytochrome c. *Mol Biol Cell* 19: 2597-608

Ostergaard S, Olsson L, Nielsen J (2001) In vivo dynamics of galactose metabolism in Saccharomyces cerevisiae: metabolic fluxes and metabolite levels. *Biotechnol Bioeng* 73: 412-25

Pakos-Zebrucka K, Koryga I, Mnich K, Ljujic M, Samali A, Gorman AM (2016) The integrated stress response. *EMBO Rep* 17: 1374-1395

Palamiuc L, Schlagowski A, Ngo ST, Vernay A, Dirrig-Grosch S, Henriques A, Boutillier AL, Zoll J, Echaniz-Laguna A, Loeffler JP, Rene F (2015) A metabolic switch toward lipid use in glycolytic muscle is an early pathologic event in a mouse model of amyotrophic lateral sclerosis. *EMBO Mol Med* 7: 526-46

Park JS, Davis RL, Sue CM (2018) Mitochondrial Dysfunction in Parkinson's Disease: New Mechanistic Insights and Therapeutic Perspectives. *Curr Neurol Neurosci Rep* 18: 21

Pasanen P, Myllykangas L, Poyhonen M, Kiuru-Enari S, Tienari PJ, Laaksovirta H, Toppila J, Ylikallio E, Tyynismaa H, Auranen M (2016) Intrafamilial clinical variability in individuals carrying the CHCHD10 mutation Gly66Val. *Acta Neurol Scand* 133: 361-6

Pear WS, Scott ML, Nolan GP (1997) Generation of high-titer, helper-free retroviruses by transient transfection. *Methods Mol Med* 7: 41-57

Penttila S, Jokela M, Bouquin H, Saukkonen AM, Toivanen J, Udd B (2015) Late onset spinal motor neuronopathy is caused by mutation in CHCHD10. *Ann Neurol* 77: 163-72

Penttila S, Jokela M, Hackman P, Maija Saukkonen A, Toivanen J, Udd B (2012) Autosomal dominant late-onset spinal motor neuronopathy is linked to a new locus on chromosome 22q11.2-q13.2. *European journal of human genetics : EJHG* 20: 1193-6

Perrone F, Nguyen HP, Van Mossevelde S, Moisse M, Sieben A, Santens P, De Bleecker J, Vandenbulcke M, Engelborghs S, Baets J, Cras P, Vandenberghe R, De Jonghe P, De Deyn PP, Martin JJ, Van Damme P, Van Broeckhoven C, van der Zee J, Belgian Neurology c (2017) Investigating the role of ALS genes CHCHD10 and TUBA4A in Belgian FTD-ALS spectrum patients. *Neurobiol Aging* 51: 177 e9-177 e16

Pfanner N, van der Laan M, Amati P, Capaldi RA, Caudy AA, Chacinska A, Darshi M, Deckers M, Hoppins S, Icho T, Jakobs S, Ji J, Kozjak-Pavlovic V, Meisinger C, Odgren PR, Park SK, Rehling P, Reichert AS, Sheikh MS, Taylor SS et al. (2014) Uniform nomenclature for the mitochondrial contact site and cristae organizing system. *J Cell Biol* 204: 1083-6

Pozo Devoto VM, Falzone TL (2017) Mitochondrial dynamics in Parkinson's disease: a role for alpha-synuclein? *Dis Model Mech* 10: 1075-1087

Purandare N, Somayajulu M, Huttemann M, Grossman LI, Aras S (2018) The cellular stress proteins CHCHD10 and MNRR1 (CHCHD2): Partners in mitochondrial and nuclear function and dysfunction. *J Biol Chem* 293: 6517-6529

Puschmann A, Dickson DW, Englund E, Wszolek ZK, Ross OA (2015) CHCHD2 and Parkinson's disease. *The Lancet Neurology* 14: 679

Quiros PM, Prado MA, Zamboni N, D'Amico D, Williams RW, Finley D, Gygi SP, Auwerx J (2017) Multi-omics analysis identifies ATF4 as a key regulator of the mitochondrial stress response in mammals. *J Cell Biol* 216: 2027-2045

Rampelt H, Zerbes RM, van der Laan M, Pfanner N (2016) Role of the mitochondrial contact site and cristae organizing system in membrane architecture and dynamics. *Biochim Biophys Acta*

Ramsden DB, Ho PW, Ho JW, Liu HF, So DH, Tse HM, Chan KH, Ho SL (2012) Human neuronal uncoupling proteins 4 and 5 (UCP4 and UCP5): structural properties, regulation, and physiological role in protection against oxidative stress and mitochondrial dysfunction. *Brain Behav* 2: 468-78

Robinson BH, Petrova-Benedict R, Buncic JR, Wallace DC (1992) Nonviability of cells with oxidative defects in galactose medium: a screening test for affected patient fibroblasts. *Biochem Med Metab Biol* 48: 122-6

Ronchi D, Riboldi G, Del Bo R, Ticozzi N, Scarlato M, Galimberti D, Corti S, Silani V, Bresolin N, Comi GP (2015) CHCHD10 mutations in Italian patients with sporadic amyotrophic lateral sclerosis. *Brain* 138: e372

Rubino E, Brusa L, Zhang M, Boschi S, Govone F, Vacca A, Gai A, Pinessi L, Lopiano L, Rogaeva E, Rainero I (2017) Genetic analysis of CHCHD2 and CHCHD10 in Italian patients with Parkinson's disease. *Neurobiol Aging* 53: 193 e7-193 e8

Rubino E, Zhang M, Mongini T, Boschi S, Vercelli L, Vacca A, Govone F, Gai A, Giordana MT, Grinberg M, Rogaeva E, Rainero I (2018) Mutation analysis of CHCHD2 and CHCHD10 in Italian patients with mitochondrial myopathy. *Neurobiol Aging* 66: 181 e1-181 e2

Ryall JG, Dell'Orso S, Derfoul A, Juan A, Zare H, Feng X, Clermont D, Koulnis M, Gutierrez-Cruz G, Fulco M, Sartorelli V (2015) The NAD(+)-dependent SIRT1 deacetylase translates a metabolic switch into regulatory epigenetics in skeletal muscle stem cells. *Cell Stem Cell* 16: 171-83

Ryan M, Zaldivar Vaillant T, McLaughlin RL, Doherty MA, Rooney J, Heverin M, Gutierrez J, Lara-Fernandez GE, Pita Rodriguez M, Hackembruch J, Perna A, Vazquez MC, Musio M, Ketzoian CN, Logroscino G, Hardiman O (2019) Comparison of the clinical and genetic features of amyotrophic lateral sclerosis across Cuban, Uruguayan and Irish clinic-based populations. *J Neurol Neurosurg Psychiatry* 90: 659-665

Santos D, Esteves AR, Silva DF, Januario C, Cardoso SM (2015) The Impact of Mitochondrial Fusion and Fission Modulation in Sporadic Parkinson's Disease. *Mol Neurobiol* 52: 573-86

Scher MB, Vaquero A, Reinberg D (2007) SirT3 is a nuclear NAD+-dependent histone deacetylase that translocates to the mitochondria upon cellular stress. *Genes Dev* 21: 920-8

Schindelin J, Arganda-Carreras I, Frise E, Kaynig V, Longair M, Pietzsch T, Preibisch S, Rueden C, Saalfeld S, Schmid B, Tinevez JY, White DJ, Hartenstein V, Eliceiri K, Tomancak P, Cardona A (2012) Fiji: an open-source platform for biological-image analysis. *Nat Methods* 9: 676-82

Scholle LM, Lehmann D, Deschauer M, Kraya T, Zierz S (2018) FGF-21 as a Potential Biomarker for Mitochondrial Diseases. *Curr Med Chem* 25: 2070-2081

Sharma K, Schmitt S, Bergner CG, Tyanova S, Kannaiyan N, Manrique-Hoyos N, Kongi K, Cantuti L, Hanisch UK, Philips MA, Rossner MJ, Mann M, Simons M (2015) Cell type- and brain region-resolved mouse brain proteome. *Nat Neurosci* 18: 1819-31

Shen S, He J, Tang L, Zhang N, Fan D (2017) CHCHD10 mutations in patients with amyotrophic lateral sclerosis in Mainland China. *Neurobiol Aging* 54: 214 e7-214 e10

Shi CH, Mao CY, Zhang SY, Yang J, Song B, Wu P, Zuo CT, Liu YT, Ji Y, Yang ZH, Wu J, Zhuang ZP, Xu YM (2016) CHCHD2 gene mutations in familial and sporadic Parkinson's disease. *Neurobiol Aging* 38: 217 e9-217 e13

Shi M, Zhang H, Wu X, He Z, Wang L, Yin S, Tian B, Li G, Cheng H (2017) ALYREF mainly binds to the 5' and the 3' regions of the mRNA in vivo. *Nucleic Acids Res* 45: 9640-9653

Shoffner JM, Watts RL, Juncos JL, Torroni A, Wallace DC (1991) Mitochondrial oxidative phosphorylation defects in Parkinson's disease. *Ann Neurol* 30: 332-9

Smith EF, Shaw PJ, De Vos KJ (2019) The role of mitochondria in amyotrophic lateral sclerosis. *Neurosci Lett* 710: 132933

Soustek MS, Balsa E, Barrow JJ, Jedrychowski M, Vogel R, Jan S, Gygi SP, Puigserver P (2018) Inhibition of the ER stress IRE1alpha inflammatory pathway protects against cell death in mitochondrial complex I mutant cells. *Cell Death Dis* 9: 658

Stein LR, Imai S (2012) The dynamic regulation of NAD metabolism in mitochondria. *Trends Endocrinol Metab* 23: 420-8

Straub IR, Janer A, Weraarpachai W, Zinman L, Robertson J, Rogaeva E, Shoubridge EA (2018) Loss of CHCHD10-CHCHD2 complexes required for respiration underlies the pathogenicity of a CHCHD10 mutation in ALS. *Hum Mol Genet* 27: 178-189

Strong DW, Hodges CV (1976) Disseminated nocardiosis presenting as testicular abscess. *Urology* 7: 57-9

Suomalainen A, Elo JM, Pietilainen KH, Hakonen AH, Sevastianova K, Korpela M, Isohanni P, Marjavaara SK, Tyni T, Kiuru-Enari S, Pihko H, Darin N, Ounap K, Kluijtmans LA, Paetau A, Buzkova J, Bindoff LA, Annunen-Rasila J, Uusimaa J, Rissanen A et al. (2011) FGF-21 as a biomarker for muscle-manifesting mitochondrial respiratory chain deficiencies: a diagnostic study. *Lancet Neurol* 10: 806-18

Teske BF, Fusakio ME, Zhou D, Shan J, McClintick JN, Kilberg MS, Wek RC (2013) CHOP induces activating transcription factor 5 (ATF5) to trigger apoptosis in response to perturbations in protein homeostasis. *Mol Biol Cell* 24: 2477-90

Tezze C, Romanello V, Sandri M (2019) FGF21 as Modulator of Metabolism in Health and Disease. *Front Physiol* 10: 419

Thangaratnarajah C, Ruprecht JJ, Kunji ER (2014) Calcium-induced conformational changes of the regulatory domain of human mitochondrial aspartate/glutamate carriers. *Nat Commun* 5: 5491

Thul PJ, Akesson L, Wiking M, Mahdessian D, Geladaki A, Ait Blal H, Alm T, Asplund A, Bjork L, Breckels LM, Backstrom A, Danielsson F, Fagerberg L, Fall J, Gatto L, Gnann C, Hober S, Hjelmare M, Johansson F, Lee S et al. (2017) A subcellular map of the human proteome. *Science* 356

Tilokani L, Nagashima S, Paupe V, Prudent J (2018) Mitochondrial dynamics: overview of molecular mechanisms. *Essays Biochem* 62: 341-360

Tio M, Wen R, Lim YL, Zukifli ZHB, Xie S, Ho P, Zhou Z, Koh TW, Zhao Y, Tan EK (2017) Varied pathological and therapeutic response effects associated with CHCHD2 mutant and risk variants. *Hum Mutat* 38: 978-987

Tkach JM, Yimit A, Lee AY, Riffle M, Costanzo M, Jaschob D, Hendry JA, Ou J, Moffat J, Boone C, Davis TN, Nislow C, Brown GW (2012) Dissecting DNA damage response pathways by analysing protein localization and abundance changes during DNA replication stress. *Nat Cell Biol* 14: 966-76

Tournier C, Hess P, Yang DD, Xu J, Turner TK, Nimnual A, Bar-Sagi D, Jones SN, Flavell RA, Davis RJ (2000) Requirement of JNK for stress-induced activation of the cytochrome c-mediated death pathway. *Science* 288: 870-4

Tseng AH, Shieh SS, Wang DL (2013) SIRT3 deacetylates FOXO3 to protect mitochondria against oxidative damage. *Free Radic Biol Med* 63: 222-34

Tsuruta F, Sunayama J, Mori Y, Hattori S, Shimizu S, Tsujimoto Y, Yoshioka K, Masuyama N, Gotoh Y (2004) JNK promotes Bax translocation to mitochondria through phosphorylation of 14-3-3 proteins. *EMBO J* 23: 1889-99

Ueda E, Tamura Y, Sakaue H, Kawano S, Kakuta C, Matsumoto S, Endo T (2019) Myristoyl group-aided protein import into the mitochondrial intermembrane space. *Sci Rep* 9: 1185

Urano F, Wang X, Bertolotti A, Zhang Y, Chung P, Harding HP, Ron D (2000) Coupling of stress in the ER to activation of JNK protein kinases by transmembrane protein kinase IRE1. *Science* 287: 664-6

Walter J, Bolognin S, Antony PMA, Nickels SL, Poovathingal SK, Salamanca L, Magni S, Perfeito R, Hoel F, Qing X, Jarazo J, Arias-Fuenzalida J, Ignac T, Monzel AS, Gonzalez-Cano L, Pereira de Almeida L, Skupin A, Tronstad KJ, Schwamborn JC (2019) Neural Stem Cells of Parkinson's Disease Patients Exhibit Aberrant Mitochondrial Morphology and Functionality. *Stem Cell Reports* 12: 878-889

Wei Y, Vellanki RN, Coyaud E, Ignatchenko V, Li L, Krieger JR, Taylor P, Tong J, Pham NA, Liu G, Raught B, Wouters BG, Kislinger T, Tsao MS, Moran MF (2015) CHCHD2 Is Coamplified with EGFR in NSCLC and Regulates Mitochondrial Function and Cell Migration. *Mol Cancer Res* 13: 1119-29

Weraarpachai W, Antonicka H, Sasarman F, Seeger J, Schrank B, Kolesar JE, Lochmuller H, Chevrette M, Kaufman BA, Horvath R, Shoubridge EA (2009) Mutation in TACO1, encoding a translational activator of COX I, results in cytochrome c oxidase deficiency and late-onset Leigh syndrome. *Nat Genet* 41: 833-7

Wiedemann FR, Manfredi G, Mawrin C, Beal MF, Schon EA (2002) Mitochondrial DNA and respiratory chain function in spinal cords of ALS patients. *J Neurochem* 80: 616-25

Wilson R, Gundamaraju R, Vemuri R, Angelucci C, Geraghty D, Gueven N, Eri RD (2020) Identification of Key Pro-Survival Proteins in Isolated Colonic Goblet Cells of Winnie, a Murine Model of Spontaneous Colitis. *Inflamm Bowel Dis* 26: 80-92

Winklhofer KF, Haass C (2010) Mitochondrial dysfunction in Parkinson's disease. *Biochim Biophys Acta* 1802: 29-44

Woo JA, Liu T, Trotter C, Fang CC, De Narvaez E, LePochat P, Maslar D, Bukhari A, Zhao X, Deonarine A, Westerheide SD, Kang DE (2017) Loss of function CHCHD10 mutations in cytoplasmic TDP-43 accumulation and synaptic integrity. *Nat Commun* 8: 15558

Wu H, Lu X, Cen Z, Xie F, Zheng X, Chen Y, Luo W (2016) Genetic analysis of the CHCHD2 gene in Chinese patients with familial essential tremor. *Neurosci Lett* 634: 104-106

Xiao T, Jiao B, Zhang W, Pan C, Wei J, Liu X, Zhou Y, Zhou L, Tang B, Shen L (2017) Identification of CHCHD10 Mutation in Chinese Patients with Alzheimer Disease. *Mol Neurobiol* 54: 5243-5247

Xiao Y, Zhang J, Shu X, Bai L, Xu W, Wang A, Chen A, Tu WY, Wang J, Zhang K, Luo B, Shen C (2019) Loss of mitochondrial protein CHCHD10 in skeletal muscle causes neuromuscular junction impairment. *Hum Mol Genet*

Yagi M, Uchiumi T, Takazaki S, Okuno B, Nomura M, Yoshida S, Kanki T, Kang D (2012) p32/gC1qR is indispensable for fetal development and mitochondrial translation: importance of its RNA-binding ability. *Nucleic Acids Res* 40: 9717-37

Yang X, Zhao Q, An R, Zheng J, Tian S, Chen Y, Xu Y (2016) Mutational scanning of the CHCHD2 gene in Han Chinese patients with Parkinson's disease and meta-analysis of the literature. *Parkinsonism Relat Disord* 29: 42-6

Ye Q, Worman HJ (1994) Primary structure analysis and lamin B and DNA binding of human LBR, an integral protein of the nuclear envelope inner membrane. *J Biol Chem* 269: 11306-11

Yin F, Sancheti H, Patil I, Cadenas E (2016) Energy metabolism and inflammation in brain aging and Alzheimer's disease. *Free Radic Biol Med* 100: 108-122

Zhang M, Xi Z, Fang S, Ghani M, Sato C, Moreno D, Liang Y, Lang AE, Rogaeva E (2016) Mutation analysis of CHCHD2 in Canadian patients with familial Parkinson's disease. *Neurobiology of aging* 38: 217 e7-8

Zhang M, Xi Z, Zinman L, Bruni AC, Maletta RG, Curcio SA, Rainero I, Rubino E, Pinessi L, Nacmias B, Sorbi S, Galimberti D, Lang AE, Fox S, Surace EI, Ghani M, Guo J, Sato C, Moreno D, Liang Y et al. (2015) Mutation analysis of CHCHD10 in different neurodegenerative diseases. *Brain* 138: e380

Zhang X, Zhang F, Guo L, Wang Y, Zhang P, Wang R, Zhang N, Chen R (2013) Interactome analysis reveals that C1QBP (complement component 1, q subcomponent binding protein) is associated with cancer cell chemotaxis and metastasis. *Mol Cell Proteomics* 12: 3199-209

Zhao M, Kim JR, van Bruggen R, Park J (2018) RNA-Binding Proteins in Amyotrophic Lateral Sclerosis. *Mol Cells* 41: 818-829

Zheng Y, Lin TY, Lee G, Paddock MN, Momb J, Cheng Z, Li Q, Fei DL, Stein BD, Ramsamooj S, Zhang G, Blenis J, Cantley LC (2018) Mitochondrial One-Carbon Pathway Supports Cytosolic Folate Integrity in Cancer Cells. *Cell* 175: 1546-1560 e17

Zhou Q, Chen Y, Wei Q, Cao B, Wu Y, Zhao B, Ou R, Yang J, Chen X, Hadano S, Shang HF (2017a) Mutation Screening of the CHCHD10 Gene in Chinese Patients with Amyotrophic Lateral Sclerosis. *Mol Neurobiol* 54: 3189-3194

Zhou W, Ma D, Sun AX, Tran HD, Ma DL, Singh BK, Zhou J, Zhang J, Wang D, Zhao Y, Yen PM, Goh E, Tan EK (2019) PD-linked CHCHD2 mutations impair CHCHD10 and MICOS complex leading to mitochondria dysfunction. *Hum Mol Genet* 28: 1100-1116

Zhou X, Liu Z, Guo J, Sun Q, Xu Q, Yan X, Tang B, Lei L (2017b) Identification of CHCHD10 variants in Chinese patients with Parkinson's disease. *Parkinsonism Relat Disord*

Zhou ZD, Saw WT, Tan EK (2016) Mitochondrial CHCHD-Containing Proteins: Physiologic Functions and Link with Neurodegenerative Diseases. *Mol Neurobiol*

Zhu L, Gomez-Duran A, Saretzki G, Jin S, Tilgner K, Melguizo-Sanchis D, Anyfantis G, Al-Aama J, Vallier L, Chinnery P, Lako M, Armstrong L (2016) The mitochondrial protein CHCHD2 primes the differentiation potential of human induced pluripotent stem cells to neuroectodermal lineages. *J Cell Biol* 215: 187-202

Appendix

Research Ethics Board approval for study on human patient fibroblasts.

MUHC REB – NEUPSY / CÉR CUSM – NEUPSY
3801, rue University, # 686
Montréal (Québec) H3A 2B4
Tel. 514.398.1046
reb.neuro@mcgill.ca
www.leneuro.ca

2018-03-28

Dr. Eric Alan Shoubridge
MNI/H 622D
email: eric.shoubridge@mcgill.ca

RE: Final REB Approval of a New Research Project
Investigation of biochemical defects in cell lines of patients with mitochondrial disease

Mito / 2017-3362

MUHC REB Co-Chair for the NEUPSY panel: Dr. Judith Marcoux

Dear Dr. Shoubridge,

Thank you for submitting your responses and corrections for the research project indicated above, as requested by the McGill University Health Centre (MUHC) Research Ethics Board (REB).

The MUHC REB, more precisely its Neurosciences and Psychiatry panel (NEUPSY) provided conditional approval for the research project after a delegated review provided by its member(s).

On 2018-03-28, delegated review of your responses and corrections was providedbymember(s) of the MUHC REB. The research project was found to meet scientific and ethical standards for conduct at the MUHC and Montreal Neurological Institute and Hospital (MNI/H).

The following documents were approved or acknowledged by the MUHC REB:

- Initial Submission Form
  - F11NIR-14543
- REB Conditions & PI Responses Form(s)
  - F20-29789
- Protocol
  - Protocol_Mito_2018-03-26_REB Approved.docx
  - MDA grantfor ethics.pdf
  - CIHR CHCHD10.docx
- Contract, Budget and Financial
  - MTA - inbound - ALS samples projet MinE.pdf
  - previewAps.pdf
- Additional Documents / Discussion
  - Email_Add Rouleau as collaborator_2018-03-28.pdf

This will be reported to the MUHC REB and will be entered accordingly into the minutes of the next NEUPSY meeting. Please be advised that you may only initiate the study after all required reviews and decisions are received and documented.

The approval of the research project is valid until 2019-03-27.

MUHC REB – NEUPSY / CÉR CUSM – NEUPSY
3801, rue University, # 686
Montréal (Québec) H3A 2B4
Tel. 514.398.1046
reb.neuro@mcgill.ca
www.leneuro.ca

2018-04-04

Dr. Eric Alan Shoubridge
MNI/H 622D
email: eric.shoubridge@mcgill.ca

RE: Neuro Authorization
Investigation of biochemical defects in cell lines of patients with mitochondrial disease **(Mito / 2017-3362)**

Dear Dr. Shoubridge,

We are writing to confirm that the study mentioned above has received all required institutional approvals.

You are hereby authorized to conduct your research at the Montreal Neurological Institute (MNI) as well as to initiate recruitment.

Please refer to the MUHC Study number in all future correspondence relating to this study.

In accordance with applicable policies it is the investigator's responsibility to ensure that staff involved in the study is competent and qualified and, when required, has received certification to conduct clinical research.

Should you have any questions, please do not hesitate to contact the support for the undersigned at brigitte.paquet@mcgill.ca.

We wish you every success with the conduct of the research.

Best Regards,

Brigitte Pâquet, LL.B.
for:
John McCall, CPA, CGA
Director of Administration and Operations
Montreal Neurological Institute